THE DEVELOPMENT OF GLYCOSAMINOGLYCAN-BASED MATERIALS TO PROMOTE CHONDROGENIC DIFFERENTIATION OF MESENCHYMAL STEM CELLS

A Dissertation
Presented to
The Academic Faculty

by

Jeremy J. Lim

In Partial Fulfillment
of the Requirements for the Degree
Doctor of Philosophy in the
Department of Biomedical Engineering

Georgia Institute of Technology
August 2012

THE DEVELOPMENT OF GLYCOSAMINOGLYCAN-BASED MATERIALS TO PROMOTE CHONDROGENIC DIFFERENTIATION OF MESENCHYMAL STEM CELLS

Approved by:

Dr. Johnna S. Temenoff, Advisor
Department of Biomedical Engineering
Georgia Institute of Technology

Dr. Andrés J. García
School of Mechanical Engineering
Georgia Institute of Technology

Dr. Ravi V. Bellamkonda
Department of Biomedical Engineering
Georgia Institute of Technology

Dr. Marc E. Levenston
Department of Mechanical Engineering
Stanford University

Dr. Kenneth A. Gall
School of Materials Science and Engineering
Georgia Institute of Technology

Dr. Todd C. McDevitt
Department of Biomedical Engineering
Georgia Institute of Technology

Date Approved: June 15, 20012

Dedicated to my loving family:
To Mom and Dad for the support, devotion, and confidence,
and to Court and T.J. for the laughter, guidance, and companionship.

ACKNOWLEDGEMENTS

I acknowledge everyone who contributed to this work and supported me during my graduate career. First, I wish to thank my thesis committee members – Dr. Ravi Bellamkonda, Dr. Ken Gall, Dr. Andrés García, Dr. Marc Levenston, and Dr. Todd McDevitt – for their insight and guidance over the years. They were always sure to challenge me to make sure that my science was strong and that my work was impactful. I deeply value the broad range of expertise that they contributed to this work at the intersection of material science and cell biology, and their advice over the years has helped me to grow as both a scientist and engineer. I feel especially fortunate to have had to opportunity to develop relationships with my committee members on both a professional and personal level. Dr. Bellamkonda always reminded me to take a step back and consider the bigger picture, and I've enjoyed the insight and assistance that he and his lab have provided me over the years. I had the pleasure of working with Dr. Gall during my internship at MedShape Solutions, and Ken taught me a great deal about engineering novel materials for use in medical applications and gave me valuable insight into how to operate a successful small business. Dr. García has been a tremendous mentor to me over these past 6 years. I had the opportunity of working with him during my research rotation in his lab and on the Cell and Tissue Engineering Training Grant. Andrés has always been a strong advocate for and an invested teacher to the students, so I greatly appreciated his leadership. When Dr. Levenston was at Georgia Tech, he was a valuable mentor as the Temenoff Lab was first getting started. He and his lab were always welcoming and willing to help in the development of protocols, use of equipment,

and assistance with experiments/analysis, and even after moving to Stanford University in 2007, Marc has continued to be an accommodating resource. I especially need to acknowledge Dr. McDevitt, along with Andrés Bratt-Leal and Kirsten Kepple, for their assistance in the synthesis and characterization of CSMA microspheres. I've greatly enjoyed working closely with Todd and his lab, and I am especially grateful that some of my work has been able to develop a closer collaboration between our research groups. In addition, I would like to acknowledge Dr. Gang Bao and Charles Glaus for use of and assistance with their dynamic light scattering system, Dr. Vladimir Tsukruk and Seth Young in the Microanalysis Center for use of and assistance with their Fourier transform infrared spectrometer, and Dr. Brani Vidakovic for valuable statistical expertise and consultation. Finally I would like to acknowledge my undergraduate academic advisor at Northwestern University, Dr. Eric Perreault, for his advice and assistance which helped me to find a field of research and graduate university that I love, leading me to where I am today.

I also wish to thank everyone in the Department of Biomedical Engineering and Institute for Bioengineering and Biotechnology for their help and support. Shannon Sullivan, Sally Gerrish, Beth Bullock, and Penelope Pollard in BME have been valuable resources, and I appreciate how they always greeted me with a smile. The work they do and community they built help to make Georgia Tech BME great. I also thank Dr. Essy Behravesh and Paul Fincannon for their friendship. I deeply appreciate the tremendous work that Steve Woodard, Aqua Asberry, and Andrew Shaw do to keep the IBB core facilities operational. Many aspects of the research we do depend on their hard work and assistance. Also thanks to Megan McDevitt, Colly Mitchell, James Godard, Alyceson

Andrews, and Floyd Wood in IBB for their work organizing the constant flow of events, and especially their work with BBUGS.

I very much need to thank my advisor, Dr. Johnna Temenoff, for all of her help and support over the years. She has always trusted in me since I first started at Georgia Tech, clueless but determined, and at times it seemed like she believed in me more that I believed in myself. Johnna encouraged me when I needed encouragement, motivated me when I needed motivation, and challenged me when I needed a challenge. Her mentorship has taught me a great deal over the years to help me to develop as a researcher and given me confidence as I move forward in my career. I value her both as a colleague and as a friend, as we share a mutual love for haikus, Harry Potter, and German gummies.

The Temenoff Lab has been like a second home for me, and my labmates have become like a second family throughout the years. The Temenoff Lab has a tremendous culture of support and cooperation, and it is something that I treasure. Derek Doroski and Kelly Brink were there in the beginning, and I will always appreciate the foundation that they built. They not only set up the lab and many of the protocols we use, but ensured that the lab was a welcoming, collaborative community going forward. I enjoyed the many extended conversations that I have had with Derek, and his quick wit and sense of humor were a constant bright spot. Kelly always had a welcoming smile, and she filled our days with plenty of laughter and joy. Peter Yang and I started in the lab together, and he has been my wingman throughout the process. I have tremendous respect for him as a loyal friend, as he treats those closest to him with great love and respect. He is a deeply committed individual, especially once he finds something that he loves, and I value his

friendship. Taymour Hammoudi, Song Seto, and Jennifer Lei have been exceptional companions both in lab and outside of lab during the past few years. Taymour has always provided a strong and fun personality that I appreciate, his stories and exploits keep life interesting, and during the past 6 months, he's been my best "bro" among a lab full of women. His passion for science is something that I greatly admire, and I appreciate his endless help and advice over the years, especially in the early development of the chondroitin sulfate-based materials. Too many times I've told people, "I'm not sure, but you should ask Taymour. He'd definitely know." Song has been a tremendous friend over the years. She seems to understand people better than most, and she has always been quick to ask about my friends and family and willing to listen to my problems and hardships. Song is forever hardworking and selfless, has always been willing to humor us in our goofy exploits, and I appreciate everything that she has done for me as a colleague and friend. Jen is always good for a big smile, and her exaggerated waves were something that I looked forward to walking into lab each day. Forever laid back and optimistic, she also kept me active during the last few months of this work by convincing me to train for the Publix Half-Marathon in Atlanta in March 2012. Though it seemed like there was always more work to be done, I treasured the times where I could go for a run and clear my head. I've also enjoying getting to know and mentoring Melissa Goude and Torri Rinker over the past year. Scientifically, they're years ahead of where I was as an incoming student, and I'm certain that they'll take the lab to new heights. I've worked closely with Melissa during the past year, and her inquisitive nature and youthful energy have been a joy. Torri was especially supportive while I was writing this dissertation, and I appreciate her constant encouragement during those long, busy days. I also give my

thanks to our former postdocs Yongzhi Qiu and Sharon Hamilton for keeping me company during the many late nights in lab. Yong is an outstandingly warm-hearted individual, and he never hesitated to go out of his way to help a friend. Sharon's been a great friend and resource. We've shared a lot of fun moments together, and her insight into the chemical modification of my materials was priceless. I also thank my undergraduate students Larry Scott, Jr. and Rachel Van Stelle for their hard work and assistance in completing this work. Larry was always hardworking, diligent, and reliable, and a he's been a supportive friend. I look forward to the promising future that he has ahead of him. Rachel was always dependable and a very fast learner, and she will continue to be successful in everything that she does. The past 6 years in the Temenoff Lab have been an absolute joy for me, as I've been able to meet new students and form a special bond with close friends each and every year.

I need to thank all of the senior students that came (and subsequently left) before me. They created a welcoming community within the department, and I could always rely on them for help, advice, and friendship. I thank Chris Wilson, John Connelly, Ashley Palmer, and Onyi Irrechukwu of the Levenston Lab for their mentorship during the early years. I also thank Richard Carpenedo, David Dumbauld, Tim Petrie, Scott Robinson, Torrence Welch, Brock Wester, and Blaine Zern for the many memories over the years that they've been a part of.

I also need to thank Casey Holliday Ankeny, Randy Ankeny, Andrés Bratt-Leal, Ashley Carson Brown, Chris Brown, Priya Santhanam, Erin Spinner, and Jason Weaver for their friendship the past 6 years. We all met during my first year of grad school in 2006-2007, and they've been amazing companions throughout the years. Andrés and Erin

have been my most loyal friends at Georgia Tech. They treated me like family and always made me feel loved, appreciated, and welcome, whether hanging out at their apartment, playing tennis, or taking weekend trips to escape Atlanta. Ashley and Chris can really bring the fun, and we've shared some great memories. We'll always have Moondogs. Casey and Randy have been especially caring and supportive, and countless times they've offered me a ride, cooked me dinner, and been the first to lend a hand and offer their encouragement when needed. They're super genuine in their words and actions, and would always greet me with a big smile. I've always been comfortable and at home with Jason and Priya, and we will always share a common love of Big Ten sports and all things Chicago.

Additionally I thank Ashley Allen, Vince Fiore, Matt Magnuson, Katie Pitz, Jonathan Suever, Jay Sy, and Brent Uhrig for their friendship. Ashley's quirky enthusiasm is contagious, Vince is a genuine, loveable guy and our wildcard, Matt is a committed friend and always made me feel appreciated, Katie is loved by everyone around her, Jonathan is a fun-loving guy who always means well, Jay was my first friend in Atlanta when we met during orientation, and Brent has always had my back and been a true friend. Also thanks to Min Cho, Chris Dosier, Alison Douglas, Chris Edens, Kelly Erby, Sarah Forte, Laura Hansen, Nathan Hotaling, Christian Lease, Ted Lee, Melissa Li, and Rachel Whitmire for their friendship over the years. Raj Patel and Burhan Khan deserve special acknowledgement as best buds from Northwestern who were always quick to ask for updates about my research, and offered their love and support from afar.

Finally, I owe everything in my life to my loving family. My parents, Allen and Carrie Lim, have been forever supportive of me and my goals in life. Mom and Dad have

been a constant inspiration to me in the way I work, the way I play, the way I live my life, and the way I treat those around me. Their high expectations and loving character have absolutely shaped every aspect of my life today. They always pushed me to never be satisfied with anything less than my best and encouraged me to never quit on something that I start. My Dad is the hardest working individual that I know, and he has forever worked to support his family, while asking for nothing in return. I try my best to live my life by his example. Mom is the steadfast leader of our family, and she can be stubbornly strong-willed but will never fail to fight for those she loves. She knows me all too well, and her strength and love throughout my life have been an inspiration. My sister Courtney Lim was a tremendous role model growing up. She unknowingly pushed me to be better as a student and as a person, and we've shared a lifetime of memories together. Even though when we were younger, it seemed like it was my older sister's job to make my life difficult, I now realize that Court has been by my side through it all and is one of the best friends that I will ever have. My brother-in-law T.J. Linz has been encouraging through the years and has always treated me like a brother, even if he occasionally likes to harass me (and beat me on Xbox) like a little brother too. Finally, my new nephew William Linz provided me with countless smiles, laughs, and hope during these first 6 months of his life, and the constant barrage of photo updates would always bring a smile to my face, even during the hardest days. I love my family more than anything in this world, and will forever appreciate their endless love and support. Living by their example drives me every day to try to leave this world better than when I entered it.

TABLE OF CONTENTS

LIST OF TABLES

LIST OF FIGURES

LIST OF ABBREVIATIONS

AcCl	acryloyl chloride
ACI	autologous chondrocyte implantation
ACL	anterior cruciate ligament
ANOVA	analysis of variance
APMAm	N-(3-aminopropyl)methacrylamide
APS	ammonium persulfate
bFGF	basic fibroblast growth factor
BMP	bone morphogenetic protein
BMSC	bone marrow stromal cell
BSA	bovine serum albumin
C4st1	chondroitin-4-sulfotransferase 1
C6st1	chondroitin-6-sulfotransferase 1
Ch-MA	chondroitin methacrylate
ChSy1	chondroitin sulfate synthase 1
COMP	cartilage oligomeric matrix protein
CS	chondroitin sulfate
CSGalNAcT1	chondroitin sulfate N-acetylgalactosaminyltransferase 1
CSMA or CS-MA	chondroitin sulfate methacrylate
CSMAm	chondroitin sulfate methacrylamide
D2959	Irgacure 2959
D_2O	deuterated water
DAB	diaminobenzidine
DAPI	4',6-diamidino-2-phenylindole

ddH_2O	distilled, deionized water
dH_2O	distilled water
DLS	dynamic light scattering
DMMB	dimethylmethylene blue
DMSO	dimethyl sulfoxide
EB	embryoid body
ECM	extracellular matrix
EDC	N-(3-dimethylaminopropyl)-N'-ethylcarbodiimide
EDTA	ethylenediaminetetraacetic acid
ELISA	enzyme-linked immunosorbent assay
ESC	embryonic stem cell
ESPA	equine systemic proteoglycan accumulation
FBS	fetal bovine serum
FGF	fibroblast growth factor
FTIR	Fourier transform infrared spectroscopy
FuCl	fumaryl chloride
GAG	glycosaminoglycan
GAPDH	glyceraldehyde-3-phosphate dehydrogenase
GDNF	glial cell line-derived neurotrophic factor
GMA	glycidyl methacrylate
H&E	hematoxylin and eosin
HB-EGF	heparin-binding epidermal growth factor-like growth factor
^1H NMR	proton nuclear magnetic resonance
HRP	horseradish peroxidase
IGF	insulin-like growth factor

IHC	immunohistochemistry
Ihh	Indian hedgehog
ITS	insulin-transferrin-selenium
LIF	leukemia inhibitory factor
MeCl	methylene chloride
MK	midkine
MMP	matrix metalloproteinase
M_n	number average molecular mass
MSC	mesenchymal stem cell
M_w	weight average molecular mass
MWCO	molecular weight cutoff
N-cadherin	neural-cadherin
N-CAM	neural cell adhesion molecule
NEAA	nonessential amino acids
OPF	oligo(poly(ethylene glycol) fumarate)
PBS	phosphate-buffered saline
PCL	poly(ε-caprolactone)
PCM	pericellular matrix
PCR	polymerase chain reaction
PDGF	platelet-derived growth factor
PEG	poly(ethylene glycol)
PEG-DA	poly(ethylene glycol)-diacrylate
PEG-DMA	poly(ethylene glycol)-dimethacrylate
PGA	poly(glycolic acid)
pI	isoelectric point

PI	polydispersity index
PLA	poly(lactic acid)
PLGA	poly(lactic-co-glycolic acid)
PPAR-γ2	peroxisome proliferator-activated receptor γ2
Ptc	Patched
PTHrP	parathyroid hormone-related protein
PTN	pleiotrophin
RGD	arginine-glycine-aspartic acid
RHAMM	receptor for hyaluronan-mediated motility
ROCK	Rho kinase
RT-PCR	reverse transcription polymerase chain reaction
SAX-HPLC	strong anion exchange high performance liquid chromatography
SEC-HPLC	size exclusion high performance liquid chromatography
SLRP	small leucine-rich proteoglycan
SPR	surface plasmon resonance
Sulfo-NHS	N-hydroxysulfosuccinimide
TCPS	tissue culture-treated polystyrene
TEA	triethylamine
TEMED	tetramethylethylenediamine
TGF-β	transforming growth factor-β
TNF-α	tumor necrosis factor-α
Tris	tris(hydroxymethyl)aminomethane
UV	ultraviolet
VEGF	vascular endothelial growth factor

SUMMARY

Tissue engineering strategies represent exciting potential therapies to repair cartilage injuries; however, difficulty regenerating the complex extracellular matrix (ECM) organization of native cartilage remains a significant challenge. Cartilaginous ECM molecules, specifically chondroitin sulfate (CS) glycosaminoglycan, may possess the ability to promote and direct MSC differentiation down a chondrogenic lineage. CS may interact with the stem cell microenvironment through its highly negative charge, generation of osmotic pressure, and sequestration of growth factors; however, the role of CS in directing differentiation down a chondrogenic lineage remains unclear. The overall goal of this dissertation was to develop versatile biomaterial platforms to control CS presentation to mesenchymal stem cells (MSCs) in order to improve understanding of the interactions with CS that promote chondrogenic differentiation.

To investigate chondrogenic response to a diverse set of CS materials, progenitor cells were cultured in the presence of CS proteoglycans and CS chains in a variety of 2D and 3D material systems. Surfaces were coated with aggrecan proteoglycan to alter cell morphology, CS-based nano- and microspheres were developed as small particle carriers for growth factor delivery, and desulfated chondroitin hydrogels were synthesized to examine electrostatic interactions with growth factors and the role of sulfation in the chondrogenic differentiation of MSCs. Together these studies provided valuable insight into the unique ability of CS-based materials to control cellular microenvironments via morphological and material cues to promote chondrogenic differentiation in the development of tissue engineering strategies for cartilage regeneration and repair.

CHAPTER 1

INTRODUCTION

1.1 Motivation

Cartilaginous tissues play important structural and mechanical roles throughout the body. Particularly in the articular joints, hyaline cartilage distributes loads across the ends of long bones and facilitates motion with low-friction gliding along its surfaces. Unfortunately, cartilage tissue possesses a low capacity for healing, largely because it is a poorly vascularized tissue [1]. As a load bearing tissue, damage to articular cartilage by arthritis and physical trauma can be both debilitating and extremely painful. Of nearly 995,000 arthroscopic procedures performed on the knee in the United States in 2006, 466,000 (47%) of those performed in an ambulatory (outpatient) setting were diagnosed with a tear of the medial or lateral cartilage or menisci. An additional 56,500 (6%) were diagnosed with osteoarthritis of the knee [2]. In 2005, an estimated 27 million adults in the US had clinical osteoarthritis with indirect costs totaling approximately $89 billion per year [3-4]. To address this growing need, novel tissue engineering therapies seek to promote repair of cartilaginous tissue and restore long-term joint function.

Tissue engineering seeks to promote regeneration of tissue replacements through the combination of cells, scaffold materials, and various soluble, physical, or mechanical differentiation stimuli. While cartilage appears to be a relatively simple tissue that lacks vascularization and nerves and primarily contains only one cell type, challenges to cartilage regeneration include maintaining the phenotype of chondrocytes *in vitro* and recapitulating the complex extracellular matrix (ECM) organization of cartilaginous

tissues [5]. Mesenchymal stem cells (MSCs) are multipotent progenitor cells, found in adult bone marrow, that are capable of differentiating into cartilaginous tissues [6], and recent research has investigated the ability of cartilaginous ECM molecules to direct differentiation of MSCs down a chondrogenic lineage [7-11]. Chondroitin sulfate (CS) is a glycosaminoglycan (GAG) that is prevalent in cartilage, primarily linked with aggrecan proteoglycan. While is it well established that the high negative charge density of CS contributes to cartilage's compressive strength by osmotically retaining water within the tissue matrix [12-13], its role in promoting the development, maintenance, and repair of cartilage tissue is not as well understood.

CS-containing proteoglycans versican and perlecan regulate mesenchymal condensation during cartilage development [14-15], and several enzymes involved in CS initiation, elongation, and sulfation are required for proper skeletal development and patterning [16-18], indicating that CS glycosaminoglycans (GAGs) play an important role in chondrogenesis *in vivo*. Recent studies have investigated the ability of CS-modified biomaterials to promote the production of cartilaginous ECM *in vitro* as well. Aggrecan-coated surfaces promoted the aggregation and production of GAG and collagen II in dermal fibroblasts [10], and culture in CS-containing hydrogels upregulated expression and production of cartilaginous ECM by encapsulated goat and mouse MSCs [8-9]. Sulfated GAGs may alter the extracellular microenvironment via altered osmotic swelling pressure, streaming potential under dynamic loading, and sequestration of growth factors [19-22]. Additionally, downstream effects of cell clustering in CS-modified materials may play a role in differentiation, including increased cell-cell contact [8, 10, 23]. While some of the effects of CS materials on ECM production have been

broadly characterized, an improved understanding of the role of GAGs in stem cell differentiation is a vital step in developing tissue engineering therapies to regenerate cartilage.

1.2 Research Objectives

The objective of the research presented is this dissertation was to develop CS-based materials as platforms to control CS presentation to MSCs in order to study the role of CS in chondrogenic differentiation. To investigate the chondrogenic response to CS, MSCs were cultured in the presence of CS proteoglycan and CS GAG chains on 2D surfaces, with nano- and microparticles, and in 3D hydrogels. MSC response on 2D aggrecan-coated surfaces was explored for cell morphology, including aggregation and cell contact, and expression and production of ECM. CS-based materials were also developed, over numerous size scales, to study their role in electrostatic complexation with positively charged growth factors. CS particles were developed for controlled delivery of growth factors within micromass culture, and particles were characterized for size, charge, cytocompatibility, and ability to bind and release growth factor. Given the role of sulfation in the high negative charge density characteristic of sulfated GAGs, a biomaterial platform was developed to explore the role of sulfate moieties in growth factor sequestration through the desulfation of CS. These materials were then used to examine the role of sulfation in electrostatic sequestration of the chondrogenic growth factor transforming growth factor-β1 (TGF-β1) and in subsequent chondrogenic differentiation of MSCs. The goal of these studies was to provide additional insight regarding the interactions with CS that alter stem cell microenvironments to drive

chondrogenic differentiation of MSCs. The **central hypothesis** of this research was that engineering of GAG-based materials to control presentation of CS matrix within a variety of 2D and 3D systems would enhance production of chondrocytic ECM in MSCs. The presence of CS matrix would drive chondrogenic differentiation of MSCs by regulating cellular response through morphological cues and through sequestration of chondrogenic TGF-β1 from the culture medium. The role of CS in chondrogenic differentiation of MSCs was explored in the following three specific aims:

Hypothesis I: 2D surfaces modified with cartilaginous GAGs will promote aggregation of bovine MSCs and differentiation toward a cartilaginous phenotype.

Specific Aim I: Determine the effect of sulfated GAGs on cellular aggregation and chondrogenic differentiation of bovine MSCs when cultured on 2D surfaces, in the absence of chondrogenic growth factors.

The cartilaginous chondroitin sulfate proteoglycan aggrecan was previously shown to promote cell aggregation and upregulation of GAG production by rabbit dermal fibroblasts [10]; therefore, aggrecan-coated surfaces were investigated as a potential pre-culture technique to promote the production of chondrogenic ECM prior to cell implantation. The morphology of bovine MSC aggregates was observed on 2D aggrecan-coated surfaces, in the absence of chondrogenic growth factors, and anterior cruciate ligament (ACL) fibroblasts were also cultured on aggrecan to examine their potential for the formation of a more fibrochondrocytic phenotype for regeneration of a fibrocartilaginous ligament-bone insertion. Aggregation promotes high density culture and cell-cell contact, similar to that seen in pre-cartilaginous condensations during

cartilage development, suggesting that aggregation may facilitate increased production of cartilaginous ECM by MSCs and ACL fibroblasts [24]. Gene expression and production of ECM were examined over the course of 2 weeks in MSCs and ACL fibroblasts isolated from 3 different bovine donors, compared to nonadhesive surfaces that promoted cell aggregation in the absence of aggrecan and MSC monolayers on unmodified tissue culture-treated polystyrene surfaces.

Hypothesis II: Chondroitin sulfate-based nanoparticles and microparticles will electrostatically sequester positively charged growth factors.

Specific Aim II: Develop CS-based nanoparticles and microparticles for growth factor delivery and characterize their ability to sequester positively charged growth factors, as a means to direct stem cell differentiation.

Micromass culture is a functional technique in the culture of embryonic stem cell embryoid bodies and chondrogenic MSC pellets; however, dense, multicellular spheroids possess numerous boundaries to diffusion, and growth factor supplementation from the culture medium may result in insufficient or heterogeneous stem cell differentiation. Small particle carriers are valuable tools for controlled delivery to a variety of tissues, and controlled size scale allows for tailored release kinetics, including diffusion rate and degradation properties; therefore, nanospheres and microspheres were fabricated over a range of different size scales from CS materials. CS particles were synthesized and characterized for size, morphology, surface charge, and cytocompatibility. To explore the ability of negatively charged GAGs to electrostatically sequester positively charged proteins, CS microparticles were loaded with the positively charged growth factor TGF-

β1, and release was observed over 5 days, compared to the negatively charged cytokine tumor necrosis factor-α (TNF-α).

Hypothesis III: Desulfation of CS will diminish its affinity to electrostatically sequester TGF-β1, and desulfated chondroitin hydrogels will promote a weaker chondrogenic differentiation response in MSCs, compared to CS.

Hypothesis IIIA: Desulfated chondroitin materials will have a weaker affinity for sequestration of TGF-β1, compared to CS, due to decreased negative charge density.

Specific Aim IIIA: Chemically desulfate CS to produce desulfated chondroitin materials, and determine the effect of sulfation on sequestration and release of TGF-β1.

While previous studies have explored the role of increased GAG sulfation on sequestration of positively charged growth factors [25-26], development of a nonsulfated variant would permit investigation on the role of decreased sulfation, and therefore decreased negative charge density, without modification of the remaining GAG structure. CS was chemically desulfated, and desulfated chondroitin materials were characterized to determine that sulfates were removed from CS without modification of the remaining CS chemical structure. Chondroitin and CS chains were then methacrylated to permit the formation of GAG-containing hydrogels, and modified materials were also examined to determine if chemical modification prevented enzymatic degradation by chondroitinase ABC enzyme. Finally, release of TGF-β1 from CS and chondroitin hydrogels over 7 days and sequestration of soluble TGF-β1 out of solution were measured by enzyme-linked

immunosorbent assay (ELISA) to determine the role of sulfation on interactions with TGF-β1.

Hypothesis IIIB: Sulfation of CS plays an essential role in CS-mediated chondrogenic differentiation, and desulfated chondroitin hydrogels will promote a weaker chondrogenic response in encapsulated human MSCs cultured in the presence of TGF-β1, compared to CS.

Specific Aim IIIB: Determine the effect of sulfation of chondroitin on the chondrogenic differentiation of human MSCs when encapsulated in CS and desulfated chondroitin hydrogels.

While CS-containing hydrogels have been shown to promote the production of chondrogenic ECM in the presence of chondrogenic media [8-9], the role of sulfation and negative charge density in directing chondrogenic differentiation is not currently well understood. The high degree of sulfation of CS carries a highly negative fixed charge density that facilitates a variety of interactions with cartilaginous ECM, signaling molecules, and interstitial fluid; therefore, sulfation is expected to play an essential role in CS-mediated chondrogenic differentiation. To independently examine the roles of TGF-β1 and sulfation of CS, human MSCs were encapsulated in PEG-based hydrogels containing 50% CS or 50% chondroitin by mass or in PEG-only controls and were cultured for 6 weeks in the presence of medium with or without 10 ng/mL TGF-β1. Encapsulated MSCs were analyzed over 42 days for viability, total DNA, gene expression by quantitative reverse transcription polymerase chain reaction (RT-PCR), and ECM production by immunostaining, compared to PEG-only control hydrogels.

1.3 Significance and Scientific Contributions

The studies in this dissertation provide significant insights into the role of sulfated GAGs in altering stem cell microenvironments to control differentiation. A variety of CS-based materials, including 2D surfaces, nano- and microparticles, and bulk hydrogels with varying degrees of sulfation, were developed, and these novel tools provided information on the diverse interactions of sulfated GAGs that may influence differentiation. Culture on 2D aggrecan surfaces provided insight on the (non)adhesive properties of cartilage proteoglycans and the role of cell-cell contact in the production of cartilaginous ECM. GAG-based particles were fabricated over a range of size scales that improve understanding of the electrostatic interactions between sulfated GAGs and positively charged growth factors. Desulfation of CS materials facilitated well-controlled study of the role of sulfation in growth factor sequestration by CS and provided new information on the role of sulfation and growth factor interactions in directing differentiation of MSCs. Controlled presentation of CS through diverse GAG-based biomaterial platforms improved understanding of the various interactions with GAGs that influence stem cell microenvironments, and these principles may be applied to direct differentiation of various multipotent and pluripotent progenitor cells down other non-cartilaginous lineages. The knowledge garnered from these studies, in turn, may advance understanding of the role of GAG matrix during development, maintenance, and repair of cartilaginous tissues.

In addition to advancing the current understanding of stem cell differentiation, development of GAG-based materials to control CS presentation has important

implications for tissue engineering and regenerative medicine. Materials that facilitate careful control of cell-cell and cell-matrix interactions could be developed as pre-culture techniques to "prime" stem cell fate prior to implantation. Novel CS-based particles have potential as delivery vehicles to promote improved growth factor transport and more homogeneous differentiation within a variety of tissue and stem cell environments, and careful control over GAG sulfation could contribute to the development of chemically and spatially controlled constructs for tissue regeneration. This research provides additional insight into the contributions of local chemical and biomolecular environments on many broader applications within the fields of cellular differentiation, tissue engineering, and treatment of orthopaedic injuries. Together these findings provide a framework for future investigations into the use of GAG-based biomaterials for cartilage repair and regeneration, and this research will aid in the development of design principles and new strategies to treat of a wide range of health-based problems.

CHAPTER 2

BACKGROUND

2.1 Cartilage

2.1.1 Articular Cartilage Composition and Function

Cartilage is connective tissue that is found throughout the body to perform a variety of mechanical and structural functions [27-28]. Cartilage can be classified as elastic cartilage, hyaline cartilage, or fibrocartilage [27-29]. Elastic cartilage contains high elastin content and is found in the ears and nose, while fibrocartilage has collagen type I and appears in the menisci, annulus fibrosis of intervertebral discs, temporomandibular joint, as well as the insertions of tendon/ligament into bone [27-29]. Hyaline cartilage includes articular cartilage which covers the ends of long bones and facilitates joint loading and motion [27-28]. The structure of articular cartilage facilitates function by providing compressive strength and allowing distribution of load across the joint [13, 30]. Cartilage also facilitates joint motion by providing a low friction surface for gliding [13, 30]. 65-80% of the total weight of hyaline cartilage is composed of water [13]. This fluid interacts with the extracellular matrix (ECM) to absorb loads, minimize peak pressures on the subchondral bone, and lubricate the joint [13]. In articular cartilage, nutrition and elimination of waste is primarily dependent on diffusion to and from the synovial fluid, so the high water content also facilitates the delivery of nutrients and removal of waste products in the largely avascular, aneural, and alymphatic tissue [28].

ECM plays critical roles in cartilage function and maintenance, including protection of chondrocytes from loading forces, storage of cytokines and growth factors,

regulation of mass transport throughout the tissue, and transduction of extracellular signals to the cells [31-32]. Cartilaginous ECM is primarily composed of collagen (60-70% dry weight), proteoglycans (20-35%), and glycoprotein (5-15%), while chondrocytes (1-5% total volume) are responsible for maintaining and remodeling the ECM network [12-13, 28, 31]. Collagen type II is the predominant collagen (90-95% of total collagen) in hyaline cartilage, and collagen II fibers form the primary fibrillar network that provides the tissue with tensile strength [31]. In lesser amounts, collagen IX forms inter-fibrillar connections, and collagen XI promotes nucleation of fibrils to form a fibrillar mesh with collagen II [13]. Collagen type VI is also present in the pericellular matrix to support chondrocyte attachment and link chondrocytes to the matrix [31]. Collagen type X is only expressed by hypertrophic chondrocytes in the mineralized zone of cartilage to support mineralization and provide structural support [13, 30-31].

Aggrecan is the most prevalent proteoglycan (90% of proteoglycan) found in adult cartilage tissue [31]. Aggrecan is a large 1-3 million Da molecule composed of a core protein with hundreds of sulfated glycosaminoglycan (GAG) side chains [12, 28, 33]. These aggrecan proteoglycans become trapped within the ECM network by aggregating along hyaluronan chains via link proteins to form massive 100-200 million Da structures [12, 28]. The sulfated GAGs in aggrecan, chondroitin sulfate and keratan sulfate, possess negatively charged sulfates and carboxylates, resulting in a highly negative fixed charge density [12-13]. This negative charge density attracts high concentrations of positively charged molecules, while repelling negatively charged molecules, thus increasing the osmolarity of cartilage and creating a Donnan effect [13]. The resulting osmotic pressure causes the tissue to swell and retain water, which is then

constrained from expansion by tension of the collagen network. This fluid-ECM interaction allows the tissue to support high compressive loads while also lubricating joint motion [12, 28]. Compressive loading of the joint causes the internal hydrostatic pressure of the cartilage to increase, and once it exceeds the osmotic pressure of the cartilage, water is pushed out of the ECM, resulting in "weeping" lubrication of the joint [28]. The natural fluid flow that occurs with loading and unloading of the joint also plays an important role to stimulate transport of nutrients and waste within the tissue [28]. In addition to aggrecan proteoglycan, biglycan, decorin, and fibromodulin are small leucine-rich proteoglycans (SLRPs) with shorter protein cores and fewer GAG chains that are found in cartilage tissue. These SLRPs interact with the collagen network to influence fibrillogenesis [31, 34], and have also been shown to bind TGF-β to influence cell signaling and function [34-35].

Glycoproteins, on the other hand, consist primarily of protein with only a few attached monosaccharides or oligosaccharides. Structural glycoproteins in cartilage interact with cellular receptors and regulate adhesion, migration, proliferation, and differentiation of chondrocytes [28]. Annexin V and cartilage oligomeric matrix protein (COMP) anchor chondrocytes to the surrounding matrix [31]. Fibronectin and tenascin have important roles in matrix organization and cell-matrix interactions. Fibronectin possesses binding affinity for fibrin, collagen, and heparin, and cell binding is mediated by integrins [28], while tenascin may bind and inhibit cell attachment to fibronectin [36]. Laminin is also present in cartilage and binds integrins to link chondrocytes to the surrounding ECM [37].

Chondrocytes are the cells that are responsible for synthesizing, degrading, and maintaining the complex ECM network of cartilage through normal ECM turnover. Their intracellular components are directly linked to the ECM through receptors on the cell surface [28]. While individual chondrocytes have high individual metabolic activity, due to their low total volume in cartilage the total metabolic activity of chondrocytes is relative low, allowing chondrocytes to function in low oxygen conditions [13, 27]. Chondrocytes, however, are quite sensitive to toxic influences, and even slight fluctuations in pH from physiological 7.4 can disrupt the highly specialized matrix infrastructure [13, 28]. Chondrocytes have also been shown to alter their expression to respond to differences in loading, including the different forces and mechanics experienced throughout the various zones in cartilage [31].

2.1.2 Cartilage Structure and Organization

In addition to the many diverse ECM components, cartilage contains four depth-dependent zones with different ECM composition and organization in each: the superficial zone, transitional zone, middle (radial) zone, and calcified cartilage zone. These zones act to facilitate load-dependent deformation in each zone [31]. The superficial zone, found at the surface of cartilage, is the thinnest zone and begins at the surface with a thin sheet of fibrils and film of synovial fluid called lamina splendens [13, 31]. Beneath this sheet, flattened ellipsoid cells lie parallel to the joint surface, within a matrix characterized by high collagen production, low proteoglycan content, and the highest water content of the zones [13, 31]. The collagen in the superficial zone is aligned parallel to the surface to provide tensile and shear strength [13, 31]. The transitional zone provides a spatial and structural intermediate between the superficial and middle zones.

In the transitional zone, spheroid shaped cells are present at a lower cell density than the superficial zone; however, larger diameter collagen fibers are randomly oriented and proteoglycan content is higher than the superficial zone [13, 31]. In the middle (radial) zone, spheroidal cells are arranged in a columnar fashion perpendicular to surface, and this zone has the largest diameter collagen fibrils, aligned perpendicular to the joint surface, as well as the highest proteoglycan concentration and lowest water content and cell density [13, 31]. A tidemark divides the middle and calcified zones, which provides a transition from cartilage to the subchondral bone. In the calcified cartilage zone, a small volume of hypertrophic chondrocytes are embedded in calcified matrix. These hypertrophic cells have very low metabolic activity and synthesize collagen X, which helps to provide structural integrity and shock absorbance with subchondral bone [13, 31].

The matrix can also be classified into three compartments, based on their cellular interactions, including the pericellular, territorial, and interterritorial matrix regions. The pericellular matrix (PCM) encompasses a thin rim of matrix in close contact with the cell membrane (~2 μm wide) [13]. The cartilaginous PCM is rich in proteoglycan and non-collagenous proteins, as well as non-fibrillar collagen VI, and links the cell surface to the matrix [13, 31]. The territorial matrix surrounds the pericellular region of individual or clusters of chondrocytes. In this region, collagen fibrils are arranged in a crisscrossing manner, forming a fibrillar basket around the chondrocytes and protecting them from mechanical impact [13, 31]. The interterritorial matrix forms most of the volume of the cartilage matrix, and contains large diameter collagen fibrils, oriented differently by zone, as well as proteoglycan aggregates [13, 31].

2.1.3 Cartilage Development

To form the complex ECM structure of cartilage, the development of cartilage and long bones *in vivo* are uniquely linked. The developmental process begins with migration of undifferentiated mesenchymal cells to areas of bone formation, followed by cellular condensation [24]. As the cells condense, they increase their cell packing and cell density, without an increase in proliferation, resulting in an increase in cell-cell contacts, cell-cell adhesion molecules, and gap junctions [24]. Undifferentiated mesenchymal cells begin the process by producing collagen I, hyaluronan, tenascin, and fibronectin; however, condensation and differentiation prompts a shift in ECM production to produce large quantities of collagen II, IX, XI, Gla protein, aggrecan, and link protein [24]. ECM deposition eventually pushes the cells apart to form chondrocytes that are encased in ECM with a characteristic rounded morphology [13, 27].

Cartilaginous condensation and differentiation appear to be directed by a variety of cell-cell and cell-matrix interactions. Prior to condensation, mesenchymal cells increase their production of hyaluronidase, remodeling the hyaluronan-rich matrix to permit increased cell-cell interaction [24]. Fibronectin is also increased in condensations and may facilitate matrix-driven translocation, while tenascin may act to inhibit cell attachment to fibronectin [24]. Within the condensing mesenchyme, neural-cadherin (N-cadherin) and neural cell adhesion molecule (N-CAM) are highly expressed, forming cell-cell contacts that play a critical role in directing differentiation of the cells toward a chondrocytic phenotype [24]. Additionally, hyaluronan receptor CD44 appears to anchor cells to the aggrecan-rich PCM and direct assembly of the chondrocyte PCM during differentiation [24]. Proteoglycans and GAGs may also act as molecular tethers of

soluble factors that play a role in condensation and differentiation, possibly through modulation of the Wnt signaling pathway [24].

During terminal differentiation, chondrocytes undergo hypertrophy, express collagen X and alkaline phosphatase, decrease expression of collagen II, and begin to mineralize the ECM. During endochondral ossification, hypertrophic cartilage is vascularized by the invasion of blood vessels from the perichondrium. Osteoblasts are transported into the tissue through the blood vessels, and begin replacing cartilage with mineralized bone [5, 24]. Indian hedgehog (Ihh) and parathyroid hormone-related protein (PTHrP) signaling may interact to regulate chondrocyte maturation and hypertrophy. It has been proposed that hypertrophic chondrocytes produce Ihh, which acts on Patched (Ptc) and Gli expressing cells in the perichondrium, adjacent to the pre-hypertrophic zone, inducing the expression of PTHrP. PTHrP then signals back to chondrocytes expressing PTHrP receptor and prevents them from proceeding down the hypertrophic pathway in a negative feedback loop that regulates maturation and hypertrophy [38]. Additional Ihh signaling pathways that are independent of PTHrP have also been identified to examine the role of Ihh signaling in promoting chondrocyte hypertrophy [38-40].

2.2 Cartilage Injury and Repair

2.2.1 Cartilage Pathology and Healing

Cartilage injury may occur from direct blunt trauma, indirect impact loading, or torsional loading of a joint [41]; however, due to the low proliferative ability and metabolic activity of chondrocytes, cartilage has a low potential for natural healing.

Additionally, cartilage does not have direct access to progenitor cells, the dense ECM may impede cell migration, and proteoglycans tend to resist cell adhesion, further undermining the healing process [1, 42-43]. If severe damage is allowed to persist, the tissue may degenerate further and progress into development of osteoarthritis, which is a chronic disease characterized by wear and tear of the cartilage surface [44]. Cartilage damage can generally be classified into three types of injury, depending on the depth of the defect: matrix disruption, partial thickness defects, and full thickness defects. During matrix disruption, the damage to the ECM is relatively mild, and viable chondrocytes are capable of repairing the tissue by increasing their natural synthetic ability [41, 45]. Partial thickness defects describe more severe injuries that disrupt the cartilage surface but do not extend to the subchondral bone. In partial thickness injuries, the surrounding chondrocytes respond by increasing their proliferation, but cellular attempts to naturally repair the tissue cease before the defect is fully healed [41, 45]. Full thickness defects, on the other hand, transverse the entire cartilage thickness and penetrate the subchondral bone. In this case, subchondral blood vessels are disrupted, defects are filled with a fibrin clot, and the classic wound healing response ensues [41, 45]. Unlike partial thickness defects, access to the subchondral bone permits access to a population of progenitor cells from the bone marrow, which can migrate to fill the defect. At the end of the healing process, the fibrin clot is replaced with an intermediate tissue with properties between those of hyaline cartilage and fibrocartilage that is typically less stiff and more permeable than healthy cartilage [27, 41-42].

2.2.2 Clinical Interventions for Cartilage Repair

While a total knee arthroplasty, in which the joint is replaced with artificial surfaces, is the most common treatment for end stage osteoarthritis, the surgery is extremely invasive, requires replacement every 10-15 years, and is not ideal for young patients with active lifestyles [13, 46]. Osteotomy can also relieve severe joint pain by removing part of the bone in order to redistribute load within the joint surface and correct misalignment of the joint [47-48]; however, these techniques are invasive and are typically only employed after less invasion interventions have failed [13, 27, 49].

To encourage the natural healing response, one strategy to treat cartilage defects involves intentionally penetrating the subchondral bone in order to stimulate the bone marrow and promote the formation of a fibrin clot. The impetus for this technique is to disrupt subchondral blood vessels, similar to full thickness defects, to form a fibrin clot and induce bone marrow-derived chondroprogenitors to migrate into the lesion, proliferate, and differentiate. [50-51]. Bone marrow stimulation may also enhance expression of cytokines to promote repair [52]. Techniques include subchondral drilling, abrasion, and microfracture, and are commonly used in conjugation with debridement to remove necrotic tissue from the joint surfaces [53-56]. Marrow stimulation techniques are fairly easy to perform and relatively low cost; however, similar to full thickness healing, the tissue is often replaced with fibrous or fibrocartilaginous tissue, that is more prone to future degeneration [50-51, 56].

In another approach, autografts are taken from non-load bearing regions to replace the injured cartilage tissue. In a mosaicplasty, cylindrical osteochondral plugs are harvested from non-weight bearing regions of the knee and transplanted into the defects.

While this approach replaces the damaged tissue with hyaline cartilage, the gaps between the plugs are often replaced with fibrocartilage, resulting in a lack of integration with the native tissue, as well as increased permeability [57-58]. As with all autografts, donor site morbidity and limited availability of autologous tissue limits this approach, especially for repair of large lesions [51, 59]. Perichondrium and periosteum have also been used as sources for autologous grafts, due to their chondrogenic and osteogenic potential; however, despite some promising results, they are still unable to consistently replace healthy cartilage tissue [13, 60-62].

More recently, autologous chondrocytes have been cultured *in vitro* and reimplanted to promote healing. Autologous chondrocyte implantation (ACI) involves taking a tissue biopsy from a non-weight bearing region of cartilage, enzymatically isolating chondrocytes from the tissue, and expanding the excised chondrocytes for 2-3 weeks *in vitro* [13]. After expansion, the defect is covered with an autologous periosteal flap, and a suspension of expanded chondrocytes is injected underneath the patch into the defect [13]. This approach has yielded some promising results; however, limitations include occasional leakage of transplanted cells, an invasive surgical method, hypertrophy of the periosteum, and the loss of chondrocytic phenotype associated with expansion of chondrocytes in culture [51, 63-65]. In addition, the regenerated cartilage is often more fibrous in nature, possibly due to the low proliferation potential of chondrocytes [66-67]. Overall, there has been large variation and contrasting degrees of success when comparing the current intervention techniques for cartilage repair. Jakobsen et al. evaluated sixty-one clinical cartilage repair studies including a total of 3,987 surgical procedures using microfracture, autologous osteochondral transplantation

(mosaicplasty), autologous periosteal transplantation, and ACI [68]. Large variation was observed between each treatment modality, and no significant differences were found across techniques, suggesting that an improved clinical approach is necessary to properly repair cartilage after injury [51].

2.3 Tissue Engineering and Regenerative Medicine

2.3.1 Tissue Engineering of Cartilage

The limited ability of cartilage to heal and the limitations of surgical repair have introduced the need for tissue engineering strategies for cartilage regeneration. Tissue engineering typically applies a combination of biological, chemical, and engineering principles to regenerate functional tissue. The typical tissue engineering approach uses a 3D scaffold to promote tissue formation, cells that can be expanded and maintained *in vitro*, and the use of differentiation factors to drive tissue development [69]. Bioreactor systems have also been developed to apply mechanical or physical stimulation to the tissue and to facilitate precise control of the extracellular culture environment [70]. Cartilaginous tissues appear to be a strong fit for tissue engineering strategies, because of their relative simplicity as a tissue. Cartilage is largely avascular, lacks nerves, and contains primarily only one cell type; however, barriers to cartilage regeneration include maintaining the phenotype of chondrocytes *in vitro* and recapitulating the complex ECM organization of cartilaginous tissues [5].

2.3.2 Current Tissue Engineering Approaches

2.3.2.1 Cell Sources

An obvious choice of cell type for cartilage tissue engineering is chondrocytes, since chondrocytes are the predominant cell type in cartilaginous tissue and are responsible for maintaining the ECM. Unfortunately, chondrocytes have a limited proliferative capacity *in vitro* and tend to de-differentiate in extended culture, especially in monolayer, becoming increasingly fibrous in nature [71-72]. 3D encapsulation in a variety of materials improves maintenance of chondrocyte phenotype; however, culture in these materials also slows cell growth. Therefore a number of bioreactors, including spinner flasks, microcarrier suspensions, perfusion systems, and rotating-wall bioreactors have been developed for mass culture of chondrocytes to maintain mature phenotype [73-76].

Mesenchymal stem cells (MSCs) are adult stem cells present in the bone marrow that can selectively differentiate into any mesenchymal cell type, including osteoblasts, chondrocytes, adipocytes, myoblasts, and ligament fibroblasts [77-79]. Marrow cells can be noninvasively collected from adult bone marrow by needle biopsy, and MSCs can be expanded *in vitro*, making them a promising cell source for cartilage tissue engineering. MSCs are mostly commonly differentiated in micromass/pellet culture to promote chondrogenesis [6]. High cell density and close cell-cell contact mimics mesenchymal condensation observed during cartilage development [24]. Common markers for chondrogenic differentiation include ECM markers collagen II, aggrecan, and cartilage oligomeric matrix protein (COMP), as well as SOX-9 transcription factor [80-82]. MSC-like progenitor cells, with similar colony forming ability and multilineage potential, have

also been isolated from adipose tissue, periosteum, synovium, skeletal muscle, tendon, trabecular bone, and umbilical cord blood [83-89]; however, the differentiation potential of each population varies. MSC-like cells have also been derived from embryonic stem cells, which are pluripotent cells isolated from the inner cell mass of the blastocyst [90]. Embryonic-derived MSCs were capable of producing cartilage-like tissue *in vitro* and *in vivo* [91].

2.3.2.2 Differentiation Factors

A variety of soluble biochemical factors have been shown to influence MSC differentiation toward a cartilaginous phenotype. Most commonly medium containing transforming growth factor-β (TGF-β) and dexamethasone is established to drive MSCs toward a chondrogenic phenotype [6]. A number of TGF-β superfamily proteins are known play a crucial role in cartilage formation. In particular, TGF-β1, -β2, and -β3 are highly expressed in pre-cartilaginous condensations of the developing mesenchyme [24, 92-93], and all three isoforms possess chondrogenic potential [94-97]. Bone morphogenetic proteins (BMPs) including BMP-2, -4, and -6 have also been shown to enhance chondrogenic differentiation of MSCs [98-99]. BMP-2, especially, has been demonstrated to exhibit an additive differentiation response in MSC pellet cultures when supplemented in combination with TGF-β [99]. Similarly, insulin-like growth factor-1 (IGF-1) has been shown to upregulate expression of chondrocytic markers in MSCs [100-102]. IGF-1 has independent signaling pathways to TGF-β and is capable of promoting a comparable chondrogenic response; however, IGF-1 has also been shown to promote an additive response when supplemented either in combination or sequentially with TGF-β [101-102].

Unfortunately, chondrogenic MSCs cultured under these conditions tend to undergo hypertrophy, as the cells produce collagen X and alkaline phosphatase and undergo terminal differentiation [97, 103-104]. Chondrogenic MSCs also do not entirely suppress expression of collagen I, often resulting in a more fibrous tissue [105]. Basic fibroblast growth factor (bFGF) and PTHrP have been investigated for their ability to delay hypertrophy and maintain chondrocytic phenotype *in vitro* [106-109]. Recently, Gawlitta et al. published that oxygen tension may also play a role in chondrogenic differentiation and hypertrophy. In this study, hypoxic conditions (5% O_2) were capable of delaying hypertrophy of chondrogenic MSC pellets [110].

2.3.2.3 Scaffold Materials

Various natural and synthetic materials have been investigated as scaffolds to support cartilage regeneration. Various synthetic hydrophobic polymers can be extruded or electrospun into micro- or nanofibers, and these fibers can be layered to form porous sponges. The resulting fibrous meshes are mechanically stiff, and MSCs can be seeded on and between the fibers [111]. Hydrolytically degradable materials, including poly(lactic acid) (PLA), poly(glycolic acid) (PGA), their copolymer poly(lactic-co-glycolic acid) (PLGA), and poly(ε-caprolactone) (PCL) have been shown to support chondrogenic differentiation and production of cartilaginous ECM by MSCs [112-116]. As these hydrolytically labile materials degrade, the scaffold can be replaced with ECM deposited by the embedded cells. These materials and their copolymers can also be chemically modified to control degradation rate [117] and modified with bioactive proteins, peptides, and molecules to support bioactivity [118-121].

Due to the high water content of native cartilage, hydrogel materials are popular scaffolds for 3D culture and chondrogenic differentiation of MSCs. Through the crosslinking of polymer chains, hydrogel scaffolds can be swelled in aqueous solution to create highly hydrated network structures [122-123]. Cells can be homogenously encapsulated within polymer networks and cultured for extended periods of time [124]. Encapsulation of MSCs reconstructs a 3D tissue environment in which the cells are immobilized within matrix with a rounded morphology, characteristic of chondrocytes, without the need for cell adhesion [71]. Prior to crosslinking, macromer solution can also be injected to a site of injury and crosslinked *in situ* for minimally invasive surgical techniques and cell delivery [124].

Naturally-derived hydrogels for cartilaginous tissue engineering include collagen types I and II, fibrin, gelatin, and hyaluronan [11, 81, 125-129]. Along with the inherent biocompatibility of natural materials, encapsulated cells and bioactive molecules can actively interact with these materials and remodel the matrix over time. While alginate and agarose are naturally-occurring polysaccharides with application in chondrogenic culture, they are derived from marine algae and are cannot be produced or degraded by mammalian cells [81, 129-133]; therefore, they can be utilized to limit cellular remodeling when desirable. Unfortunately, the inherent complexity of natural scaffolds, along with batch-to-batch variability and limitations on chemical modification, are significant limitations for cartilage regeneration [134].

While synthetic hydrogels do not possess inherent bioactivity, these materials can be precisely engineered to exhibit specific chemical and mechanical properties, and bioactive functionality must be expressly designed into the system [135]. Poly(ethylene

glycol) (PEG) is a common synthetic polymer used to support chondrogenic differentiation of MSCs [136-137]. By engineering bioactive moieties into the polymer network in a functionally, spatially, and temporally tailored fashion, one can study specific cell stimuli and responses in a discrete and controlled way. Design of PEG-based hydrogels for chondrogenic differentiation of MSC will be discussed in further detail in Section 2.3.3.

2.3.2.4 Physical Stimuli

Due to the established importance of mechanical forces in the development, maintenance, and remodeling of orthopaedic tissues, mechanical loading has been investigated as a technique to stimulate cartilage tissue formation. Cyclic, compressive loading has been shown to increase production of cartilage specific ECM, including collagen II and aggrecan, in MSCs encapsulated in a variety of hydrogel materials [125, 138-141]. Similarly, application of cyclic, hydrostatic pressure increased collagen and proteoglycan production in encapsulated chondrogenic MSCs [142], as well as in scaffold-free MSC aggregates [143]. Huang et al. found that cyclic compression improved the matrix distribution and increased mechanical stiffness of chondrogenic MSC-laden agarose scaffolds after long-term culture for 42 days [144]. In studies by Kisiday et al., proteoglycan content was found to increase in agarose gels in response to loading after 15 days, even in the absence of chondrogenic cytokines [145].

Other physical stimuli, including cell shape and the stiffness of the surrounding matrix, interact with chemical, molecular, and genetic factors to regulate stem cell fate [146]. McBeath et al. demonstrated that cell shape and area regulated osteogenic and adipogenic differentiation in MSCs [147]. Small cell areas and rounded shape dictated a

more adipogenic fate, while large areas and spreading promoted an osteogenic phenotype in identical mixed media, via RhoA/Rho kinase (ROCK) regulation of cytoskeletal tension. Kilian et al. followed up this finding by showing that cell shapes that enabled higher acto-myosin contractility, even under identical cell areas, promoted osteogenic differentiation over adipogenic differentiation [148]. These studies implicated a relationship between cytoskeletal organization and differentiation lineage.

In chondrocyte culture or chondrogenic differentiation of MSCs, it has been well established that micromass culture and encapsulation, which maintain a rounded cell shape, are beneficial to maintaining or promoting a chondrocytic phenotype, compared to monolayer culture, suggesting that cell shape, cytoskeletal tension, and matrix interactions may also play important roles in chondrogenesis [149]. Gao et al. demonstrated that in the presence of TGF-β3 a rounded cell shape promoted chondrogenic differentiation of MSCs on 2D surfaces, while spreading promoted a myogenic smooth muscle cell phenotype [150]. In addition, while RhoA exhibited little change in activity, another GTPase Rac1 inhibited chondrogenesis, upregulated expression of N-cadherin, and induced smooth muscle differentiation. In an examination of nucleus shape, McBride and Knothe Tate also demonstrated that rounder nuclei were associated with greater expression of chondrogenic markers by C3H/10T1/2 stem cells on 2D surfaces [151-152]. A series of studies on 2D surfaces demonstrated that chemical disruption of cytoskeletal tension and inhibition of RhoA/ROCK signaling promoted expression of chondrogenic markers by stem cells [153-157]; however, RhoA/ROCK and Rac1 signaling has been found to be vastly different in 3D micromass culture. Woods and Beier observed that in 3D micromass cultures of primary mouse mesenchymal limb bud

cells, RhoA/ROCK inhibition instead decreased expression of chondrogenic markers [158]. Furthermore, Woods et al. showed that Rac1 promoted chondrogenic differentiation in micromass culture through enhanced N-cadherin expression [159]. These studies suggest that while cytoskeletal tension and RhoA-ROCK and Rac1 signaling may play important roles in chondrogenic differentiation, significant differences occur between 2D and 3D culture, possibly due to inherent differences in cell-cell interactions, cell-matrix interactions, and cell shape.

Along with geometry, matrix stiffness also influences stem cell lineage. In a seminal paper by Engler et al., stiff poly(acrylamide) substrates (Young's modulus 25-40 kPa) directed MSCs toward a more osteogenic phenotype, compared to moderate stiffness (8-17 kPa) for myogenic, and soft (0.1-1 kPa) for neurogenic differentiation. As formation of focal adhesions increased on stiffer substrates, nonmuscle myosin II was required for matrix stiffness-based direction of MSC lineage [160]. For culture of chondrocytes, it appears that relatively soft substrates which limit cytoskeletal tension encourage chondrogenic phenotype. Schuh et al. observed that softer poly(acrylamide) substrates (Young's modulus 4 kPa) promoted greater production of collagen II and aggrecan by chondrocytes, along with decreased proliferation and actin organization, compared to stiffer substrates in 2D culture [161]. In addition, Park et al. determined that stiffness regulated MSC response to TGF-β1, promoting expression of chondrogenic markers on soft collagen I and poly(acrylamide) substrates and myogenic phenotype on stiffer substrates [162]. Overall, these studies have established that cell shape and matrix stiffness appear to regulate cell phenotype through cell-matrix interactions and cytoskeletal organization and tension in 2D. In 3D culture, however, these effects are

more difficult to discern, because cell shape and matrix stiffness are also highly dependent on the material properties of the scaffold, including crosslinking density, porosity, and resulting transport properties. In 3D, local ECM organization also regulates cellular interactions with the matrix. While Schuh et al. found that softer agarose constructs supported greater GAG production by encapsulated chondrocytes, softer constructs also supported formation of larger cell clusters and a different local ECM environment than stiffer gels [163].

2.3.3 PEG-Based Hydrogels for Cartilage Tissue Engineering

Poly(ethylene glycol) (PEG) is a nonadhesive synthetic material that is highly resistant to protein adsorption, making it an attractive material for cartilage tissue engineering [164-166]. These non-fouling properties enable PEG-based materials to act as a "blank slate" upon which additional bioactive functionality can be specifically tailored into the hydrogel formulation. PEG hydrogels have been extensively investigated for bone, cartilage, vascular, and neural engineering [136, 167-173]. To crosslink and form PEG-based hydrogels, PEG is most often chemically modified to include acrylate groups. The resulting PEG-diacrylate (PEG-DA) or -dimethacrylate (PEG-DMA) can be crosslinked via free radical initiation, where polymerization occurs through a chain-growth mechanism that involves chain transfer of the radical to a free double bond on another acrylate group [174]. Radical initiators include the thermally responsive tandem ammonium persulfate (APS) and tetramethylethylenediamine (TEMED), as well as the photosensitive Irgacure 2959 [175-178]. Alternative step-growth crosslinking mechanisms, including Michael-type addition and "click" chemistry, have been utilized for crosslinking of PEG-based materials, and these techniques can also be used together

with chain-growth initiators for sequential or mixed-mode crosslinking reactions [174, 179-182].

PEG's mechanical and biochemical properties can be easily modified for a variety of tissue engineering applications [167, 183-184]. Hydrolytically labile components have been added into PEG networks to control degradation [169, 185], and enzymatically degradable peptides have also been incorporated within PEG hydrogels for cell-mediated degradation [186-187]. More recently, novel photodegradable groups have been investigated as a means to degrade PEG networks on demand in the presence of ultraviolet (UV) light [188]. Functional peptides like the adhesive peptide arginine-glycine-aspartic acid (RGD) and growth factors including TGF-β, bFGF, and vascular endothelial growth factor (VEGF) have been tethered into PEG networks to modulate cell response [171, 189-191]. Additionally, PEG hydrogels are capable of micropatterning to create well-defined physical and biochemical features via photolithography [192-197].

Oligo(poly(ethylene glycol) fumarate) (OPF) is a PEG-based, hydrolytically degradable hydrogel material that supports various *in vivo* and *in vitro* tissue engineering applications, including chondrogenic and osteogenic differentiation of MSCs [175, 198-202]. OPF's swelling, degradation, and mechanical properties can be easily controlled by altering the molecular weight of its initial PEG chains [45, 202]. Using PEG-DA as a crosslinker, OPF/PEG-DA scaffolds have been modified with functional peptides, including RGD [201], and OPF hydrogels have also been utilized as a delivery vehicle for a variety of growth factors [203-205]. OPF is a versatile and biocompatible hydrogel biomaterial with potential for use in the regeneration of a variety of tissues.

For these reasons, PEG and OPF-based materials have been used in controlling chondrogenic differentiation of MSCs [136, 199, 206-208]. PEG-DA hydrogels encourage increased production of cartilaginous matrix, over monolayer culture, in chondrogenic media [136], and the network structure and mesh size can be precisely controlled to influence differentiation [207, 209]. Many forms of biofunctionality have also been designed into the hydrogel system to promote enhanced bioactivity, including various ECM molecules and biological mimics. Most commonly the adhesive peptide RGD has been incorporated into PEG-based hydrogels to promote adhesion and MSC viability [210-211]. The role of RGD, an integrin binding peptide located in the III_{10} repeat of fibronectin, in chondrogenic differentiation of MSCs has yet to be fully elucidated [212]. While fibronectin is expressed in pre-chondrogenic condensations during cartilage development, RGD incorporation into PEG hydrogels has been shown to increased differentiation of chondrogenic MSCs [211], while RGD inhibited chondrogenesis in agarose gels [213]. Hypothesizing that RGD may promote early chondrogenic differentiation of MSCs, Salinas et al. used a matrix metalloproteinase (MMP)-sensitive peptide to achieve temporal presentation of RGD to cells [137]. As the cells underwent early differentiation in the presence of RGD, the RGD was enzymatically cleaved and released from the network by cell-secreted MMP-13. After 21 days, chondrogenic MSCs encapsulated with cleavable RGD moieties exhibited significantly greater production of cartilaginous ECM than those with uncleaveable RGD, suggesting that both spatial and temporal presentation of biological cues may be necessary for regeneration. Additional work has incorporated collagen types I and II, collagen mimetic peptides GFOGER and $(POG)_7$, decorin sequence KLER, and GAGs hyaluronan and

chondroitin sulfate to examine their roles in chondrogenic differentiation [7-9, 214-216]. Together, the research presented here strongly suggests that ECM interactions play a critical role in directing MSCs down a chondrogenic lineage for cartilage repair and regeneration. Specifically, chondroitin sulfate (CS) is a cartilaginous GAG that plays important structural and biological roles in cartilaginous tissues; however, the role of CS in chondrogenic differentiation and the interactions between CS and MSCs are not well understood.

2.4 Chondroitin Sulfate Interactions to Promote Chondrogenic Differentiation

2.4.1 Role of CS Proteoglycans in Chondrogenesis

Perlecan and versican are proteoglycans that play important roles in tissue development. CS proteoglycan versican influences embryonic cell adhesion, migration, proliferation, and ECM assembly in a variety of tissues [217], and versican exhibits increased expression during mesenchymal condensation in early cartilage development [14, 218-219]. Versican may act as an anti-adhesion molecule during the initiation of matrix assembly, and versican expression ceases after deposition of aggrecan in the ECM [220]. Perlecan is also essential for proper cartilage development [221-223]. Perlecan is expressed within cartilaginous condensations after expression of collagen II and aggrecan, and remains in the adult pericellular matrix where it interacts with other ECM molecules including laminin and fibronectin [224]. Perlecan containing both heparan sulfate and CS has been implicated in bFGF signaling to regulate chondrocyte proliferation during endochondral ossification in the growth plate [15, 223, 225-226]. Heparan sulfate chains bind bFGF in perlecan, sequestering it from FGF receptors, while

CS chains on perlecan appear to block FGF receptor binding [15]. Additionally, aggrecan also plays a critical role in skeletal formation and patterning, ECM production, and collagen fibrillogenesis [33, 227]. The major influence of CS proteoglycans in chondrogenesis suggests that CS GAGs may play an important role in directing chondrogenic differentiation.

Furthermore, chondroitin sulfate production and patterning play critical roles in the development of cartilage and the skeleton, as mutations affecting production and patterning of CS are largely not viable. A recent study by Wilson et al. demonstrated that chondroitin sulfate synthase 1 (Chsy1), which is one member of a family of enzymes responsible for extension of chondroitin sulfate chains, is required for proper bone development and joint/digit patterning in mice [16]. Chsy1 mutations resulted in chondrodysplasia, decreased bone density, and abnormal digit patterning, possibly resulting from abnormal sulfation of CS. Similarly, Watanabe et al. showed that chondroitin sulfate N-acetylgalactosaminyltransferase 1 (CSGalNAcT1), another enzyme responsible for the initiation and elongation of CS chains, is required for normal cartilage development, as knockout in mice resulted in 50% decrease in chondroitin sulfate production and significantly thinner growth plate cartilage with disorganized arrangement of collagen fibers [17]. Kluppel et al. also showed that chondroitin-4-sulfotransferase 1 (C4st1) expression, which is responsible for transfer of sulfate groups onto the 4-O position of chondroitin, was required for development and growth factor signaling during cartilage morphogenesis in mice [18]. C4st1 mutations demonstrated underexpression and mislocalization of CS in the growth plate, resulting in disorganized ECM and abnormal chondrocyte orientation. Defective CS balance in C4st1 mutants also resulted

in upregulation of TGF-β3 signaling, and downregulation of BMP, suggesting a role in growth factor signaling. Interestingly, while deletion of chondroitin-6-sulfotransferase 1 (C6st1), which transfers sulfates onto the 6-O position, did not affect skeletal development in mice, mutations in C6st1 in humans are associated with chondrodysplasia [228].

CS structure is regulated during cartilage differentiation and development, as sulfation patterns may regulate the affinity of CS to bind growth factors [229-230], and CS sulfation and structure continues to change through maturation and into adulthood. In human articular cartilage, CS is primarily monosulfated on either the 4- or 6-carbon of N-acetylgalactoseamine; however, CS structure and patterning in cartilage continues to change through adulthood. As the tissue matures and growth cartilage is replaced by adult cartilage, the ratio of 6-sulfated CS to 4-sulfated CS increases from ~0.77 to ~23, indicating a shift in the sulfation balance by adulthood [20, 231]. Additionally, sulfation pattern varies by zone, as deeper zones of cartilage contain more 4-sulfated CS than superficial zones [20]. In addition to sulfation pattern, the average CS chain length also decreases over time. The average chain size decreases from ~32 kDa in fetal cartilage to ~20 kDa in postnatal cartilage, then down to ~8 kDa by skeletal maturity [231]. The change in structure and sulfation pattern from fetal cartilage to adulthood suggests that CS may actively regulate its structure over time to facilitate specific interactions and signaling mechanisms within the maturing tissue.

2.4.2 Chondroitin Sulfate Hydrogels for Tissue Engineering

Recent work has investigated the ability of ECM molecules to direct stem cell differentiation down specific lineages, including GAGs for chondrogenic differentiation.

Culture on aggrecan-coated surfaces was shown to promote cell aggregation and production of GAG and collagen II in rabbit dermal fibroblasts, following pretreatment with IGF-1 [10]. Studies have also shown that encapsulation of chondrocytes and mesenchymal stem cells within hyaluronan-based hydrogels increased production of cartilaginous ECM [11, 232-236], suggesting that cells interact with GAGs and that CS hydrogels may be a useful tool in promoting chondrogenic differentiation of MSCs.

Various research groups have developed CS-containing hydrogels as tool to study 3D interactions with cells, most often in combination with PEG. The Elisseeff research group has developed several forms of crosslinkable CS-based tissue adhesives to promote repair and regeneration. By chemically modifying CS with methacrylates, aldehydes, or N-hydroxysuccinimde, CS adhesives were crosslinked to themselves, PEG-DA, or with the amine groups present in proteins. These adhesives have demonstrated the ability to bond articular cartilage and cornea tissue with good biocompatibility [237-241].

CS proteoglycans also play important roles in directing growth in neural systems, so Conovaloff and Panitch used CS/PEG hydrogels to study neurite growth for neural regeneration applications [242]. Chondroitin-6-sulfate was shown to bind NGF, BDNF, and NT-3 cytokines with high affinity, compared to heparin, by capillary electrophoresis, while hyaluronan bound NGF with higher affinity than CS. Culture of E8 chick dorsal root ganglia in the presence of NGF demonstrated more robust neurite outgrowth in 2% CS/98% PEG-DA hydrogels, compared to 2% hyaluronan/98% PEG-DA after 3 days, suggesting CS acts as a better scaffold than hyaluronan despite weaker affinity for NGF, possibly due to inhibition of growth by HA. While this study suggested that CS/PEG hydrogels support neurite growth, this result contrasts other studies that have shown that

CS and various CS proteoglycans inhibited neurite growth in glial scar and that inhibition is dependent on the degree of sulfation [243-247]; however, differences in sulfation pattern, CS presentation without the proteoglycan core protein, and growth factor supplementation may account for these differences.

As a prominent GAG in cartilaginous tissues, CS/PEG hydrogels have also been developed for 3D culture of chondrocytes. Bryant et al. crosslinked varying amounts of methacrylated chondroitin-4-sulfate into PEG hydrogels to alter the macroscopic properties of the hydrogels. 40% CS/60% PEG hydrogels were shown to promote greater production of cartilaginous ECM by chondrocytes, than CS-only gels, suggesting that the addition of PEG-DA was necessary to support ECM deposition in these CS-containing hydrogels [248]. To compare CS hydrogels to other ECM components, Hwang et al. showed that chondrocytes encapsulated in CS/PEG hydrogels supported greater accumulation of cartilaginous matrix by superficial and deep zone chondrocytes than gels with collagen type I or hyaluronan, suggesting that CS possesses tissue specific benefits for maintaining chondrocytic phenotype [249]. Furthermore, to investigate the role of mechanical loading in CS/PEG hydrogels, Villanueva et al. demonstrated that 20% CS/80% PEG hydrogels simulated greater production of GAG and collagen by bovine chondrocytes under dynamic compression, compared to loaded PEG gels [21]. These studies suggest that CS/PEG hydrogels interact with chondrocytes in 3D hydrogels and may support the production of cartilaginous ECM.

Sulfated GAGs generate osmotic swelling pressure in cartilaginous tissues as a result of the associated high negative charge density [20]. Mobile positive ions in solution rush into the tissue to shield the negatively charged GAGs, and the resulting osmotic

pressure provides the tissue with enhanced ability to withstand compressive loads [20]. Osmotic swelling pressure also facilitates streaming potential during loading, in which the mobile positive ions are forced in and out of the matrix resulting in an electric potential [21, 250]. Sulfation, osmotic swelling, and streaming potential appear to influence ECM production in chondrocytes [21]; however, its role in differentiation of MSCs remains unclear.

To examine the role of CS interactions in differentiation of MSCs, Varghese et al. examined the chondrogenic differentiation of MSCs in CS/PEG hydrogels. Goat bone marrow MSCs aggregated in 50% CS/50% PEG-DA hydrogels and upregulated production of chondrocytic markers in chondrogenic media, compared to PEG-only controls [8]. Cadherin11 expression was also temporally upregulated at early stages of aggregation, suggesting that increased cell-cell contact in CS materials may encourage a more chondrogenic phenotype. Additional analysis by Nguyen et al. suggested that controlled presentation of the CS matrix could direct differentiation toward the different cartilaginous zones [9]. 50% CS/50% PEG-DA hydrogels promoted production of high levels of collagen II and proteoglycan similar to that found in transitional zone of cartilage by D1 mouse bone marrow stem cells. Meanwhile, incorporation of MMP-cleavable peptide sequences into the CS/PEG hydrogel promoted a more superficial zone-like ECM with low proteoglycan, and hyaluronan/PEG produced proteoglycan production with lower collagen II similar to the middle (radial) zone of cartilage. CS-only hydrogels, on the other hand, produced higher levels of collagen X, reminiscent of the calcified zone of cartilage.

Of these studies investigating CS hydrogels, few studies have investigated the effect of CS on human MSCs. Chen et al. observed that 2D surfaces with crosslinked chondroitin-6-sulfate supported greater differentiation of human MSCs than MSCs cultured with CS and CS oligosaccharide present in the culture medium [251]. Steinmetz and Bryant also examined the effect of cyclic compressive loading on the chondrogenic differentiation of human MSC in CS/PEG hydrogels [252]. While the effects of CS in 20% CS/80% PEG-DA hydrogels were not as apparent after 14 days as previously reported in animal-derived MSCs with little ECM accumulation, the results suggested that CS may slow the terminal differentiation process in response to loading, as observed by downregulation of collagen X production and Runx2 expression.

2.4.3 Growth Factor Sequestration by Chondroitin Sulfate

Charged GAGs, primarily associated with proteoglycans *in vivo*, play a major role in sequestration of growth factors, stabilizing growth factors and preventing denaturation [22, 253-254]. Negatively charged GAGs, including heparin, heparan sulfate, and CS, bind positively charged growth factors, such as bFGF, IGF, VEGF, platelet-derived growth factor (PDGF), and TGF-β, by electrostatic interactions [255-264]. GAGs electrostatically complex with growth factors due to their highly negative charge density, and increased degree of sulfation appears to correlate with stronger electrostatic interaction. Heparin binds with bFGF, IGF, VEGF, and glial cell line-derived neurotrophic factor (GDNF) in a sulfation-dependent manner and with special importance of 2-O-sulfation for binding [265-272]. While a majority of studies have focused on heparin and heparan sulfate, due to their relatively higher charge densities, CS has also been shown to bind to various growth factors *in vitro* [22, 261-264], indicating that

sequestration of chondrogenic growth factors by CS hydrogels may be a promising strategy to enhance chondrogenic differentiation of MSCs.

Deepa et al. found that CS-E, which is 4,6-disulfated, bound directly to a variety of heparin-binding growth factors including midkine (MK), pleiotrophin (PTN), heparin-binding epidermal growth factor-like growth factor (HB-EGF), FGF-2, FGF-10, FGF-16, and FGF-18. [261]. Binding affinity to CS-E was greater than or comparable to that observed in heparin, and growth factors bound CS-E in a specific and concentration dependent manner. Additionally, Hintze et al. demonstrated that chemical sulfation of CS and hyaluronan enhanced affinity for TGF-β1 and BMP-4 [25, 273]. Electrostatic binding was enhanced as degree of sulfation was increased from 0 to 3 sulfates per disaccharide, and interaction was inhibited by increasing the salt concentration of the buffer and through competitive inhibition by soluble GAGs, indicating that CS possesses sulfate-dependent affinity for chondrogenic growth factors of the TGF-β superfamily.

In an examination to determine the binding mechanism of sulfated GAGS to TGF-β, Lyon et al. demonstrated that heparin and highly sulfated liver heparan sulfate electrostatically bound TGF-β1 and TGF-β2 by affinity chromatography, while TGF-β3 isoform did not [274]. The bound fraction was eluted with ≥0.5 M NaCl. These highly sulfated GAGs also potentiated TGF-β1 activity in mink lung epithelial cells, while a low sulfated mucosal heparan sulfate did not. TGF-β1 and TGF-β2 are reported to have isoelectric points (pI) of approximately 9.5 and 8.5, respectively [275-276], while TGF-β3 has a lower pI of 6.8, suggesting that it is actually negatively charged at physiological pH and unable to electrostatically complex with sulfated GAGs [275].

Based on analysis of the TGF-β1 crystal structure (Figure 2.1a) and amino acid differences with TGF-β3, Lyon et al. predicted that TGF-β1 interacts with heparin via basic arginine and lysine residues at positions 25, 26, 31, and 37 and a histidine at 34 at the tip of first β-strand loop in TGF-β1, along with Arg/Lys at position 94 on the adjacent tip of another β-strand loop [272, 274]. In TGF-β3, the basic amino acid at position 26 is replaced with a neutral amino acid, suggesting that position 26 is critical for binding. While the proposed binding sites form two distinct sites at opposite poles but on the same face in the TGF-β dimer, they could be potentially be engaged by a single heparin chain at two points approximately 60 Å (or ~7 disaccharides) apart, as well as by two separate heparin chains (Figure 2.1b). The proposed binding site is also in a similar location, at the tips of the β-strand loops, to where TGF-β binds its receptors; however, little competition has been reported and in many cases heparin appears to potentiate the effect [272].

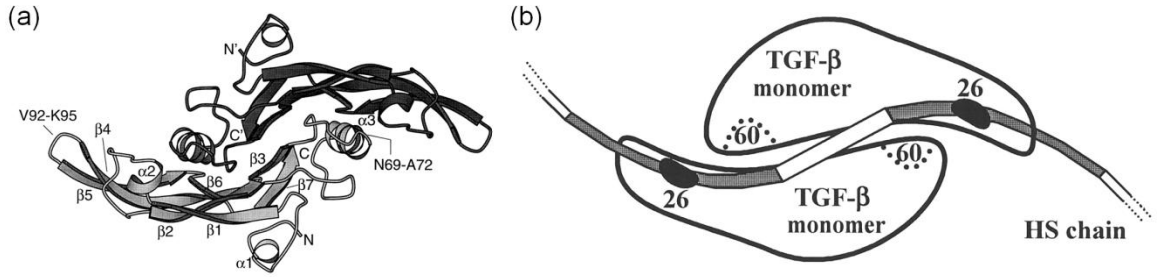

Figure 2.1. GAG binding site in TGF-β1. Crystal structure of TGF-β1 as determined by Hinck et al. [277] (b) Diagram of heparin/heparan sulfate binding sites as proposed by Lyon et al. [274]

Sulfation-dependent GAG/TGF-β1 interactions may play important roles in TGF-β1 signaling, feedback to subsequently regulate GAG sulfation, as well as disease. Merceron et al. reported that sulfated polysaccharides may potentiate TGF-β1 signaling for chondrogenic differentiation [278]. The oversulfated marine polysaccharide GY785 DRS possessed greater binding affinity to TGF-β1 than its less sulfated counterpart

GY785 DR, as determined by surface plasmon resonance (SPR). Additionally, human adipose-derived MSCs produced greater GAG and collagen when cultured with GY785 DRS in the medium, and ERK1/2 phosphorylation and MAPK signaling suggested that GY785 DRS potentiated TGF-β1 signaling to promote chondrogenesis and that this interaction was dependent on the sulfation of the polysaccharide. Additionally, Zanni et al. reported that TGF-β1 signaling in cartilage explants resulted in reduction in chondroitin-4-sulfation and an increase in nonsulfated disaccharides, suggesting that a potential feedback loop may exist between sulfate-dependent GAG/TGF-β signaling and subsequent CS sulfation patterning via altered activity or synthesis of sulfotransferases [279]. Kim et al. also demonstrated that abnormal balance of 4- or 6-sulfation pattern and subsequent growth factor affinity may play a role in disease [280]. Decorin from the tendons of horses with equine systemic proteoglycan accumulation (ESPA) possessed enhanced 6-sulfation, as well as a decrease in 4- to 6-sulfation ratio, and that ESPA decorin exhibited diminished TGF-β1 binding *in vitro*. These finding may have relation to Ehlers-Danlos syndrome, a genetic disorder characterized by abnormal collagen synthesis in connect tissue, which has been linked to a mutation in galactosyl transferase I gene.

Electrostatic interactions between CS and growth factors have been exploited for delivery and controlled release. Park et al. developed a porous chitosan-CS sponge for controlled sequestration and release of PDGF-BB [262]. Release kinetics were dependent on CS content in the sponge composition, up to 40% CS, and PDGF-BB-loaded sponges were shown to promote migration and proliferation of rat osteoblasts *in vitro*, compared to chitosan-only scaffolds. Mullen et al. also designed collagen-CS materials for gradual,

sustained release of the chondrogenic growth factor IGF-1 over 14 days [264]. IGF-1 adsorption was characterized over time and as a function of loading concentration, and binding also varied with buffer ionic strength, indicating electrostatic interaction. Released IGF-1 retained bioactivity and promoted proteoglycan production of seeded human osteoarthritic chondrocytes *in vitro*, compared to unloaded constructs.

Collectively , these studies suggest that CS sequesters and regulates important interactions with growth factors, including the chondrogenic growth factor TGF-β1, and that the degree of sulfation may play a role in binding affinity. Further examination of the role of CS in TGF-β1 signaling and the cellular interactions that promote chondrogenic differentiation of MSCs may aid in the development of novel tissue engineering strategies to promote cartilage repair and regeneration.

CHAPTER 3

AGGREGATION OF BOVINE MARROW STROMAL CELLS AND ANTERIOR CRUCIATE LIGAMENT FIBROBLASTS PROMOTES AGGRECAN PRODUCTION[1]

3.1 Introduction

Several recent studies have demonstrated that adult dermal fibroblasts may possess multilineage potential and specifically the ability to produce cartilaginous extracellular matrix (ECM) in controlled culture conditions [10, 281-284]. Previous work has also investigated the ability of ECM molecules to direct cell differentiation and promote ECM production. Aggrecan is a cartilaginous ECM proteoglycan, and culture on aggrecan-coated surfaces has been shown to promote cell aggregation and production of glycosaminoglycan (GAG) and collagen II in RAB-9 adult rabbit dermal fibroblasts pre-treated with insulin-like growth factor-1 (IGF-1) [10]. These results suggest that adult dermal fibroblasts maintain the ability to differentiate/transdifferentiate and produce cartilaginous ECM on aggrecan-coated surfaces, and that aggrecan-modified materials could potentially be used to promote production of chondrocytic ECM.

Production of cartilaginous ECM by a fibroblastic cell type may possess particular application for regeneration of fibrocartilaginous tissues. Fibrocartilage appears in the menisci, annulus fibrosis of intervertebral discs, and temporomandibular joint, and

[1] Portions of this chapter were adapted from Lim JJ, Scott L, Jr., Temenoff JS. Aggregation of bovine anterior cruciate ligament fibroblasts or marrow stromal cells promotes aggrecan production. Biotechnol Bioeng. 2011;108(1):151-62.

contains a fibrous collagen I matrix along with cartilaginous ECM, including collagen II and aggrecan [27-29]. Fibrocartilaginous tissues also mediate direct insertions of tendon/ligament into bone [285-286], as fibrocartilaginous regions permit a gradual increase in stiffness from the fibrous tendon/ligament to the highly mineralized bone, thus preventing the formation of stress concentrations in the tissue and decreasing the risk of failure [287-288]. Production of chondrocytic ECM in fibroblastic cell types may possess unique application to tendon/ligament insertions, because fibroblasts are the predominant cell type in tendons and ligaments [69, 78, 289]; therefore the production of cartilaginous ECM in ligament fibroblasts may present a novel approach to regenerate fibrocartilaginous interfaces for ligament repair.

The anterior cruciate ligament (ACL) of knee is one of the most commonly injured ligaments with 250,000 ACL ruptures each year in the United States, resulting in over 100,000 ACL reconstructions annually [290]. In ACL reconstruction surgery, graft tissue is drawn across the knee to replace the ligament, and the graft is commonly held in place within bone tunnels using interference screws [287, 291]. During healing, collagenous fibers and mineralized tissue formation in the bone tunnels help anchor the graft to the bone; however, these fixation methods are unable to physiologically replicate the native fibrocartilaginous insertion points that are present at many interfaces of ligament and bone [287]. In addition, secondary surgeries for harvest of autograft tissue often results in significant donor site morbidity [78, 291], and deficiencies in fixation strength and graft positioning may lead to secondary pathologies, such as osteoarthritis [287, 292].

The limitations of surgical repair have introduced a need for tissue engineering strategies for ligament regeneration. A potential approach would be to develop a tissue-engineered bone-ligament-bone graft that possesses a fibrous ligament midsubstance with the mechanical strength to restore function to the injured joint, as well as fibrocartilaginous insertions and osseous tissue for improved fixation of the graft to bone. In order to function similarly to native ligaments, the fibrous ligament body would possess structurally organized collagen type I fibers aligned in parallel to maximize tensile strength, along with sparsely distributed fibroblasts to maintain the ECM [293-294]. The fibrocartilaginous insertions, on the other hand, would contain chondrocyte-like cells within a matrix of collagen I, collagen II, aggrecan, and some collagen X [287-288, 295-296].

To engineer such tissue interfaces, methods to produce zonally-varied ECM similar to that found in the ligament-bone insertion point are needed. In prior work, fibrous poly(lactic-co-glycolic acid) (PLGA) has been combined with bioactive glass in a composite scaffold to support both ligament and bone development [297-298], and these scaffolds have been used as a multiphasic co-culture system for ligament fibroblasts, chondrocytes, and osteoblasts [298-299]. Additionally, gradients of retroviral transfection with RUNX2/CBFA1 osteogenic transcription factor in fibroblasts have been utilized to produce graded distributions of mineral deposition for transitional tissue interfaces [300]. While the experiments detailed above have explored the culture of multiple cell types or biomaterial-based induction of phenotypic changes to produce the ECM gradient required for these applications, few studies have examined the possibility of altering pre-culture techniques to encourage one cell type to produce the range of phenotypes needed for this

complex tissue structure. Therefore, the focus of this set of experiments was to examine the potential for formation of cartilaginous ECM through altering cell pre-culture parameters for ACL fibroblasts. This was then compared with the response under the same culture conditions for bone marrow stromal cells (BMSCs), which are known to differentiate into various mesenchymal cell types, including osteoblasts, chondrocytes, adipocytes, myoblasts, and tendon/ligament fibroblasts [77-79].

Specifically, the purpose of this study was to investigate the role of aggrecan in chondrogenic differentiation of bovine ACL fibroblasts and BMSCs. We hypothesized that cells would aggregate on aggrecan-coated surfaces, and that aggrecan-coated surfaces would promote the expression and production of cartilaginous ECM by both ACL fibroblasts and BMSCs. Because cells were found to aggregate on aggrecan-coated surfaces, another aggrecan-free surface treatment that induced aggregation was used as a control to determine whether the resulting phenotypic differences were aggrecan-dependent. In particular, cell morphology, gene expression, and ECM production were examined over 14 days for bovine ACL fibroblasts and BMSCs cultured on uncoated tissue culture-treated polystyrene (TCPS), aggrecan-coated TCPS, and nonadhesive culture plates in order to determine how the culture surface affected phenotypic responses for both cell types.

3.2 Materials and Methods

3.2.1 Bovine ACL Fibroblast and BMSC Harvest

Bovine ACL fibroblasts were harvested according to a previously described protocol [174]. The femur and tibia of an immature calf (Research 87, Marlborough, MA)

were isolated, and the ACL was sterilely removed and cut into ~1 mm^3 pieces. Ligament tissue was then digested in 0.4% (w/v) collagenase type II (Invitrogen, Carlsbad, CA) solution in high-glucose DMEM (Mediatech, Manassas, VA), 1% penicillin/streptomycin/neomycin (Invitrogen), 1% kanamycin (Mediatech), 0.1% gentamicin (Mediatech), and 0.1% Fungizone (Invitrogen) for 24 hr. The digested cell solution was filtered through a cell strainer with 80 µm mesh (Small Parts, Miramar, FL), collagenase was removed by centrifugation, and cells were resuspended in "fibroblast medium" containing high-glucose DMEM, 10% fetal bovine serum (FBS; Thermo Scientific HyClone, Waltham, MA), 1% antibiotic/antimycotic (Mediatech), 1% nonessential amino acids (Mediatech), 1% HEPES buffer (Mediatech), and 50 µg/ml ascorbate (Sigma-Aldrich, St. Louis, MO) and cryopreserved until use.

Bovine bone marrow stromal cells (BMSCs) were harvested according to a previously described protocol [213]. The femur and tibia of an immature calf were isolated, and marrow was placed into phosphate-buffered saline (PBS) with 1% antibiotic/antimycotic. The resulting mixture was physically disrupted by repeatedly pipetting through 50 and 10 mL pipettes, followed by 16, 18, and 20 gauge syringe needles. After centrifugation, the fatty layer was aspirated off, and the cell solution was plated for 30 minutes in "BMSC medium" containing low-glucose DMEM (Mediatech), 10% FBS, 1% antibiotic/antimycotic, and 1 ng/mL basic fibroblast growth factor (bFGF, Peprotech, Rocky Hill, NJ) to allow rapidly adhering cells to attach to the tissue culture plastic. The remaining cells in solution were then plated in tissue culture flasks. After 24 hours, nonadherent cells were aspirated off, culture medium was replaced, and BMSCs

were allowed to expand until confluency. Confluent cells were trypsinized in 0.05% trypsin/EDTA (Mediatech) and cryopreserved until use.

For long-term storage, ACL fibroblasts and BMSCs were placed in medium supplemented with 20% FBS and 10% dimethyl sulfoxide (DMSO; Sigma-Aldrich) and stored in liquid nitrogen until further use. Before use, cells were replated at $1.0x10^6$ cells/flask for at least 3 days in T-150 flasks to eliminate transitory effects from the thawing process. To examine the effects of interdonor variability, ACL fibroblasts and BMSCs were each isolated from 3 different animals (donors) for this study, including 1 donor from which both ACL fibroblasts and BMSCs were isolate from a single leg (donor #3).

3.2.2 Cell Culture on Aggrecan, Nonadhesive, and Control Surfaces

Similar to [10], wells of a tissue culture-treated 24-well plate were coated with 5 µg of bovine aggrecan (Sigma-Aldrich) by suspending aggrecan in PBS at a concentration of 50 µg/mL and allowing the PBS to evaporate overnight in a sterile environment at room temperature. After washing wells with PBS to remove residual unadsorbed aggrecan, wells were stained for 30 minutes with 16 µg/mL dimethylmethylene blue (DMMB; pH 3.0; Sigma-Aldrich) for sulfated GAGs to determine the distribution of aggrecan on the surfaces. For other samples, bovine ACL fibroblasts (P1) and BMSCs (P2) were plated at $8.8x10^4$ cells/well on aggrecan-coated surfaces and TCPS control surfaces in FBS-supplemented media. ACL fibroblasts were cultured in fibroblast medium as described above and including 1% nonessential amino acids, 1% HEPES buffer, and 50 µg/mL ascorbate. BMSCs were cultured in BMSC medium as described above and including 1 ng/mL bFGF. For all experiments in FBS-

supplemented media, FBS from a single lot was used to prevent variability between serum lots. These two cell types were also cultured on nonadhesive surfaces that resist cell attachment (Ultra-Low Attachment surfaces, Corning, Lowell, MA). To examine the nature of the cellular interaction with aggrecan, ACL fibroblasts and BMSCs were cultured in FBS-free media on aggrecan-coated and control surfaces.

Additionally, for specific experiments, aggrecan was added to the media of ACL fibroblasts and BMSCs cultured on control surfaces to examine the effect of aggrecan when suspended in the culture medium. 5 µg of aggrecan was added to the medium either at the time of seeding or 24 hours after seeding, instead of pre-treating the wells prior to seeding. For all experiments, culture medium was replaced every 2-3 days, and cell morphology was observed with a phase contrast microscope using a 10X objective (Nikon Eclipse TE2000-U, Tokyo, Japan).

3.2.3 Reverse Transcription Polymerase Chain Reaction

Gene expression of ACL fibroblasts and BMSCs on both aggrecan-coated surfaces and nonadhesive surfaces was analyzed after 3, 7, and 14 days by reverse transcription polymerase chain reaction (RT-PCR) for collagen I (fibroblastic marker), collagen II (chondrocytic marker), aggrecan (chondrocytic marker), and peroxisome proliferator-activated receptor γ2 (PPAR-γ2; adipocytic marker). ACL fibroblasts and BMSCs isolated from 3 different bovine donors, including 1 donor from which both ACL fibroblasts and BMSCs were isolated from a single leg (donor #3), were analyzed for interdonor variability. On aggrecan-coated surfaces, aggregates were separated from non-aggregating cells for analysis using a 1000 µL pipette tip to isolate the samples.

Nonadherent aggregates on nonadhesive surfaces were simply resuspended in culture medium, and TCPS monolayers were trypsinized and resuspended.

RNA was extracted from cell samples using a QIAshredder tissue homogenizer and RNeasy kit with DNase I digestion (Qiagen, Hilden, Germany). Reverse transcription was performed using SuperScript III Reverse Transcriptase (Invitrogen) with Oligo$(dT)_{15}$ primers (Promega, Madison, WI) and nucleotides (Promega). Custom primers (Invitrogen) specific to bovine mRNA for the target sequences are shown in Table 3.1, and quantitative PCR amplification was performed on a StepOnePlus System (Applied Biosystems, Carlsbad, CA) with SYBR Green master mix (Applied Biosystems). Fold regulation over control TCPS surfaces was calculated using the $\Delta\Delta C_T$ method with glyceraldehyde-3-phosphate dehydrogenase (GAPDH) as an endogenous control [301].

Table 3.1. Bovine primer sequences for quantitative polymerase chain reaction

Target	Primer Sequences (5'-3')	GenBank
Collagen I (α2)	AAGAACCCAGCTCGCACATG	AB008683
	GGTTAGGGTCAATCCAGTAGTAACCA	
Collagen II (α1)	GCATTGCCTACCTGGACGAA	X02420
	CGTTGGAGCCCTGGATGA	
Aggrecan	CCTCAGGGTTTCCTGACATTA	NM_173981
	TAAGCTCAGTCACGCCAGATA	
PPAR-γ2	CGCACTGGAATTAGATGACAGC	NM_181024
	CACAATCTGTCTGAGGTCTGTC	
GAPDH	CCTTCATTGACCTTCACTACATGGTCTA	NM_001034034
	TGGAAGATGGTGATGGCCTTTCCATTG	

3.2.4 Dimethylmethylene Blue (DMMB) and PicoGreen Assay

ACL fibroblast and BMSC aggregates were also analyzed by DMMB assay for sulfated GAG production and by PicoGreen assay for DNA content. ACL fibroblast (donor #1) and BMSC (donor #3) aggregates cultured on aggrecan-coated and nonadhesive surfaces were isolated as described above and digested in 1 mg/mL proteinase K (Sigma-Aldrich) in tris(hydroxymethyl)aminomethane

(Tris)/ethylenediaminetetraacetic acid (EDTA) digestion buffer (pH 6.5) with 185 µg/mL iodacetamide (Sigma-Aldrich) and 10 µg/ml pepstatin A (Sigma-Aldrich) for 16 hours at 56°C, and analyzed by DMMB assay, measuring absorbance at 520 nm (SpectraMax M2e; Molecular Devices, Sunnyvale, CA), compared to acellular blanks and a chondroitin sulfate standard curve [302]. Cells were then lysed through a series of freeze/thaw cycles and sonication, and PicoGreen assay (Invitrogen) was used to evaluate the total DNA content in each sample, according to established protocols [303]. Fluorescence was read at excitation 485 nm, emission 525 nm (SpectraMax M2e), and DNA content was determined using a standard curve of DNA and translated to cell number, compared to known numbers of bovine ACL fibroblasts and BMSCs. GAG content and cell number was normalized to the approximate number of aggregates per sample, and GAG content was also normalized to cell number.

3.2.5 Histological Staining

For this study, staining was only undertaken for proteins that were upregulated according to gene expression results (in this case, aggrecan only). Nonadherent ACL fibroblast and BMSC aggregates, from a single bovine donor (donor #3), cultured on nonadhesive surfaces were rinsed in PBS and fixed for 60 minutes in 10% buffered formalin after 3, 7, and 14 days. Fixed aggregates were encapsulated in Histogel (Richard-Allan, Waltham, MA), embedded in paraffin wax, and sectioned at 5 µm thickness. Sections were either stained with hematoxylin and eosin (H&E; Leica Autostainer XL, Wetzlar, Germany) or stained by immunohistochemistry (IHC) for aggrecan. For immunostaining, antigen retrieval was achieved with 20 µg/mL proteinase K for 10 minutes. Samples were deglycosylated with 10 µL of 0.75 U/mL chondroitinase

ABC (Sigma-Aldrich) for 1.5 hours to uncover the aggrecan core protein epitope. After blocking nonspecific binding with a solution of 2% goat serum, 1% bovine serum albumin (BSA), 0.1% gelatin, and 0.1% Triton-X in PBS and blocking endogenous peroxidases with 0.3% H_2O_2 in methanol, monoclonal mouse antibodies to bovine aggrecan (Abcam, Cambridge, UK) were allowed to bind overnight, and horseradish peroxidase-conjugated (HRP) secondary goat anti-mouse antibodies (Abcam) were allowed to incubate for 30 minutes, before diaminobenzidine (DAB) chromogen (Abcam) was used to develop the brown color that indicated positive immunostaining for aggrecan. Histological sections were imaged using a brightfield microscope at 10X and 40X magnifications (Nikon Eclipse E600).

3.2.6 Statistical Analysis

All values were reported as mean ± standard deviation. Statistical significance of quantitative results was determined using a two-way (quantitative PCR, DMMB) or three-way (PicoGreen) analysis of variance (ANOVA) with Tukey's multiple comparison test ($p \leq 0.05$). For quantitative PCR analysis, the two factors were surface and time. For DMMB analysis, the two factors were cell type and time. For PicoGreen analysis, the three factors were surface, cell type, and time. Statistical analysis was carried out using Minitab (v15.1, State College, PA).

3.3 Results

3.3.1 Aggregation of ACL fibroblasts and BMSCs on aggrecan-coated and nonadhesive surfaces

Aggrecan-coated surfaces induced formation of dense cellular aggregates along the periphery of the wells within 24 hours of cell seeding (Figure 3.1a,e), compared to TCPS surfaces (Figure 3.1d,h). DMMB staining of aggrecan-coated surfaces verified that the majority of aggrecan adsorbed in a ring along the periphery of each well, aligning closely with where cell aggregation occurred. These aggregates were tethered to the surface, but some aggregates were still able to move when the medium surrounding them was agitated. Aggregation occurred in both ACL fibroblasts (Figure 3.1a) and BMSCs (Figure 3.1e). Aggregates were consistently less than 100 μm in diameter with most aggregates between 30 and 80 μm. Aggregate formation on aggrecan-coated surfaces was not dependent on the presence of serum proteins, with ACL fibroblast and BMSC aggregates forming in serum-free media (Figure 3.1b,f). When aggrecan was suspended in the culture medium, rather than pre-adhered on culture surfaces, the cells appeared morphologically similar to cells on control surfaces, indicating that aggrecan must be adsorbed to the surface prior to cell seeding to induce aggregation. Large cellular aggregates also formed on nonadhesive surfaces in the absence of aggrecan (Figure 3.1c,g), and unlike aggrecan-coated surfaces, these aggregates were not adhered to the culture surface. Aggregate size for both ACL fibroblasts and BMSCs on nonadhesive surfaces was highly variable with aggregates ranging from less than 100 up to 400 μm in diameter.

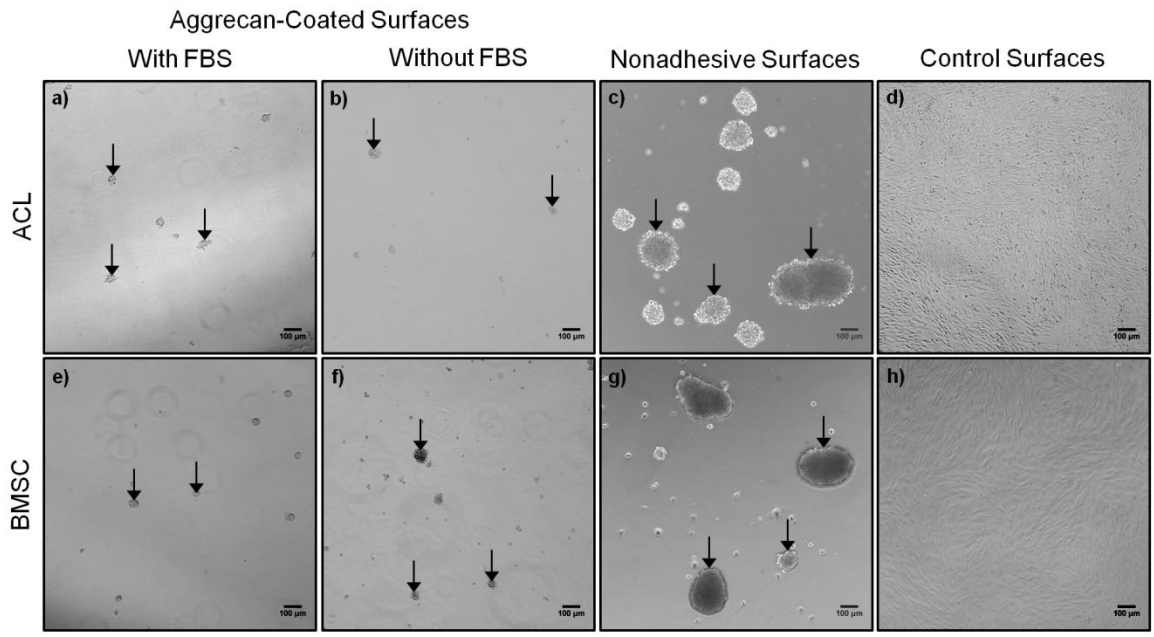

Figure 3.1. ACL fibroblasts (a-d) and BMSCs (e-h) on aggrecan-coated, nonadhesive, and control tissue culture-treated polystyrene surfaces in serum-supplemented and serum-free media after 3 days. Within 24 hours, aggregation (arrows) was observed on aggrecan-coated (a,e) and nonadhesive (c,g) surfaces, and aggregate morphology was maintained over 14 days. Aggregate formation on aggrecan-coated surfaces was not dependent on the presence of serum proteins (b,f). Scale bars in all images are 100 µm.

PicoGreen DNA assay was used to estimate the number of cells in ACL fibroblast (donor #1) and BMSC (donor #3) aggregates cultured on aggrecan-coated and nonadhesive surfaces. On aggrecan-coated surfaces, ACL fibroblast aggregates were composed of approximately 150±34 cells, and BMSC aggregates contained 51±17 cells on day 3. Aggregates cultured on nonadhesive surfaces, however, demonstrated higher cell number than those on aggrecan-coated surfaces, regardless of cell type; ACL fibroblast aggregates possessed approximately 3,920±480 cells, and BMSC aggregates contained 600±95 cells on nonadhesive surfaces on day 3. From statistical analysis, ACL fibroblast aggregates had significantly higher cellularity than BMSC aggregates when cultured on nonadhesive surfaces, although aggregate cell number was not significantly

different between cell types on aggrecan-coated surfaces. PicoGreen results further indicated that aggregate cell number did not significantly change over time on either surface.

3.3.2 Upregulation of aggrecan gene expression in ACL fibroblast and BMSC aggregates on aggrecan-coated and nonadhesive surfaces

Overall, ACL fibroblast and BMSC aggregates on aggrecan-coated and nonadhesive surfaces showed significantly upregulated aggrecan gene expression. Though some interdonor variability was evident, in all donors (donors #1-3), ACL fibroblast aggregates on aggrecan-coated surfaces demonstrated significantly upregulated aggrecan expression at all time points, compared to cells on TCPS controls (Figure 3.2a-c). On nonadhesive surfaces, ACL fibroblasts experienced significant upregulation of aggrecan expression on day 14 in all donors (Figure 3.2d-f), and donor #1 also showed upregulated aggrecan expression on days 3 and 7, compared to TCPS controls (Figure 3.2d). In addition, collagen I expression was significantly downregulated in ACL fibroblasts on nonadhesive surfaces over all time points in all 3 donors. Collagen II and PPAR-γ2 were generally downregulated over most time points on nonadhesive surfaces in cells from donors #1 and #2. Minimal change in gene expression of collagen I, collagen II, and PPAR-γ2 was observed on aggrecan-coated surfaces with ACL fibroblasts.

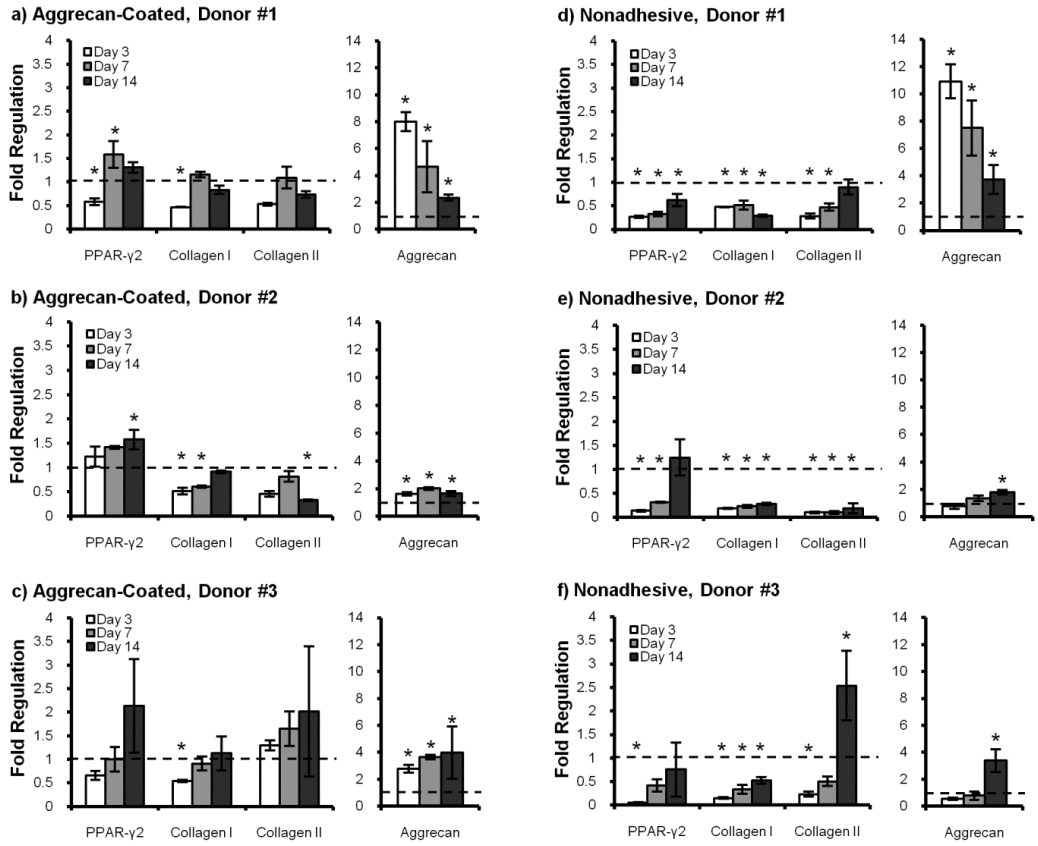

Figure 3.2. Gene expression of ACL fibroblasts from 3 different bovine donors on aggrecan-coated (a-c) and nonadhesive (d-f) surfaces over 14 days, relative to cells on untreated control surfaces. (Aggrecan expression is depicted on separate axes using a different vertical scale.) Some interdonor variability was evident; however, ACL aggregates significantly upregulated aggrecan gene expression on aggrecan-coated and nonadhesive surfaces (n=3), particularly by day 14. * indicates significantly different from control samples ($p \leq 0.05$).

Similar to ACL fibroblasts, BMSC aggregates on aggrecan-coated and nonadhesive surfaces also demonstrated an increase in aggrecan gene expression. Though some interdonor variability was evident, BMSC aggregates on aggrecan-coated surfaces showed significantly upregulated aggrecan expression on day 3, compared to TCPS controls, in all bovine donors (donors #3-5; Figure 3.3a-c); however, expression diminished to control levels on days 7 and 14. On nonadhesive surfaces, BMSCs from all 3 donors experienced significant upregulation of aggrecan expression over TCPS controls

on all time points (Figure 3.3d-f). Collagen II was significantly downregulated on both surfaces over all times in cells from donor #5 and on nonadhesive surfaces over most time points with donor #3. Collagen I and PPAR-γ2 were significantly downregulated over most time points on nonadhesive surfaces in cells from donors #3 and #4. Minimal change in gene expression of collagen I and PPAR-γ2 was observed on aggrecan-coated surfaces.

3.3.3 Production of sulfated GAG in ACL fibroblast and BMSC aggregates

ACL fibroblast (donor #1) and BMSC (donor #3) aggregates on nonadhesive surfaces were analyzed by DMMB assay for production of sulfated GAG. ACL fibroblast aggregates produced 69±3 ng GAG per aggregate, while BMSC aggregates produced 12±2 ng GAG per aggregate, suggesting that ACL aggregates contained significantly more GAG than BMSC aggregates; however, GAG production was not statistically significant across cell types when normalized to cell number. ACL aggregates contained 18±1 pg GAG per cell, while BMSC aggregates contained 20±4 pg GAG per cell after day 3 (Table 3.2). GAG content in ACL and BMSC aggregates on nonadhesive surfaces did not significantly change over time.

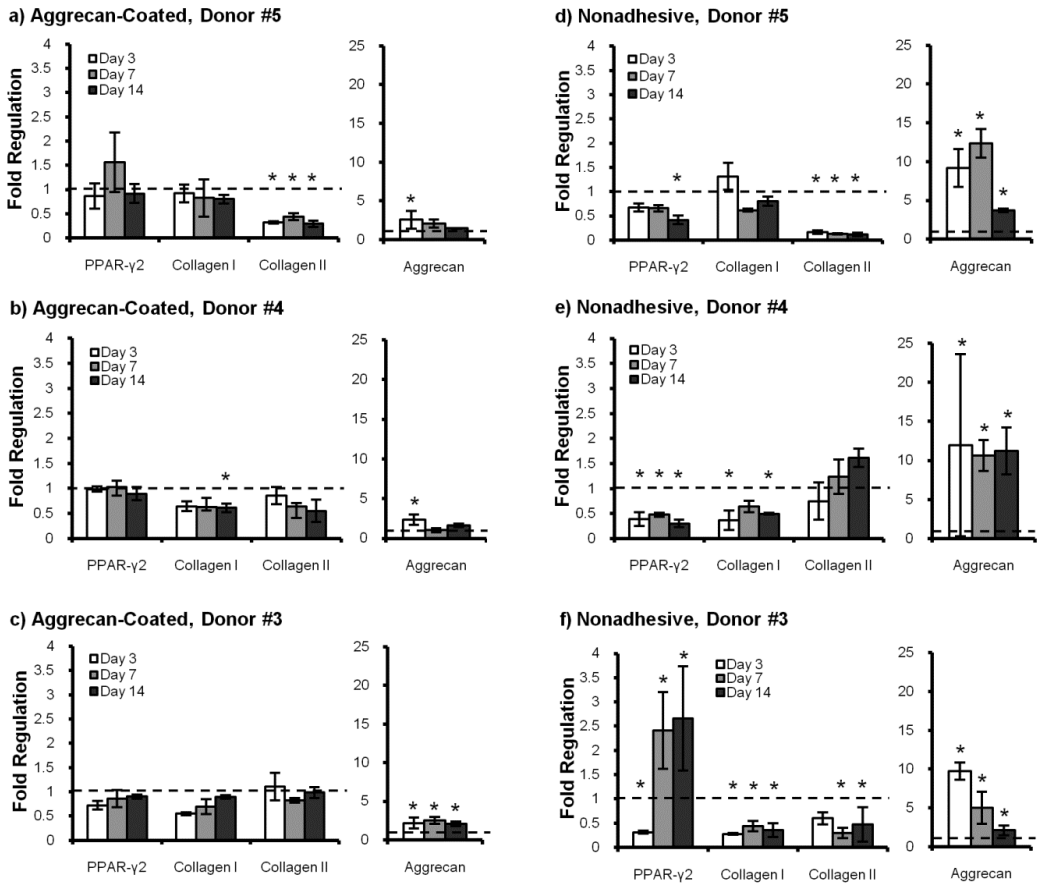

Figure 3.3. Gene expression of BMSCs from 3 different bovine donors on aggrecan-coated (a-c) and nonadhesive (d-f) surfaces over 14 days, relative to cells on untreated control surfaces. (Aggrecan expression is depicted on separate axes using a different vertical scale.) Some interdonor variability was evident; however, BMSC aggregates significantly upregulated aggrecan gene expression on aggrecan-coated and nonadhesive surfaces on day 3 (n=3). * indicates significantly different from control samples ($p \leq 0.05$).

Table 3.2. Sulfated GAG content within cell aggregates cultured on nonadhesive surfaces as determined by DMMB assay, normalized by cell number (n=3)

Cell Type	Mass of GAG (pg per cell)		
	Day 3	Day 7	Day 14
ACL Fibroblasts	18±1 pg/cell	21±6 pg/cell	21±4 pg/cell
BMSCs	20±4 pg/cell	24±2 pg/cell	16±14 pg/cell

3.3.4 Production of aggrecan in ACL fibroblast and BMSC aggregates

Immunostaining of ACL fibroblast and BMSC (both donor #3) aggregates cultured on nonadhesive surfaces verified the presence of aggrecan after 3, 7, and 14 days

(Figure 3.4b-d,f-h), compared to negative control samples stained without primary antibody for aggrecan (Figure 3.4a,e). Also, BMSCs formed noticeably better defined aggregates than ACL fibroblasts. While ACL aggregates showed some sectioning artifact, especially at early time points, in which cells dissociated from the aggregate body, BMSC aggregates appeared to possess a thin, smooth layer surrounding each aggregate and remained intact during sectioning. In immunostaining and hematoxylin and eosin staining, a distinct change in aggregate morphology was observed in BMSC aggregates from 3 to 14 days (Figures 3.4f-h, 3.5d-f). Starting at day 7 and increasing by day 14, small pocket-like spaces were present in BMSC aggregates with ECM organization appearing as a circular, interconnected network. ACL aggregates, however, did not observe this pocket-like ECM organization, and morphology did not appear to greatly change over the course of 14 days (Figure 3.4b-d, 3.5a-c).

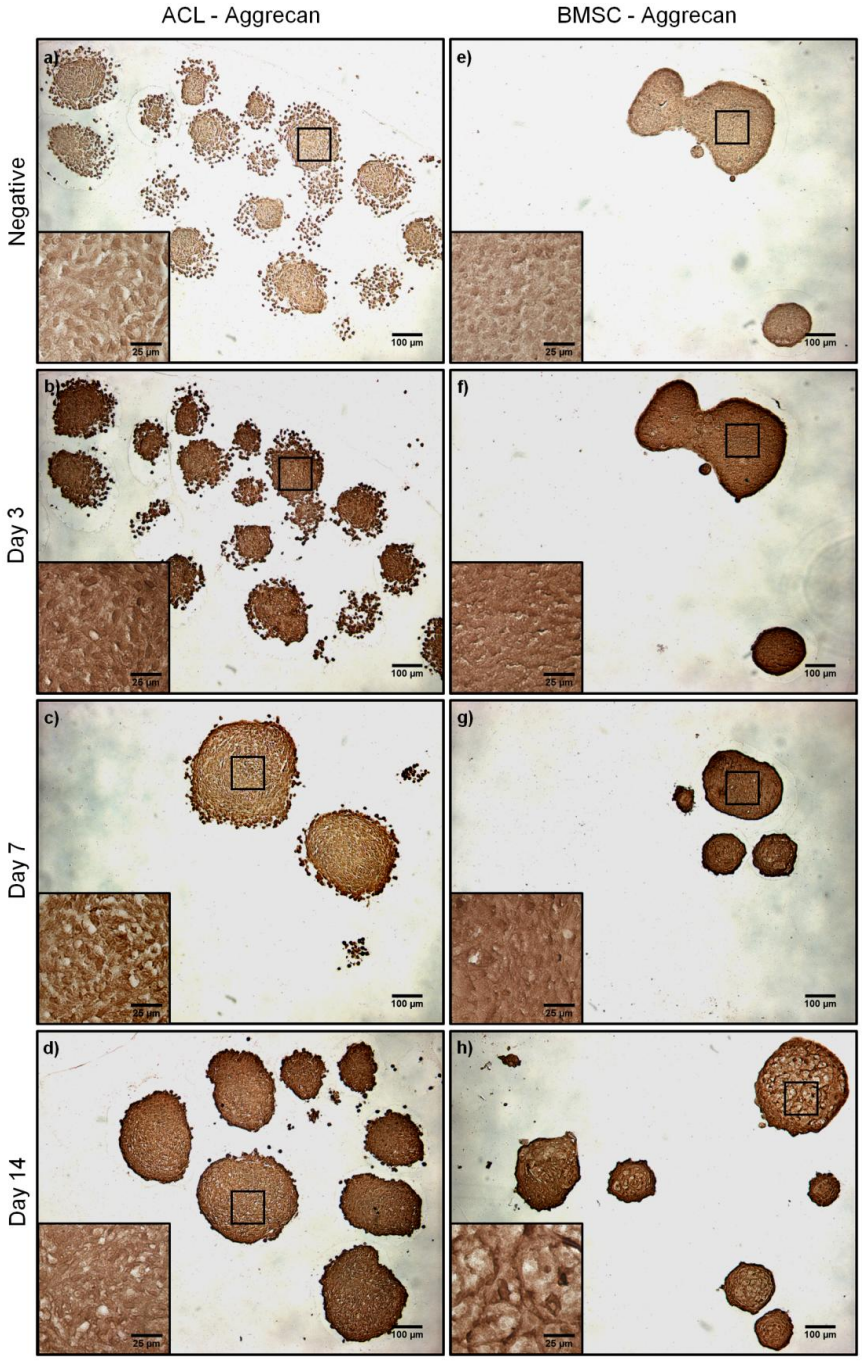

Figure 3.4. Presence of aggrecan within ACL fibroblast (a-d) and BMSC (e-h) aggregates as indicated by immunohistochemistry staining. ACL and BMSC aggregates stained strongly for aggrecan (b-d, f-h), compared to negative control samples stained without primary antibody for aggrecan (a,e). A noticeable change in ECM morphology is evident over 14 days in BMSC aggregates. Boxed regions are magnified in insets located in the lower left corner of each image. Scales bars in images are 100 µm, and insets are 25 µm.

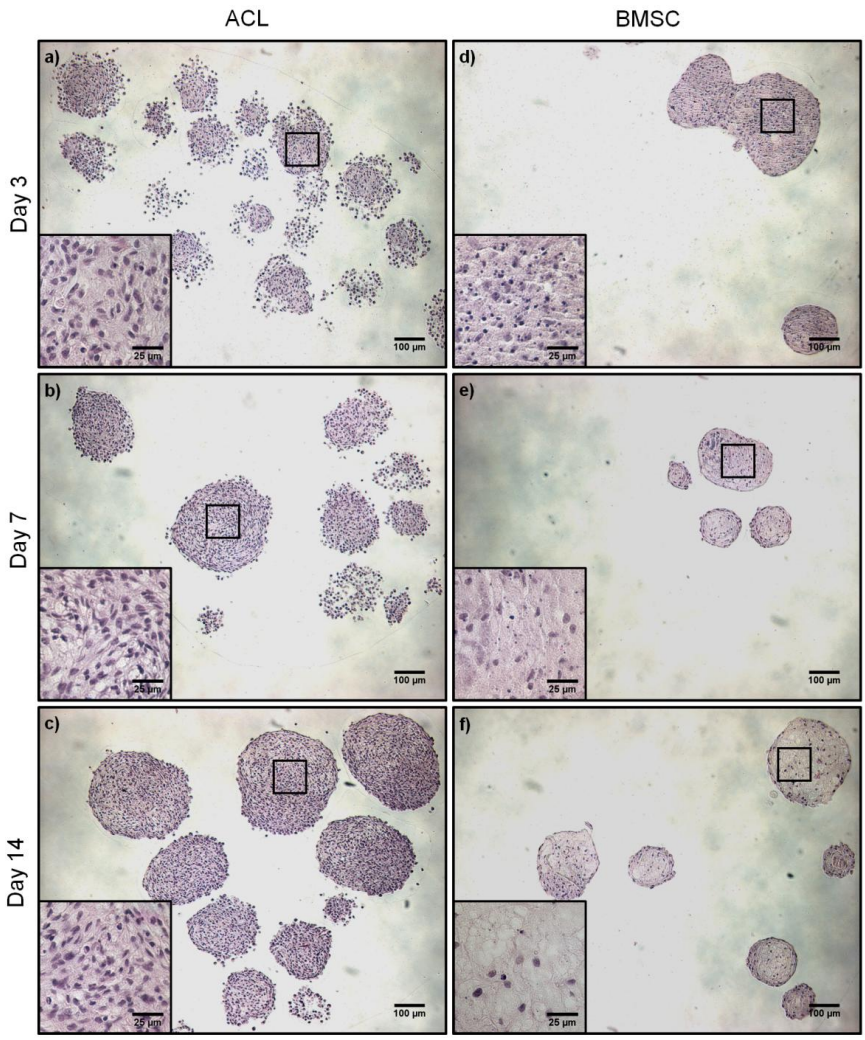

Figure 3.5. Hematoxylin and eosin (H&E) staining of ACL fibroblast (a-c) and BMSC (d-f) aggregates. A noticeable change in ECM morphology is evident over 14 days in BMSC aggregates. Boxed regions are magnified in insets located in the lower left corner of each image. Scales bars in images are 100 µm, and insets are 25 µm.

3.4 Discussion

The results from this study demonstrated that aggrecan-coated surfaces can be used to alter the morphology of both bovine ACL fibroblasts and BMSCs. Modification of surfaces with aggrecan molecules promoted the formation of ACL fibroblast clusters and BMSC aggregates (Figure 3.1). DMMB staining verified that the localization of aggrecan on tissue culture surfaces aligned closely with areas of cell aggregation.

Aggregation required that aggrecan molecules be adsorbed to the surface prior to cell seeding, and the presence of aggrecan suspended in the culture medium did not induce aggregate formation, suggesting that the interaction between the aggrecan and the surface prior to cell seeding reduced cell adhesion to the culture dish and thus encouraged cell clustering. However, aggregation on aggrecan-coated surfaces was not dependent on the presence of serum proteins, with aggregates forming in FBS-free media (Figure 3.1). After formation, ACL fibroblast and BMSC aggregates on aggrecan-coated surfaces contained significantly fewer cells than aggregates on nonadhesive surfaces, and aggregate cellularity did not change with time.

Aggregation of bovine ACL fibroblasts and BMSCs, even in the absence of aggrecan (as shown on nonadhesive surfaces), promoted gene expression and production of aggrecan, a key cartilaginous ECM proteoglycan (Figures 3.2-4, Table 3.2). In general, there was variability between the 3 bovine donors tested for gene expression, suggesting intrinsic differences in how these cells respond to culture conditions; however, the general trend of aggrecan upregulation was maintained regardless of cell source, which indicated that aggregation is a robust method to promote cartilaginous gene expression in these cells. Results from the DMMB assay and immunostaining verified that ACL fibroblast and BMSC aggregates cultured on nonadhesive surfaces also produced detectable amounts of sulfated GAG/aggrecan. However, direct comparison of aggrecan production between culture surfaces was not possible as cells on aggrecan-coated surfaces could not be isolated without releasing the original aggrecan coating as well, thus potentially contaminating the samples.

These data suggested that cells could potentially be pre-cultured as aggregates in order to promote the production of cartilaginous ECM within a cell population, prior to their incorporation into a portion (insertion points) of a 3D scaffold for ligament tissue engineering applications. Alternatively, biomaterial scaffolds may be designed with means to induce differing degrees of cellular aggregation along their length [174], thereby predisposing a certain population of cells to produce larger amounts of aggrecan in areas near the insertion point. RT-PCR results indicated that cells responded similarly in aggregates, regardless of the cell culture surface employed (Figures 3.2-3.3), suggesting aggregation itself was a major stimulus for the changes in gene expression observed. This leaves open the possibility of using a wide variety of pre-culture methods, including those tissue culture surfaces presented here, to encourage cells to form cartilaginous ECM for insertion point regeneration.

Similar to culture of these cell aggregates on nonadhesive surfaces, pellet culture and micromass culture are established methods to prevent the dedifferentiation of chondrocytes or to promote chondrogenic differentiation of BMSCs [6, 98, 132, 304-307]. High-density culture may mimic the cell environment of mesenchymal condensation that occurs during cartilage development prior to chondrogenesis, including cell-cell and cell-matrix interactions [24, 308]. However, to our knowledge, this is the first time aggregate culture has been investigated for chondrogenic differentiation of tendon/ligament fibroblasts. High-density culture of human tenocytes, including pellet formation by centrifugation or clustering in response to ultra-confluent monolayer culture, has been examined for maintenance of tenocyte phenotype [309-311], and one group reported accumulation of proteoglycan over 14 days with no change in collagen II

[309]; however, further implications for chondrogenic differentiation were not explored. In contrast, this study induced aggregate formation via culture on nonadherent 2D surfaces, both with or without aggrecan treatment, to investigate expression of cartilaginous ECM by ACL fibroblasts. Micromass culture has also been applied with lactic acid treatment to promote production of cartilaginous ECM by human dermal fibroblasts [281]. These results suggest that ligament fibroblasts retain the plasticity to alter their gene expression and possibly differentiate toward a chondrogenic phenotype under the appropriate conditions.

While aggrecan was significantly upregulated in clustered cells, collagen type II, another chondrocytic ECM marker, was either significantly downregulated or remained unchanged in both ACL fibroblast and BMSC aggregates on both surfaces. This decoupled expression of aggrecan and collagen type II suggests that while aggrecan expression is upregulated in cell aggregates, the cells are not completely committed to a chondrocytic phenotype. For use as part of a tissue-engineered ligament replacement, cartilaginous ECM (aggrecan and collagen II) should be upregulated, while fibrous ECM (collagen I) expression should be either upregulated or maintained within ACL fibroblasts and BMSCs; however, this system may be useful to investigate the basic interactions of cells with aggrecan in the absence of a collagen II matrix. Also, it is important to note that gene expression of other markers such as PPAR-γ2 was either downregulated or unchanged over most time points, indicating that ACL fibroblasts and BMSCs are not differentiating down an alternate (adipogenic) lineage. Further work is required to determine the optimal culture conditions that would simultaneously upregulate collagen I, collagen II, and aggrecan expression for production of

fibrochondrogenic ECM. A combination of aggregate-inducing culture substrates with soluble factors or mechanical loading (not explored in this study) may be necessary to achieve an optimal cell phenotype for use in the insertion sites of future tissue-engineered ACL replacements.

The ability of BMSCs and ACL fibroblasts to alter their gene expression and ECM production may be dependent on the presence of a subpopulation of multipotent progenitor cells in both cases. BMSCs and ACL fibroblasts in this study are heterogeneous populations of cells from the bone marrow and ACL, respectively. BMSCs likely include a subpopulation of multipotent mesenchymal stem cells [77], and while cells from the ACL are mostly ligament fibroblasts, they may include a small subpopulation of ligament progenitor cells, similar to progenitor/stem cells isolated from tendon and periodontal ligament [312-313]. Overall, BMSCs displayed greater and more consistent upregulation of aggrecan expression than ACL fibroblasts (Figures 3.2-3.3), suggesting that, even though ACL fibroblasts are capable of altering their gene expression profiles, BMSCs are more consistently responsive to cell aggregation and may possess are larger population of progenitor cells than ACL fibroblasts. Ligament fibroblasts, however, have been extensively explored as a cell source for ligament tissue engineering [69, 314-315], as an injured ACL could be surgically removed and the harvested fibroblasts used as an autologous cell source to populate a ligament graft [316]. The ability of ACL fibroblasts to alter their gene expression and produce cartilaginous ECM suggests that ACL fibroblasts may also be a promising cell type in the development of a tissue-engineered bone-ligament-bone graft including fibrocartilaginous insertions.

From histological sections, distinct differences were observed between the morphology of ACL fibroblast and BMSC aggregates cultured on nonadhesive surfaces (Figure 3.4-3.5). Most noticeably, in this study, small pocket-like spaces were observed in day 14 BMSC aggregates with ECM appearing as a circular, interconnected network. The matrix organization in day 14 BMSC aggregates may be an effect of nutrient transport into these large cell aggregates. It should be noted that this ECM network has not been reported by similar studies examining micromass culture of bovine BMSCs over similar time scales [132, 307]. However, in these other studies, aggregates were formed by centrifugation resulting in much larger cell pellets, which could account for differences in observed pellet morphology. Additionally, cells in this study were cultured with 10% FBS, while other studies replaced serum with insulin-transferrin-selenium (ITS) supplement with and without transforming growth factor-β1 or -β3 (TGF-β). Further work is needed to fully understand the timing and events involved in differentiation and matrix production that may lead to this unique ECM structure within these aggregates.

Together the results of these studies present aggregate culture of ACL fibroblasts and BMSCs as a potential pre-culture technique to promote the regeneration of cartilaginous and fibrocartilaginous tissues.

3.5 Conclusions

These studies have shown that aggrecan-coated surfaces induce the aggregation of bovine ACL fibroblasts and BMSCs, and cell clusters (on aggrecan-coated surfaces and in the absence of aggrecan) demonstrated upregulated aggrecan gene expression,

regardless of cell type. Immunostaining also confirmed the presence of aggrecan in cell aggregates over 14 days. These findings suggest that both cell types could potentially be pre-cultured as aggregates to promote production of cartilaginous ECM, specifically aggrecan proteoglycan, prior to seeding on scaffolds, for orthopaedic tissue engineering applications requiring the presence of this molecule. This is particularly attractive as it suggests that altering pre-culture conditions like degree of clustering could produce a range of phenotypes from a single cell source, such as the ACL fibroblast. As such, these findings represent a first step which may inform future approaches to producing tissue-engineered alternatives for current ACL grafting procedures through regeneration of physiological fibrocartilaginous interfaces.

CHAPTER 4

DEVELOPMENT OF NANO- AND MICRO-SCALE CHONDROITIN SULFATE PARTICLES FOR CONTROLLED GROWTH FACTOR DELIVERY[2]

4.1 Introduction

Chondroitin sulfate (CS) is a sulfated glycosaminoglycan (GAG) that is covalently bound to a variety of protein cores to form proteoglycans that are found throughout the human body [317]. During development, one of the key roles of GAGs is to establish morphogen gradients that pattern tissue morphogenesis by sequestering secreted growth factors at the cell membrane [318]. Negatively charged GAGs, including heparin, heparan sulfate, and CS, are capable of electrostatically interacting with positively charged growth factors, including basic fibroblast growth factor (bFGF), insulin-like growth factor (IGF), vascular endothelial growth factor (VEGF), platelet-derived growth factor (PDGF), and transforming growth factor-β (TGF-β), to stabilize and prevent degradation of the growth factors in solution [206, 262, 319], indicating that CS biomaterials may be a promising vehicle for delivery of cationic growth factors, particularly to direct differentiation of stem cells.

Size scale plays an important role in the release kinetics of a given delivery vehicle, including the diffusion rate of molecules out of the material and the degradation

[2] Portions of this chapter were adapted from Lim JJ, Hammoudi TM, Bratt-Leal AM, Hamilton SK, Kepple KL, Bloodworth NC, et al. Development of nano- and microscale chondroitin sulfate particles for controlled growth factor delivery. Acta Biomater. 2011;7(3):986-95.

properties of the material [320]; therefore, control of size enables one to tailor the release profile for a variety of applications. Nanospheres and microspheres possess a high surface area-to-volume ratio, accelerating the diffusion of molecules from the particles and potentially enhancing the hydrolytic or enzymatic degradation of the carrier and further accelerating release [320-321]. The small size of nano- and microspheres, relative to cells and tissues, make them especially advantageous carriers for delivery and sustained release within dense tissues, high-density cell pellets, or tissue engineering scaffolds with numerous barriers to diffusion [322], because these small particle carriers can be incorporated or locally injected within a tissue for controlled release of specific molecules to achieve a localized or more homogenous cell response [321].

Additionally, nano-sized particles (< 500 nm diameter) are capable of being internalized by cells, permitting efficient transport across the cell membrane [321]. Generally, smaller particles are endocytosed more effectively than larger particles, though an optimal size range commonly exists around 100-200 nm [323]. Larger micro-scale delivery vehicles, however, may be advantageous for preventing cell endocytosis if extracellular release is desired, and their larger size scales also possess potential for greater molecule loading and prolonged release due to their larger volumes.

In this study, we explored the means to fabricate both micron-scale particles and nano-scale micelles from CS. Micelles are nanoscale, self-assembling particles composed of amphiphilic molecules. In an aqueous environment, micelles self-assemble into sphere-like structures with a hydrophilic shell surrounding a hydrophobic core, making them largely stable in the aqueous environment of the body [324]. Due to its negative charge density and hydrophilic nature, CS can be utilized as a hydrophilic segment of a

polymeric micelle. CS has been previously reported as the hydrophilic component with poly(L-lactic acid) (PLLA) and poly(lactic-co-glycolic acid) (PLGA) copolymers to form amphiphilic microspheres for use as drug and protein delivery carriers [324-326]. With its nanoscale size and high negative charge density, CS-derived micelles have promising potential for many drug and protein delivery applications.

The long term goal of this research was to examine CS interactions with stem cells, particularly as a means to control growth factor release in order to direct differentiation. Therefore, the first set of experiments in this study were designed to develop facile means to control the size of CS-based particles over a broad range of size scales (at least two orders of magnitude) and characterize the resulting materials. Subsequently, the ability of these CS-based biomaterials to interact electrostatically with positively charged growth factors, as well as the cytocompatibility of these materials with both embryonic and mesenchymal stem cells was demonstrated, confirming the potential for these materials as naturally-derived carriers for growth factor delivery for a variety of stem cell-based tissue engineering and regenerative medicine applications.

4.2 Materials and Methods

4.2.1 Modification of Chondroitin Sulfate

4.2.1.1 Chondroitin Sulfate Modification for Micelle and Hydrogel Fabrication

To examine the effects of reaction stoichiometry on the resulting modification of CS, N-(3-dimethylaminopropyl)-N'-ethylcarbodiimide (EDC) chemistry, which forms an amide bond between a primary amine and a carboxylic acid, was used to synthesize chondroitin sulfate methacrylamide (CSMAm; Figure 4.1a). N-(3-

aminopropyl)methacrylamide (APMAm) was conjugated to chondroitin sulfate A, using EDC chemistry adapted from [327]. 2.5 mM CS (~48.7 kDa; Sigma-Aldrich, St. Louis, MO) [328] based on CS disaccharide molecular weight was reacted with APMAm (Polysciences, Warrington, PA), EDC (Sigma-Aldrich), and N-hydroxysulfosuccinimide (sulfo-NHS; Sigma-Aldrich) at various molar ratios depicted in Table 4.1. Since CS possesses 1 carboxyl moiety per disaccharide, this represented the molar ratio of reagent to each reactive carboxyl group. The reaction mixture was incubated at room temperature and pH 5.0 for 2 hours with stirring.

Sulfo-NHS stabilizes the EDC reaction and was used to control the degree of substitution of the reaction; however, to reduce the degree of modification for micelle formation, the reaction with the highest molar ratio of 4:1 was repeated in the absence of sulfo-NHS. Initially a 2:1 ratio of APMAm and EDC to CS was used and allowed to react for 2 hours, and then a second round of APMAm and EDC was added to the solution for a total 4:1 molar ratio to CS. The reaction without sulfo-NHS was allowed to proceed for 2 more hours at pH 5.0. All reaction mixtures were dialyzed in 1,000 Da molecular weight cutoff (MWCO) dialysis membrane (Spectrum Laboratories, Rancho Dominguez, CA) against distilled water (dH_2O) for 3 days, and the product was then lyophilized (Labconco FreeZone 4.5, Kansas City, MO) for 4 days and stored at 4°C until use.

4.2.1.2 Chondroitin Sulfate Modification for Microsphere Fabrication

For microsphere formation, CS was reacted with methacrylic anhydride (Sigma-Aldrich) to conjugate methacrylate groups to the existing hydroxyl groups in CS (Figure 4.1b). Methacrylation of CS was carried out per established protocols [328]. After complete dissolution, 60 mL methacrylic anhydride was added dropwise into 60 mL of a

25% w/v chondroitin sulfate A solution (20.6:1 molar ratio of methacrylic anhydride to reactive hydroxyl) under basic conditions. The reaction solution was stirred at 60°C for 24 hours, then precipitated and washed in cold methanol:isopropanol (10:1). The resulting chondroitin sulfate methacrylate (CSMA) precursor was subsequently dried under vacuum at room temperature. The resulting product was dialyzed (1,000 Da MWCO) against dH_2O for 3 days, followed by lyophilization for 4 days.

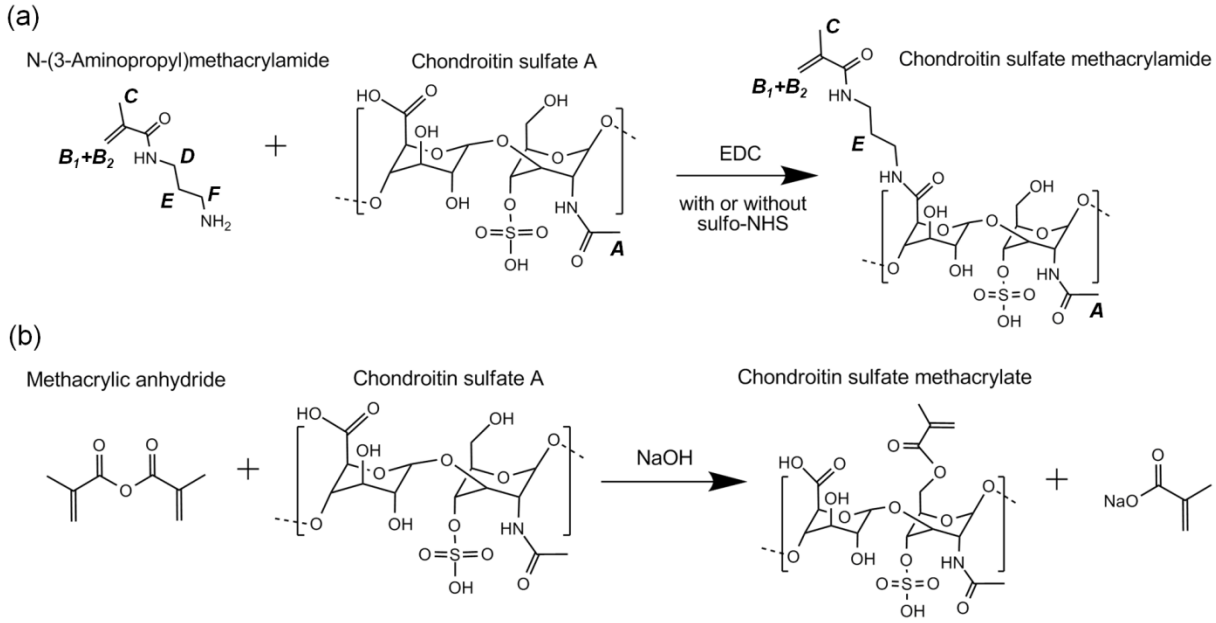

Figure 4.1. Modification reactions of chondroitin sulfate. (a) Chondroitin sulfate A (CS) and N-(3-aminopropyl)methacrylamide (APMAm) were reacted in the presence of N-(3-dimethylaminopropyl)-N'-ethylcarbodiimide (EDC) with or without N-hydroxysulfosuccinimide (sulfo-NHS) to yield chondroitin sulfate methacrylamide (CSMAm). Protons are labeled for ^{1}H NMR results in Figure 4.2. (b) CS and methacrylic anhydride were reacted in the presence of NaOH to yield chondroitin sulfate methacrylate (CSMA).

4.2.2 Characterization of CS Nano- and Microspheres

4.2.2.1 Proton Nuclear Magnetic Resonance Spectroscopy

Proton nuclear magnetic resonance (^{1}H NMR) was utilized to determine the degree of the conjugation of the APMAm groups to the CS chains. The initial components (CS and APMAm) and resulting modified CS products (CSMAm and CSMA) were solubilized in deuterated water (D_2O; Sigma-Aldrich), and ^{1}H NMR was measured on a Bruker AMX-400 spectrometer (Billerica, MA) at 400 MHz. The resulting spectra were analyzed by calibrating the region from 3.61-3.88 ppm according to the known number of protons in the chondroitin sulfate backbone. This provided an internal standard which allowed monitoring of the amount of modification attached to the different modification reactions.

4.2.2.2 Formation and Characterization of Bulk CS Hydrogels

Solutions of CSMAm or CSMA at 90% water content in phosphate buffered saline (PBS) were crosslinked between 2 glass slides at 1 mm thickness under 15 mW/cm^2, 365 nm UV light (UVP, Upland, CA) with 0.2 wt% Irgacure 2959 photoinitiator (D2959, Ciba, Ludwigshafen, Germany) for 12.5 minutes, and 6 mm diameter discs were punched out using a cork borer. After 1 day swelling in PBS, the wet weight of crosslinked hydrogels was recorded, and following lyophilization overnight, dry weight was recorded. Swelling ratio was calculated as wet weight/dry weight (n=4).

4.2.2.3 Dynamic Light Scattering and Zeta Potential Measurements of CS Micelles

Dynamic light scattering (DLS) measurements were taken to determine the average diameter of CSMAm micelles in distilled, deionized water (ddH_2O), and zeta potential measurements were also recorded as a measure of surface charge and colloidal

stability in ddH_2O. DLS and zeta potential measurements were taken on a NICOMP 380ZLS (Particle Sizing Systems, Santa Barbara, CA) at 23°C. A helium-neon laser at 632.8 nm wavelength was used at a detector angle of 90°. Samples of 1.0 mg/mL CSMAm were run in ddH_2O, while samples of unmodified CS at the same concentration served as controls (n=4). Prior to measurement, the solutions were filtered through a 5 µm pore size cellulose acetate filter (Sartorius, Goettingen, Germany), and the sample was briefly centrifuged (14,000 RPM) to remove any dust particles from the solution. Hydrodynamic diameter was calculated using the inverse Laplace transform of the correlation function [329].

Zeta potential measures colloid mobility of charged particles in solution under an electric field. Zeta potential measurements were taken on 0.1 mg/mL CSMAm solutions in an electric field of 4 V/cm (1.6 V, 0.4 cm electrode distance; n=3). Zeta potential was calculated according to the Smoluchowski limit [330].

4.2.2.4 CS Microsphere Fabrication and Characterization

CS microspheres were fabricated using a water-in-oil, single-emulsion technique similar to a previously described protocol [331]. CSMA (55.6 mg) was dissolved in PBS (440 µL) and combined with ammonium persulfate (30 µL, 0.3 M) (Sigma-Aldrich) and tetramethylethylenediamine (30 µL, 0.3 M) (Sigma-Aldrich) free radical initiators on ice. This mixture was added drop-wise into corn oil at 4°C and homogenized at 3,800 RPM for 5 minutes. The temperature was then raised to 50°C with stirring for 30 minutes to promote crosslinking. The resulting solution was centrifuged at 300 RCF, and the corn oil was removed. Microspheres were then washed with dH_2O and stored in dH_2O at 4°C. The diameter of the microsphere population was analyzed using a Z2 Coulter Particle

Counter (Beckman Coulter, Fullerton, CA) equipped with a 100 µm aperture. Microspheres were suspended in Isoton II diluent (Beckman Coulter) prior to counting.

For imaging, microspheres were treated with a solution of 1,9-dimethylmethylene blue (DMMB; Sigma-Aldrich) for 30 minutes to stain CS purple, washed with ddH_2O, and imaged using an inverted microscope (Nikon Eclipse TE2000-U, Melville, NY).

4.2.2.5 Complexation and Release from CS Microspheres

To examine the ability of negatively charged CS microspheres to electrostatically bind positively charged TGF-β1, approximately 2 mg of lyophilized microspheres were suspended in 500 µL of 50 ng/mL human recombinant TGF-β1 (Peprotech, Inc., Rocky Hill, NJ) and 1% bovine serum albumin (BSA) in PBS. Microspheres were incubated with TGF-β1 overnight at 4°C with shaking (n=3).

To examine the release kinetics of positively charged TGF-β1 and negatively charged tumor necrosis factor-α (TNF-α), approximately 2 mg of lyophilized CS microspheres were loaded with 5 µL of 5 µg/mL human recombinant TGF-β1 or TNF-α (R&D Systems, Minneapolis, MN) per mg of microspheres overnight at 4°C. Microspheres were then suspended in 750 µL of solution containing 1% BSA in PBS (time 0) and incubated at 37°C with gentle shaking for 5 days.

At various time points, samples were centrifuged for 90 seconds at 4,000 RPM, and the supernatant was sampled and analyzed for factor content using the corresponding enzyme-linked immunosorbent assay (ELISA; R&D Systems) kit specific to human TGF-β1 or TNF-α (n=3).

4.2.3 Cytocompatibility of CS Nano- and Microspheres

4.2.3.1 *In Vitro* Cytotoxicity of CS Micelles and Microspheres on 2D BMSC Monolayers

For CSMAm micelle cytotoxicity studies, bovine bone marrow stromal cells (BMSCs) were isolated in a modification of the procedure outlined in [213]. Briefly, bone marrow was harvested from the tibia and femur of an immature calf (Research 87, Marlborough, MA). Cells were cultured in medium composed of low-glucose DMEM (Mediatech, Manassas, VA) supplemented with 10% fetal bovine serum (FBS; Thermo Scientific Hyclone, Logan, Utah), 1% antibiotic/antimycotic, 0.1% Fungizone antimycotic (Invitrogen, Carlsbad, CA), and 1 ng/mL bFGF (Peprotech). The adherent BMSCs were expanded until confluence and were then detached with 0.05% trypsin/EDTA (Mediatech), frozen in medium containing 20% FBS and 10% dimethyl sulfoxide (DMSO; Sigma-Aldrich), and cryopreserved in liquid nitrogen until use (P1).

Prior to use, BMSCs were thawed and plated for at least 3 days to eliminate transitory effects from the thawing process. After this time, cells were trypsinized (P2) and plated at 10,000 cells/cm^2 in a tissue culture-treated 96-well plate. After 24 hours to allow cell attachment, culture medium was replaced with 100 µl of medium containing CSMAm micelles or CSMA microparticles equivalent to 1, 10, 100, 320 mg per 10^6 cells (0.064, 0.64, 6.4, and 20.5 mg/ml, respectively). After 24 hours of exposure to the CSMAm- or CSMA-containing media, cells were stained (30 minutes) with LIVE/DEAD stain (Invitrogen). Calcein stains live cells to fluoresce green (excitation/emission: 494/517 nm), and ethidium homodimer-1 stains dead cells to fluoresce red (excitation/emission: 528/617 nm). Dead controls were exposed to 70% methanol prior to staining, while live controls were cultured in normal culture medium without CS

particles. Fluorescent images were captured using an inverted microscope, and total fluorescence of each well was measured in a SpectraMax M2^e plate reader (Molecular Devices, Toronto, Canada) at the wavelengths specified above (n=3). Relative viability was analyzed in comparison to live controls, using the following equation:

$$Fraction\ of\ live\ cells = \frac{F(517)_{sample} - F(517)_{DEAD}}{F(517)_{LIVE} - F(517)_{DEAD}},$$

where $F(517)_{sample}$, $F(517)_{LIVE}$, and $F(517)_{DEAD}$ are the fluorescence at 517 nm of the sample, live controls, and dead controls, respectively.

4.2.3.2 *In Vitro* Cytotoxicity of CS Microspheres when Incorporated within 3D ESC Embryoid Bodies

Undifferentiated D3 murine embryonic stem cells (ESCs) were maintained on gelatin-coated tissue culture dishes in DMEM supplemented with 15% FBS and 10^3 U/mL leukemia inhibitory factor (LIF; Millipore, Billerica, MA). Embryoid bodies (EBs) were formed using a single-cell suspension by forced aggregation in AggreWell^{TM} 400 inserts (Stem Cell Technologies, Vancouver, CA) [332]. Briefly, 1.2 x 10^6 cells in 0.5 mL of medium were inoculated into AggreWell^{TM} inserts, containing approximately 1,200 wells per insert, and centrifuged at 200 RCF for 5 minutes to cluster cells in the wells. Subsequently, 200 µL of CS microsphere solution was added in a 4:1 microsphere-to-ESC ratio, and a second centrifugation was performed at 200 RCF for 5 minutes. After 24 hours of culture, aggregates were removed from the wells using a wide-bore pipette and transferred to suspension culture on a rotary orbital shaker (40 RPM) to maintain the homogeneity of the population [333].

CS microsphere incorporation within EBs was examined through histological sections of EBs after 3 days of culture. EBs were sampled and fixed in a 10% formalin

solution. The EBs were washed in PBS and resuspended in HistoGel (Thermo Richard-Allan Scientific, Kalamazoo, MI) prior to paraffin processing. Sections of 5 μm were stained using Safranin-O (Sigma-Aldrich) for GAG detection, Fast Green (Sigma-Aldrich) for cytoplasm, and Weigert's hematoxylin (Sigma-Aldrich) for cell nuclei and imaged using a brightfield microscope (Nikon Eclipse 80i).

EBs with and without CSMA microspheres were also stained with LIVE/DEAD stain (30 minutes) and imaged by laser-scanning confocal microscopy (LSM 510; Carl Zeiss, Oberkochen, Germany) to examine the cytotoxicity of CSMA microspheres on ESCs within 3D EBs.

4.2.4 Statistical Analysis

All values were reported as mean ± standard deviation. Statistical significance was determined using Minitab Statistical Software (v15, State College, PA) with a one-way analysis of variance (ANOVA) with Tukey's multiple comparison test ($p \leq 0.05$) for swelling ratio and cytotoxicity analysis and with a 2-sample t-test ($p \leq 0.05$) for growth factor loading efficiency and cumulative release. For swelling ratio analysis, the factor was hydrogel formulation. For cytotoxicity analysis, the factor was CS concentration. For growth factor loading efficiency and cumulative release, TGF-β1 and TNF-α cumulative release were compared at time 0 and day 5, respectively.

4.3 Results

4.3.1 Characterization of CS nano- and microspheres

4.3.1.1 Proton nuclear magnetic resonance spectroscopy

^{1}H NMR spectra indicate that APMAm was successfully conjugated to CS by the EDC reaction. CSMAm product synthesized in the presence of sulfo-NHS clearly showed the appearance of vinyl groups, found in the APMAm moiety (Figures 4.2b-d; peaks B_1 and B_2, corresponding to the labeled protons in Figure 4.1a). The modified CS product also possessed proton peaks C and E, as labeled in Figures 4.2b-c, which were present in APMAm. ^{1}H NMR spectra also suggested that the degree of modification increased with increased ratio of starting reagents per CS disaccharide equivalent. While vinyl groups were clearly visible in 4:1, 3:1, and 5:2 molar ratio reactions, vinyl peaks were barely distinguishable in the 7:10 reaction product (Figure 4.2c,d). At 1:5 molar ratio and when synthesized at 4:1 ratio without sulfo-NHS, vinyl peaks were not visible (Figure 4.2e,f). Similarly, peaks C and E did not appear in these reaction products. This indicated that despite a modification of the CS from the original reagent (as indicated by the light scattering data below), APMAm protons were not visible by ^{1}H NMR at 1:5 molar ratio and without sulfo-NHS. Successful methacrylation of CS to form CSMA via reaction with methacrylic anhydride was also verified by ^{1}H NMR.

4.3.1.2 Hydrogel formation and swelling

CSMAm crosslinking and swelling results in PBS also indicated that the degree of modification increased with increasing ratio of starting reagents per CS disaccharide equivalent. While 1:5 and 7:10 ratio reactions and the reaction without sulfo-NHS resulted in products that did not form robust hydrogels, at 5:2 molar ratio and above,

CSMAm crosslinked to form bulk hydrogels (Table 4.1). As the molar ratio increased from 5:2 to 3:1 to 4:1, swelling ratio significantly decreased from 39.8 ± 1.8 to 20.4 ± 1.2 to 12.8 ± 0.6, respectively. Decreased swelling is indicative of increased crosslinking density [123], likely as a result of higher degree of substitution of the methacrylamide in the EDC reaction. For comparison, crosslinked CSMA materials used for microsphere fabrication possessed a swelling ratio of 31.3 ± 3.6.

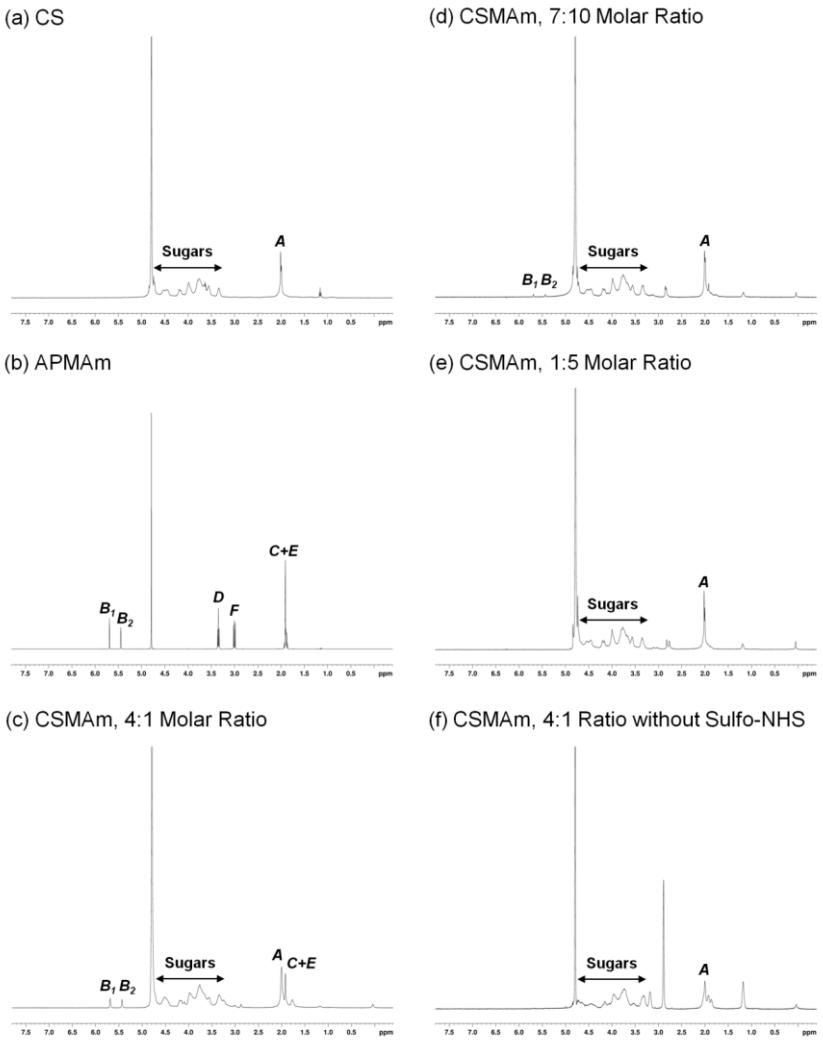

Figure 4.2. ^{1}H NMR spectra of (a) chondroitin sulfate, (b) APMAm, and reaction products synthesized at (c) 4:1, (d) 7:10, and (e) 1:5 molar ratios of APMAm, EDC, and sulfo-NHS to CS disaccharide, as well as (f) 4:1 ratio without sulfo-NHS. Protons are labeled according to corresponding diagrams in Figure 4.1a, and spectra indicated successful addition of methacrylamide moieties to the chondroitin sulfate.

Table 4.1. Molar ratios of reactants in EDC modification of CS and resulting swelling ratios of crosslinked hydrogels in PBS

CS (by disaccharide MW)	Molar Ratio to CS			Swelling Ratio
	APMAm	EDC	Sulfo-NHS	
2.5 mM	4:1	4:1	None	No Gel
2.5 mM	1:5	1:5	1:5	No Gel
2.5 mM	7:10	7:10	7:10	No Gel
2.5 mM	5:2	5:2	5:2	39.8 ± 1.8 *
2.5 mM	3:1	3:1	3:1	20.4 ± 1.2 *
2.5 mM	4:1	4:1	4:1	12.8 ± 0.6 *

* indicates statistically different from all other samples ($p \leq 0.05$)

4.3.1.3 Size distribution of CS micelles

Highly substituted CSMAm synthesized in the presence of sulfo-NHS did not appear to form stable micelles in an aqueous environment; therefore, only the 4:1 molar ratio without sulfo-NHS was used for micelle characterization. In order to accurately characterize the size of the CSMAm micelles, DLS analysis was performed. Micelle formation was examined by DLS for independent synthesis batches (n=4) and was verified to possess similar diameters. CSMAm micelles formed with an average diameter of 324.1 ± 8.5 nm in ddH_2O (Figure 4.3). A lower intensity collection of smaller CSMAm micelles appeared to form at 73.2 ± 4.4 nm, as well. Unmodified CS at the same concentration, did not produce detectable scattering by DLS. Zeta potential measurements indicated that the CS micelles possessed a zeta potential of -38.7 ± 1.1 mV.

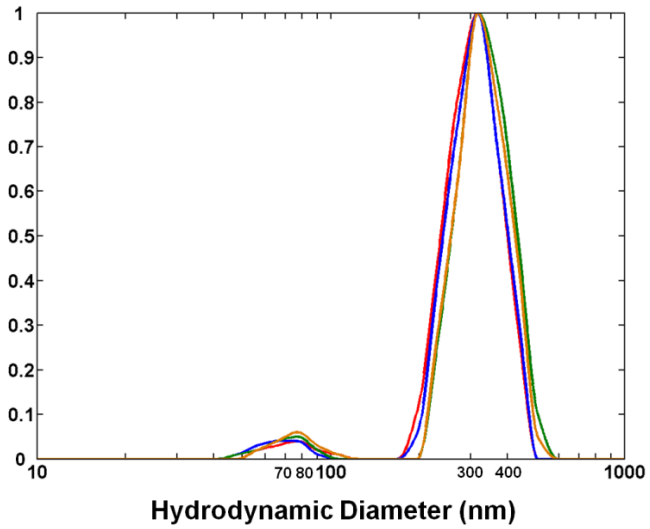

Figure 4.3. Size characterization of CSMAm micelles. Dynamic light scattering measurements of hydrodynamic diameter indicated that a bimodal distribution was present with average diameters of 324.1 ± 8.5 nm and 73.2 ± 4.4 nm. Particle sizing measurements were consistent for 4 separate samples (shown in red, blue, green, and orange).

4.3.1.4 Morphology and size distribution of CS microspheres

The CS microspheres had a smooth, round morphology, and Coulter Counter analysis indicated that the microspheres exhibited a unimodal size distribution with an average diameter of 4.3 ± 0.93 μm (Figure 4.4a,b). Additionally, the microparticles stained positively by DMMB for sulfated GAG, appearing purple (Figure 4.4a).

4.3.1.5 Complexation and release from CS microspheres

To verify that a model positively charged growth factor was able to electrostatically complex with CS, the ability of CS microspheres to bind TGF-β1 in solution was examined. When the CS microspheres were incubated overnight with 25 ng of TGF-β1 (500 μL at 50 ng/mL), 97.4 ± 1.3% of free TGF-β1 in solution became incorporated with the CS microspheres. Additionally, in the following release study, positively charged TGF-β1 exhibited no appreciable release after loading in CS microspheres. Only 1.4 ± 0.3% (0.34 ± 0.08 ng per mg microspheres) of loaded TGF-β1

was observed in solution at time 0, representing a low amount of unloaded or loosely affiliated growth factor and high loading efficiency, and only 0.2% (0.04 ng) additional release was detected over the following 5 days (Figure 4.4c). In contrast, negatively charged TNF-α, loaded identically to TGF-β1, demonstrated 17.7 ± 3.5% (4.43 ± 0.87 ng per mg microspheres) of loaded TNF-α in solution at time 0, representing a significantly lower loading efficiency than TGF-β1, and 43.9 ± 9.1% cumulative release (10.97 ± 2.27 ng) over the first 15 hours from CS microspheres with no further detectable release after 15 hours (Figure 4.4c). Cumulative release of TNF-α from 3 hours to 5 days, correcting for differences in loading, was significantly greater than TGF-β1 released. Overall, after 5 days, significantly more release of TNF-α was observed compared to TGF-β1.

4.3.2 Cytocompatibility of CS nano- and microspheres

4.3.2.1 *In vitro* cytotoxicity of CS micelles and microspheres on 2D BMSC monolayers

LIVE/DEAD staining of bovine BMSCs cultured in monolayer in the presence of increasing concentrations of CSMAm micelles and CSMA microspheres revealed that cells remained largely viable at the lowest concentrations of 1 and 10 mg/10^6 cells with 1.21 ± 0.14 and 0.77 ± 0.05 viability, respectively, for CSMAm micelles and 1.09 ± 0.11 and 1.12 ± 0.29 viability, respectively, for CSMA microspheres, compared to live controls which possessed normalized viabilities of 1.00 ± 0.08 and 1.00 ± 0.13 for CSMAm and CSMA experiments, respectively (Figure 4.5a). Viability of all 1 and 10 mg/10^6 cells samples was not statistically different from live controls. Cells appeared mostly green (live) and possessed a spread morphology, characteristic of BMSCs (Figure 4.5b,c). At 100 mg/10^6 cells, a significant decrease in viability was observed in the presence of CSMAm with 0.38 ± 0.06 viability, compared to live controls, as BMSCs

experienced a large decrease in cell density and spreading (Figure 4.5a,d), while viability did not significantly decrease in CSMA-containing medium (0.98 ± 0.16 viability; Figure 4.5a,d). At the 320 mg/10^6 cells concentration, very few cells remained adhered to the surface (Figure 4.5e) in both CSMAm and CSMA samples, resulting in a significant decrease in viability to 0.18 ± 0.07 and -0.05 ± 0.06, respectively.

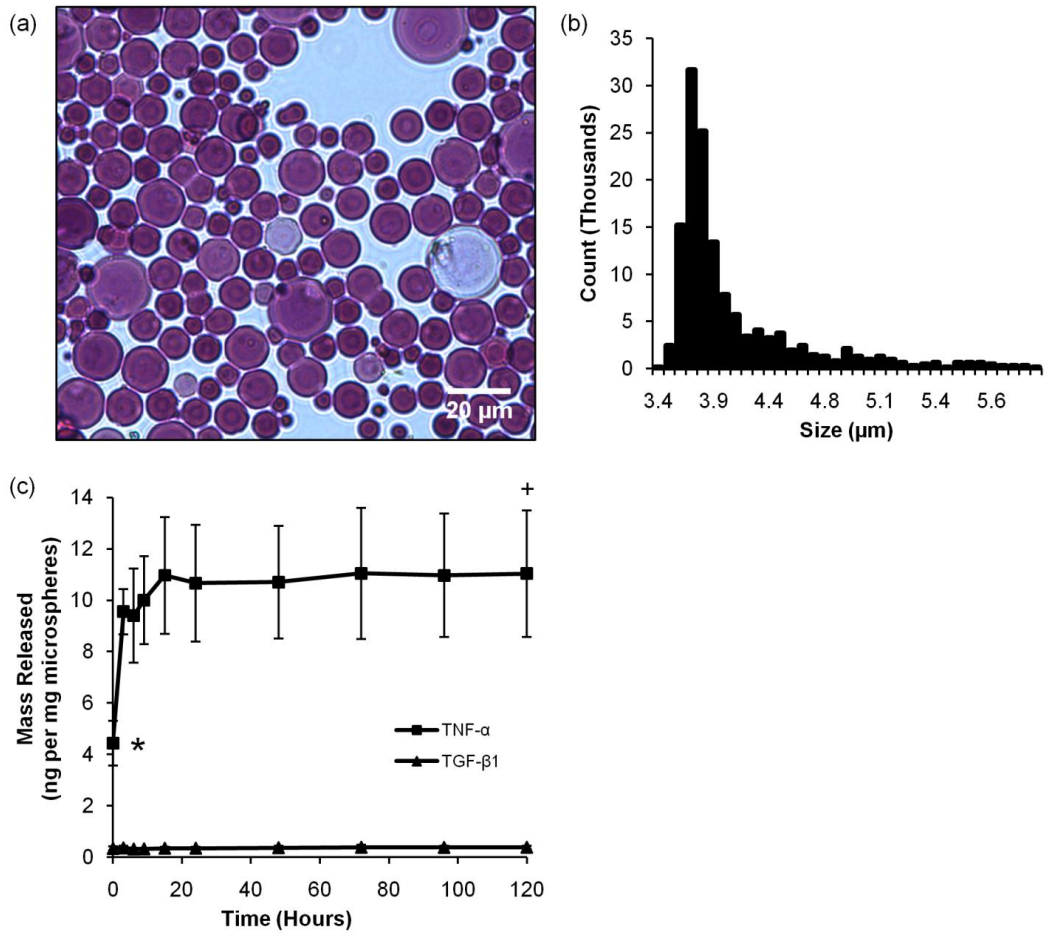

Figure 4.4. Characterization of CSMA microspheres. (a) CS microspheres possessed a smooth, rounded morphology and stained positively for sulfated GAG by DMMB (purple). Scale bar = 20 µm. (b) CS microspheres exhibited a unimodal distribution with an average diameter of 4.3 ± 0.93 µm. (c) Positively charged TGF-β1 (triangles) experienced very little release from negatively charged CS microspheres after 5 days; however, negatively charged TNF-α (squares) experienced large early release within 15 hours. * indicates statistically different loading efficiency (0 hours) compared to TGF-β1 loaded samples. + indicates statistically different cumulative release from 3 hours to 5 days compared to TGF-β1 release samples ($p \leq 0.05$).

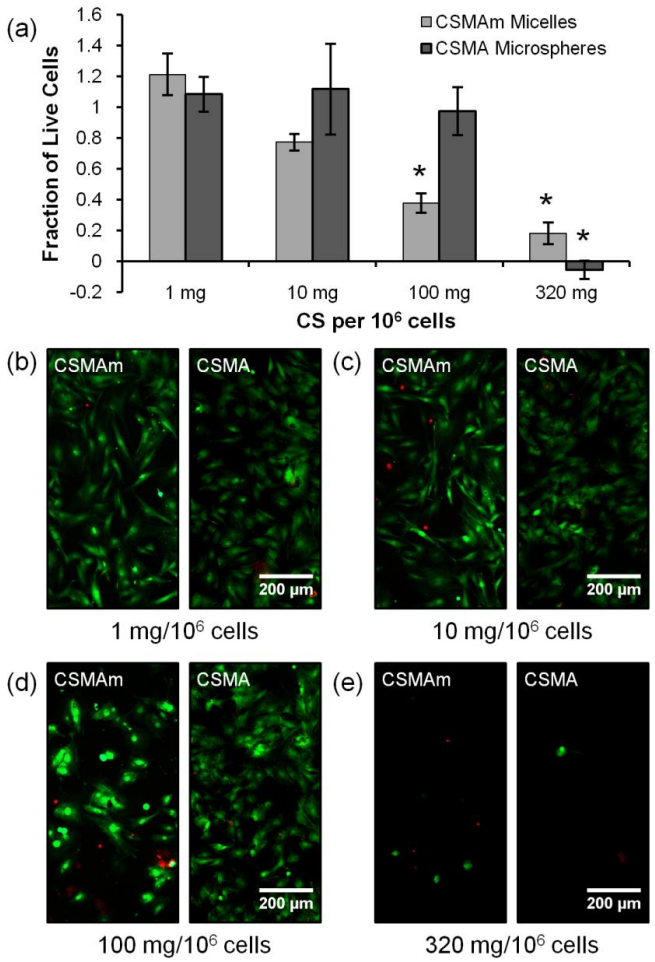

Figure 4.5. LIVE/DEAD cytotoxicity analysis of bovine marrow stromal cells cultured in 2D monolayer in the presence of CSMAm micelles and CSMA microparticles. (a) Fraction of live cells per well compared to live controls, as determined by fluorescence values recorded at 517 nm wavelength. LIVE/DEAD fluorescence images in the presence of (b) 1 mg, (c) 10 mg, (d) 100 mg, and (e) 320 mg CSMAm or CSMA per 10^6 cells for 24 hours. Live cells appeared green, while dead cells appeared red. Scale bar = 200 µm. * indicates statistically different from live controls ($p \leq 0.05$).

4.3.2.2 *In vitro* cytotoxicity of CS microspheres when incorporated within 3D ESC embryoid bodies

CS microspheres were successfully incorporated within embryoid bodies using the forced aggregation method described. The microspheres stained positively in histological sections for sulfated GAG by Safranin-O, appearing red (Figure 4.6b).

Surrounding ESCs also appeared to be morphologically normal, compared to control EBs (Figure 4.6a), with no signs of cell death or adverse cell response after 3 days, suggesting that the incorporation of CS microspheres within 3D stem cell aggregates does not negatively impact the extracellular microenvironment. Additionally, LIVE/DEAD staining of EBs observed similar degrees of viability with CSMA microspheres incorporated (Figure 4.6d), when compared to control EBs (Figure 4.6c), indicating that ESCs remained largely viable when CSMA microspheres were incorporated within 3D EBs.

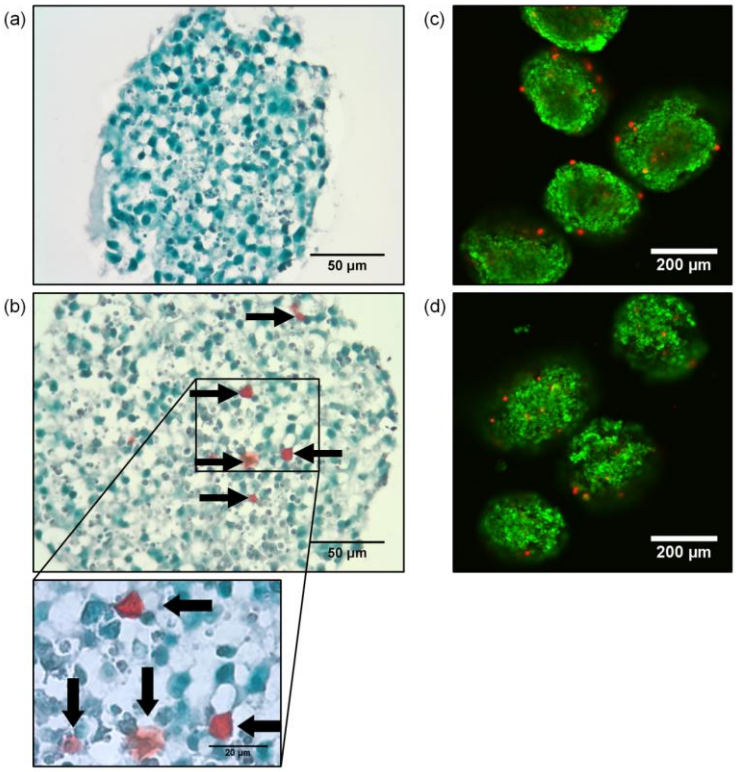

Figure 4.6. Cytotoxicity of mouse embryonic stem cells with CS microspheres incorporated within 3D embryoid bodies. (a) Cells in embryoid bodies without CS microspheres. (b) CS microspheres stained positively for sulfated GAGs by Safranin-O (red stain; black arrows). Surrounding cells appeared morphologically normal, with no signs of cell death after 3 days. Scale bar = 50 µm. A boxed region of cells and microspheres is also shown at higher magnification. Scale bar = 20 µm. (c) LIVE/DEAD fluorescence images of embryoid bodies without CS microspheres and (d) with incorporated CS microspheres, showed similar degrees of viability. Live cells appeared green, while dead cells appeared red. Scale bar = 200 µm.

4.4 Discussion

In the first part of this study, a model reaction using EDC (and sulfo-NHS) to conjugate a methacrylamide moiety to CS was used to determine the effects of degree of modification on the properties of the resulting GAG-based material. This approach can be applied to any polysaccharide possessing a carboxylic acid moiety, including dermatan sulfate, heparin, heparan sulfate, and hyaluronic acid [334]. The resulting CSMAm material demonstrated increasing degrees of modification with greater molar ratios of starting reagents, resulting in higher degrees of crosslinking, as verified by ^{1}H NMR data and significantly decreased swelling in bulk hydrogels (Figure 4.2 and Table 4.1).

Interestingly, at lower degrees of modification, CSMAm self-assembled into micelles in aqueous solution. When reacted at 1:5 molar ratio and without sulfo-NHS, proton peaks associated with APMAm were not visible by ^{1}H NMR (Figure 4.2e,f), though a modification of CS was apparent by the formation of nanospheres, as confirmed by DLS analysis (Figure 4.3). It is likely that the APMAm groups were not visible by ^{1}H NMR, because these hydrophobic moieties were internalized within the micelle structure that formed in the NMR solvent (water). Similar results were observed in ^{1}H NMR spectra of CS-PLLA micelles in D_2O, where internal protons were not visible due to limited mobility within the micelle core [324].

In this study, EDC chemistry was used to confirm that the degree of conjugation, and resulting molecular structure, could be controlled by altering the ratios of the starting reactants during synthesis; however, in order to efficiently scale up the size of the reaction while maintaining crosslinking capabilities to form microparticles, methacrylate

groups were added to CS by reacting the GAG with methacrylic anhydride. Resulting CSMA was crosslinked in a water-in-oil, single-emulsion to form CS microspheres. While the microspheres described here had an average diameter of 4.3 ± 0.93 μm (Figure 4.4a,b), the size of the microparticles could be easily modified by altering the emulsion conditions, such as speed of mixing and CSMA concentration, prior to crosslinking [335]. The results of this work suggested that by altering the degree of conjugation, CS-based materials can be developed that can be presented to cells on different size scales, including nanoscale micelles and larger microspheres, as well as controlled degree of crosslinking within particles. Therefore, this set of materials provides a versatile platform to explore presentation and release of various growth factors because the basic chemistry of the delivery vehicle is not altered, while a wide range of particle sizes is achieved.

Zeta potential results indicated that CSMAm micelles possessed of zeta potential of -38.7 ± 1.1 mV, confirming that the micelles were negatively charged and stable in solution and suggesting that these micelles may have application in delivery of various cationic factors. Similarly, CSMA microspheres were shown to electrostatically complex with TGF-β1 at physiological pH. TGF-β1 was capable of a higher loading efficiency than TNF-α1, as indicated by the time 0 data point, despite identical loading conditions, likely due to electrostatic interactions. Considerable release of TNF-α was also observed from CS microspheres over the first 15 hours; however, minimal TGF-β1 release was seen over 5 days, indicating that TGF-β1 remained bound to the CS microspheres during this time (Figure 4.4c). TGF-β1 possesses an isoelectric point (pI) of 9.5 and thus was selected to represent a positively charged growth factor [276], while TNF-α has a pI of 5.3, making it negatively charged at physiological pH [336]. Such results are comparable

to other CS-based hydrogels and microspheres, which have been reported to retain positively charged lysozyme, aprotonin, and vasopressin [325, 337]. TGF-β isoforms are important for a number of processes in mammalian development [338-339], and have been particularly implicated in chondrogenesis *in vivo* [340] and *in vitro* [341-342], making this a relevant growth factor to investigate for directing differentiation of stem cells. While 100% of loaded TNF-α was not released over the time course of this study, as might be expected with little affinity between the cytokine and the CS matrix, this could be explained by the potential degradation of the protein over time in solution, resulting in artificially low ELISA readings after release [343].

Cumulative release data from these experiments suggested that significantly more TNF-α was liberated than TGF-β1, thus supporting the use of these materials for controlled delivery via electrostatic interaction with growth factors. Delivery kinetics can be further tailored by customizing the size and crosslinking density of the particles by altering the synthesis and fabrication parameters [344-345]. In combination with the release of growth factors through dissociation from the CS-based carrier, these biomaterial carriers could potentially be enzymatically cleaved by chondroitinase, a naturally secreted enzyme that digests chondroitin sulfate [346], thereby providing a second method for localized delivery.

In addition to control over size and the potential for degradation, the CS-based particles presented here are particularly advantageous because both types of particles are fabricated almost entirely from only CS molecules, for nearly uniform biochemical presentation to target cells. In previous work, CS has been combined with synthetic polymers like PLLA and PLGA, as well as natural materials including chitosan, alginate,

and gelatin [324, 326, 347-349] to produce micron-scale particles. However, to the best of our knowledge, this is the first time that CS microspheres and micelles have been synthesized without significant modification with other large polymers, making this system beneficial for specifically probing GAG-stem cell interactions.

While CS plays a role in many developmental processes, CS delivery vehicles may be particularly useful to promote chondrogenesis. CS-containing proteoglycans versican and perlecan regulate mesenchymal condensation and growth factor signaling during cartilage development [14-15], and culture in CS-containing hydrogels upregulated expression and production of chondrocytic ECM by encapsulated mesenchymal stem cells [8]. Therefore, in the future, the use of CS-based materials for controlled growth factor delivery may be advantageous as a means to direct cell differentiation to promote regeneration of cartilaginous tissues.

As a next step in the development of these materials as bioactive factor delivery vehicles, the cytotoxicity of CS was investigated *in vitro* using bovine BMSCs and murine ESCs. BMSCs and ESCs were chosen for their multipotent and pluripotent potential, respectively [77, 350]. In this study, BMSC monolayers were cultured with the presence of CS micelles and microspheres in the media for 24 hours to determine cytotoxicity in 2D, and CS microspheres were incorporated into ESC embryoid bodies for 3 days to examine cytocompatibility within 3D cell spheroids. ESCs are often cultured and differentiated within embryoid bodies; however, these dense, multicellular spheroids possess numerous boundaries to diffusion [322]. CS particles could potentially be utilized to deliver growth factors throughout the EB to improve homogeneous differentiation, compared to diffusion of soluble factors from the medium [322].

BMSCs, cultured in 2D with moderate concentrations of CSMAm micelles and CSMA microspheres of 1 and 10 mg/10^6 cells, remained viable with no statistical difference from live controls (Figure 4.5a-c), while CSMA microspheres also remained cytocompatible up to 100 mg/10^6 cells. Similarly, ESCs surrounding CS microspheres incorporated into EBs appear to be morphologically healthy with no apparent cell death (Figure 4.6), suggesting that CS microspheres could potentially be used to deliver growth factors within dense cell aggregates. At the highest concentration tested, 320 mg/10^6 cells (as well as 100 mg/10^6 cells for CSMAm), BMSCs experienced statistically decreased viability after 24 hours with the presence of CSMAm micelles and CSMA microspheres in the culture media (Figure 4.5a,d-e). Cell death may have resulted at high concentrations due to endocytosis of nanoscale CSMAm micelles by cells [323], or the high negative surface charge of CS particles may have interacted with receptors on the cell membrane [351] or altered the osmotic pressure of the medium, though these mechanisms were not further explored in this study. The range of concentrations in these studies, equivalent to 0.064, 0.64, 6.4, and 20.5 mg/ml, included and exceeded previously reported values used for cytotoxicity testing of CS-based microspheres and were defined according to ASTM International Standards F1903 and F813 regarding cytotoxicity testing of particles and materials, respectively [324, 326, 352-353]. Only 1 and 10 mg CS/10^6 cells samples (0.064 and 0.64 mg/ml, respectively), which experienced no significant difference in cell viability from live controls, fell within previously reported ranges for cytotoxicity testing (0-5 mg/mL) of CS-PLLA microspheres [326]. Taken together, these results indicated that CS materials did not appear to affect the morphology of stem cells when cultured at moderate concentrations.

Overall, these studies have demonstrated the formation of novel CS-based particles over a range of size scales with significant potential for use as ECM-derived carriers for delivery of charged growth factors to promote stem cell differentiation.

4.5 Conclusions

The results of these studies demonstrated that CS chains were successfully modified to form amphiphilic self-assembling CS micelles on a nanoscale (~73 nm and ~320 nm), as well as microscale fabrication of CS microspheres (~4 μm) for a wide range of sizes, and that CS microspheres retained their ability to bind positively charged growth factors. This flexibility in particle size can potentially provide a large degree of control for release of cationic factors from these CS materials, and the use of naturally-derived polysaccharide matrix without modification by other polymers may be especially advantageous in better understanding the role of GAGs in cell differentiation. Therefore, CS nano- and microspheres with the ability to deliver growth factors via electrostatic interaction provides a controlled, yet extremely versatile platform to further explore means to direct differentiation of stem cells for a variety of applications in tissue engineering and regenerative medicine.

CHAPTER 5

CHEMICAL DESULFATION OF CHONDROITIN SULFATE FOR CONTROLLED GROWTH FACTOR RELEASE FROM GAG-BASED HYDROGELS

5.1 Introduction

The highly sulfated GAGs heparin and heparan sulfate are known to play important roles in sequestration of positively charged growth factors *in vivo*, including basic fibroblast growth factor (bFGF), insulin-like growth factor (IGF), vascular endothelial growth factor (VEGF), platelet-derived growth factor (PDGF), and transforming growth factor-β (TGF-β) [263, 272, 319]. Specifically, sulfate groups contribute to the highly negative fixed charge density of sulfated GAGs and their associated proteoglycans, facilitating electrostatic interactions with basic amino acid residues in positively charged growth factors. Due to its high sulfation, heparin possesses a stronger affinity than less sulfated GAGs, including chondroitin sulfate and the nonsulfated GAG hyaluronan [268, 354-357], and selective desulfation of heparin modulates binding in a sulfation-dependent manner and with special importance of 2-O-sulfation for binding [265-267, 269-271, 358-359].

While heparin binding has been investigated in detail *in vivo* and *in vitro*, growth factor interactions with chondroitin sulfate (CS) have not been as well characterized. CS is especially prominent in cartilaginous tissues, as part of aggrecan proteoglycan, and while CS is known to play an important role in maintaining osmotic pressure within cartilaginous tissues, its role in growth factor signaling is currently not well understood.

Despite its lower degree of sulfation, compared to heparin, CS has also been shown to sequester several "heparin-binding" growth factors *in vitro*, and these electrostatic interactions have been exploited for controlled delivery and sustained release of growth factors, including PDGF-BB and IGF-1 [22, 262, 264]. Additionally, oversulfation of CS has been shown to enhance binding affinity in a sulfation-dependent manner, including to the chondrogenic growth factor TGF-β1, suggesting that sulfation regulates CS interactions with growth factors [25, 261].

While oversulfation of CS has been investigated to determine the role of sulfates in growth factor interactions, the nonsulfated GAG hyaluronan has commonly been used as a nonsulfated control. While hyaluronan is structurally similar to CS, hyaluronan plays very different roles than CS *in vivo*, and hyaluronan has activity independent of CS, including roles in ECM interactions, growth factor signaling, and known cell surface receptors like CD44 and receptor for hyaluronan-mediated motility (RHAMM) [360-364]. Use of a nonsulfated chondroitin variant would facilitate proper comparison across varying degrees of sulfation, while maintaining a consistent polysaccharide backbone and structure and only altering the sulfation pattern and resulting charge density of CS-based materials. The role of a nonsulfated chondroitin in growth factor binding and signaling has yet to be investigated; therefore, to further investigate the role of sulfation in interactions with growth factors, CS was chemically desulfated via acid methanol treatment to produce chondroitin. Desulfated chondroitin was then characterized for sulfation pattern and total charge to ensure that sulfates were removed without significant modification of the remaining GAG backbone.

As a naturally-derived cartilaginous ECM molecule, CS is a promising material for cartilage differentiation and repair. Additionally, the natural ability of CS to sequester growth factors may facilitate interaction with chondrogenic growth factors, such as TGF-β1, IGF-1, and various bone morphogenetic proteins (BMPs), while controlled desulfation of CS materials would offer further control over growth factor retention and release to promote differentiation of mesenchymal stem cells (MSCs). To examine the role of sulfation in growth factor interactions, CS and chondroitin were methacrylated and crosslinked in order to form bulk CS and chondroitin-based hydrogels containing varying ratios of CS and chondroitin to alter the relative degree of sulfation within the constructs. Release of chondrogenic growth factor TGF-β1 from CS and chondroitin hydrogels over 7 days and sequestration of soluble TGF-β1 out of solution were determined to examine the role of sulfation on interactions with TGF-β1.

5.2 Materials and Methods

5.2.1 Desulfation of Chondroitin Sulfate

Chondroitin sulfate was desulfated using an acidic methanol treatment for up to 7 days per established protocols [365-366]. Chondroitin sulfate A (primarily chondroitin-4-sulfate, Sigma-Aldrich, St. Louis, MO) or chondroitin sulfate C (primarily chondroitin-6-sulfate, Wako Chemicals USA, Richmond, VA) was stirred at 5.0 mg/mL in methanol (VWR, Radnor, PA) containing 0.5% v/v acetyl chloride (Acros Organics, Geel, Belgium). CS was centrifuged and acidic methanol was replaced either on days 1, 2, and 3 for a 3-day reaction or on days 1, 3, and 7 for a 7-day reaction to produce a methyl ester of chondroitin (Figure 5.1). The product was then dissolved in 20 mL distilled, deionized

water (ddH_2O) per gram of starting CS before precipitation in an excess of ethanol. The methyl ester of chondroitin was washed in ethanol and ethyl ether (Fisher, Waltham, MA), vacuum dried at <5 mmHg, and stored at 4 °C.

Methyl ester of chondroitin was demethylated at 25 mg/mL in 0.1 M potassium hydroxide (KOH, Fisher) for 24 hours to produce chondroitin (Figure 5.1). The chondroitin product was then neutralized in 4 mL 100 mg/mL potassium acetate (Fisher) in 10% v/v acetic acid (VWR) per gram of starting product, and precipitated in an excess of ethanol. Chondroitin was washed in ethanol and ethyl ether, vacuum dried, and stored at 4°C until use.

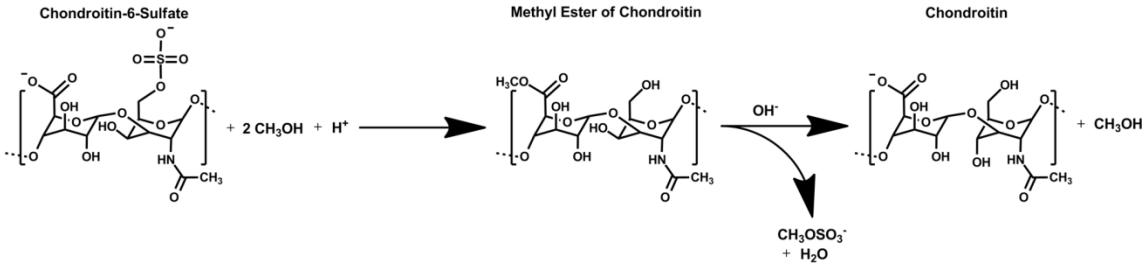

Figure 5.1. Desulfation reaction of chondroitin sulfate. Chondroitin sulfate was desulfated in acidic method for up to 7 days to form a methyl ester of chondroitin. The methyl ester was demethylated in potassium hydroxide for 24 hours to yield chondroitin.

5.2.2 Characterization of Desulfated Chondroitin

5.2.2.1 Dimethylmethylene Blue Assay

Removal of sulfate groups in chondroitin was confirmed by dimethylmethylene blue (DMMB) assay for sulfated GAGs [302]. Standard curves from 0 to 50 µg/mL chondroitin or chondroitin sulfate were assayed according to established protocols by DMMB, and absorbance was measured at 520 nm in a plate reader (SpectraMax M2e; Molecular Devices, Sunnyvale, CA) as a measure of sulfation. The slopes of the

chondroitin standard curves were compared to the CS standard curve to determine percent desulfation of the chondroitin product.

5.2.2.2 Fourier Transform Infrared Spectroscopy

Because chondroitin sulfate C after 7 days in acidic methanol showed the greatest degree of sulfation, that chondroitin product was used in all future experiments, and compared to unmodified CS-C. To further verify the removal of sulfate groups in chondroitin, CS and chondroitin materials were analyzed by Fourier transform infrared (FTIR) spectroscopy. A 3 mg/mL solution of CS and desulfated chondroitin in deuterated water (D_2O; Sigma-Aldrich) were spin coated onto a silicon crystal and FTIR was measured using a Bruker Vertex 70 ATR-FTIR spectrometer (Billerica, MA) with atmospheric compensation.

5.2.2.3 Strong Anion Exchange High Performance Liquid Chromatography

Samples were analyzed by strong anion exchange high performance liquid chromatography (SAX-HPLC) by the University of Georgia Complex Carbohydrate Research Center (CCRC) to determine the disaccharide composition and average charge density of the CS and chondroitin materials. A 1 mg/mL GAG solution of either CS or chondroitin in 50 mM ammonium acetate (NH_4OAc) buffer, pH 8 was digested into disaccharides by 0.1 mU/mL of chondroitinase ABC (Sigma-Aldrich) at 37°C for 24 hours. The chondroitinase enzyme was inactivated by heating to 100°C for 2 minutes, and the sample was centrifuged prior to HPLC analysis.

SAX-HPLC was carried out on an Agilent 1200 system (Santa Clara, CA) using a 4.6×250 mm Waters Spherisorb analytical column (Milford, MA) with 5 μm particle size at 25°C, using an injection volume of 10 μL and a flow rate of 1.0 mL/min. The 2.5 mM

sodium phosphate (Na_3PO_4) solvent at pH 3.5 was transitioned from a concentration of 0.036 M NaCl up to 1.2 M NaCl over the course of 55 minutes, gradually increasing the ionic strength of the buffer and causing elution of the disaccharides based on electrostatic charge, with more negatively charged disaccharides eluting later.

Disaccharide detection was performed by post-column derivatization. A 1:1 mixture of 0.25 M NaOH and 1% 2-cyanoacetamide was added to the eluent from the column from a binary HPLC pump at 0.5 mL/min. The eluent was then heated to 120°C in a 10-m reaction coil, followed by cooling in a 50-cm cooling coil, and directed into a Shimadzu fluorescence detector (excitation: 346 nm, emission: 410 nm; Kyoto, Japan). Based on these results, a predictive model was used to calculate average charge, based on known disaccharide structures containing negatively charged sulfate and carboxylate groups.

5.2.2.4 Size Exclusion High Performance Liquid Chromatography

CS and chondroitin samples were also analyzed by size exclusion high performance liquid chromatography (SEC-HPLC) by the University of Georgia CCRC to determine the average molecular weight of the CS and chondroitin chains. Solutions of CS or chondroitin were prepared at 2 mg/mL in 50 mM sodium sulfate (Na_2SO_4) buffer, pH 5.0, and partially depolymerized heparin fractions (4.2, 9.0, 12.0, 15.0, and 20.0 kDa) were used as molecular weight standards. Separations were carried out using a TSKGel G3000SWXL column (Tosoh Bioscience, Stuggart, Germany, 7.8 mm ID x 30 cm) and a TSKGel G2000SWXL column (7.8 mm ID x 30 cm), connected in series, on an Agilent 1200 LC instrument using refractive index detection with an injection volume of 50 μL and a flow rate of 0.5 mL/min.

A standard curve was constructed based on the molecular weights and elution volumes of the heparin standards. The data were baseline corrected, and the retention times were converted to molecular weights using the standard curve. The weight fraction w_i of each data point was calculated by dividing the detector response by the sum of detector responses over the whole peak width. The weight average molecular mass was calculated as $M_w=\sum w_i M_i$, and the number average molecular mass was calculated as $M_n=1/\sum(w_i/M_i)$. Polydispersity index (PI) was calculated as $PI=M_w/M_n$.

5.2.3 Synthesis of Crosslinkable Hydrogel Materials

5.2.3.1 PEG-DA Synthesis

Poly(ethylene glycol)-diacrylate (PEG-DA) polymers were synthesized according to established protocols [191]. 3,400 Da (M_n) PEG (Sigma-Aldrich) was solubilized in distilled, anhydrous methylene chloride (MeCl, Fisher) to produce a 60% (m/v) solution. Triethylamine (TEA, Sigma-Aldrich) was added to the dissolved PEG, and acryloyl chloride (AcCl, Sigma-Aldrich) was slowly added dropwise at 2:1 AcCl:PEG and 1:1 AcCl:TEA molar ratios to create a 40% w/v solution. The reaction was allowed to proceed at room temperature under nitrogen gas, and the reaction was left stirring overnight to ensure completion. 2 M potassium carbonate (K_2CO_3, Fisher) was used at a 2:1 K_2CO_3:AcCl molar ratio to extract TEA to the aqueous phase. The organic phase was allowed to separate from the aqueous phase, and anhydrous magnesium sulfate ($MgSO_4$, Fisher) was used to remove any remaining aqueous phase from the solution. PEG-DA was then precipitated in ethyl ether and filtered, followed by vacuum drying at <5 mmHg. Dry polymers were stored in sealed containers at -20°C until use.

5.2.3.2 OPF Polymer Synthesis

Oligo(poly(ethylene glycol) fumarate) 10K polymers were synthesized according to established protocols [367]. 10,000 Da (M_n) PEG (Sigma-Aldrich) was azeotropically distilled in toluene (Fisher) and then combined with distilled, anhydrous MeCl to produce a 40% (v/v) solution. Fumaryl chloride (FuCl, Sigma-Aldrich) and TEA were slowly added dropwise over a period of 2 hours at 0.9 FuCl:PEG and 1:2 FuCl:TEA molar ratios. During this time, the reaction was allowed to proceed at 0°C under nitrogen gas, after which the reaction was left stirring for 72 hours under nitrogen at room temperature to ensure reaction completion. After rotovaporing (Buchi, Flawil, Switzerland) to remove excess MeCl, the resulting polymer was recrystallized twice with ethyl acetate (Fisher) and washed three times in ethyl ether, followed by vacuum drying at <5 mmHg. Dry polymers were stored in sealed containers at -20°C before use.

5.2.3.3 Methacrylation of Chondroitin Sulfate and Chondroitin

CS and chondroitin were methacrylated with glycidyl methacrylate per established protocols [368]. CS or chondroitin was dissolved at 1% w/v in a 50:50 mixture of acetone (VWR) and ddH_2O and allowed to stir at room temperature overnight. A 20-fold molar excess of TEA per CS or chondroitin disaccharide was added to the solution, and a 20-fold molar excess of glycidyl methacrylate (GMA, Sigma-Aldrich) per disaccharide was added dropwise to the solution. The reaction was allowed to stir at room temperature for 24 hours to produce CS-methacrylate (CS-MA) (Figure 5.2) and chondroitin-methacrylate (Ch-MA). The resulting products were dialyzed first in 50:50 acetone:water for 24 hours (1,000 Da MWCO), and then in distilled water (dH_2O) for 2 days to remove unreacted reagents. The methacrylated products were lyophilized

(Labconco, Kansas City, MO) for 4 days to produce a dry product, and stored at -20°C until use.

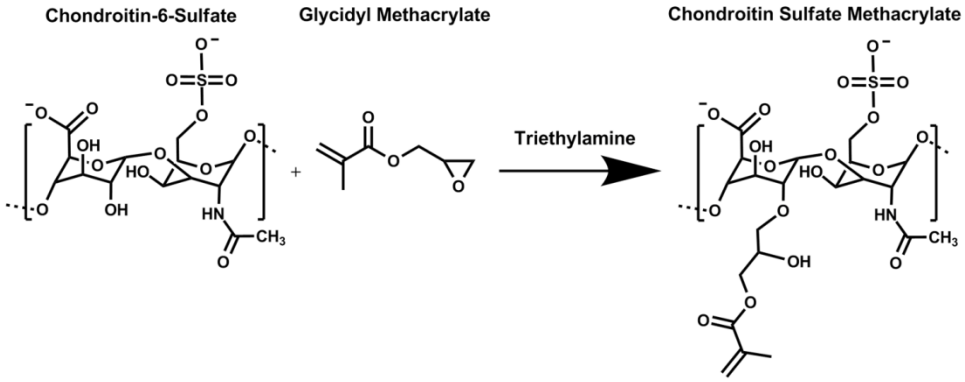

Figure 5.2. Chondroitin sulfate methacrylation reaction. Chondroitin sulfate was methacrylated with glycidyl methacrylate in 50:50 acetone:ddH_2O for 24 hours in the presence of triethylamine to form chondroitin sulfate methacrylate (CS-MA).

5.2.4 Characterization of Crosslinkable Hydrogel Materials

5.2.4.1 Gel Permeation Chromatography

PEG-DA (M_n = 3760 ± 50, PI = 1.1 ± 0.02), PEG 3.4K (M_n = 3440 ± 30, PI = 1.1 ± 0.001), OPF 10K (M_n = 28,100 ± 760, PI = 5.2 ± 0.4), and PEG 10K (M_n = 12,900 ± 210; PI = 1.1 ± 0.002) were characterized via gel permeation chromatography as previously reported [174]. The molecular weight distribution of PEG-based polymers was characterized by gel permeation chromatography (Prominence; Shimadzu) equipped with a refractive index detector (Shimadzu). Polymer samples were dissolved in chloroform, filtered (0.45 μm filter, Whatman, Maidstone, UK), and injected into a column (Waters) at a flow rate of 1 mL/min (n=3).

5.2.4.2 Proton Nuclear Magnetic Resonance

Proton nuclear magnetic resonance (^{1}H NMR) was utilized to determine the degree of the conjugation of the GMA groups to the CS and chondroitin chains. The

initial components (CS, chondroitin, and GMA) and resulting modified products (CS-MA and Ch-MA) were solubilized in D_2O, and ^1H NMR was measured on a Bruker AMX-400 spectrometer at 400 MHz. The resulting spectra were analyzed by calibrating the region from 4.18-3.75 ppm according to the known number of protons in the chondroitin sulfate backbone, providing an internal standard to determine the degree of modification by the methacrylation reaction.

5.2.4.3 Degradation of Modified Chondroitin Sulfate and Chondroitin Materials

To determine if the ability of chondroitinase enzyme to degrade CS was affected by either desulfation, methacrylation, or crosslinking, the degradation of modified CS-MA and Ch-MA was determined in solution and in crosslinked hydrogels. Soluble chondroitinase activity was assayed per established protocols [369-371]. 2 mg/mL CS-MA and chondroitin-MA solutions in a buffer of 250 mM tris(hydroxymethyl)aminomethane (Tris, Sigma-Aldrich), 300 mM sodium acetate (Sigma-Aldrich) with 0.05% bovine serum albumin (BSA, Sigma-Aldrich) at pH 8.0 were incubated with 0.06 U/mL chondroitinase ABC. Accumulation of the $\Delta^{4,5}$-unsaturated disaccharide degradation product at 37°C was monitored by measuring the increase in absorbance at 232 nm UV light in a UV-transparent 96-well assay plate (Corning Incorporated, Corning, NY) by a plate reader (SpectraMax M2e; Molecular Devices) every minute for 1 hour, compared to CS-MA and Ch-MA blanks without enzyme (n=3).

To determine the ability of crosslinked CS-MA and Ch-MA hydrogels to degrade in the presence of chondroitinase enzyme, 100% CS-MA or 100% Ch-MA hydrogels at 90 wt% H_2O were crosslinked in 6 mm diameter, 1 mm deep cylindrical molds with

0.018 M ammonium persulfate (APS, Sigma-Aldrich) and tetramethylethylenediamine (TEMED, Sigma-Aldrich) for 10 minutes at 37 °C, and swelled overnight in phosphate-buffered saline (PBS). CS-MA and Ch-MA hydrogels were then transferred into 0.125 U/mL chondroitinase ABC in 250 mM Tris, 300mM sodium acetate buffer with 0.05% BSA at pH 8.0 and incubated at 37°C. Complete degradation was determined when the bulk hydrogel was no longer visible in solution (n=3).

5.2.4.4 Swelling of GAG/PEG Hydrogels

Polymer solutions containing a 1:1 ratio of OPF 10K:PEG-DA and either 10% or 50% CS-MA or Ch-MA at 90% water content in PBS were crosslinked in 6 mm diameter, 1 mm deep cylindrical molds with 0.018 M APS/TEMED thermal initiator system for 10 minutes at 37°C, and swelled overnight in PBS. A 60% PEG-DA:40% OPF mixture that possessed similar swelling properties to 50% Ch-MA formulations was used as a PEG-only swelling control for 50% Ch-MA. After 1 day swelling in PBS, the wet weight of crosslinked hydrogels was recorded, and following lyophilization overnight, dry weight was recorded. Swelling ratio was calculated as wet weight/dry weight (n=5).

As an estimate of osmotic pressure based on fixed negative charge in GAG hydrogels, Donnan swelling pressure was estimated in a 0.15 M NaCl solution at 37°C. According to Donnan equilibrium, electroneutrality, and osmotic pressure laws, Donnan osmotic pressure is calculated by the equation:

$$\pi = RT[\sqrt{(c^F)^2 + 4(c^*)^2} - 2c^*]$$

where π is the Donnan osmotic pressure, R is the universal gas constant (8.314 L kPa K^{-1} mol^{-1}), T is the absolute temperature (310 K), c^F is the fixed charge density in mol of charge per L of interstitial fluid, and c^* is the salt concentration of the external electrolyte

solution (0.15 M NaCl) [372-374]. Fixed charge density was calculated based on the GAG disaccharide concentration in the hydrogels, as well as the average charge per disaccharide, determined by SAX-HPLC, as described in Section 5.2.2.3.

5.2.5 Interaction of CS and Chondroitin Hydrogels with TGF-β1

5.2.5.1 Release of TGF-β1 from CS and Chondroitin Hydrogels

To investigate the role of sulfate moieties in the electrostatic complexation and release of positively charged TGF-β1, 1:1 OPF:PEG-DA hydrogels containing 10% CS-MA, 50% CS-MA, or 50% Ch-MA (90 wt% H_2O) were sterilely crosslinked in 6 mm diameter, 1 mm deep cylindrical molds with 0.018 M APS/TEMED for 10 minutes at 37°C, and swelled overnight in PBS. Hydrogels were then lyophilized for 24 hours, and loaded by reswelling with 15 µL of 12.5 µg/mL TGF-β1 solution (Peprotech, Rocky Hill, NJ) for 16 hours at 4°C. Loading correlated to a ~1:500,000 TGF-β:disaccharide molar ratio in 50% GAG hydrogels and to a ~1:100,000 TGF-β:disaccharide molar ratio in 10% CS. Hydrogels were then incubated at 37°C in 500 µL 1% BSA in PBS for 7 days. At 0, 5, 12, and 24 hours, and after 2, 3, 5, and 7 days, the supernatant was sampled and analyzed for TGF-β1 content by enzyme-linked immunosorbent assay (ELISA, R&D Systems, Minneapolis, MN). Cumulative release was calculated for each hydrogel over 7 days (n=4).

5.2.5.2 Formation of 50% Total GAG Hydrogels with Varying Sulfation

To demonstrate that hydrogels can be fabricated with a constant GAG content and varying degrees of sulfation, CS-MA and Ch-MA were incorporated into 1:1 OPF:PEG-DA hydrogels at varying mass ratios while maintaining total GAG content constant at 50 wt%, according to Table 5.1. A 60% PEG-DA:40% OPF mixture that possessed similar

swelling properties to 50% Ch-MA formulations was used as a PEG-only swelling control for 50% Ch-MA. Polymer was dissolved in PBS for an initial water content of 90% w/w, and all macromer solutions were filter sterilized through a 0.2 μm pore filter (Nalgene, Rochester, NY). 30 μL of macromer solution was crosslinked with 0.018 M APS/TEMED for 10 minutes at 37°C in cylindrical molds, resulting in hydrogel disks that were 6 mm diameter and 1 mm thick. All hydrogels were swelled in PBS. After 7 days in PBS to demonstrate the retention of GAG, hydrogels were stained overnight in DMMB solution (n=2).

Table 5.1. Hydrogel formulations with 50 wt% total GAG

	Mass Ratios of Total Dry Polymer			
	CS-MA	**Ch-MA**	**PEG-DA**	**OPF 10K**
50% CS-MA	50%	0%	25%	25%
10% CS-MA/ 40% Ch-MA	10%	40%	25%	25%
1% CS-MA/ 49% Ch-MA	1%	49%	25%	25%
50% Ch-MA	0%	50%	25%	25%
PEG Control	0%	0%	60%	40%

5.2.5.3 Pull-Down (Depletion) of TGF-β1 from Solution by CS-MA and Ch-MA Hydrogels

To investigate the role of sulfation in TGF-β1 sequestration by 3D hydrogels, TGF-β1 pull-down (or depletion) from solution by PEG-based hydrogels containing varying amounts of CS-MA or desulfated Ch-MA was investigated. CS-MA and Ch-MA hydrogels were fabricated as described in Section 5.2.5.2, according to the 50% CS-MA, 10% CS-MA/40% Ch-MA, and 50% Ch-MA formulations in Table 5.1. A 60% PEG-DA:40% OPF mixture that possessed a similar swelling properties to 50% Ch-MA

formulations was used as a PEG-only swelling control. All hydrogels were swelled overnight in PBS.

After unconstrained swelling in PBS overnight, hydrogels were incubated in 1.0 mL solution of 2.0 ng/mL TGF-β1 in 1% BSA in PBS for 24 hours at 37°C with gentle shaking. To inhibit electrostatic binding with hydrogels, pull-down was also measured with an additional 0.5 M NaCl or 10 mg/mL soluble CS in the TGF-β1 solution. The TGF-β:disaccharide molar ratio in the solutions correlated to a ~1:50,000,000 molar ratio in 50% GAG hydrogels and to a ~1:10,000,000 molar ratio in 10% CS. After 24 hours, the supernatant was collected and frozen at -20°C until analysis. TGF-β1 pull-down by the hydrogels was determined by assaying the remaining TGF-β1 in solution by ELISA (n=5).

5.2.6 Statistical Analysis

All values were reported as mean ± standard deviation. A one- or two-factor analysis of variance (ANOVA) was used to determine statistical significance of groups, and Tukey's *post hoc* multiple comparison test with significance set at $p \leq 0.05$ indicated significance between individual samples. For all one-factor ANOVAs (swelling and TGF-β1 release), the factor was hydrogel type. For pull-down experiments, the two factors were hydrogel type and buffer composition. Statistical analysis was carried out using Minitab (v15.1, State College, PA).

5.3 Results

5.3.1 CS-C was desulfated after 7-day acidic methanol treatment

DMMB assay was used to measure sulfation level of the chondroitin products after acidic methanol treatment. While CS-A only experienced 54% desulfation after 3 days, CS-C experienced removal of 80% of the sulfates after the same time (Figure 5.3a). Extension of the acidic methanol treatment time from 3 to 7 days resulted in nearly complete desulfation of CS-C, as indicated by zero slope in the desulfated chondroitin standard curve by DMMB assay. As further confirmation of desulfation, FTIR spectroscopy was used to examine the bonds present in CS and chondroitin. FTIR spectroscopy verified the disappearance of sulfate peaks at 1100-1250 cm^{-1} (Figure 5.3b, black box), while the remaining bonds in CS appeared to remain unchanged.

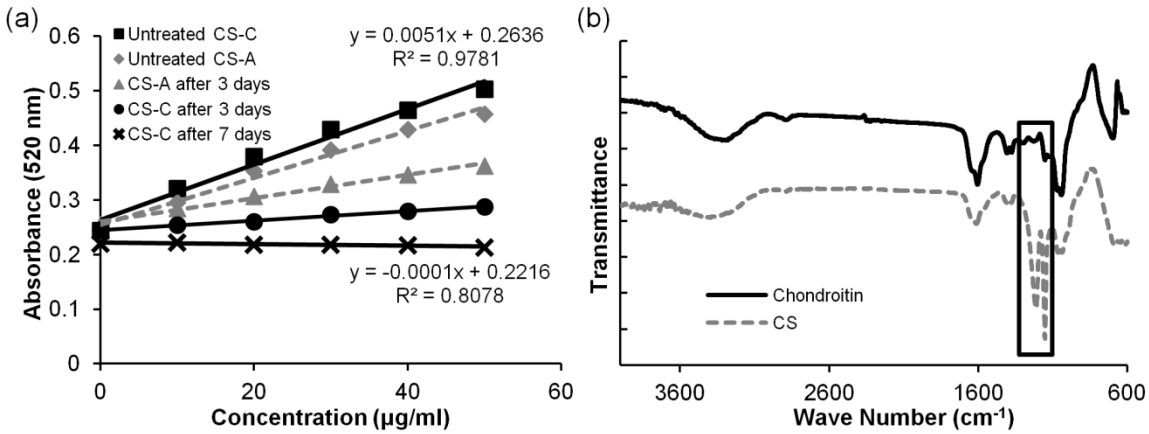

Figure 5.3. CS-C was desulfated by acidic methanol treatment for 7 days. (a) Dimethylmethylene blue (DMMB) assay standards for CS showed a linear trend with positive slope, indicating the presence of sulfates; however, the standard for the chondroitin product from CS-C desulfated for 7 days showed zero slope indicating the absence of sulfate groups in chondroitin. CS-A and CS-C experienced incomplete desulfation after 3 days, but CS-C showed greater susceptibility to desulfation in the same time than CS-A. (b) Fourier transform infrared (FTIR) spectroscopy showed the absence of sulfate peaks from 1100-1250 cm^{-1} (in black box) in chondroitin materials, compared to CS.

5.3.2 Disaccharide composition of chondroitin indicated a reduction of negative charge density

SAX-HPLC analysis was performed to determine the disaccharide composition of CS-C and desulfated chondroitin. It was determined that CS-C disaccharides were approximately 57.8% 6-sulfated and 26.8% 4-sulfated, as well as 1.3% nonsulfated (Table 5.2). The desulfated chondroitin product, however, was 98.5% nonsulfated and only 1.5% 6-sulfated. From the elution profiles, nonsulfated disaccharides, which are the least charged, eluted earliest (9-11 min), followed by the monosulfated disaccharides (18-23 min), and the most negatively charged disulfated disaccharides eluting latest (41-47 min) (Figure 5.4a-b). The observed shift in desulfated chondroitin to a primarily nonsulfated form also indicates a reduction in negative charge density in chondroitin, compared to CS. Based on these results, a predictive model calculated CS to have an average charge of -2.3 per disaccharide, while chondroitin had an average charge of -1.02, indicating that desulfation resulted in a decrease in negative charge density of CS by over two-fold.

Table 5.2. CS and chondroitin disaccharide composition by SAX-HPLC analysis

	ΔUA-GalNAc	ΔUA-GalNAc(6S)	ΔUA-GalNAc(4S)	ΔUA(2S)-GalNAc(6S)	ΔUA-GalNAc(4S,6S)	ΔUA(2S)-GalNAc(4S)
CS	1.3%	57.8%	26.8%	12.7%	0.7%	0.7%
Chondroitin	98.5%	1.5%	nd	Nd	nd	nd

ΔUA = $\Delta^{4,5}$-unsaturated uronic acid, GalNAc = N-acetylgalactosamine, nd = not detected

SEC-HPLC analysis was also performed to determine the average molecular weight of the full CS and chondroitin chains. It was determined that CS had a weight averaged molecular mass (M_w) of 17,880 Da and a number averaged molecular mass

(M_n) of 16,300 Da (PI=1.1) (Figure 5.4c). Chondroitin, however, was notably smaller with an M_w of 6,310 Da and an M_n of 5,230 Da (PI=1.2), resulting in a later elution time than CS (Figure 5.4d). This represented a 67.9% decrease in molecular weight (M_n) from CS, while sulfates only accounted for 17.1% of mass based on disaccharide composition.

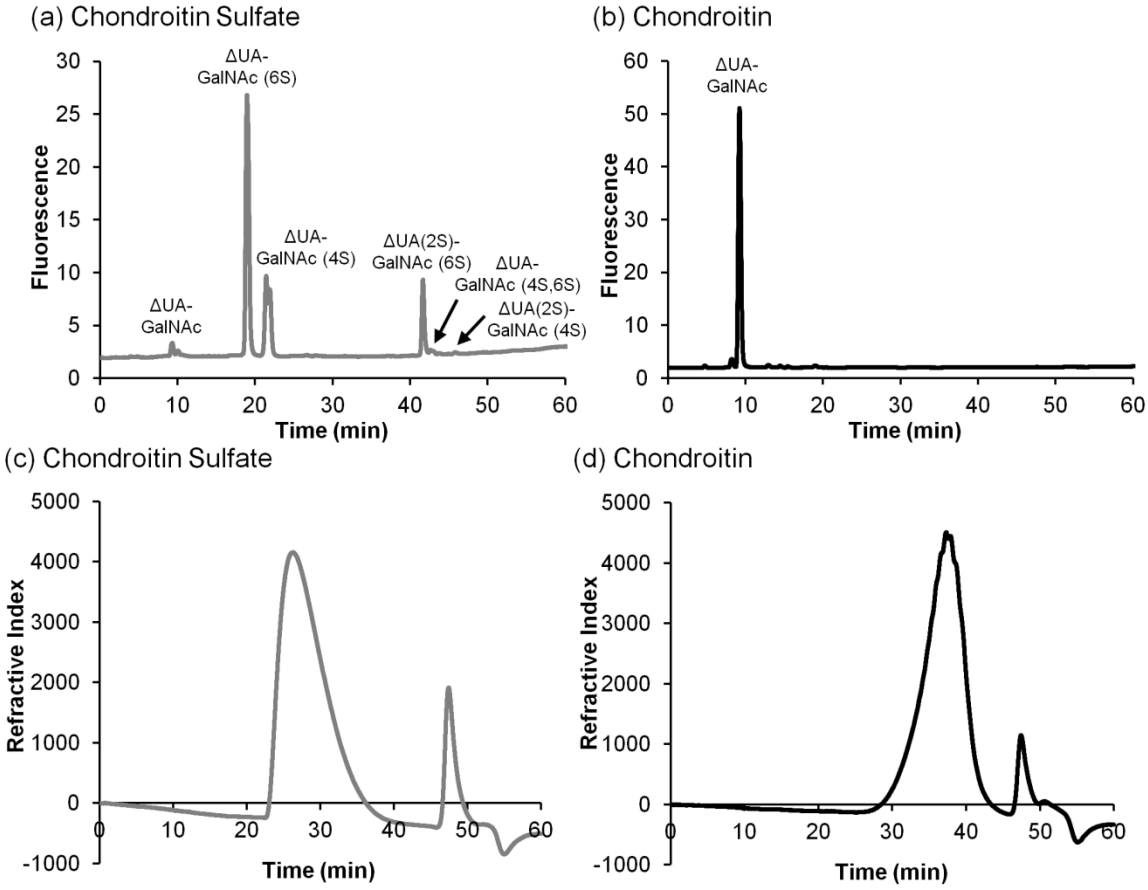

Figure 5.4. SAX-HPLC and SEC-HPLC analysis of CS and chondroitin. (a-b) SAX-HPLC analysis of (a) CS and (b) chondroitin disaccharide composition showed a shift in negative charge density in CS and chondroitin materials. Nonsulfated disaccharides (charge: -1) eluted from 9-11 min, monosulfated disaccharides (charge: -2) eluted from 18-23 min, and disulfated disaccharides (charge: -3) eluted from 41-47 min. Based on disaccharide composition, CS possessed an average charge of -2.3 per disaccharide, while chondroitin was 98.5% nonsulfated and possessed an average charge of -1.02 per disaccharide. (c-d) SEC-HPLC analysis of (c) CS and (d) chondroitin molecular weight suggested that while CS had a M_n of 16.3 kDa (PI=1.1), and chondroitin was smaller with an M_n of 5.23 kDa (PI=1.2), resulting in a later elution time than CS.

5.3.3 Degree of methacrylation by glycidyl methacrylate by H^1 NMR

H^1 NMR spectra indicated that GMA was successfully conjugated to CS. Vinyl peaks were visible at 5.6 and 6.0 ppm, confirming the methacrylation of CS and chondroitin by GMA to form CS-MA and Ch-MA, respectively (Figure 5.5, in black boxes). Peak integration also indicated that on average one GMA molecule was conjugated per every 4.3 disaccharides in CS-MA and every 3.7 disaccharides in Ch-MA.

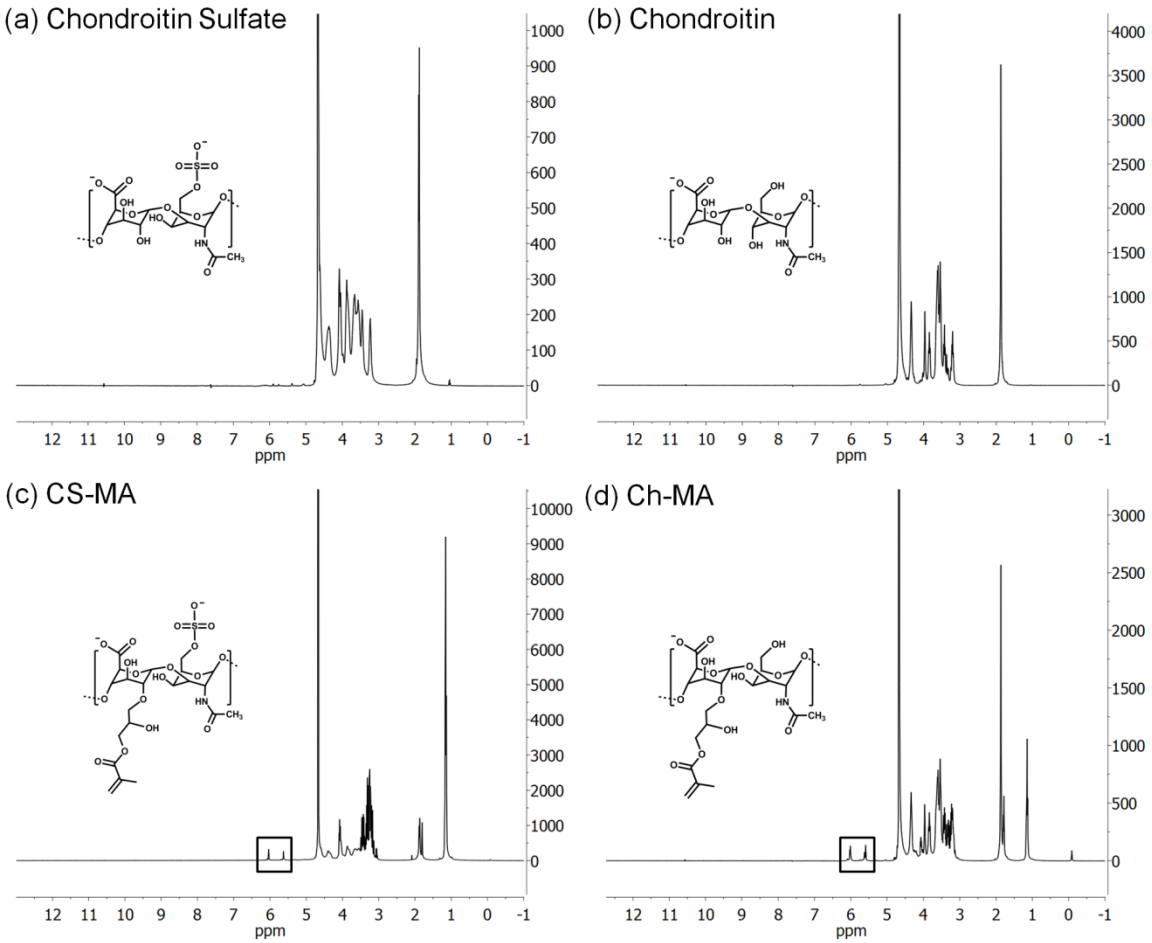

Figure 5.5. ^{1}H NMR analysis of methacrylated CS and chondroitin. ^{1}H NMR confirmed methacrylation of CS and chondroitin with glycidyl methacrylate. Compared to (a) CS and (b) chondroitin, ^{1}H NMR spectra verified the presence of vinyl groups (in black boxes) in (c) CS-MA and (d) Ch-MA at 5.6 and 6.0 ppm, resulting from methacrylation of CS and chondroitin.

5.3.4 Chondroitinase ABC maintains enzymatic activity to degrade CS-MA and Ch-MA

Soluble methacrylated CS and chondroitin degraded in chondroitinase ABC with an increase in absorbance of 232 nm UV light over time, indicating an increase of $\Delta^{4,5}$-unsaturated disaccharide degradation products (Figure 5.6). Complete degradation of CS-MA and Ch-MA occurred within ~30 minutes in solution. Additionally, crosslinked CS-MA and Ch-MA hydrogels completely degraded overnight in chondroitinase enzyme.

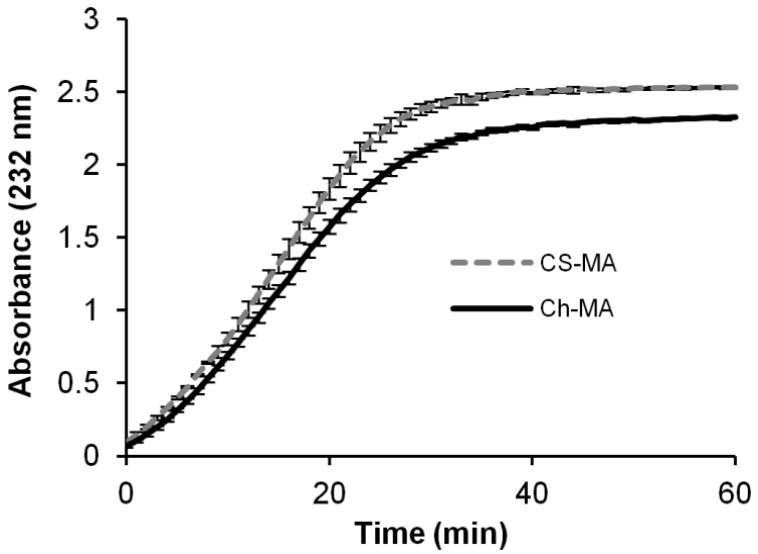

Figure 5.6. Degradation of CS-MA and Ch-MA by chondroitinase ABC. 2 mg/mL soluble CS-MA and chondroitin-MA materials were degradable in the presence of 0.06 U/mL chondroitinase ABC, as detected by absorbance of 232 nm light.

5.3.5 Swelling of PEG hydrogels containing CS-MA and Ch-MA

50% CS-MA hydrogels possessed a fold swelling ratio of 25.2 ± 1.4, and 50% CS-MA swelled signficantly more than 50% Ch-MA hydrogels which swelled 16.9 ± 2.1 fold. 10% CS-MA with a 22.7 ± 2.4 fold swelling ratio, however, did not swell significantly differently from 50% CS-MA (Figure 5.7a). 60% PEG-DA/40% OPF 10K hydrogels (17.1 ± 0.5 fold) that swell similarly to 50% Ch-MA hydrogels were fabricated

as a PEG-based swelling control. Based on estimatations of Donnan osmotic pressure in a 0.15 M NaCl electrolyte solution, 50% CS-MA hydrogels possessed an osmotic pressure of 280 kPa while 50% Ch-MA hydrogels had lower osmotic pressure of 93 kPa, representing a 3.0-fold difference in osmotic swelling pressure based on charge alone.

5.3.6 TGF-β1 retention and release by CS and chondrotin

TGF-β1 release studies from CS-MA and Ch-MA hydrogels observed increased release of TGF-β1 correlating with decreased sulfation. Hydrogels containing 50% CS displayed the greatest retention of TGF-β1 over 7 days, with only 3.6 ± 1.0 ng TGF-β1 released after 7 days (Figure 5.7b). 10% CS hydrogels demonstrated significantly greater TGF-β1 release than 50% CS-MA with 5.6 ± 0.5 ng TGF-β1 released. Additionally, 50% chondroitin hydrogels exhibited the greatest release of 6.8 ± 0.2 ng TGF-β1.

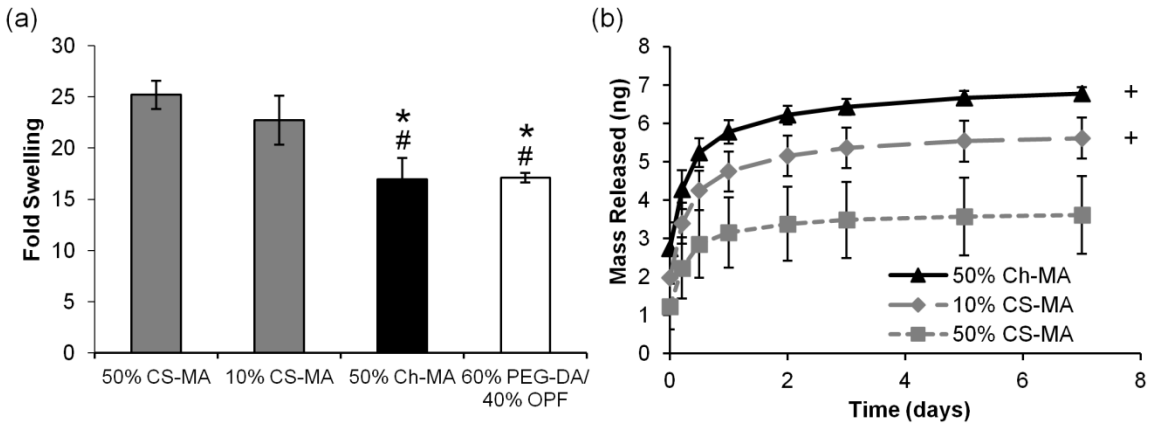

Figure 5.7. Swelling and TGF-β1 release from CS-MA and Ch-MA hydrogels. (a) Crosslinked 50% Ch-MA hydrogels swelled significantly less than 50% CS-MA and 10% CS-MA hydrogels. 40% OPF/60% PEG-DA hydrogels were formed as PEG-based swelling controls for 50% Ch-MA. (b) 50% CS-MA hydrogels demonstrated greatest retention of TGF-β1 over 7 days, while 10% CS-MA gels exhibited greater release, and 50% chondroitin-MA gels displayed the greatest release, indicating that TGF-β1 release decreased with increasing degrees of sulfation. * indicates significantly lower fold swelling that 50% CS-MA ($p \leq 0.05$). # indicates significantly lower fold swelling that 10% CS-MA ($p \leq 0.05$). + indicates significantly greater release than 50% CS-MA after 7 days ($p \leq 0.05$).

5.3.7 TGF-β1 pull-down by hydrogels with varying CS content

GAG-containing hydrogels were fabricated containing varying amounts of CS-MA. While total GAG was maintained at 50 wt%, the fraction of CS-MA was varied with the remainder balanced with nonsulfated Ch-MA. A pink/purple color indicated the present of sulfated GAG in a concentration-dependent manner, while a blue color indicated the absence of sulfates. Staining with DMMB indicated that CS-containing hydrogels stained positively for sulfation after 7 days, and increasing degrees of staining were apparent in hydrogels as sulfation increased up to 50% CS, while PEG only hydrogels remained blue (Figure 5.8a).

In pull-down (depletion) studies from solution, all hydrogels exhibited significant pull-down of TGF-β1, compared to blank wells without gels, where less TGF-β1 remaining in solution indicated greater pull-down; however, pull-down in 50% CS-MA hydrogels was significantly greater than less sulfated hydrogel formulations (Figure 5.8b). 50% CS-MA depleted 55.9 ± 1.5% of available TGF-β1 out of solution, compared to blanks. Ch-MA and PEG control hydrogels, on the other hand, experienced the least pull-down of TGF-β1 with 29.4 ± 2.7% and 33.8 ± 3.0% depletion, respectively. Hydrogels containing 10% CS-MA/40% Ch-MA responded in a concentration-dependent manner with 36.4 ± 3.3% depletion, which was significantly greater pull-down than 50% Ch-MA and less than 50% CS-MA, indicating that greater depletion of TGF-β1 was observed with increasing sulfation.

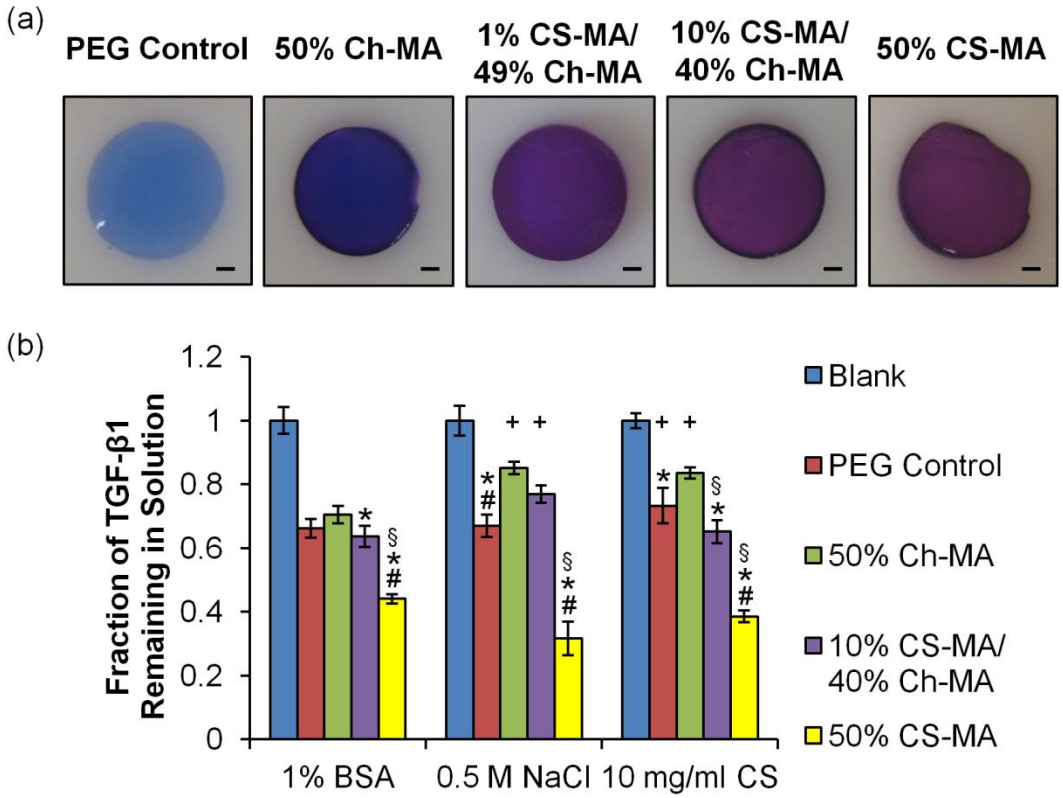

Figure 5.8. TGF-β1 pull-down by CS-MA and Ch-MA hydrogels with varying degrees of sulfation. (a) DMMB staining indicated increasing degrees of sulfation in hydrogels from 0% to 50% CS-MA content after 7 days. Sulfated GAGs stained purple/pink, while nonsulfated materials remained blue. All hydrogels contained 50% total GAG (with CS balanced with chondroitin). Scale bars = 1.0 mm. (b) All hydrogels demonstrated significant pull-down compared to blanks ($p \leq 0.05$), where less TGF-β1 remaining in solution indicated greater pull-down. 50% CS-MA hydrogel exhibited the greatest pull-down of soluble TGF-β1 out of solution, while nonsulfated 50% Ch-MA and PEG control hydrogels exhibited the least depletion in 1% BSA. 10% CS-MA/40% Ch-MA hydrogels corresponded in a sulfation-dependent manner with an intermediate level of depletion. Incubation in 0.5 M NaCl and 10 mg/ml soluble CS significantly decreased depletion by 50% Ch-MA, but not 50% CS-MA hydrogels. § indicates significantly greater pull-down than PEG controls ($p \leq 0.05$). * indicates significantly greater pull-down than 50% Ch-MA ($p \leq 0.05$). # indicates significantly greater pull-down than 10% CS-MA/40% Ch-MA ($p \leq 0.05$). + indicates significantly less pull-down than the same hydrogel type in 1% BSA ($p \leq 0.05$).

In the presence of 0.5 M NaCl, pull-down of TGF-β1 by 50% Ch-MA and 10% CS-MA/40% Ch-MA hydrogels significantly decreased, while pull-down by 50% CS-MA did not decrease. Depletion by 50% Ch-MA hydrogels decreased to 14.8 ± 2.0%, and

depletion by 10% CS-MA/40% Ch-MA decreased to 23.0 ± 2.7% in 0.5 M NaCl. Additionally, in 10 mg/mL soluble CS, a similar response was observed. In the presence of 10 mg/mL soluble CS, pull-down by 50% Ch-MA hydrogel was significantly decreased to 16.4 ± 1.8% depletion; however, pull-down by crosslinked 50% CS-MA hydrogels did not decrease. TGF-β1 pull-down by PEG control hydrogels, on the other hand, remained unchanged in 0.5 M NaCl, compared to in 1% BSA, with 33.1 ± 3.5% depletion, while soluble CS resulted in a slight decrease in depletion by PEG controls to 26.7 ± 5.5%.

5.4 Discussion

Together these studies demonstrated that CS could be desulfated without modification of the original CS chemical structure, CS and chondroitin materials could be crosslinked to form hydrogels, and CS-based hydrogels sequestered TGF-β1 in a sulfation-dependent manner. Chondroitin sulfate C was successfully desulfated by acidic methanol treatment after 7 days to yield chondroitin. DMMB assay, FTIR spectroscopy, and SAX-HPLC collectively indicated that chondroitin was ~98.5% nonsulfated after 7 days of chemical desulfation (Figures 5.3, 5.4a-b). FTIR and SAX-HPLC analysis also suggested that the remaining bonds and chemical structure of the CS disaccharides appeared to remain unmodified, and that desulfation was specific to removal of the sulfate groups. SAX-HPLC estimated that desulfation of CS resulted in a 2.3-fold reduction in negative charge density, due to removal of negatively charged sulfates (Figure 5.4a-b); however, due to the presence of carboxylates in the GAG backbone, chondroitin chains remained moderately negatively charged with approximately one

negatively charged group per disaccharide unit. These results present desulfated chondroitin materials as a highly controlled system to investigate of the role of sulfation and resulting negative charge density, without altering the chemical composition of the remaining polysaccharide GAG backbone.

Additionally, results from the DMMB assay suggested that CS-C, which is primarily sulfated at the 6-carbon, may be more susceptible to desulfation by acidic methanol treatment than CS-A, which is sulfated at the 4-carbon. After 3 days, CS-C underwent 80% desulfation, while CS-A only exhibited 54% desulfation, as measured by DMMB assay, suggesting that sulfation of the 6-carbon was more susceptible to cleavage by acidic methanol treatment. The 6-carbon of the N-acetylgalactosamine sugar of CS hangs away from the ring structure (Figure 5.1), while the 4-carbon is one of the members of the ring. This suggests that the ring structure may either limit accessibility to 4-O-sulfates for cleavage or may decrease the susceptibility of the 4-carbon to modification, slowing the rate of desulfation. Extended treatment with acid methanol after 7 days resulted in nearly complete desulfation of CS-C, suggesting that desulfation of CS was time-dependent with increasing desulfation over time (Figure 5.3a). These results suggested that a wide range of degrees of sulfation could be produced by increasing or decreasing the treatment time up to 7 days. In conjugation with various chemical methods of oversulfation [25-26], a diverse assortment of sulfated materials, with varying degrees of charge, could be developed from a single GAG structure. While desulfated chondroitin remains moderately negatively charged due to the presence of carboxylates, desulfation by acid methanol treatment methylated these carboxylate groups, producing a neutrally charged methyl ester intermediate. While this intermediate

was subsequently demethylated in KOH to form chondroitin for the purposes of these studies in which only sulfation was altered, the methyl ester of chondroitin could potentially be used as a neutrally charged alternative for further control of charge to study electrostatic interactions with GAGs.

SEC-HPLC analysis, however, suggested that desulfated chondroitin chains may be of shorter average length than the starting CS chains (Figure 5.4c-d). Acidic methanol treatment for 7 days may result in some degradation or chain shortening in chondroitin materials, possibly due to hydrolysis at low pH. To accurately characterize the true molecular weight of these materials, however, HPLC analysis would require further investigation to examine the interaction of charged GAG chains with the chromatography columns. In these experiments, the molecular weights of CS and chondroitin, which possess varying degrees of charge, were quantified relative to standards of partially depolymerized heparin, which is even more negatively charged than CS; therefore, a more thorough investigation would be required in differing buffer compositions to minimize the differential interactions of negatively charged GAG chains with the columns and to accurately quantify the molecular masses of CS and chondroitin. If further analysis determines that the average chain length of chondroitin is, in fact, substantially shorter than CS, the reaction parameters of the acid methanol treatment may be altered to minimize degradation. While shorter reaction time in 0.5% v/v acetyl chloride resulted in incomplete desulfation after 3 days, altering the concentration of reagents along with reaction time may be able to limit potential degradation of chondroitin. Reaction in either lower concentrations of acetyl chloride for a longer time or higher concentrations for a shorter time may be able to minimize potential chain

shortening in chondroitin materials. Additionally, other chemical and enzymatic procedures have been developed to desulfate CS, and these techniques could be explored as alternative chemistries to prevent degradation of chondroitin chains [375-378].

Nevertheless, while molecular weight is important in material properties and growth factor interactions, methacrylation and crosslinking of CS-MA and Ch-MA materials, as performed in these studies, were expected to mitigate potential differences in molecular mass, as GAG chains were crosslinked together and became immobilized with a highly crosslinked polymer network. Methacrylation of CS and chondroitin with GMA permitted crosslinking of GAG materials by free radical initiation, and ^{1}H NMR analysis suggested that CS-MA and Ch-MA were similarly methacrylated, approximately once every ~4 disaccharides on average (Figure 5.5), indicating that similar crosslinking density of the two GAGs may result in comparable materials. Crosslinked CS-MA and Ch-MA hydrogels, however, did demonstrate significant differences in swelling properties, as 50% CS-MA hydrogels swelled significantly more than 50% Ch-MA gels in PBS (Figure 5.7a). These differences in swelling may be attributed in part to differences in osmotic pressure within the hydrogel networks, resulting from the disparity in negative charge density. The high negative charge density in CS-MA hydrogels is expected to attract high concentrations of positively charged molecules, while repelling negatively charged molecules, thus increasing the osmolarity of the interstitial fluid and creating a Donnan effect [379]. Donnan osmotic pressure in these materials was estimated to be approximately 3.0-fold higher in 50% CS-MA hydrogels in a 0.15 M NaCl solution than in 50% Ch-MA, based the higher negative charge of CS GAGs [45, 380]. Therefore, for use as a swelling control for release studies and future cellular

experiments, PEG-based controls composed of 60% PEG-DA/40% OPF were designed to possess similar swelling properties to 50% Ch-MA hydrogels, but in the absence of charged GAGs.

Chemical modification though desulfation of CS and subsequent methacrylation of CS and chondroitin did not appear to inhibit the ability of chondroitinase enzyme to degrade these products in solution (Figure 5.6). Additionally, crosslinked CS and Ch hydrogels completely degraded in chondroitinase enzyme, indicating that crosslinking of CS-MA and Ch-MA also did not prevent degradation of the hydrogel networks by chondroitinase. Enzymatic degradation of these biomaterials is especially important to permit interaction of the naturally-derived GAG matrix with surrounding cells. Cell-secreted chondroitinase enzyme could facilitate cell-mediated degradation of CS-MA and Ch-MA materials, and enzymatic degradation may permit localized remodeling of GAG matrix.

Desulfation of CS was found to alter the ability of CS to both retain and release the chondrogenic growth factor TGF-β1 *in vitro*. CS-MA and Ch-MA hydrogels were loaded with TGF-β1 and release was monitored over 7 days. In these studies, 50% CS-MA materials were found to largely retain TGF-β1, while decreasing the CS content to 10% CS-MA resulted in significantly greater release (Figure 5.7b). Additionally 50% Ch-MA, which maintained a constant GAG content compared to 50% CS-MA but with a reduction in sulfation and negative charge, showed significantly more release than 50% CS-MA, suggesting that sulfation of CS plays a fundamental role in the retention of growth factors. These differences in growth factor retention were observed in spite of differences in swelling between CS-MA and Ch-MA hydrogels. CS-MA hydrogels

swelled significantly more than Ch-MA gels (Figure 5.7a); therefore, the estimated mesh size of CS-MA materials would be expected to be higher than Ch-MA [380]. While one would expect an increase in mesh size to facilitate greater growth factor release from CS-MA hydrogels, Ch-MA materials with a smaller mesh size experienced significantly greater release of TGF-β1 than CS-MA. These results suggested that TGF-β1 was retained via electrostatic interactions with negatively charged sulfates in CS, rather than simply physical entrapment within the hydrogel network, and that sulfation can be carefully controlled within this system to alter the release kinetics of TGF-β1 from CS-based materials.

In particular, sulfated and desulfated CS-based materials may be promising tools to deliver TGF-β1 for cartilage regeneration. CS proteoglycans are expressed during early cartilage development [14-15], and sulfated GAGs have been shown to potentiate TGF-β1 signaling [274, 278]. TGF-β1 plays a critical role in promoting chondrogenesis and is positively charged at physiological pH, facilitating electrostatic interaction with sulfated GAGs [6, 24]. In response to TGF-β1 signaling, cartilage may also regulate subsequent CS production and sulfation patterning, suggesting that a potential feedback loop may exist in which sulfated GAGs regulate growth factor signaling [230, 279].

In addition to examining release from CS-MA and Ch-MA materials, the ability of CS-MA and Ch-MA hydrogel to "pull-down" soluble TGF-β1 out of solution was explored in CS-MA and Ch-MA hydrogels. Sequestration and retention appear to be more analogous to *in vivo* environments, in which proteoglycans are believed to sequester growth factors and possibly direct these signals for tissue patterning and differentiation [220, 230]. This system is also comparable to culture of GAG-based constructs in

chondrogenic media, in which hydrogels may be able to sequester TGF-β1 to promote signaling and differentiation. Pull-down was examined using hydrogels in which the total GAG content was maintained at 50% while the balance of CS-MA and Ch-MA was varied proportionally to alter the degree of sulfation (Figure 5.8a). Staining with DMMB demonstrated CS was retained within the hydrogel scaffolds after 1 week and increasing CS content was visible from 0% CS-MA (with 50% Ch-MA) up to 50% CS-MA (with 0% Ch-MA) by increased intensity of DMMB staining. Pull-down experiments in these gels demonstrated that 50% CS-MA hydrogels sequestered soluble TGF-β1, "pulling" it out of solution and sequestering TGF-β1 within the hydrogel network in 1% BSA (Figure 5.8). Decreasing the sulfation of the GAG matrix reduced the observed interaction with TGF-β1 in a concentration-dependent manner in 10% CS-MA/40% Ch-MA hydrogels and in 50% Ch-MA hydrogels, indicating that sulfation and charge play important roles in facilitating depletion of TGF-β1. Interestingly, increasing the ionic strength of the buffer with an additional 0.5 M NaCl significantly inhibited pull-down of TGF-β1 by 50% Ch-MA, while pull-down by 50% CS-MA did not appear to decrease. The moderate negative charge of chondroitin may retain a weaker electrostatic interaction with TGF-β1 that was inhibited in 0.5 M NaCl; however, 0.5 M NaCl was not sufficient ionic strength to shield TGF-β1 interactions with 50% CS-MA hydrogels, suggesting that CS-MA may possess a stronger ability to bind TGF-β1. Similarly, 10 mg/mL soluble CS decreased depletion in 50% Ch-MA, but was unable to competitively inhibit sequestration in 50% CS-MA gels. This suggested that TGF-β1 may preferentially bind crosslinked CS-MA hydrogels over soluble CS chains in solution.

In related studies, Hintze et al. demonstrated that chemically oversulfated CS and hyaluronan were able to sequester TGF-β1 in a sulfation-dependent manner when covalently conjugated onto 2D surfaces, as determined by ELISA and surface plasmon resonance (SPR), and incubation with 0.3 M NaCl inhibited electrostatic interactions with TGF-β1[25]. Similarly, Lyon et al. found that TGF-β1 bound heparin by affinity chromatography, and 0.5 M NaCl was sufficient to elute TGF-β1 from the heparin-agarose columns [274]. This was consistent with a number of studies that have reported shielding of a variety of electrostatic protein interactions with sulfated GAGs in 0.5 M NaCl [381-383]; however, binding of a number of stronger protein-GAG interactions have required concentrations up to 1.5 M NaCl [384-388], suggesting that 50% CS-MA hydrogels may possess a relatively strong electrostatic interaction with TGF-β1 in this system and that greater ionic strength may be required to shield these interactions. An additional study by Hintze el al. showed that 10 mg/mL of soluble GAGs, including CS, was able to competitively inhibit binding of BMP-4 to surfaces conjugated with oversulfated hyaluronan by ELISA [273]. It is important to note that these other studies tested binding to GAG-conjugated 2D surfaces or affinity columns, while the work in this dissertation represents the first time that TGF-β1 sequestration has been examined in crosslinked GAG hydrogels. Crosslinked hydrogels may immobilize GAG chains in close proximity to alter their ability to sequesterTGF-β1.

TGF-β1 is a growth factor that plays a critical role in promoting chondrogenesis and is positively charged at physiological pH, facilitating electrostatic interaction with sulfated GAGs. Heparin has been found to electrostatically interact with TGF-β1 and TGF-β2, but not the TGF-β3 isoform [274]. TGF-β1 and TGF-β2 are reported to have

isoelectric points (pI) of approximately 9.5 and 8.5, respectively [275-276], while TGF-β3 has a lower pI of 6.8, suggesting that it is actually negatively charged at physiological pH and unable to electrostatically complex with sulfated GAGs [275]. Highly sulfated GAGs were also capable of potentiating TGF-β1 activity in mink lung epithelial cells, suggesting that GAGs may also have a synergistic effect in TGF-β1 signaling. It was hypothesized that TGF-β1 interacts with sulfated GAGs via basic arginine and lysine residues at positions 25, 26, 31, and 37 and a histidine at 34 in TGF-β1, along with Arg/Lys at position 94 [272, 274]. In the TGF-β1 dimer, these two sites could be potentially be engaged by a single GAG chain approximately 60 Å apart or by two separate GAG chains. The proposed binding site was also in a similar location, at the tips of the β-strand loops, to where TGF-β binds its receptors; however, little competition has been reported and in many cases sulfate GAGs appeared to potentiate the signaling effects [272]. These studies suggested that GAG-based materials may have significant application in controlling interactions with TGF-β1 to promote chondrogenic differentiation of MSCs.

Overall, desulfated chondroitin hydrogels provide a highly controlled system to examine the interactions between charged GAGs and growth factors, and these materials may have tremendous potential to promote chondrogenic differentiation through sequestration of growth factors.

5.5 Conclusions

These studies present desulfated chondroitin as a potential tool to further investigate the role of sulfation in GAG interactions with growth factors. Chondroitin

sulfate was chemically desulfated by acidic methanol treatment, and characterization supported significant desulfation with little modification of the remaining CS chemical structure. Desulfation also resulted in a 2.3-fold decrease in negative charge density in chondroitin materials. Methacrylation of CS and chondroitin allowed the formation of CS-MA and Ch-MA hydrogels, which remained degradable by chondroitinase enzyme for potential cell-mediated degradation. 50% CS-MA hydrogels were able to sequester greater amounts of TGF-β1 than desulfated 50% Ch-MA hydrogels, as shown by retaining TGF-β1 from release and through TGF-β1 pull-down from solution, suggesting that sulfates play an important role in facilitating the electrostatic interactions between growth factors and CS. These results present desulfated chondroitin materials as a valuable tool to alter GAG sulfation in a highly controlled manner as a promising strategy to control binding and interaction with positively charged growth factors, particularly the chondrogenic growth factor TGF-β1. Sulfated and desulfated CS-based materials may present a promising platform to modulate growth factor interactions to control release or sequestration for chondrogenic differentiation of MSCs and development of novel tissue engineering therapies for cartilage regeneration and repair.

CHAPTER 6

DESULFATED CHONDROITIN HYDROGELS UPREGULATED GENE EXPRESSION OF CARTILAGINOUS MARKERS BY ENCAPSULATED HUMAN MESENCHYMAL STEM CELLS IN THE PRESENCE OF TGF-β1

6.1 Introduction

As a load bearing tissue, damage to articular cartilage can be both debilitating and extremely painful. Nearly 466,000 arthroscopic procedures performed on the knee in an ambulatory (outpatient) setting were diagnosed with a tear of the medial or lateral cartilage or menisci in the United States in 2006 [2]. If severe cartilage damage is allowed to persist without appropriate repair, the tissue may degenerate further and progress into development of osteoarthritis. In 2005, an estimated 27 million adults in the US had clinical osteoarthritis with indirect costs totaling approximately $89 billion per year [3-4]. Due to cartilage's low capacity for healing, novel tissue engineering therapies seek to promote repair and regeneration of cartilaginous tissues. Mesenchymal stem cells (MSCs) are multipotent progenitor cells that are capable of differentiating into cartilaginous tissues, making them a promising cell source for tissue repair [6]; however, difficulty recapitulating the complex extracellular matrix (ECM) composition and organization of native cartilage remains a significant challenge. Recent research has suggested that cartilaginous ECM molecules may play a central role in directing differentiation of MSCs down a chondrogenic lineage.

Chondroitin sulfate (CS) is a cartilaginous glycosaminoglycan (GAG) that appears to play an important role in chondrogenesis *in vivo*. CS-containing proteoglycans versican and perlecan regulate mesenchymal condensation during cartilage development [14, 218-219, 223-224], and several enzymes involved in CS initiation, elongation, and sulfation are required for proper skeletal development and patterning [16-18]. Recent studies have investigated the ability of CS-modified biomaterials to promote chondrogenic differentiation *in vitro* as well. Culture in CS-containing hydrogels upregulated expression and production of cartilaginous ECM by encapsulated goat and mouse MSCs [8-9], suggesting that CS may play a particularly important role in directing stem cell differentiation down a chondrogenic lineage; however, relatively few studies have specifically investigated the effect of CS on chondrogenic differentiation of human MSCs (as opposed to other mammalian species) [251-252].

In cartilaginous tissues, sulfated GAGs play essential roles in maintaining cartilage function. Specifically, the high degree of sulfation of CS carries a highly negative fixed charge density that facilitates a variety of interactions with cartilaginous ECM, signaling molecules, and interstitial fluid. In Chapter 5 of this dissertation, nonsulfated chondroitin materials were characterized as a potential system to control material interactions with growth factors, including the chondrogenic growth factor TGF-β1; however, the effects of sulfation of CS in chondrogenic differentiation of MSCs have not been investigated. To examine the chondrogenic response to sulfated and nonsulfated GAG materials, human MSCs were encapsulated in CS- and chondroitin-containing hydrogels and cultured in the presence of chondrogenic medium containing TGF-β1 over the course of 6 weeks *in vitro*. Cell viability and total DNA content were monitored over

time, and gene expression and ECM production of encapsulated MSCs were determined as measures of chondrogenic differentiation.

6.2 Materials and Methods

6.2.1 Synthesis of Materials

6.2.1.1 Desulfation of Chondroitin Sulfate

Chondroitin sulfate was desulfated using an acidic methanol treatment for up to 7 days per established protocols [365-366]. Chondroitin sulfate C (primarily chondroitin-6-sulfate, Wako Chemicals USA, Richmond, VA) was stirred at 5.0 mg/mL in methanol (VWR, Radnor, PA) containing 0.5% v/v acetyl chloride (Acros Organics, Geel, Belgium). CS was centrifuged and acidic methanol was replaced on days 1, 3, and 7 to produce a methyl ester of chondroitin. The product was then dissolved in 20 mL distilled, deionized water (ddH_2O) per gram of starting CS before precipitation in an excess of ethanol. The methyl ester of chondroitin was washed in ethanol and ethyl ether (Fisher, Waltham, MA), vacuum dried at <5 mmHg, and stored at 4°C.

Methyl ester of chondroitin was demethylated at 25 mg/mL in 0.1 M potassium hydroxide (KOH, Fisher) for 24 hours to produce chondroitin. The chondroitin product was then neutralized in 4 mL of 100 mg/mL potassium acetate (Fisher) in 10% v/v acetic acid (VWR) per gram of starting product, and precipitated in an excess of ethanol. Chondroitin was washed in ethanol and ethyl ether, vacuum dried, and stored at 4°C until use. Removal of sulfate groups in chondroitin was confirmed by dimethylmethylene blue (DMMB) assay for sulfated GAGs [302].

6.2.1.2 Methacrylation of Chondroitin Sulfate and Chondroitin

CS and chondroitin were methacrylated with glycidyl methacrylate per established protocols [368]. CS or chondroitin was dissolved at 1% w/v in a 50:50 mixture of acetone (VWR) and ddH_2O and allowed to stir at room temperature overnight. A 20-fold molar excess of triethylamine (TEA, Sigma-Aldrich, St. Louis, MO) per CS or chondroitin disaccharide was added to the solution, and a 20-fold molar excess of glycidyl methacrylate (GMA, Sigma-Aldrich) per disaccharide was added dropwise to the solution. The reaction was allowed to stir at room temperature for 24 hours to produce CS-methacrylate (CS-MA) and chondroitin-methacrylate (Ch-MA). The resulting products were dialyzed first in 50:50 acetone:water for 24 hours (1,000 Da MWCO), and then in distilled water (dH_2O) for 2 days to remove unreacted reagents. The methacrylated products were lyophilized (Labconco, Kansas City, MO) for 4 days to produce a dry product, and stored at -20°C until use. Proton nuclear magnetic resonance (^{1}H NMR) was utilized to determine the degree of the conjugation of the GMA groups to the CS and chondroitin chains.

6.2.1.3 PEG-DA Synthesis

Poly(ethylene glycol)-diacrylate (PEG-DA) polymers were synthesized according to established protocols [191]. 3,400 Da (M_n) PEG (Sigma-Aldrich) was solubilized in distilled, anhydrous methylene chloride (MeCl, Fisher) to produce a 60% (m/v) solution. TEA was added to the dissolved PEG, and acryloyl chloride (AcCl, Sigma-Aldrich) was slowly added dropwise at 2:1 AcCl:PEG and 1:1 AcCl:TEA molar ratios to create a 40% w/v solution. The reaction was allowed to proceed at room temperature under nitrogen gas, and the reaction was left stirring overnight to ensure completion. 2 M potassium

carbonate (K_2CO_3, Fisher) was used at a 2:1 K_2CO_3:AcCl molar ratio to extract TEA to the aqueous phase. The organic phase was allowed to separate from the aqueous phase, and anhydrous magnesium sulfate ($MgSO_4$, Fisher) was used to remove any remaining aqueous phase from the solution. PEG-DA was then precipitated in ethyl ether and filtered, followed by vacuum drying at <5 mmHg. Dry polymers were stored in sealed containers at -20°C until use. PEG-DA (M_n = 3760 ± 50, PI = 1.1 ± 0.02) and PEG 3.4K (M_n = 3440 ± 30, PI = 1.1 ± 0.001) were characterized via gel permeation chromatography as previously reported [174].

6.2.1.4 OPF Polymer Synthesis

Oligo(poly(ethylene glycol) fumarate) (OPF) 10K polymers were synthesized according to established protocols [367]. 10,000 Da (M_n) PEG (Sigma-Aldrich) was azeotropically distilled in toluene (Fisher) and then combined with distilled, anhydrous MeCl to produce a 40% (v/v) solution. Fumaryl chloride (FuCl, Sigma-Aldrich) and TEA (Sigma-Aldrich) were slowly added dropwise over a period of 2 hours at 0.9 FuCl:PEG and 1:2 FuCl:TEA molar ratios. During this time the reaction was allowed to proceed at 0°C under nitrogen gas, after which the reaction was left stirring for 72 hours under nitrogen at room temperature to ensure reaction completion. After rotovaporing (Buchi, Flawil, Switzerland) to remove excess MeCl, the resulting polymer was recrystallized twice with ethyl acetate (Fisher) and washed three times in ethyl ether (Fisher), followed by vacuum drying at <5 mmHg. Dry polymers were stored in sealed containers at -20°C before use. OPF 10K (M_n = 28,100 ± 760, PI = 5.2 ± 0.4) and PEG 10K (M_n = 12,900 ± 210; PI = 1.1 ± 0.002) were characterized via gel permeation chromatography as previously reported [174].

6.2.2 Encapsulation of Human MSC

Human MSCs were obtained from the Texas A&M Health Science Center College of Medicine Institute for Regenerative Medicine at Scott & White (Temple, TX) at passage 1. Cells were seeded at 50 cells/cm^2 following recommended protocols, in growth medium containing α-MEM (Mediatech, Manassas, VA) with 16.3% fetal bovine serum (FBS, Atlanta Biologicals, Lawrenceville, GA), 1% antibiotic/antimycotic (Mediatech), and 2 mM L-glutamine (Mediatech). Following expansion, cells were frozen at passage 2 in liquid nitrogen until further use. For these studies, cells from three separate donors were thawed, expanded separately, and combined prior to encapsulation at passage 3.

For cell encapsulation, human MSCs were incorporated at a final cell concentration of 20x10^6 cells/mL into macromer solutions containing a 1:1 ratio of OPF 10K:PEG-DA and 50% CS-MA or 50% Ch-MA by dry mass. PEG controls containing 60% PEG-DA:40% OPF, which were designed to swell similarly to 50% Ch-MA as described in Chapter 5, were used as swelling controls. Dispersed MSCs were crosslinked in hydrogels using 6 mm diameter, 1 mm deep cylindrical molds with 0.018 M ammonium persulfate (APS, Sigma-Aldrich) and tetramethylethylenediamine (TEMED, Sigma-Aldrich) for 10 minutes at 37 °C. Hydrogels were cultured for 6 weeks at 37°C and 5% CO_2 in chondrogenic medium composed of high glucose DMEM (Mediatech) containing 1% ITS+ culture supplement (Becton, Dickenson, Franklin Lakes, NJ), 1% nonessential amino acids (NEAA, Mediatech), 50 μg/mL ascorbate-2-phosphate (Sigma-Aldrich), and 1% antibiotic/antimycotic (Mediatech). Chondrogenic medium was also supplemented with 10 ng/mL TGF-β1 (Peprotech, Rocky Hill, NJ) and 100 nM

dexamethasone (Sigma-Aldrich), and culture medium was replaced every 2 days throughout the course of the study.

6.2.3 Analysis of MSC Response in CS-MA and Ch-MA Hydrogels

6.2.3.1 LIVE/DEAD Staining for Viability

Viability of human MSCs encapsulated in 50% CS-MA and 50% Ch-MA hydrogels was observed by LIVE/DEAD staining over 6 weeks. In this stain, calcein is cleaved within the cytosol of viable cells, fluorescing green (ex/em: 494/517 nm), while ethidium homodimer-1 is able to enter the ruptured cell membranes of nonviable cells, binding nuclear DNA and fluorescing red (ex/em: 528/617 nm). On days 1, 21, and 42, after rinsing samples of excess media in PBS with 100 μg/mL $CaCl_2$ and 47 μg/mL $MgCl_2$ (Invitrogen, Carlsbad, CA), hydrogels were stained for 60 minutes in LIVE/DEAD stain containing 1 μM calcein and ethidium homodimer-1 (Invitrogen). Viability within all hydrogel formulations was imaged in PBS via confocal microscopy (Carl Zeiss LSM 510, Oberkochen, Germany). Images were captured every 10 μm through the entire depth of the hydrogel from three separate regions in each sample (n=4).

6.2.3.2 PicoGreen DNA assay

Hydrogels were analyzed by PicoGreen assay for DNA content on days 1, 21, and 42. The PicoGreen assay uses a fluorescent dye that binds to double stranded DNA to quantify DNA content. After rinsing in PBS, samples were massed and wet mass was recorded. Hydrogels were then homogenized with pestle grinders and mixed with 500 μL of distilled water before being frozen at -80°C until analysis. Cells were lysed through a series of freeze/thaw cycles and sonication. PicoGreen assay (Invitrogen) was used to

evaluate the total DNA content in each sample, according to established protocols [303]. Fluorescence was read at excitation 485 nm, emission 525 nm (Molecular Devices SpectraMax M2e, Sunnyvale, CA), and DNA content was determined using a standard curve of DNA. Within each hydrogel formulation, DNA content of each gel was normalized to wet mass to correct for small differences in gel size (n=4).

6.2.3.3 Reverse transcription polymerase chain reaction

Gene expression of encapsulated MSCs was analyzed after 1, 21, and 42 days by reverse transcription polymerase chain reaction (RT-PCR). After rinsing in PBS, RNA was extracted from samples using a QIAshredder tissue homogenizer and RNeasy kit with DNase I digestion (Qiagen, Hilden, Germany). Reverse transcription was performed using SuperScript III Reverse Transcriptase (Invitrogen) with Oligo$(dT)_{15}$ primers (Promega, Madison, WI) and nucleotides (Promega). Custom designed primers (Invitrogen) specific to human mRNA for collagen II, aggrecan, and SOX9 (chondrocytic markers), collagen X (hypertrophic chondrocyte marker), collagen I (fibroblastic marker), osteocalcin (osteoblastic marker), myoD (myofibroblastic marker), and peroxisome proliferator-activated receptor γ2 (PPAR-γ2; adipocytic marker) are shown in Table 5.2. Quantitative PCR amplification for each gene target was performed on a StepOnePlus System (Applied Biosystems, Carlsbad, CA) with SYBR Green master mix (Applied Biosystems). To determine fold regulation over PEG control hydrogels on day 1, the raw fluorescence data was processed using LinRegPCR (v12.11; http://www.hartfaalcentrum.nl) [389] with glyceraldehyde-3-phosphate dehydrogenase (GAPDH) as an endogenous control (n=6).

Table 6.1. Human primer sequences for quantitative polymerase chain reaction

Target	Primer Sequences (5'-3')	GenBank
Collagen II (α1)	ACCCCAATCCAGCAAACGTT	NM_001844
	ATCTGGACGTTGGCAGTGTTG	
Aggrecan	ACAGCTGGGGACATTAGTGG	NM_001135
	GTGGAATGCAGAGGTGGTTT	
SOX9	GCGGAGGAAGTCGGTGAAGAACGGGCA	NM_000346
	TGTGAGCGGGTGATGGGCGGG	
Collagen X (α1)	GGCCCAGCAGGAGCAAAGGG	NM_000493
	GTGGCCCGGTGGGTCCATTG	
Collagen I (α2)	GAAAACATCCCAGCCAAGAA	NM_000089
	GCCAGTCTCCTCATCCATGT	
Osteocalcin (BGLAP)	GTGCAGAGTCCAGCAAAGGT	NM_199173
	AGCAGAGCGACACCCTAGAC	
MyoD	GTCGAGCCTAGACTGCCTGT	NM_002478
	GTATATCGGGTTGGGGTTCG	
PPAR-γ2	TCCATGCTGTTATGGGTGAA	NM_015869
	GGGAGTGGTCTTCCATTACG	
GAPDH	GAGTCAACGGATTTGGTCGT	NM_002046
	TTGATTTTGGAGGGATCTCG	

6.2.3.4 Histological staining

ECM production by encapsulated MSCs was determined by immunostaining on days 1, 21, and 42. After rinsing in PBS, samples were placed into a solution of 5% w/v sucrose (EMD, Darmstadt, Germany) in PBS under vacuum (-25 inHg). The sucrose concentration was gradually increased over the course of 2 hours to 15% sucrose. Next, gels were subjected to increasing concentrations of 20% sucrose:OCT (VWR) over the course of 4 hours until samples were infiltrated with a 1:2 volume ratio of 20% sucrose:OCT. After vacuum infiltration overnight, samples were embedded in 1:2 20% sucrose:OCT solution by gentle freezing in liquid nitrogen and stored at -80ºC. Infiltrated hydrogels were cryosectioned at 20 µm thickness (Thermo Scientific, Cryostar NX70).

Sections were fixed in acetone, and OCT was rinsed in PBS. For aggrecan and collagen X staining, samples were deglycosylated with 30 µl of 0.75 U/ml chondroitinase ABC (Sigma-Aldrich) for 1.5 hours. Samples were blocked with Image-iT FX signal enhancer (Invitrogen). For primary antibody binding, sections were incubated overnight

at 4°C in monoclonal mouse anti-human collagen I, collagen II, aggrecan (Abcam), or collagen X (Sigma). Sections were then incubated for 30 minutes with highly cross-adsorbed Alexa Fluor 488-conjugated goat polyclonal anti-mouse immunoglobulin G (IgG, Molecular Probes, Carlsbad, CA) or IgM (Molecular Probes) for collagen X, and counterstained with 0.1 μg/mL 4',6-diamidino-2-phenylindole (DAPI, Anaspec, Fremont, CA). Negative controls were stained as described, but using a monoclonal mouse IgG1 isotype control (Abcam) with no known reactivity with human antigens as the primary antibody at 10 μg/mL. Histological sections were imaged using an epifluorescence microscope with a 20X magnification objective (Nikon Eclipse 80i, Tokyo, Japan) (n=2).

6.2.4 Statistical Analysis

All values were reported as mean ± standard deviation. For statistical analysis, PCR amplification data for each gene were first transformed using a Box-Cox transformation to obtain a normal distribution for analysis [390]. A two-factor analysis of variance (ANOVA) was used to determine statistical significance of groups, and Tukey's *post hoc* multiple comparison test with significance set at $p \leq 0.05$ indicated significance between individual samples. For DNA and gene expression analysis, the factors were hydrogel type and time. Statistical analysis was carried out using Minitab (v15.1, State College, PA).

6.3 Results

6.3.1 Viability in CS-MA and Ch-MA hydrogels during 6 weeks of culture

LIVE/DEAD staining of human MSCs in 50% CS-MA and 50% Ch-MA hydrogels indicated that visible MSCs appeared mostly viable over 6 weeks of culture

(Figure 6.1a). Cells remained dispersed evenly throughout the hydrogel scaffolds with a spherical shape, and no cell aggregation or spreading was observed. Total DNA content, as a measure of cell number, suggested that cellularity decreased over time in all hydrogel formulations (Figure 6.1b). DNA content significantly decreased by approximately half from day 1 to day 21 in all hydrogels; however, no significant differences were observed in DNA content between day 21 and day 42. Additionally, DNA content was significantly greater in 50% Ch-MA hydrogels than 50% CS-MA or PEG control hydrogels on days 1 and 21, suggesting that 50% Ch-MA hydrogels contained a higher cellularity.

6.3.2 Upregulation of gene expression for chondrocytic markers by MSCs encapsulated in 50% Ch-MA hydrogels

Human MSCs encapsulated in nonsulfated 50% Ch-MA hydrogels significantly upregulated gene expression of the cartilaginous ECM molecules collagen II and aggrecan on days 21 and 42, over 50% CS-MA hydrogels (Figure 6.2). MSCs in 50% Ch-MA expressed 83,100 ± 38,800 fold upregulation of collagen II expression, compared to only 28 ± 174 in 50% CS-MA and 2,650 ± 6,410 fold in PEG controls (Figure 6.2a). Similarly, aggrecan expression in Ch-MA gels was upregulated 76.0 ± 37.3 fold on day 42, compared to 4.9 ± 11.5 in CS-MA and 59.6 ± 25.5 in PEG (Figure 6.2c). Cartilaginous transcription factor SOX9 experienced slight upregulation on day 42 in 50% Ch-MA with 2.0 ± 1.5 fold regulation, while CS-MA only expressed 0.19 ± 0.11 fold regulation (Figure 6.2d). Collagen X, an ECM marker of hypertrophic chondrocytes, was also significantly upregulated in Ch-MA hydrogels over CS-MA and PEG controls

on days 21 and 42 (Figure 6.2e). MSCs in 50% Ch-MA upregulated collagen X by 202 ± 93 fold on day 42, compared to 11.0 ± 11.0 in CS-MA and 31.8 ± 14.1 in PEG controls.

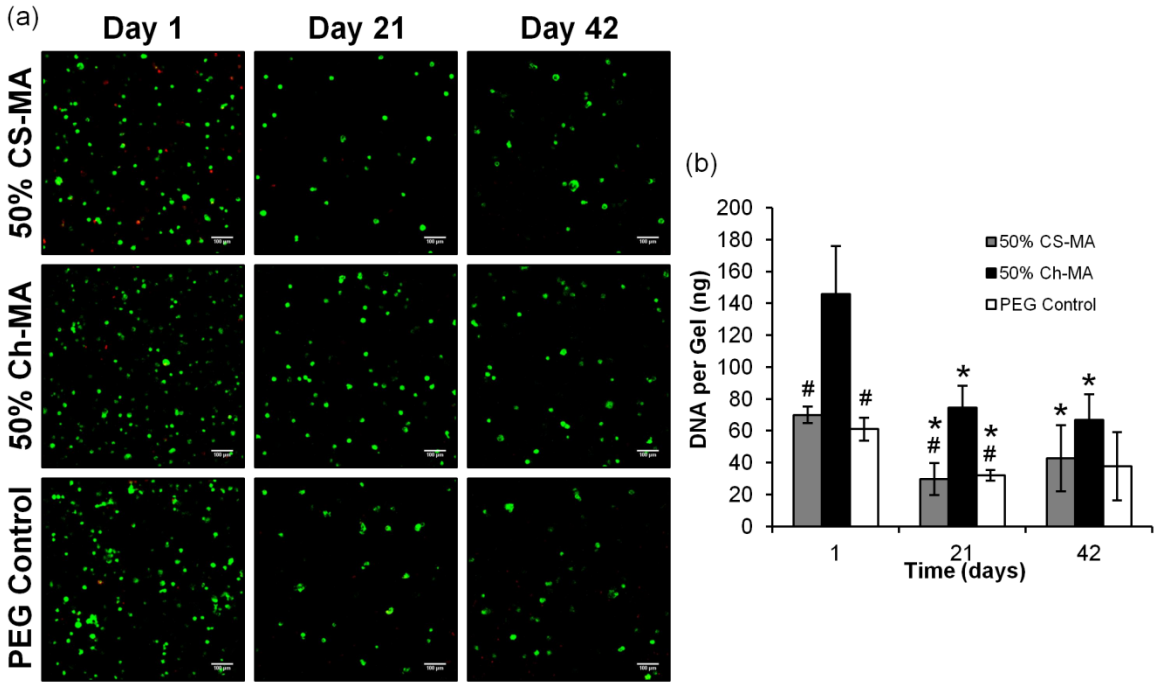

Figure 6.1. Viability and cellularity of human MSCs encapsulated in 50% CS-MA and 50% Ch-MA hydrogels. (a) Human MSCs appeared largely viable in all hydrogel formulations over 42 days of culture. Cells remained dispersed with a rounded morphology. Scale bars = 100 µm. (b) DNA content, as a measure of cellularity, decreased over time with a significant decrease observed between day 1 and day 21 in all hydrogel formulations. Additionally, greater DNA content was measured in 50% Ch-MA hydrogels on days 1 and 21, compared to 50% CS-MA and PEG controls. * indicates significantly less DNA than day 1 ($p \leq 0.05$). # indicates significantly less DNA than 50% Ch-MA hydrogels at the same time point ($p \leq 0.05$).

Markers for other tissues including fibroblastic marker collagen I, osteoblastic marker osteocalcin, myofibroblastic marker MyoD, and adipocytic marker PPAR-γ2 were also examined. Collagen I did not exhibit downregulation over the course of this study (Figure 6.3a). MSCs in PEG hydrogels actually exhibited 23.3 ± 15.2 fold upregulation of collagen I by day 42, and Ch-MA gels expressed 6.2 ± 4.2 fold regulation. The ratio of collagen II:collagen I relative expression suggested that MSCs in

50% Ch-MA hydrogels exhibited nearly equal expression of collagen II and collagen I after 42 days with a ratio of 1.03 ± 1.20, indicating significant upregulation from only $6.9x10^{-5}$ ± $2.6x10^{-3}$ on day 1 (Figure 6.2b). Osteocalcin displayed slight upregulation in encapsulated MSCs over time, but did not exhibit significant differences across hydrogel types (Figure 6.3b). MyoD expression demonstrated high variability and no significant trends (Figure 6.3c), while PPAR-γ2 did not amplify within 40 PCR cycles, indicating low PPAR-γ2 expression at all time points.

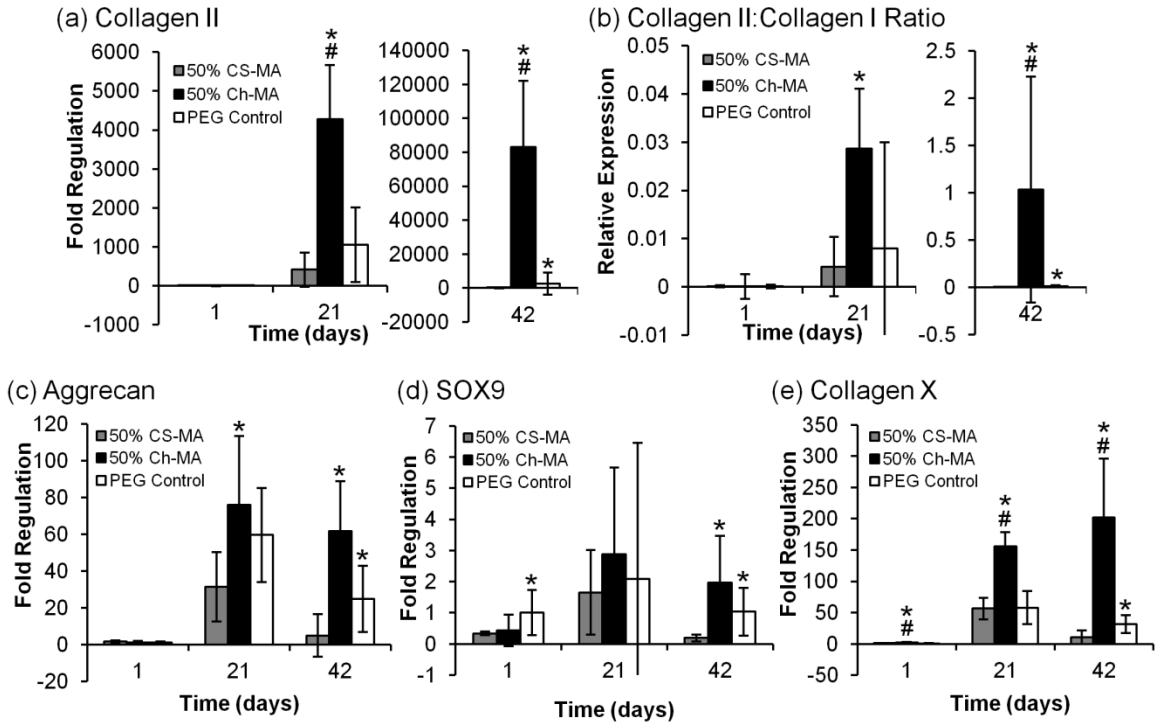

Figure 6.2. Gene expression of chondrocytic markers by MSCs in 50% CS-MA and 50% Ch-MA hydrogels. MSCs in 50% Ch-MA hydrogels significantly upregulated gene expression of (a) collagen II, (b) ratio of collagen II:collagen I relative expression, (c) aggrecan, and (d) SOX9 after 42 days, compared to 50% CS-MA. (e) Hypertrophic chondrocyte marker collagen X was also significantly upregulated in 50% Ch-MA gels on day 21 and 42 over 50% CS-MA and PEG controls. * indicates significantly greater than 50% CS-MA at same time point ($p \leq 0.05$). # indicates significantly greater than PEG controls at same time point ($p \leq 0.05$).

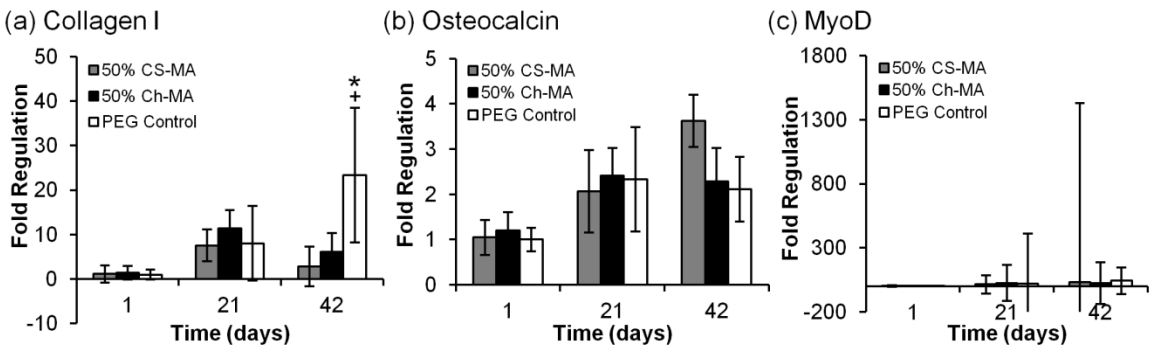

Figure 6.3. Gene expression of negative tissue markers by MSCs in 50% CS-MA and 50% Ch-MA hydrogels. While (a) collagen I, (b) osteocalcin, and (c) MyoD displayed some gene regulation in encapsulated MSCs over time, few differences were observed across hydrogel types. * indicates significantly greater than 50% CS-MA at same time point ($p \leq 0.05$). + indicates significantly greater than 50% Ch-MA at same time point ($p \leq 0.05$).

6.3.3 ECM deposition in GAG-containing hydrogels

Immunostaining for ECM production demonstrated that greater ECM production overall was observed in GAG-containing hydrogels over PEG control hydrogels, which showed relatively little staining for ECM (Figure 6.4). While some accumulation of cartilaginous ECM collagen II and aggrecan was observed pericellularly over 42 days, clear differences were not apparent between Ch-MA and CS-MA formulations (Figure 6.4a-b). Staining for collagen X, however, exhibited noticeably greater staining in 50% CS-MA hydrogels than Ch-MA gels (Figure 6.4c). Deposition of collagen I appeared to persist over time but few differences were observed between CS-MA and Ch-MA hydrogels (Figure 6.4d).

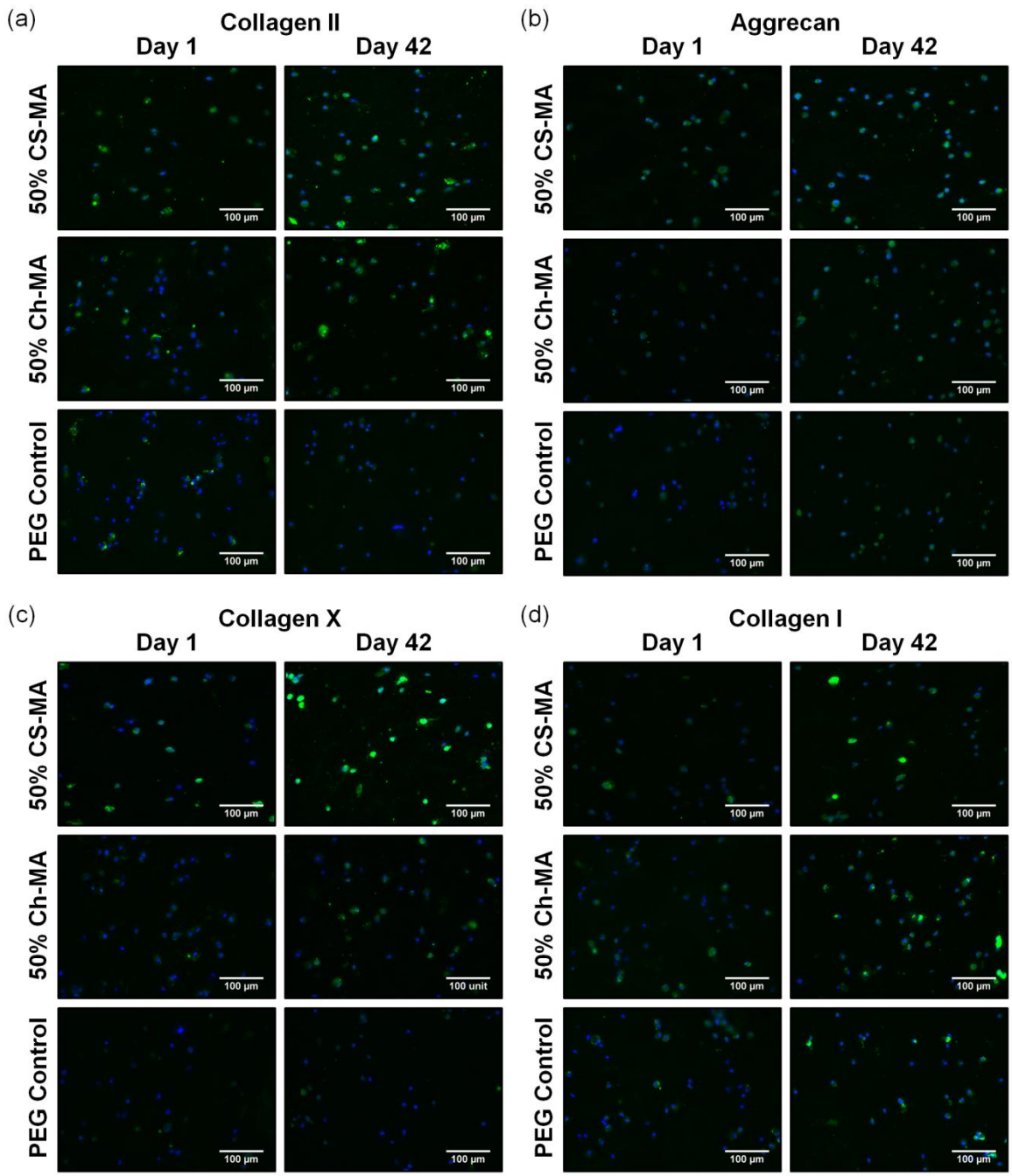

Figure 6.4. Immunostaining for ECM deposition by MSCs in 50% CS-MA and 50% Ch-MA hydrogels. (a) Collagen II and (b) aggrecan were produced in small quantities by MSCs in CS-MA and Ch-MA hydrogels, compared to relatively little deposition in PEG gels. Little difference was observed between 50% CS-MA and 50% Ch-MA. (c) Greater staining for collagen X was observed in 50% CS-MA gels. (d) Collagen I was produced by MSCs, but few differences were observed across gel types. Cell nuclei = blue. Scale bars = 100 µm.

6.4 Discussion

These studies demonstrated that viable MSCs remained dispersed throughout GAG-based hydrogels after 6 weeks of culture *in vitro*, despite significant decreases in DNA content over time (Figure 6.1), and that nonsulfated chondroitin materials upregulated gene expression of chondrogenic markers in human MSCs, compared to CS materials, when cultured in chondrogenic medium (Figure 6.2). MSCs encapsulated in 50% Ch-MA hydrogels exhibited significantly greater gene expression of collagen II, aggrecan, and SOX9 than MSCs in 50% CS-MA gels after 42 days of culture in chondrogenic medium containing TGF-β1, suggesting that nonsulfated chondroitin materials may promote greater chondrogenic differentiation over CS. As described in Chapter 5, 50% Ch-MA hydrogels swelled significantly less than 50% CS-MA; therefore, in these experiments, PEG hydrogels that swelled similarly to 50% Ch-MA hydrogels were used as swelling controls. MSCs have been shown to regulate differentiation in response to both substrate stiffness and pore size *in vitro* [160, 162, 391-392]; therefore, PEG swelling controls were used as approximate controls for material stiffness and porosity/mesh size in the absence of charged polysaccharides [45, 380]. In this experiment, MSCs in uncharged PEG control hydrogels expressed significant upregulation of collagen II, aggrecan, and SOX9 gene expression over 50% CS-MA hydrogels after 6 weeks; however, gene expression of chondrogenic markers remained less than that observed in MSCs in Ch-MA materials, suggesting that upregulation in 50% Ch-MA hydrogels was not solely due to differences in swelling properties.

An investigation of CS-MA and Ch-MA hydrogels, compared to PEG-based swelling controls, at earlier time points (1, 7, 14, 21 days) and lower cell density ($10x10^6$

cells/mL) demonstrated similar trends of upregulation of gene expression by MSCs in Ch-MA hydrogels in the presence of chondrogenic medium; however, in the absence of TGF-β1 and dexamethasone, chondroitin materials did not exhibit significant upregulation of gene expression for cartilaginous markers (Figure A.2). These results indicated that nonsulfated chondroitin materials alone were not sufficient to upregulate gene expression of cartilaginous markers by MSCs, and that upregulation of chondrogenic markers may be dependent on interactions between the chondroitin material and chondrogenic cues from exogenously supplemented TGF-β1. Interestingly, CS materials did significantly upregulate collagen II gene expression, in the absence of TGF-β1 and dexamethasone on day 21, while chondroitin materials did not (Figure A.2), suggesting that CS materials may possess the unique ability to promote chondrogenic differentiation in the absence of exogenous soluble cues. While this presents an interesting potential utility of CS-based materials, due to inconsistency within these CS samples and the greater overall response observed in chondroitin materials in the presence of chondrogenic medium, these trends have not been examined in further detail. Together, these contrasting responses in the presence and absence of chondrogenic media suggested that MSCs encapsulated in CS and chondroitin materials differentially regulate their response to soluble chondrogenic cues.

The ability of CS and chondroitin materials to differentially "pull-down" soluble TGF-β1 out of solution, as discussed in Chapter 5, is analogous to culture in chondrogenic medium, as GAG scaffolds may electrostatically bind and retain TGF-β1 within their networks. The pull-down experiments presented in Chapter 5 demonstrated that 50% CS-MA depleted greater amounts of TGF-β1 from solution than 50% Ch-MA in

a sulfation-dependent manner, suggesting that CS-based materials may sequester TGF-β1 from chondrogenic medium, thus increasing the local concentration of growth factor in close proximity to cells or modulating signaling efficiency within GAG-based scaffolds. Although enhanced upregulation of chondrogenic markers in Ch-MA materials over CS-MA hydrogels may appear to contradict this hypothesis, the high negative charge density of CS in these materials could potentially decrease TGF-β1 activity or inhibit transport within the hydrogel network; therefore, removal of sulfate groups may promote MSC differentiation via enhanced growth factor signaling. In studies by Seto et al., similar PEG hydrogels containing 10% heparin, a highly sulfated GAG, exhibited restricted diffusion of a positively charged model protein into the hydrogel network, and encapsulated MSCs co-cultured with osteoblasts demonstrated preferential mineralization at the surface of these hydrogels, potentially suggesting sequestration and limited transport of osteoblast-secreted soluble factors into the hydrogel scaffolds [393]. Noticeable spatial differences in ECM production, as observed by immunostaining, were not apparent in the experiments presented here; however, overall ECM deposition appeared to remain relatively low throughout all hydrogel types. The highly charged CS matrix may also prevent transport of other cell-secreted signals within the hydrogel, effectively inhibiting intercellular communication, which plays important roles in supporting chondrogenic differentiation and maintaining a chondrocytic phenotype [24, 38, 394-395]. Nevertheless, it is important to note that chondroitin remains moderately negatively charged at physiological pH despite the absence of sulfates, due to the presence of carboxylates in the GAG structure, and may retain electrostatic interactions with TGF-β1, albeit to a lesser degree than CS. These results suggest that decreasing the

degree of sulfation in GAG-based hydrogels may be better suited for promoting chondrogenic differentiation of MSCs than highly sulfated CS, and that differential sequestration or altered presentation of TGF-β1 to encapsulated MSCs may contribute to the observed differences in the gene expression between CS-MA and Ch-MA materials.

TGF-β1 pull-down experiments, as presented in Chapter 5, also found that PEG control hydrogels demonstrated similar degrees of TGF-β1 depletion to 50% Ch-MA gels in 1% BSA solutions, even though retention was not influenced by increased ionic strength in the presence of 0.5 M NaCl. These results suggested that PEG materials may be trapping similar amounts of TGF-β1 from solution as 50% Ch-MA, although the observed interaction with neutrally charged PEG-based materials is likely by non-electrostatic means. Nevertheless, 50% Ch-MA hydrogels enhanced gene expression of chondrogenic markers over PEG control hydrogels, despite similarities in TGF-β1 adsorption and swelling properties (Figure 6.2). These results suggested that the GAG-based matrix in Ch-MA hydrogels may play a unique role in supporting chondrogenic differentiation over PEG-based materials, independent of electrostatic growth factor sequestration and swelling, and the polysaccharide network or intermediate degree of negative charge in Ch-MA materials may have other undetermined influences on chondrogenic differentiation that warrant further investigation. As opposed to TGF-β1 sequestration by the material scaffolds to enhance MSC response, the materials themselves may alter the chondrogenic response by MSCs in the presence of soluble chondrogenic cues. As a moderately negatively charged component of cartilaginous matrix, chondroitin may alter the stem cell microenvironment through various interactions with ECM, cell surface receptors, and signaling molecules (besides TGF-β1)

to promote chondrogenic gene expression in encapsulated MSCs, in ways where synthetically-derived, neutrally charged PEG materials likely would not.

Despite significant differences in gene expression between MSCs encapsulated in Ch-MA and CS-MA hydrogels, these material effects were not as apparent in immunostaining for chondrogenic ECM markers. In general, greater ECM deposition was observed pericellularly in GAG-based CS-MA and Ch-MA materials than PEG control gels, which exhibited limited staining for ECM overall (Figure 6.4); however, notable differences in collagen II and aggrecan deposition were not evident between Ch-MA and CS-MA hydrogels, despite significant differences in gene expression. It appears that MSCs may have lacked sufficient extracellular space for significant matrix production in these tightly crosslinked hydrogel scaffolds, suggesting that degradation of the hydrogel network may play a key role in facilitating ECM deposition by encapsulated MSCs. While PEG-DA and OPF materials contain hydrolytically degradable ester moieties, PEG control hydrogels were not expected to experience significant degradation over the course of the 6-week study presented here. CS-MA and Ch-MA are degradable by chondroitinase enzyme, as described in Chapter 5; however, chondrogenic human MSCs may not produce sufficient amounts of chondroitinase enzyme to effectively degrade the GAG network, thus inhibiting the deposition of cartilaginous ECM by encapsulated MSCs. A previously study by Varghese et al. reported significant cellular aggregation of goat MSCs encapsulated in CS/PEG hydrogels, suggesting that cells of other mammalian species may possess greater ability to degrade and remodel the dense CS matrix [8]. Both hydrolytic and cell-mediated enzymatic degradation have been functionally incorporated into PEG-based hydrogels in order to support scaffold degradation in a controlled manner

[169, 185-187, 396], suggesting that similar techniques to enhance material degradation may support greater ECM deposition in Ch-MA and CS-MA materials.

While MSCs significantly upregulated expression of chondrogenic markers in 50% Ch-MA hydrogels, gene expression of collagen I did not decrease and actually appeared to increase over the time course of these experiments (Figure 6.3a). Collagen type I is normally produced in high amounts by undifferentiated MSCs, but is not normally present in hyaline cartilage [105]. While expression of collagen type II was very low at day 1 relative to collagen I expression, with only a $6.9x10^{-5} \pm 2.6x10^{-3}$ ratio of collagen II:collagen I relative expression, by day 42 MSCs exhibited a significantly greater collagen II:collagen I ratio of 1.03 ± 1.20, despite some large variability, suggesting that collagen II and collagen I may have been expressed in comparable amounts at the mRNA level after 6 weeks (Figure 6.2b). As key differentiation markers of osteogenic, myofibroblastic, and adipocytic phenotypes were not significantly regulated in these studies, these gene expression results are representative of a more fibrochondrocytic phenotype. Fibrocartilaginous tissues appear in the menisci, annulus fibrosis of intervertebral discs, temporomandibular joint, as well as the insertions of tendon/ligament into bone, and contain a fibrous collagen I matrix along with cartilaginous ECM, including collagen II and aggrecan [27-29].

Hypertrophy of chondrogenic MSCs remains a key challenge to *in vitro* chondrogenic differentiation [97, 103-104], and gene expression of collagen X, an ECM marker of hypertrophic chondrocytes, was significantly upregulated in 50% Ch-MA hydrogels, compared to CS-MA and PEG control gels. In contrast, immunostaining results suggested that CS-MA materials may actually facilitate greater production or

retention of collagen X matrix than Ch-MA hydrogels, even though relatively little ECM production by encapsulated cells was observed overall. Because sulfated GAGs are known to interact with a variety of ECM molecules [334, 397], it is important to consider that CS hydrogels may also differentially retain ECM within the scaffolds, compared to chondroitin. While some collagens can electrostatically interact with GAGs [398] and collagen X is highly glycosylated *in vivo* [399], the differential effects of sulfation on ECM retention require further investigation in greater depth, specifically in degradable or larger mesh size materials that may support greater degrees of ECM production.

DNA content within hydrogel constructs appeared decrease over time with a significant decrease between days 1 and 21 in all hydrogel types. This result is consistent with long-term culture in other PEG-based hydrogels in which the small mesh size and low overall degradability of the scaffold prevent cell division, due to limited space within the dense polymer matrix. A fraction of encapsulated cells likely undergo cell death over time, resulting in a decrease in total DNA [197, 207, 393]. Additionally, undifferentiated MSCs require the presence of adhesive cues that promote integrin binding to maintain cell viability in hydrogel materials [400]; however, persistence of these adhesive cues over time may inhibit the long-term chondrogenic response of MSCs [213]. MSCs express fibronectin during pre-cartilaginous condensation in the developing mesenchyme, then downregulate expression during differentiation into chondrocytes [24, 401], suggesting that early presentation of adhesive proteins or peptides may promote MSC viability following encapsulation and that removal of these adhesive signals over time may be necessary to support chondrogenic differentiation of MSCs [137].

It is also important to note that the DNA content in 50% Ch-MA was significantly greater than in 50% CS-MA and PEG controls by approximately two-fold on days 1 and 21, based on PicoGreen assay results. Though later time points may be explained by improved viability in Ch-MA materials, the difference in DNA on day 1 indicated a difference in encapsulation density, which could potentially confound results. However, based on the large differences in gene expression in Ch-MA hydrogels, along with similar trends of upregulation observed at early time points (days 7, 14, 21) in hydrogels with more similar DNA contents (Figure A.1-2), it appears that the cellular response in Ch-MA materials was primarily influenced by material interactions with Ch-MA in the presence of soluble chondrogenic factors, rather than simply increased cell density.

Together, these results have demonstrated that nonsulfated chondroitin hydrogels promote gene expression of chondrogenic markers by MSCs in a TGF-β1-dependent manner, and in Chapter 5, desulfation of CS was shown to reduce sequestration of TGF-β1, suggesting that electrostatic interactions with GAGs may play a role regulating TGF-β1 signaling to promote differentiation. However, it is important to consider that sulfation and charge may also alter the extracellular microenvironment through related differences in osmotic swelling pressure or through various interactions with the ECM, cell surface receptors, or other signaling molecules to influence MSC gene expression in response to soluble chondrogenic cues, independent of biomaterial sequestration of TGF-β1. Therefore, to fully elucidate the role of GAG-based materials in promoting chondrogenic differentiation, further investigation would be required to determine the cellular interactions with CS and downstream signals that result in an enhanced chondrogenic response. Controlled systems of study may clarify the importance of electrostatic growth

factor interactions in promoting differentiation. TGF-β3 would offer a closely related molecule with similar signaling mechanism and chondrogenic response to TGF-β1 (pI ~9.5), but TGF-β3 (isoelectric point, pI ~6.8) would not be expected to electrostatically interact with sulfated GAGs at physiological pH due to its difference in charge [274-276], providing a closely related comparison to examine the role of electrostatic growth factor interactions in differentiation.

CS and nonsulfated chondroitin may be combined in varying ratios to develop materials with a range of negative charge densities, and the results presented here suggest that these materials may be valuable tools to examine the role of charge in directing differentiation of MSCs in a highly controlled manner. The combined roles of sulfation in modulating TGF-β1 sequestration in Chapter 5 and chondrogenic gene expression by MSCs in nonsulfated materials in the presence of soluble chondrogenic cues in these studies suggested that an intermediate degree of sulfation may be advantageous to enhance TGF-β1 signaling and MSC response for greater chondrogenic differentiation. Alternatively, altering the presentation of TGF-β1 through a dose response may examine the ability of CS-based materials to regulate signaling in response to low TGF-β1 concentration environments, or temporal control of TGF-β1 presentation by withdrawing exogenously supplemented TGF-β1 after a period of pre-culture may examine the persistence of these signals in CS-based hydrogels.

Sulfated and nonsulfated GAG materials provide a highly controlled system to examine the interactions between charged GAGs and MSCs to promote chondrogenic differentiation, possibly through sequestration of growth factors, and these materials

possess tremendous potential as tissue engineering constructs for controlled tissue regeneration and patterning.

6.5 Conclusions

These studies have demonstrated that encapsulation in CS and chondroitin hydrogels enhanced gene expression of chondrogenic markers by MSCs in 50% Ch-MA materials in the presence of TGF-β1, compared to 50% CS-MA and PEG-only hydrogels, suggesting that chondroitin materials may be better suited for supporting chondrogenic differentiation than CS, due to their reduced sulfation and negative charge density. However, differences in production of cartilaginous ECM were not apparent in between Ch-MA and CS-MA hydrogels, as MSCs may lack sufficient space for significant matrix deposition in these tightly crosslinked hydrogel scaffolds. Greater degradation of the hydrogel network, either through hydrolytic or enzymatic means, may be required to facilitate ECM deposition in these GAG-based materials. These results present CS and nonsulfated chondroitin materials as valuable tools to alter GAG sulfation in a highly controlled manner as a biomaterial approach to differentially regulate MSC response to soluble differentiation cues. These concepts represent a first step in the development of novel biomaterials for regulating chondrogenic cues to regenerate the complex ECM architecture of cartilaginous tissues for long-term repair.

CHAPTER 7

CONCLUSIONS AND RECOMMENDATIONS

7.1 Summary

Tissue engineering strategies offer exciting and innovative approaches to treat cartilage injuries for long-term regeneration and repair; however, difficulty regenerating the complex extracellular matrix (ECM) composition and organization of native cartilage remains a significant challenge. Mesenchymal stem cells (MSCs) are multipotent progenitor cells that are capable of forming cartilaginous tissues, making them a promising cell source for tissue repair [6]. In cartilage tissue, cells are expected to synthesize, maintain, and remodel the ECM to maintain function and integrity; however, the complex cues necessary to promote cartilage formation are not fully understood [5]. Recent research has begun to investigate the ability of cartilaginous ECM molecules to promote and direct MSC differentiation down a chondrogenic lineage.

Chondroitin sulfate (CS), a cartilaginous glycosaminoglycan (GAG) that is expressed both during cartilage development and in adult cartilage associated with proteoglycans, has been shown to promote production of cartilaginous ECM by MSCs [8-9]; therefore, CS appears to play a role in altering stem cell microenvironments to direct differentiation down a chondrogenic lineage. The overall goal of this dissertation was to develop versatile biomaterial platforms to control CS presentation to MSCs in order to improve understanding of the role of CS in promoting chondrogenic differentiation. To investigate chondrogenic response to a diverse set of CS materials, progenitor cells were cultured in the presence of CS proteoglycans and CS GAG chains in a variety of 2D and

3D material systems, including surfaces coated with aggrecan proteoglycan, CS-based nanospheres and microspheres, and desulfated chondroitin hydrogels. Together these studies provided valuable insight into the unique ability of CS materials to alter cell morphology and growth factor sequestration to promote chondrogenic differentiation as part of tissue engineering strategies to promote cartilage regeneration and repair.

In Chapter 3, cellular interactions with 2D aggrecan-coated surfaces were examined for morphology and production of cartilaginous ECM. Aggrecan was passively adsorbed onto tissue culture-treated surfaces, and bovine bone marrow stromal cells (BMSCs) and anterior cruciate ligament (ACL) fibroblasts were cultured on aggrecan-coated 2D surfaces, compared to tissue culture-treated control surfaces and nonadhesive surfaces that promoted cell aggregation. Culture on aggrecan surfaces promoted cell aggregation, and BMSC and ACL fibroblast aggregates significantly upregulated aggrecan gene expression and production over 14 days of culture in the absence of chondrogenic media supplements, regardless of how cell clustering was induced. These findings support the use of aggregate-inducing materials, including CS-modified surfaces, to encourage production of aggrecan and emphasize the role of high-density culture in promoting production of chondrocytic ECM.

In Chapter 4, small particle carriers were developed to study CS interactions with charged growth factors. CS-derived nanoscale micelles and microscale particles were fabricated as potential growth factor carriers to enhance stem cell differentiation, and particles were characterized for size, surface charge, cytocompatibility, as well as growth factor release. Conjugation with a hydrophobic methacrylamide group induced spherical CS micelles to self-assemble in an aqueous environment, and micelles were negatively

charged with a bimodal distribution of ~320 and ~73 nm diameters. Larger CS microspheres, synthesized from crosslinking of methacrylated CS in a water-in-oil emulsion, possessed a rounded morphology and a diameter of ~4.3 μm. Positively charged transforming growth factor-β1 (TGF-β1) demonstrated minimal release from CS microspheres over 5 days, while negatively charged tumor necrosis factor-α (TNF-α) exhibited substantial burst release, suggesting that TGF-β1 electrostatically complexed with negatively charged CS. These studies suggested that CS-based carriers can be fabricated over a variety of nano- and microscale sizes, as potential ECM-derived carriers of positively charged growth factors to direct stem cell differentiation.

In Chapters 5 and 6, desulfated chondroitin materials were synthesized to study sulfation-dependent CS interactions in growth factor sequestration and chondrogenic differentiation. CS was chemically desulfated by acidic methanol treatment, and desulfated chondroitin materials were thoroughly characterized to ensure desulfation and decreased charge density without significant modification of the CS chemical structure. Desulfated chondroitin demonstrated ~98.5% desulfation after 7 days of chemical treatment. Crosslinked CS hydrogels consistently demonstrated greater sequestration of TGF-β1 as indicated by greater depletion from solution and less release after loading, than desulfated chondroitin; however, human MSCs encapsulated in nonsulfated chondroitin hydrogels experienced significantly greater gene expression of cartilaginous markers when cultured for 6 weeks in chondrogenic medium containing TGF-β1. These results suggested that controlled desulfation of GAG-based materials modulated growth factor interactions, and less sulfated chondroitin materials may support greater chondrogenic differentiation of human MSCs in the presence of chondrogenic medium.

Together, these findings presented in this dissertation suggested that CS plays an important role in directing chondrogenic differentiation via morphological and electrostatic interactions, and CS and chondroitin materials are promising tools to control GAG presentation within a variety of stem cell microenvironments to promote differentiation for cartilage repair.

7.2 Conclusions

The research presented in this dissertation advances understanding of how diverse CS-based biomaterials can control the presentation of GAGs within a variety of stem cell microenvironments to promote differentiation. Due to the abundance of CS in cartilaginous tissues, both during development and in adult tissues, highly controlled GAG presentation may have important implications in the engineering of novel strategies for cartilage repair. 2D surfaces, small scale particle carriers, and 3D bulk hydrogels were developed from CS-based materials to investigate stem cell interactions with sulfated GAGs, and the results of these studies suggested that highly negatively charged CS-based materials can 1) present morphological cues to promote cell aggregation and 2) regulate biomaterial interactions with charged growth factors to promote differentiation. The sulfation and resulting negative charge density of CS appears to play a critical role in morphological and growth factor signaling cues that may direct the chondrogenic differentiation of MSCs. Together, these results suggested that CS-based materials may possess the unique ability to deliver and modulate growth factor interactions through delivery and sequestration within stem cell aggregates.

Adsorption of the cartilaginous CS proteoglycan aggrecan onto 2D surfaces, as described in Chapter 3, promoted cellular aggregation of bovine BMSCs and ACL fibroblasts. The presence of aggrecan appeared to resist cell attachment and spreading on tissue culture surfaces, forcing adherent cells to cluster in close contact with one another. Formation of these dense BMSC and ACL fibroblast aggregates was accompanied by upregulation of aggrecan gene expression; however, upregulation was found to be a response to morphological cues rather than a response to the aggrecan-coated surfaces. Cell aggregates on nonadhesive culture surfaces that encouraged clustering in the absence of aggrecan also promoted upregulation of aggrecan gene expression, as well as aggrecan production within the cell spheroids. Aggregation may enhance ECM production through changes in cell shape, cell-cell contact, or intercellular signaling. These results demonstrated that CS-based materials could be used as a naturally-derived material to promote cell clustering and emphasized the importance of high density culture in promoting and supporting expression and production of cartilaginous ECM.

Pellet culture and micromass culture are established methods to delay the dedifferentiation of chondrocytes or to promote chondrogenic differentiation of MSCs [6, 98, 304-305]; therefore, it is not surprising that aggregation promoted a more cartilaginous phenotype in these studies. High-density culture supports close cell-cell contact and appears to mimic the cell environment of mesenchymal condensation that occurs during early cartilage development [24, 308]. Within the condensing mesenchyme, neural-cadherin (N-cadherin), neural cell adhesion molecule (N-CAM), and gap junctions form cell-cell contacts that facilitate intercellular communication and play a critical role in regulating the deposition of cartilaginous ECM [24]. As increasing

amounts of ECM are produced, the cells are pushed apart until individual chondrocytes become embedded in cartilaginous matrix [13, 27]. In this dissertation, aggrecan-coated surfaces used a native cartilage proteoglycan to control cell morphology by promoting self-assembly into dense cell aggregates, possibly due to the anti-adhesive properties of negatively charged CS [402-404]. Subsequent production of aggrecan proteoglycan by bovine BMSC and ACL fibroblast aggregates in the absence of exogenous chondrogenic factors suggested that aggrecan-mediated clustering may be especially advantageous to promote stem cell differentiation toward more cartilaginous or fibrocartilaginous phenotypes. CS-containing 3D hydrogels have also been demonstrated to support cell aggregation and subsequent production of chondrocytic ECM by encapsulated MSCs in the presence of chondrogenic medium [8]. Together, these data suggested that GAG-based materials could potentially be used as ECM-derived cell carriers to promote cell clustering and production of chondrocytic ECM in the development of tissue engineering strategies for cartilage repair.

The importance of high-density culture in chondrogenesis suggested that the development of biomaterial platforms to control presentation of CS within dense cell aggregates may be advantageous to promote chondrogenic differentiation. A significant challenge that accompanies micromass culture of stem cells involves transport properties within cell pellets. These dense, multicellular spheroids present numerous barriers to diffusion, in particular limited transport of soluble growth factors from the culture medium [322]. Insufficient transport may result in heterogeneous or disorganized differentiation within MSC pellets or embryonic stem cell (ESC) embryoid bodies; therefore, micromass culture presented a need to enhance growth factor signaling within

dense cell aggregates. CS-based materials may possess the unique ability to enhance growth factor signaling through sequestration, delivery, and release of growth factors to promote stem cell differentiation; therefore, CS-based biomaterial platforms were developed to examine electrostatic interactions between sulfated GAGs and positively charged growth factors.

Negatively charged GAGs have been shown bind and sequester a variety of charged growth factors [263, 272, 319], and these interactions can be exploited for controlled growth factor retention and release by GAG-based carriers [262, 264]. CS is a naturally occurring ECM component that is abundant in cartilaginous tissues, and TGF-β1 plays critical roles in promoting chondrogenesis *in vivo* and *in vitro* [340-342]; therefore, electrostatic interactions between CS and TGF-β1 may be particularly advantageous to promote chondrogenic differentiation of stem cells. Sulfated GAGs appear to interact with TGF-β1 via basic amino acid residues at the tips of its β-strand loops [272, 274], and highly sulfated GAGs may potentiate TGF-β1 activity, suggesting that GAG interactions may have a synergistic effect in TGF-β1 signaling [251, 272, 278]. CS proteoglycans are highly regulated during mesenchymal condensation during early cartilage development [14-18], and culture in CS-containing hydrogels has demonstrated upregulated expression and production of chondrocytic ECM by encapsulated mesenchymal stem cells in the presence of chondrogenic medium [8-9], suggesting that CS may play a unique role in directing growth factor signaling to promote chondrogenic differentiation of progenitor cells [14-15].

Because the high negative charge density of CS is largely attributable to the abundance of sulfate groups along its repeating GAG backbone, sulfation was expected

to play a significant role in modulating interactions with charged growth factors; therefore, in Chapter 5, the role of sulfation in growth factor sequestration was examined through chemical desulfation of the primary CS backbone. CS was chemically desulfated by acidic methanol treatment for 7 days, and desulfation yielded a nonsulfated chondroitin product, resulting in a significant reduction in negative charge density, with little modification of the native CS chemical structure. Subsequent methacrylation of these chains allowed CS and chondroitin to be covalently crosslinked to form bulk 3D hydrogels; therefore, CS and desulfated chondroitin materials provided a highly controlled system to study the role of sulfation and resulting negative charge in electrostatic sequestration of growth factors, specifically TGF-β1.

Desulfation of CS was found to alter the sequestration and release of TGF-β1 in a sulfation-dependent manner *in vitro*. In release studies, in which PEG hydrogels containing varying amounts of CS and chondroitin were loaded with TGF-β1, 50% CS materials demonstrated the greatest retention and the least cumulative release of TGF-β1 over 7 days, while decreasing the CS content to 10% CS-MA resulted in significantly more release, suggesting that CS retained TGF-β1 in a concentration-dependent manner. Additionally, 50% chondroitin hydrogels, which maintained an identical total GAG content to 50% CS hydrogels but with reduced sulfation, exhibited significantly greater release of TGF-β1 than 50% CS-MA, and these results suggested that sulfation and corresponding negative charge were critical in facilitating electrostatic interaction with growth factors. The ability of CS to retain growth factors, sequestering them from release, proposed that CS-based biomaterials may have potential applications in sequestering growth factors for enhanced stem cell differentiation.

To examine an alternate system of sequestration, rather than release from CS materials, hydrogels containing varying ratios of CS and nonsulfated chondroitin while maintaining a 50% total GAG content were examined for their ability to deplete soluble TGF-β1 by "pulling" it out of solution and trapping it with their hydrogel networks. After incubation in a 2 ng/mL TGF-β1 solution, 50% CS hydrogels demonstrated significant depletion of soluble TGF-β1 out of solution, while decreasing the sulfation of the GAG matrix reduced the observed interaction with TGF-β1 in a sulfation-dependent manner. Nonsulfated 50% chondroitin gels exhibited significantly less pull-down of TGF-β1, while 10% CS/40% chondroitin hydrogels sequestered an intermediate degree of TGF-β1. In addition, incubation in 0.5 M NaCl or 10 mg/mL soluble CS significantly inhibited the amount of depletion by 50% Ch-MA hydrogels; however, a similar decrease in depletion was not observed in 50% CS-MA hydrogels. These results suggested that while chondroitin materials retain some ability to electrostatically sequester TGF-β1, likely due the presence of negatively charged carboxylates along its repeating backbone, binding with chondroitin appeared to be much weaker than with CS. The inability of soluble CS to competitively inhibit binding to 50% CS-MA also suggested that TGF-β1 may specifically possess a stronger ability to bind to crosslinked CS hydrogels over soluble CS. Together these results suggested that CS-MA hydrogels possessed a relatively strong ability to sequester soluble TGF-β1 out of solution, and that binding of TGF-β1 can be controlled in a sulfation-dependent manner through chemical desulfation of CS.

Desulfation of CS provides a well-controlled biomaterial system to alter the electrostatic interactions between CS and charged growth factors, and these materials could therefore be used to control presentation of growth factors to stem cells for

differentiation. The ability of CS and chondroitin to differentially "pull-down" soluble TGF-β1 out of solution provided rationale to examine the effect of differentially sulfated materials on the chondrogenic differentiation of MSCs, as CS may similarly sequester TGF-β1 from chondrogenic media for controlled presentation to encapsulated MSCs. To characterize the cellular response while entrapped in CS and nonsulfated chondroitin matrix, human MSCs were encapsulated in PEG hydrogels containing either 50% CS or 50% chondroitin and cultured for 6 weeks in chondrogenic medium containing TGF-β1, as discussed in Chapter 6. Encapsulation in PEG-based hydrogels provided an established model for chondrogenic differentiation of MSCs *in vitro* [136, 199, 206-208], and PEG-based materials, in particular, have been used in the past as systems to investigate the effects CS matrix on chondrogenic differentiation of MSCs [8-9, 252].

CS- and chondroitin-containing materials were shown to differentially modulate the chondrogenic response of encapsulated MSCs in response to chondrogenic growth factor, suggesting that sulfation may play a role in regulating chondrogenic differentiation; however, MSCs in 50% chondroitin hydrogels displayed significantly greater upregulation of chondrogenic markers than 50% CS gels after 6 weeks of culture in chondrogenic medium. Chondrogenic gene expression in chondroitin hydrogels was dependent on the presence of exogenously supplemented TGF-β1 in the medium, suggesting that chondroitin materials alone were not sufficient to upregulate expression and that desulfation of the CS matrix enhanced the chondrogenic response to TGF-β1. Despite a higher degree of TGF-β1 sequestration, as shown in Chapter 5, the high negative charge density of CS in these materials could possibly decrease TGF-β1 signaling activity or inhibit transport within the hydrogel network. The highly charged

CS matrix may also prevent transport of other cell-secreted signals within the hydrogel, effectively inhibiting intercellular communication, which plays an important role in supporting chondrogenic differentiation and maintaining a chondrocytic phenotype [24, 38, 394-395]. Removal of sulfate groups from CS, however, appeared to promote MSC differentiation, possibly through enhanced growth factor signaling. Desulfated chondroitin materials remained moderately negatively charged at physiological pH, due to the presence of carboxylates in the chondroitin structure, and chondroitin may still possess electrostatic interactions with TGF-β1, though binding appeared to be weaker than with CS. These results suggested that decreasing the degree of sulfation in GAG-based hydrogels may be better suited for supporting chondrogenic differentiation than highly sulfated CS, despite stronger electrostatic interaction with CS, and that CS and chondroitin materials possess potential as biomaterials to alter stem cell microenvironments to differentially regulate chondrogenic differentiation of MSCs.

Unfortunately, despite large differences in gene expression after 42 days of culture *in vitro*, relatively little ECM deposition was observed within the hydrogel constructs with no noticeable difference between CS and chondroitin hydrogels. This is likely due to the small mesh size of these highly-crosslinked hydrogel constructs, as MSCs may have lacked sufficient extracellular space for significant matrix production. Controlled degradation of the hydrogel network may play a key role in facilitating ECM deposition by encapsulated MSCs, either by hydrolytic or cell-mediated enzymatic means. Hydrolytic degradation of crosslinked hydrogel scaffolds is dependent on the number of ester moieties within the polymer backbone; however, the degradation rate of these esters can be systematically controlled by altering the hydrophilicity of the

surrounding environment. Cell-mediated degradation through the incorporation of matrix metalloproteinase (MMP)-cleavable peptide sequences can encourage controlled degradation localized to the extracellular environment, and degradation rate can be customized through these peptides for susceptibility to cleavage, as well as specificity to a single MMP type that is expressed by specific cell populations [169, 185-187, 396]. Controlled degradation of CS-MA and Ch-MA hydrogel networks may facilitate greater ECM deposition and enhanced chondrogenic differentiation by encapsulated MSCs.

Despite significant upregulation of chondrogenic markers, collagen X, an ECM marker of hypertrophic chondrocytes, was also significantly upregulated in 50% chondroitin hydrogels; however, 50% CS gels exhibited visibly greater deposition of pericellular collagen X after 42 days than 50% chondroitin. Hypertrophy of chondrogenic MSCs remains a key challenge to *in vitro* differentiation [97, 103-104]; however, just as specific signals may promote chondrogenic differentiation of MSCs, it is also likely that additional signals may be required to maintain a mature chondrocyte phenotype, while inhibiting progression toward hypertrophy. Indian hedgehog (Ihh) and parathyroid hormone-related protein (PTHrP) signaling appear to interact *in vivo* through paracrine signaling from the perichondrium to regulate chondrocyte maturation and hypertrophy [38]. Basic fibroblast growth factor (bFGF) and PTHrP have also been investigated for their ability to delay hypertrophy and maintain chondrocytic phenotype *in vitro* with some success [106-109]. Additionally, collagen type I gene expression and production did not appear to decrease in 50% chondroitin materials, representative of a more fibrocartilaginous response. Collagen type I is normally produced in high amounts by undifferentiated MSCs; however, during cartilaginous condensation in early

development, collagen I expression is turned off and replaced with production of collagen type II and aggrecan proteoglycan in the formation of articular cartilage [24]. Together these results suggested that a variety of diverse signals may be required, along with both spatial and temporal control of these signals, to properly support chondrogenic differentiation and maintenance of a chondrocytic phenotype.

The desulfation of CS provided a highly controlled biomaterial system to alter both the sulfation and charge of CS-based materials, with minimal modification of the GAG chemical structure, to examine sequestration of soluble signals for MSC differentiation toward a chondrogenic phenotype. The combined roles of sulfation in modulating TGF-β1 sequestration and chondrogenic gene expression by MSCs in the presence of soluble chondrogenic cues in these studies suggested that an intermediate degree of sulfation may be advantageous to enhance TGF-β1 signaling and MSC response for greater chondrogenic differentiation. The ability of desulfation to promote chondrogenic gene expression in these studies suggested that an optimal amount a charge may exist to facilitate growth factor interaction, while possibly permitting intercellular communication. As demonstrated in Chapters 5, CS materials can be either be partially desulfated by time-dependent acidic methanol treatment or CS and nonsulfated chondroitin can be combined in varying ratios to develop materials with a range of negative charge densities without altering the total GAG content or composition within the bulk material. Additionally these materials may possess the unique ability to potentiate signaling in low TGF-β1 concentration environments or to retain growth factor for sustained signaling after removal of soluble TGF-β1 from the medium. This

demonstrates that CS and chondroitin are versatile systems for highly controlled interaction with stem cells and growth factors.

Due to the low degree of total ECM deposition observed in these tightly crosslinked hydrogel systems, ECM production may be enhanced by increasing the ratio of cells to matrix, thus allowing the encapsulated cells to further remodel the GAG network. While this model system involved encapsulation of MSCs in a large amount of crosslinked GAG matrix to examine its role in promoting a chondrogenic response, at the other extreme, lesser amounts of CS-based materials could be incorporated into a multicellular mass to allow unrestricted ECM deposition in response to cues from the incorporated CS matrix. Specifically, CS-based small particle carriers could potentially be incorporated to MSC aggregates to permit close cell-cell contact and used to deliver various growth factors throughout the cell aggregates for enhanced differentiation, compared to diffusion of soluble factors from the medium [322].

As described in Chapter 4, CS-based small particle carriers were developed for controlled delivery of charged growth factors. As a first step, CS-based nanoscale micelles and microscale particles were fabricated and characterized as small particle carriers for growth factor delivery. With low degrees of modification, methacrylamide-conjugated CS (CSMAm) self-assembled into ~73 nm and ~320 nm diameter micelles in aqueous solution. These micelle particles were found to possess a highly negative surface charge, suggesting that they may electrostatically interact with positively charged growth factors. Crosslinking of methacrylated CS (CSMA) in a water-in-oil, single-emulsion resulted in the formation of larger CS microspheres with an average diameter of 4.3 μm. CSMA microspheres were shown to retain positively charged TGF-β1 with little release

over 5 days, while negatively charged TNF-α exhibited substantial burst release within 15 hours at physiological pH. These results suggested that negatively charged CSMA microspheres electrostatically interacted with TGF-β1, sequestering it from release. CSMA microspheres were successfully incorporated into ESC embryoid bodies with good cytocompatibility, suggesting that CSMA microspheres may possess unique application as carriers for controlled delivery and presentation of growth factors within dense multicellular aggregates. Together with techniques for desulfation of CS to control electrostatic interactions and the ability of CS matrix to differentially modulate chondrogenic response in the presence of TGF-β1, this work represents a first step in the development of novel biomaterials to control presentation of CS in high-density micromass culture to promote chondrogenic differentiation of MSCs.

While traditional tissue engineering paradigms involve the culture of dispersed cells within a biomaterials scaffold and supplementation of exogenous differentiation cues through the culture medium, this work presents an alternative approach in which small scale biomaterials are entrapped throughout a cellular mass with delivery of differentiation factors from the embedded biomaterial carriers. This is a novel idea for tissue engineering of cartilaginous tissues in which high-density culture and formation of cell-cell contacts play important roles in differentiation. The ability of CS to electrostatically sequester TGF-β1 also may resolve transport limitations associated with traditional micromass culture. GAG-based materials have been shown to possess electrostatic interactions with a number of other chondrogenic growth factors including bone morphogenetic protein-4 (BMP-4), insulin-like growth factor-1 (IGF-1), and bFGF, some of which have demonstrated additive effects when supplemented in combination or

sequentially with TGF-β [25, 256, 264, 273]. These results suggest that CS-based carriers could be used as an ECM-derived carrier to deliver a variety of signals within a spatially and temporally controlled environment to promote differentiation of stem cell aggregates.

The CS-based biomaterials presented in this dissertation provide highly controlled systems to alter a variety of signals within stem cell microenvironments. CS-based materials were shown to regulate cell aggregation, presentation of sulfation and charge, growth factor interactions, and MSC response to soluble chondrogenic cues, and these materials possess tremendous potential to control growth factor signaling within stem cell microenvironments. Therefore, CS-based materials are valuable tools to investigate the role of a diverse array of soluble, physical, and morphological cues in stem cell differentiation, and additional spatial and temporal control can be engineered into this unique biomaterial system to modulate the stem cell environment to promote differentiation.

7.3 Future Directions

The findings presented in this dissertation provide significant insights into the potential interactions of sulfated GAGs that alter stem cell microenvironments to promote chondrogenic differentiation, including cell aggregation and electrostatic interactions with growth factors. A variety of CS-based materials, including 2D surfaces, small scale particles, and bulk hydrogels with varying degrees of sulfation, were developed as novel tools to control CS presentation to stem cells to investigate the role of CS in chondrogenic differentiation; however, future work can expand on the insights gained

from this dissertation to examine mechanisms through which GAG-based materials control stem cell differentiation.

The results of these experiments suggested that careful control of GAG structure may present a unique opportunity to further investigate the control of charge and sulfation in supporting chondrogenic differentiation. The studies in this dissertation represent a broad examination of how sulfated CS and nonsulfated chondroitin independently influence chondrogenic differentiation; however, significant differences in gene expression in chondroitin materials suggested that an intermediate level of sulfation and negative charge may be more optimal for chondrogenic differentiation, as greater degree of TGF-β1 sequestration in CS materials did not translate to a stronger chondrogenic response. An intermediate charge density may facilitate moderate interaction with growth factors while still permitting transport of soluble factors and potential intercellular communication.

For a thorough investigation of charge, CS materials can either be partially desulfated by time-dependent acidic methanol treatment or CS and nonsulfated chondroitin can be combined in varying ratios to develop materials with a range of negative charge densities without altering the total GAG content or composition within the bulk material; however, the distribution of sulfation would differ in these two approaches, as the former would contain a homogenous undersulfated CS variant, while the latter would include primarily monosulfated CS chains in a mixture of completely desulfated chondroitin. Differences in these two approaches may be able to address the role of sulfation patterning and density, compared to the role of bulk charge, in CS-based materials for growth factor sequestration and chondrogenic differentiation. In addition,

greater charge than the primarily monosulfated CS used in this dissertation can be achieved through a variety of chemical techniques to oversulfate CS [25-26], and desulfated chondroitin, which remains negatively charged at physiological pH due to the presence of carboxylates in the chondroitin structure, could be chemically modified to possess a neutral charge. A neutrally charged chondroitin material may be especially valuable to examine the effects of uncharged GAG variants, and such a material could be easily obtained in the methyl ester intermediate as a part of the acid methanol treatment, as described in Chapter 5, in which the carboxylates of chondroitin are methylated, resulting in a neutral charge. This versatility to control charge over a wide range from uncharged to oversulfated CS chains offers a highly controlled system to investigate the various roles of sulfation and charge in growth factor interactions and differentiation, without modification of the primary CS backbone.

Besides total degree of sulfation or total charge density, sulfation pattern may also play important roles in modulating GAG interactions with cells, signaling molecules, and the ECM. It has been documented that 2-O-sulfation is especially critical for growth factor interactions in heparin [266-267, 270, 358], and CS sulfation pattern has been shown to alter electrostatic interactions with $Co(NH_3)_6^{+3}$ cations, in which monosfulated chondroitin-4-sulfate possessed greater affinity than equally sulfated chondroitin-6-sulfate [405]. In Chapters 5 and 6 of this dissertation, the chondroitin sulfate used contained a mixture of 58% chondroitin-6-sulfate and 27% chondroitin-4-sulfate disaccharides, along with a 15% mixture of other nonsulfated and disulfated disaccharides, as determined in Chapter 5. This CS composition was chosen both as a result of its increased susceptibility to desulfation as described in Chapter 5, as well as

chondroitin-6-sulfate's relative prevalence in adult human articular cartilage; however, chondroin-4-sulfate is more highly expressed during growth and development of human cartilage before decreasing expression in the mature tissues [20, 231], suggesting that 4-sulfation may potentially play an increased role in differentiation and development. Differences in sulfation pattern, specifically increased chondroitin-4-sulfate composition, may exhibit important differences in growth factor interaction and stem cell differentiation that were not observed in this examination of a single CS mixture that was a majority chondroitin-6-sulfate.

It is also important to recall that CS is predominantly associated as part of proteoglycans *in vivo* in which GAGs are bound to a core protein. In cartilage specifically, versican is expressed in cartilaginous condensations during development [218-219], while aggrecan is the predominant proteoglycan in mature cartilage [31]; therefore, presentation of GAGs in conjunction with the full proteoglycan structure may further alter GAG presentation to control ECM interactions and cellular presentation. To fully understand the role of GAGs in cartilaginous tissues, a thorough investigation of cellular response in the presence of CS proteoglycans would be necessary to elucidate the roles of the protein core, GAG presentation, and interplay between GAGs and their protein cores in signaling and tissue formation.

Although these studies demonstrated that sulfation of CS influenced growth factor interactions and that differential sulfation also altered the chondrogenic response, the cellular response was not conclusively linked to growth factor signaling, as differences in charge also could potentially alter osmotic swelling pressure or other various ECM interactions that influence the extracellular microenvironment [20-21, 250]. Therefore, to

fully understand the role of CS in promoting chondrogenic differentiation, further investigation is also required to determine the cellular interactions with CS that result in an enhanced chondrogenic response. While it is difficult to completely separate the independent effects of sulfation, fixed charge, osmotic pressure, swelling, and electrostatic interactions with a variety of molecules without significant modification of these materials, due to their high interdependency, controlled systems of study may begin to start clarifying the importance of these factors in promoting differentiation.

Specifically, regarding growth factor interactions with TGF-β1 as presented in this dissertation, use of TGF-β3 would offer a closely related molecule with similar signaling mechanism and chondrogenic response to TGF-β1; however, TGF-β3 is not expected to electrostatically interact with sulfated GAGs at physiological pH [274-275]. The isoelectric point of TGF-β3 is ~6.8, compared to ~9.5 in TGF-β1, suggesting that TGF-β3 is slightly negatively charged at physiological pH [275-276]. Additionally, a basic amino acid at position 26 in TGF-β1, a central part of the hypothesized GAG-binding site, appears to be replaced with a neutral amino acid in TGF-β3, suggesting that it may be less likely to interact with CS [274].

To fully implicate TGF-β1 in the chondrogenic response observed in chondroitin hydrogels, a comprehensive investigation of the downstream receptors and signaling molecules, such as SMAD and ERK/MAPK pathways, would be required to determine the differential effects of growth factor signaling in these materials [406-408]. Subsequent receptor blocking and inhibition of these pathways could begin to answer these questions; however, signaling from chondrogenic growth factors appeared to play an important role in these interactions, as culture of MSCs in chondroitin materials in the

absence of chondrogenic medium did not observe comparable effects from the material alone.

It is, however, important to note that MSCs encapsulated in CS-MA hydrogels did significantly upregulate collagen II gene expression, and to a lesser extent aggrecan, in the absence of TGF-β1 and dexamethasone on day 21, while chondroitin materials did not, in an investigation of these materials at earlier time points and lower cell density (Figure A.2). Investigation of CS and chondroitin materials in low TGF-β1 environments warrants further examination to determine the corresponding roles of TGF-β1 signaling in these two materials. The effects of a TGF-β1 dose response on MSC expression in the presence of CS and chondroitin materials may clarify these patterns, particularly at low and intermediate TGF-β1 concentrations. Chondrogenic medium commonly uses 10 ng/mL TGF-β1 to promote chondrogenic response [6]; however, this concentration is quite high, in order to promote a strong signaling response and encourage chondrogenic differentiation. CS-based materials, however, may potentiate chondrogenic response by sequestering TGF-β1 and increasing the local concentration of growth factor in close proximity to cells or enhancing signaling efficiency within a GAG-based scaffold. CS and chondroitin materials may be uniquely capable of capturing and potentiating signals in low TGF-β1 concentrations, while overwhelming TGF-β1 concentrations may negatively impact the additional signals necessary to promote chondrogenic differentiation.

As the goal of tissue engineering is to develop replacement tissues for tissue repair, it remains critically important that chondrogenic MSCs in these CS-based systems produce cartilaginous ECM in a controlled fashion. The hydrogel materials discussed in

Chapter 6, however, supported relatively little ECM production, and all matrix production was restricted to the pericellular domains. It is likely that enhanced degradation of the hydrogel network may be required to support deposition of cartilaginous ECM, and because human MSCs do not appear to produce sufficient amounts of chondroitinase enzyme to encourage substantial degradation of the GAG matrix, additional mechanisms of degradation may be required to support ECM production. Hydrolytically degradable and cell-mediated enzymatically cleavable functionality have been investigated in similarly crosslinked PEG-based system [169, 185-187, 396]; therefore, similar functionality could be incorporated in GAG-based systems to examine the role of degradation on enhanced ECM deposition.

The unique ability of CS-based materials to selectively sequester soluble signals from solution suggests that CS-based materials may also possess considerable potential in spatial patterning of scaffolds to control differential effects of signaling. CS and chondroitin materials may be used to either trap soluble signals to potentiate signaling, or alternatively to sequester cell-secreted signals and restrict paracrine signaling in a spatially-defined fashion. These principles can be applied to spatially patterned hydrogel materials through photolithographic techniques to promote differential signaling from a single cell type within a single media formulation, by differentially trapping soluble cues from the medium in the CS matrix [192, 195, 197]. Spatially controlled GAG-based scaffolds may represent novel biomaterial systems to regenerate tissue interfaces through co-culture of multiple cell types through differential signaling, as well as promoting formation of various properties within a single tissue, such as the depth-dependent zones of cartilage.

Due the importance of cell-cell contact in production of cartilaginous ECM exhibited in Chapter 3, CS-based microparticles demonstrate a versatile delivery system to examine the effects of CS within chondrogenic MSC spheroids. The use of CS microparticles within MSC micromass cultures offers an innovative system to control growth factor presentation for "inside-out" delivery, as opposed out "outside-in" signaling via diffusion from the medium, through the use of naturally-derived GAG materials that may potentiate signaling and support further interaction with surrounding cells. While microparticle carriers were developed for growth factor delivery within MSC and ESC spheroids, as described in Chapter 4, a thorough examination is required to characterize their role in promoting chondrogenic differentiation. A few studies have begun to investigate the role of adhesion peptides and TGF-β delivery in MSC pellets to promote chondrogenic differentiation [409-410], and these experiments can be used as guiding principles in the optimization of this CS-based delivery system as an ECM-derived growth factor carrier for cartilage regeneration. Additional incorporation of desulfated chondroitin materials into this microparticle carrier system may offer further control of growth factor affinity, release kinetics, and signaling activity to control differentiation, as has been suggested in Chapters 5 and 6 of this dissertation.

Aside from being a system to promote differentiation through growth factor interactions, GAG-based materials may possess significant application as an analytical tool to study stem cell signaling. GAG-based materials may be capable of "trapping" specific cell-secreted signals for characterization and potential future delivery. Microparticles may be incorporated into stem cell aggregates, such as ESC embryoid bodies, to sequester cell-secreted signals involved in the maintenance and self-renewal of

differentiation potential. Dissociation of the cell spheroids and retrieval of the microparticles for molecular analysis may be able to clarify the complex array of secreted signals that are involved in stem cell signaling. Use of GAG-based materials as an analytical tool to identify molecular players in stem cell signaling may be a novel paradigm for stem cell engineering and development of regenerative therapies for tissue repair.

Future work can expand on the various principles presented in this dissertation to develop precisely controlled temporal, spatial, and physical cues to enhance chondrogenic differentiation for tissue engineering repair, such as controlled release and presentation of numerous signaling molecules, inclusion of biomimetic peptides or adhesive cues, and application of mechanical strain. Additionally, while this dissertation chose to focus on CS and chondrogenic differentiation, due to the prevalence of CS matrix in cartilaginous tissues, numerous GAGs are found throughout the body for a variety of functions. GAGs such as heparin, heparan sulfate, dermatan sulfate, keratan sulfate, and hyaluronan may support similar roles, including interaction with a variety of signaling molecules, and these materials may possess significant application in strategies to promote tissue repair. The research presented in this thesis provided valuable insights into the contributions of GAG matrix in the development, maintenance, and repair of cartilaginous tissues, and these findings improve understanding of the role of local chemical, biomolecular, and overall physical environments in the development of therapies to promote tissue regeneration and repair.

APPENDIX A

SUPPLEMENTARY FIGURES

A.1 Viability in CS-MA and Ch-MA hydrogels at $10x10^6$ cells/mL

A.1.1 Materials and Methods

Materials and methods were performed as described in Chapter 6, with the lone exceptions being that MSCs were incorporated at $10x10^6$ cells/mL, hydrogels were cultured both in the presence and absence of 10 ng/mL TGF-β1 and 100 nM dexamethasone, and time points for analysis were performed on days 1, 7, 14, and 21.

A.1.1.1 Encapsulation of Human MSCs

Human mesenchymal stem cells (MSCs) were encapsulated in hydrogels containing a 1:1 ratio of OPF 10K:PEG-DA and 50% chondroitin sulfate methacrylate (CS-MA) or 50% chondroitin methacrylate (Ch-MA) by dry mass at a final cell concentration of $10x10^6$ cells/mL. PEG controls containing 60% PEG-DA:40% OPF were used as swelling controls for 50% Ch-MA materials. Hydrogels were cultured for 3 weeks in basal medium composed of high glucose DMEM containing 1% ITS+ culture supplement, 1% nonessential amino acids, 50 μg/mL ascorbate-2-phosphate, and 1% antibiotic/antimycotic, or in chondrogenic medium supplemented with 10 ng/mL TGF-β1 and 100 nM dexamethasone.

A.1.1.2 LIVE/DEAD Staining for Viability

On days 1, 7, 14, and 21, hydrogels were stained for 60 minutes in LIVE/DEAD stain, and viability was imaged via confocal microscopy (n=4).

A.1.1.3 PicoGreen DNA Assay

PicoGreen assay was used to evaluate the total DNA content in each sample on days 1, 7, 14, and 21. Within each hydrogel formulation, DNA content of each gel was normalized to wet mass to correct for small differences in gel size (n=4).

A.1.1.4 Statistical Analysis

A two-factor analysis of variance (ANOVA) was used to determine statistical significance of groups, and Tukey's *post hoc* multiple comparison test with significance set at $p \leq 0.05$ indicated significance between individual samples. For DNA analysis, the factors were hydrogel type and time.

A.1.2 Results

LIVE/DEAD staining of human MSCs in 50% CS-MA and 50% Ch-MA hydrogels indicated that visible MSCs remained mostly viable over 3 weeks of culture (Figure A.1a). Cells remained dispersed evenly throughout the hydrogel scaffolds with a spherical shape, and no cell aggregation or spreading was observed. Total DNA content, as a measure of cell number, suggested that cellularity decreased over time in all hydrogel formulations (Figure A.1b). DNA content significantly decreased from day 1 to day 7 in CS-MA and Ch-MA hydrogels and by day 14 in PEG controls. DNA content was fairly consistent across hydrogel types from day 1 until day 14; however, PEG control hydrogels experienced a significant decrease in DNA content on day 21, compared to both CS-MA and Ch-MA.

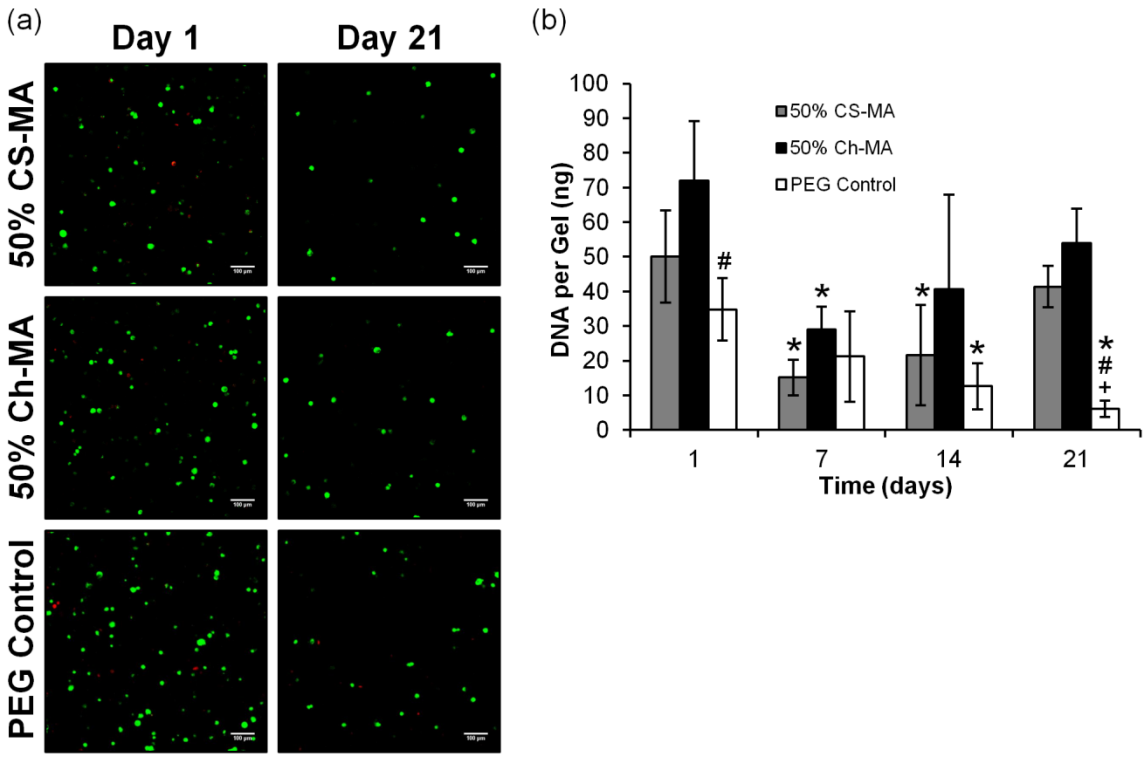

Figure A.1. Viability and cellularity of human MSCs encapsulated in 50% CS-MA and 50% Ch-MA hydrogels at 10x10^6 cells/mL in chondrogenic medium. (a) Human MSCs appeared largely viable in all hydrogel formulations over 21 days of culture. Cells remained dispersed with a rounded morphology. Scale bars = 100 µm. (b) DNA content, as a measure of cellularity, decreased over time with a significant decrease observed between day 1 and day 7 in CS-MA and Ch-MA hydrogels and by day 14 in PEG controls. Additionally, a significant decrease in DNA content was measured in PEG control hydrogels on day 21. * indicates significantly less DNA than day 1 ($p \leq 0.05$). # indicates significantly less DNA than 50% Ch-MA at the same time point ($p \leq 0.05$). + indicates significantly less DNA than 50% CS-MA at the same time point ($p \leq 0.05$).

A.2 Gene expression in the presence and absence of TGF-β1 at 10x10^6 cells/ml

A.2.1 Materials and Methods

Materials and methods were performed as described in Chapter 6, with the lone exceptions being that MSCs were incorporated at 10x10^6 cells/mL, hydrogels were cultured both in the presence and absence of 10 ng/mL TGF-β1 and 100 nM dexamethasone, and time points for analysis were performed on days 1, 7, 14, and 21.

These differences in cell encapsulation and culture conditions are described in detail in Section A.1.1.1.

A.2.1.1 Reverse transcription polymerase chain reaction

Gene expression of encapsulated MSCs was analyzed after 1, 7, 14, and 21 days by reverse transcription polymerase chain reaction (RT-PCR). RNA was extracted and reverse transcribed, and quantitative PCR amplification for each gene target was performed for gene expression of human mRNA for collagen II, aggrecan, and SOX9 (chondrocytic markers), and for collagen X (hypertrophic chondrocyte marker). To determine fold regulation over 50% Ch-MA hydrogels in the absence of TGF-β1 on day 1, the raw fluorescence data was processed using LinRegPCR with glyceraldehyde-3-phosphate dehydrogenase (GAPDH) as an endogenous control (n=6).

A.2.1.2 Statistical Analysis

PCR amplification data for each gene were first transformed using a Box-Cox transformation to obtain a normal distribution for analysis. A three-factor analysis of variance (ANOVA) was used to determine statistical significance of groups, and Tukey's *post hoc* multiple comparison test with significance set at $p \leq 0.05$ indicated significance between individual samples. For gene expression analysis, the factors were hydrogel type, media type, and time.

A.2.2 Results

In the presence of chondrogenic medium, human MSCs encapsulated in nonsulfated 50% Ch-MA hydrogels significantly upregulated gene expression of the cartilaginous ECM molecules collagen II and aggrecan on days 7, 14, and 21, over 50% CS-MA hydrogels (Figure A.2a-b). MSCs in 50% Ch-MA expressed 186 ± 162 fold

upregulation of collagen II expression on day 21, compared to only 0.022 ± 0.015 in 50% CS-MA and 9.9 ± 19.2 fold in PEG controls (Figure A.2a). Similarly, aggrecan expression in Ch-MA gels was upregulated 27.6 ± 9.5 fold on day 21 in the presence of TGF-β1, compared to 10.8 ± 3.7 in CS-MA and 7.8 ± 1.5 in PEG (Figure A.2b). Cartilaginous transcription factor SOX9 experienced slight upregulation on day 7 only in 50% Ch-MA with 1.57 ± 0.29 fold regulation, while CS-MA only expressed 0.51 ± 0.41 fold regulation (Figure A.2c). Collagen X, an ECM marker of hypertrophic chondrocytes, was also significantly upregulated in Ch-MA hydrogels over CS-MA controls in chondrogenic medium on days 7, 14, and 21 (Figure A.2d). MSCs in 50% Ch-MA exhibited large upregulation of collagen X of 4,350 ± 1390 fold on day 21, compared to 655 ± 371 in CS-MA.

In the absence of chondrogenic medium, MSCs encapsulated in 50% Ch-MA hydrogels did not upregulate any of the chondrogenic markers analyzed here. 50% CS-MA hydrogels, on the other hand, significantly upregulated collagen II gene expression compared to both Ch-MA hydrogels in basal medium and CS-MA gels in chondrogenic medium on days 14 and 21. MSCs in CS-MA hydrogels expressed 69.9 ± 19.2 fold upregulation of collagen II on day 21 in basal medium, compared to 1.28 ± 1.66 fold in Ch-MA. Aggrecan and collagen X were also upregulated on day 21 in 50% CS-MA in basal medium, compared to Ch-MA in basal medium, but not compared to CS-MA in chondrogenic medium.

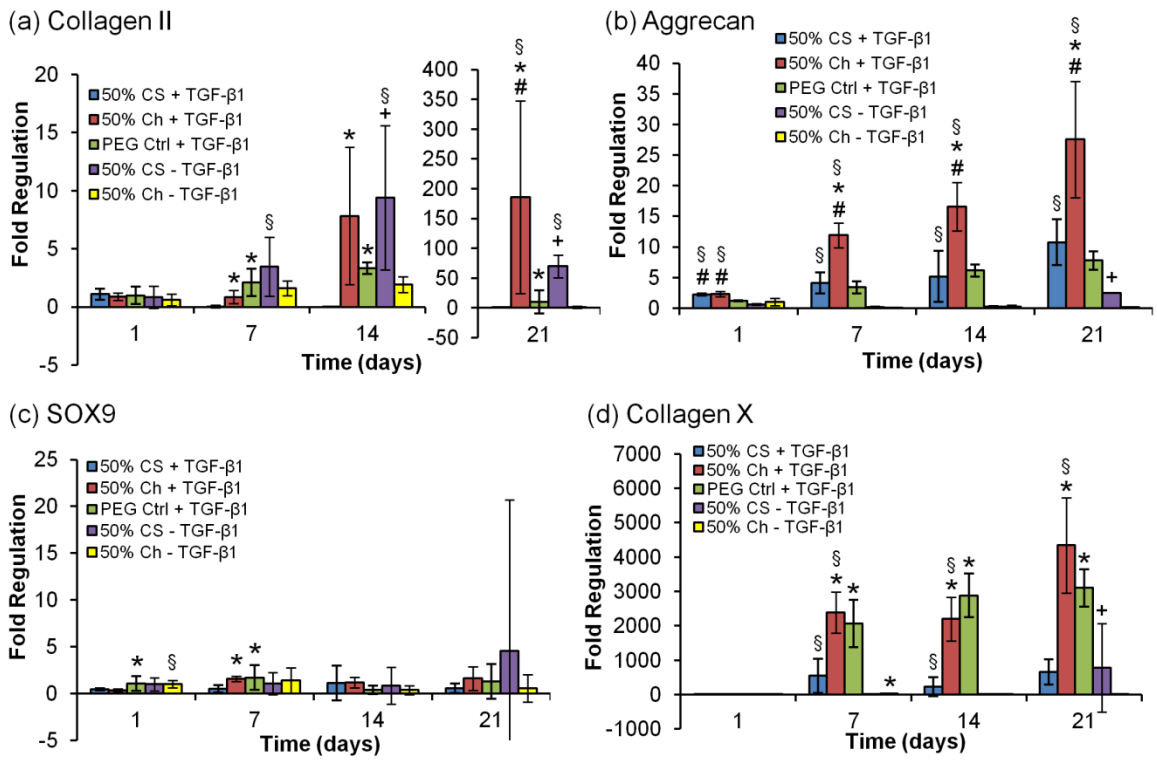

Figure A.2. Gene expression of chondrocytic markers by MSCs in 50% CS-MA and 50% Ch-MA hydrogels at 10x10^6 cells/mL in chondrogenic and basal medium. MSCs in 50% Ch-MA hydrogels significantly upregulated gene expression of (a) collagen II and (b) aggrecan on days 7, 14, and 21 in chondrogenic medium, and (c) SOX9 on day 7 only, compared to 50% CS-MA. 50% CS-MA hydrogels in basal medium, however, upregulated expression of (a) collagen II and (b) aggrecan after 21 days, compared to 50% Ch-MA. (d) Hypertrophic chondrocyte marker collagen X was also significantly upregulated in 50% Ch-MA gels on days 7, 14, and 21 in chondrogenic medium over 50% CS-MA, while 50% CS-MA in basal medium upregulated collagen X expression only on day 21, compared to 50% Ch-MA. * indicates significantly greater than 50% CS-MA in same medium and at same time point ($p \leq 0.05$). # indicates significantly greater than PEG controls in same medium and at same time point ($p \leq 0.05$). + indicates significantly greater than 50% Ch-MA in same medium and at same time point ($p \leq 0.05$). § indicates significantly greater than the same hydrogel type in the other media type and at same time point ($p \leq 0.05$).

A.3 Immunostaining for ECM in CS-MA and Ch-MA hydrogels at $10x10^6$ cells/mL

A.3.1 Materials and Methods

Materials and methods were performed as described in Chapter 6, with the lone exceptions being that MSCs were incorporated at $10x10^6$ cells/mL, hydrogels were cultured both in the presence and absence of 10 ng/mL TGF-β1 and 100 nM dexamethasone, and time points for analysis were performed on days 1, 7, 14, and 21. These differences in cell encapsulation and culture conditions are described in detail in Section A.1.1.1.

A.3.1.1 Histological staining

ECM production by encapsulated MSCs was determined by immunostaining on days 1, 7, 14, and 21. For aggrecan staining, samples were deglycosylated with 30 µl of 0.75 U/ml chondroitinase ABC for 1.5 hours. For primary antibody binding, sections were incubated in monoclonal mouse anti-human collagen I, collagen II, or aggrecan. Sections were then incubated with highly cross-adsorbed Alexa Fluor 488-conjugated goat polyclonal anti-mouse immunoglobulin G (IgG), and counterstained with 0.1 µg/mL 4',6-diamidino-2-phenylindole (DAPI) (n=2). Negative controls were stained as described, but using a monoclonal mouse IgG1 isotype control with no known reactivity with human antigens as the primary antibody at 10 µg/mL.

A.3.2 Results

Immunostaining for ECM production demonstrated that while some accumulation of cartilaginous ECM collagen II and aggrecan was observed pericellularly over 21 days, staining was generally weak and clear differences were not apparent between CS-MA and

Ch-MA formulations (Figure A.3a-b). Deposition of collagen I appeared to persist over time, but few differences were observed between CS-MA and Ch-MA hydrogels (Figure A.3c). Isotype controls demonstrated little non-specific staining (Figure A.3d).

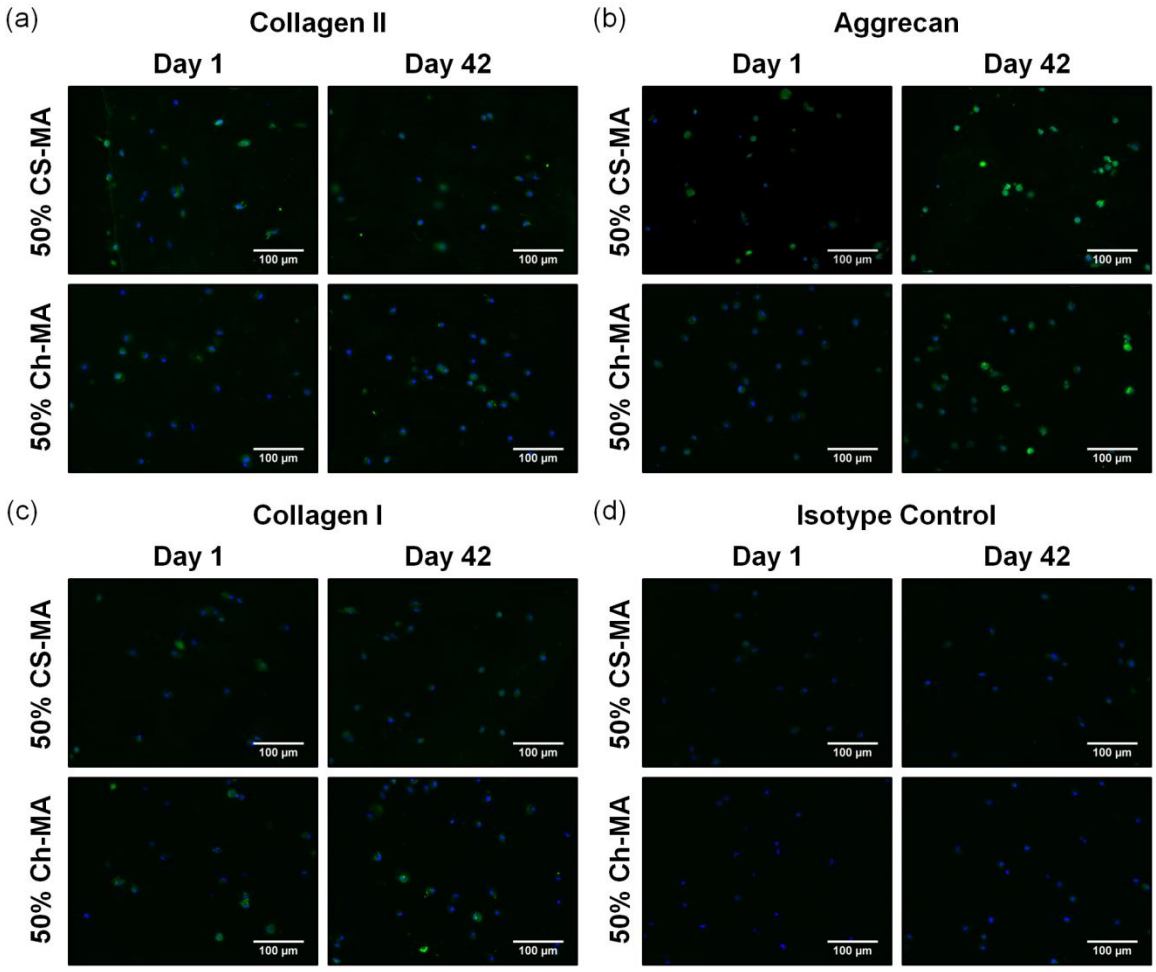

Figure A.3. Immunostaining for ECM deposition by MSCs in 50% CS-MA and 50% Ch-MA hydrogels at $10x10^6$ cells/mL in chondrogenic medium. (a) Collagen II, (b) aggrecan, and (c) collagen I were produced in relatively small quantities by MSCs in CS-MA and Ch-MA hydrogels, and there were no distinguishable differences across gel types. (d) Isotype controls demonstrated little non-specific staining. Cell nuclei = blue. Scale bars = 100 µm.

APPENDIX B

LABORATORY PROTOCOLS

B.1 OPF Synthesis

Fumaryl Chloride (FuCl) Distillation (if necessary)

Warning: Fumaryl chloride has a very pungent odor. Work only in the fume hood with the sash down as far as possible. Double glove, and leave jars, glassware, used gloves in the hood overnight to air out.

1) Wash and dry:

   2 x 500 ml round-bottom flasks, 1 x joint for thermometer, 1 x thermometer to fit joint (~160°C), 1 x large condenser, 1 x glass elbow, 1 x joint for desiccators, 1 x glass stopper, 1 x glass funnel, 1 x egg-shaped FuCl stir bar.

2) Set up the distillation apparatus as shown, without the FuCl flask and collection flask:

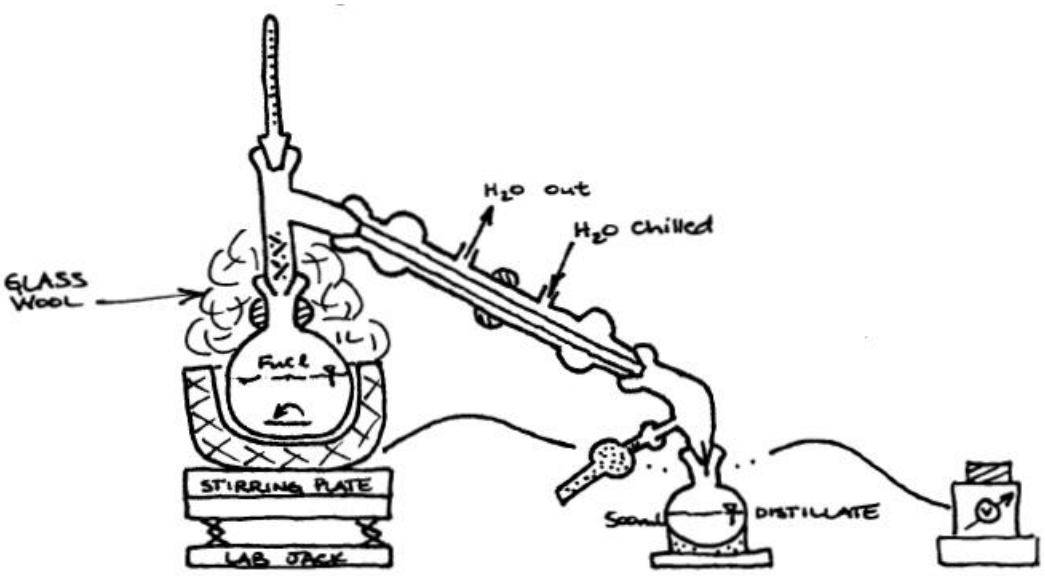

3) Replace the 500 ml collection flask with a 100 ml round bottom flask to collect the first 30 ml of distillate.

4) Clamp the apparatus to the scaffolding in the back of the fume hood.
5) Vacuum grease and clamp all connections.
6) Run cold, ice water UP the condenser tube using the circulation pump. This allows any bubbles to flow up and out of the condenser. Make sure that the circulation pump is not actively heating the water by turning the temperature control all the way down to -20°C.
7) Tie a KimWipe around the bottom of the condenser to catch external condensation.
8) Use the funnel to pour 150 ml (100 g) of FuCl into a 500 ml round-bottom flask.
9) Add the FuCl stir bar into the FuCl flask.
10) Vacuum grease the FuCl flask, and connect the flask to apparatus.
11) Place the flask in heating mantle with magnetic stirring at ~3.
12) Insulate the flask and neck with glass wool all the way up to the condensing tube to promote boiling and prevent condensation.
13) Start the transformer at 40 units.
14) Increase the transformer by 10 units, every 5 minutes.
15) Increase the transformer until the vapor temperature is 160°C (~80 units on transformer).
16) Dispose of the first ~30 ml of distillate by turning the neck up, removing the 1st 100 ml collection flask, and quickly replacing it with a clean 500 ml round-bottom flask.
17) FuCl distillate should be a light amber color.
18) The solution in the heated FuCl flask will become darker and more viscous.

19) When ~50-75 ml remains the heated FuCl flask and the solution is dark brown, turn off the transformer, remove the glass wool, turn the condenser off, and replace the heating mantle with a cork ring.

20) Stopper the FuCl distillate, parafilm the stopper, cover the flask with aluminum foil, and label it.

21) Store the distillate in the 4°C explosion-proof refrigerator.

22) Dilute the FuCl waste with tap water, and leave it in the hood overnight. Be careful of HCl production in the reaction with water, and pour the water in SLOWLY.

23) On the next day, use a spatula to break up the FuCl waste, retrieve the stir bar, and disposed of the waste in the aqueous waste container.

24) Glassware can be cleaned with acetone and the base bath.

Methylene Chloride (MeCl) Distillation

Warning: Use nitrile or silver-shield gloves when handling MeCl.

1) Wash and dry:

   1 x 1000 ml round-bottom flask, 1 x joint for thermometer, 1 x thermometer to fit joint (~40°C), 1 x large condenser, 1 x glass elbow, 1 x joint for desiccators, 1 x glass stopper, 1 x glass funnel.

2) Set up the distillation apparatus as shown, without the MeCl flask and collection flask:

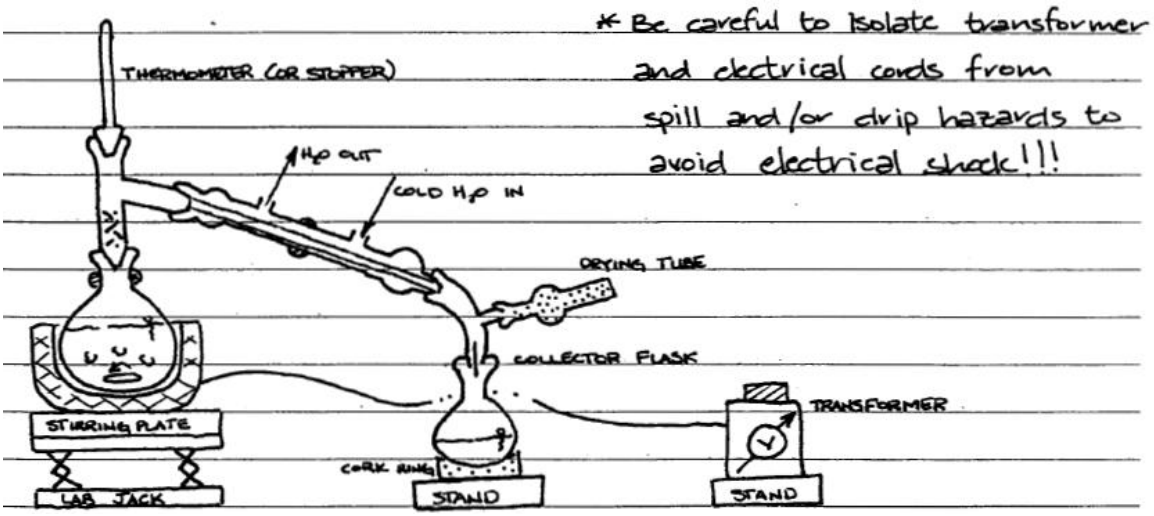

3) Replace the 500 ml collection flask with a 100 ml round bottom flask to collect the first 30 ml of distillate. Clamp the apparatus to the scaffolding in the back of the fume hood.
4) Vacuum grease and clamp all connections.
5) Run cold, ice water UP the condenser tube using the circulation pump. This allows any bubbles to flow up and out of the condenser. Make sure that the circulation pump is not actively heating the water by turning the temperature control all the way down to -20°C.
6) Tie a KimWipe around the bottom of the condenser to catch external condensation.
7) Use funnel to add 750 ml of MeCl and calcium hydride (CaH_2, if needed) into the existing MeCl + CaH_2 flask.
8) Vacuum grease the MeCl flask, and connect the flask to apparatus.
9) The MeCl + CaH_2 flask already contains a stir bar. Place the flask in heating mantle with magnetic stirring at ~4.
10) Insulate the flask and neck with glass wool all the way up to the condensing tube to promote boiling and prevent condensation.

11) Set the transformer to 35 units.

12) Vapor temperature should increase to ~40°C.

13) Dispose of the first ~30 ml of distillate by turning the neck up, removing the 1st collection flask, and quickly replacing it with a clean 1000 ml round-bottom flask.

14) When ~150-200 ml remains in the heated MeCl flask, turn off the transformer, remove the glass wool, turn the condenser off, and replace the heating mantle with a cork ring. You should have ~500 ml MeCl distillate in your collection flask (need 340-380 ml for remaining steps).

15) Vacuum grease the glass stopper, and stopper the MeCl distillate, and label it.

16) Store the anhydrous MeCl distillate in the hood overnight. Do not parafilm the stopper.

17) Vacuum grease the original MeCl + CaH_2 stopper, stopper the undistilled MeCl + CaH_2, and store it in the back of the hood.

18) Dispose of the MeCl waste in the chlorinated organic solvents waste container.

19) Glassware can be dried in the hood, and then cleaned normally.

Azeotropic Distillation of PEG

Warning: Use nitrile or silver-shield gloves when handling toluene.

1) Wash and dry:

   1 x 500 ml or 1000 ml round-bottom flask, 1 x Dean stalk, 1 x condenser,

   1 x glass stopper, 1 x Kontes #2 glass valve with LARGE hole,

   1 x egg-shaped stir bar, 1 x glass funnel, 1 x 250 ml glass graduated cylinder.

2) Set up the distillation apparatus as shown, without the PEG/toluene flask:

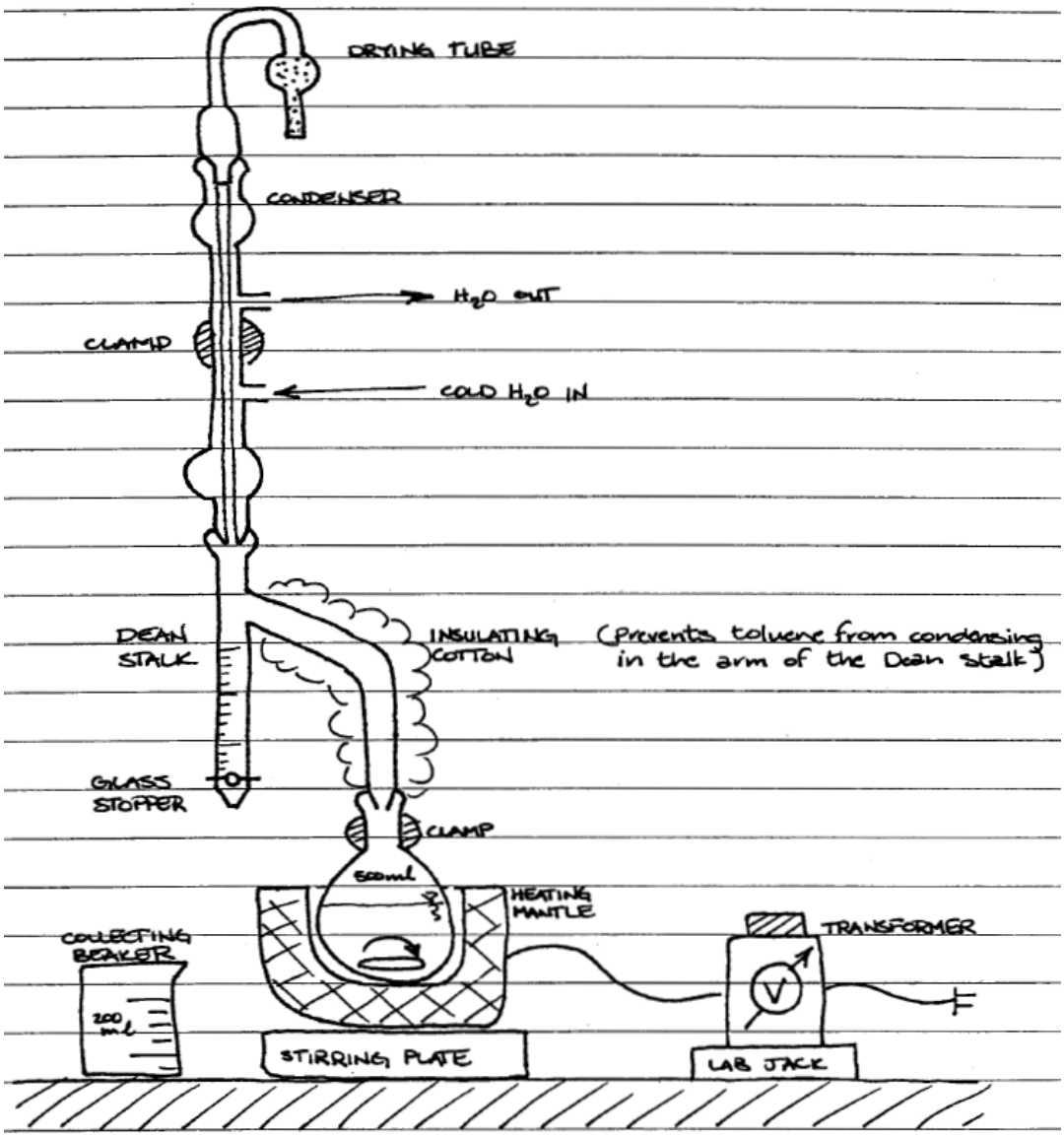

3) Clamp the apparatus to the scaffolding in the back of the fume hood.

4) Vacuum grease and clamp all connections.

5) Run cold, ice water UP the condenser tube using the circulation pump. This allows any bubbles to flow up and out of the condenser. Make sure that the circulation pump is not actively heating the water by turning the temperature control all the way down to -20°C.

6) Tie a KimWipe around the bottom of the condenser to catch external condensation.

7) Weigh 50 g PEG 3.4K or 10K in the 500 ml round-bottom flask.
8) Use the graduated cylinder and funnel to add 200 ml of toluene to the PEG in the 500 ml flask.
9) Add the stir bar to the flask, vacuum grease the flask, and connect the flask to apparatus.
10) Place the flask in heating mantle with magnetic stirring at ~5. The PEG will dissolve with stirring and heating.
11) Insulate the flask and neck with glass wool all the way up to the condensing tube to promote boiling and prevent condensation.
12) Set the transformer to 65 units.
13) When the Dean stalk fills to 20 ml, dispose of the toluene by draining the solution from the Dean stalk into a 250 ml waste beaker. The first few batches of waste may be partially cloudy, while others should be clear.
14) Repeat step 13 seven more times, removing 20 ml toluene at a time until ~160-180 ml toluene has been removed.
15) Turn off the transformer, remove the glass wool, turn the condenser off, and replace the heating mantle with a cork ring. 2-5 ml extra toluene waste may condense as you do this.
16) Allow the distilled PEG and toluene to cool, and then vacuum grease the glass stopper and stopper the distilled PEG. Parafilm the stopper, and label the flask.
17) Store the distilled PEG in the hood overnight. The PEG will solidify as it cools.
18) Dispose of the toluene waste in the nonchlorinated organic solvent waste container.
19) Glassware can be dried in the hood, and cleaned normally.

OPF Reaction

Warning: Use nitrile or silver-shield gloves when handling MeCl.

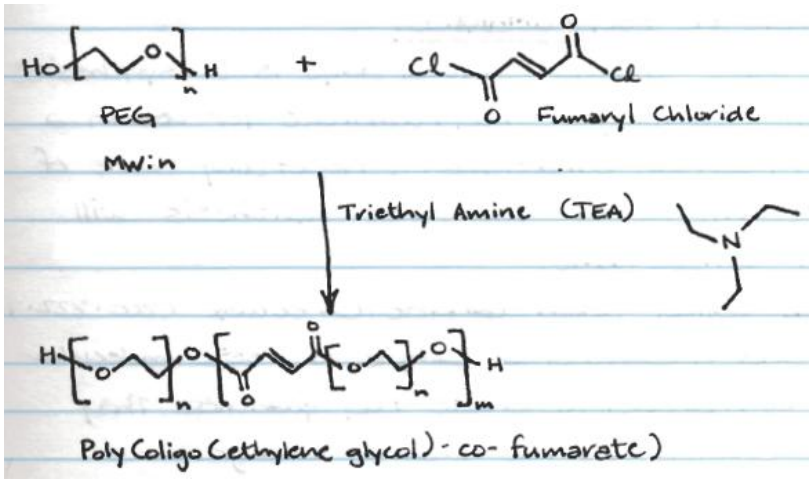

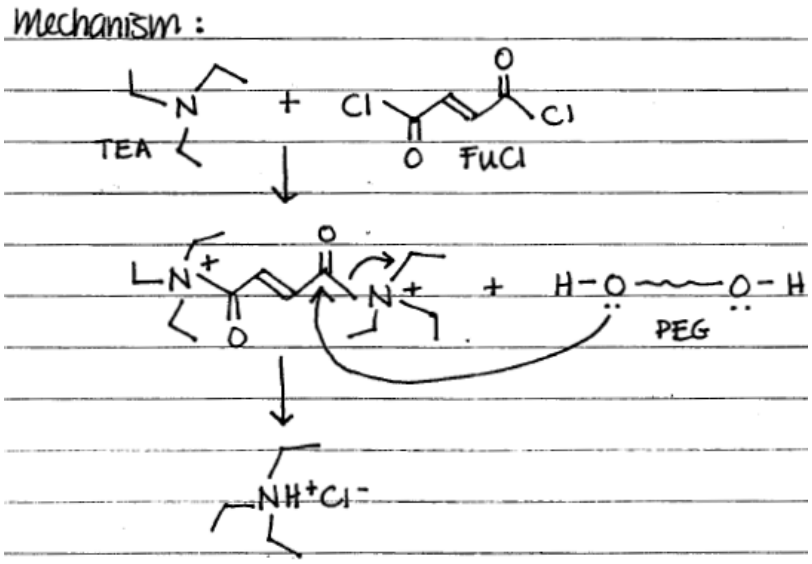

3.4K Calculations:

PEG MW = 3,400 Da

50 g PEG = 0.01471 mol PEG

1 PEG : 0.9 FuCl → 10% molar excess for PEG addition to ends of FuCl

(0.9 mol FuCl / mol PEG) * (0.01471 mol PEG) = 0.01324 mol FuCl

FuCl MW = 153 g/mol

(0.01324 mol) * (153 g/mol) = 2.025 g FuCl

FuCl density = 1.415 g/ml

(2.0235 g) / (1.415 g/ml) = **1.431 ml FuCl**

1 FuCl : 2 TEA → TEA removes Cl from ends of FuCl, 2 Cl per FuCl → Twice as much TEA as FuCl

(2 mol TEA / mol FuCl) * (0.01324 mol FuCl) = 0.02648 mol TEA

TEA MW = 101.2 g/mol

(0.02648 mol) * (101.2 g/mol) = 2.6798 g TEA

TEA density = 0.726 g/ml

(2.6798 g) / (0.726 g/ml) = **3.6912 ml TEA**

10K Calculations:

PEG MW = 10,000 Da

50 g PEG = 0.005 mol PEG

1 PEG : 0.9 FuCl → 10% molar excess for PEG addition to ends of FuCl

(0.9 mol FuCl / mol PEG) * (0.005 mol PEG) = 0.0045 mol FuCl

FuCl MW = 153 g/mol

(0.01324 mol) * (153 g/mol) = 0.6885 g FuCl

Density FuCl = 1.415 g/ml

(0.6885 g) / (1.415 g/ml) = **0.4866 ml FuCl**

1 FuCl : 2 TEA → TEA removes Cl from ends of FuCl, 2 Cl per FuCl → Twice as much TEA as FuCl

(2 mol TEA / mol FuCl) * (0.0045 mol FuCl) = 0.009 mol TEA

TEA MW = 101.2 g/mol

(0.009 mol) * (101.2 g/mol) = 0.9108 g TEA

TEA density = 0.726 g/ml

(0.9108 g) / (0.726 g/ml) = **1.2545 ml TEA**

Reaction

1) Wash and dry:

   1 x 1000 ml 3-arm round-bottom flask, 2 x 60 ml dropping funnels,

   1 x joint for the N_2 balloon, 1 x PTFE valve for the N_2 balloon,

   2 x Kontes #2 glass valves with LARGE holes, 2 x glass stoppers,

   1 x 250 ml or 1000 ml glass graduated cylinder.

2) Use the funnel and graduated cylinder to add 320 ml MeCl to the distilled PEG/toluene. Dissolve PEG with stirring.

3) Use the funnel to pour the PEG/MeCl into the 3-arm flask. The PEG distillation stir bar can be reused in this step.

4) Set up the reaction apparatus as shown, without the glass stoppers and N_2 balloon:

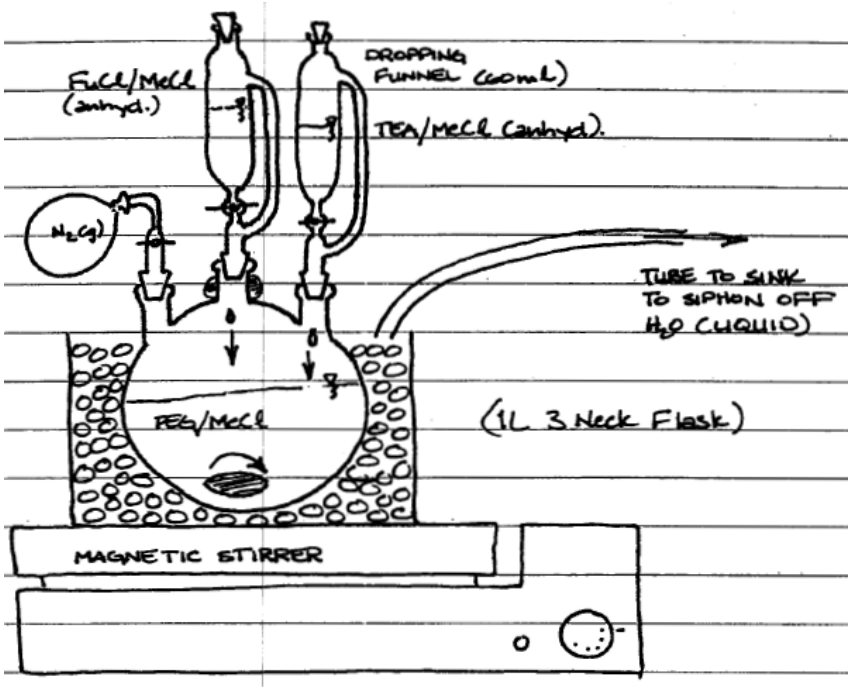

5) Clamp the apparatus to the scaffolding in the back of the fume hood.
6) Vacuum grease and clamp all connections. Be careful not to vacuum grease over the holes in the valves, or else the FuCl and TEA will not flow through. Also the PTFE valve for the N_2 balloon does not require vacuum grease.
7) Place the 3-arm flask in a small autoclave bin, filled with ice on a large stir plate. Optional: Add salt to the ice to keep the ice from melting.
8) For PEG 3.4K, use glass pipettes to add 30 ml MeCl to volumes of FuCl and TEA calculated above (3.4K: 1.431 ml FuCl and 3.6912 ml TEA). Add MeCl to dropping funnels first, then FuCl and TEA. MeCl removes the markings from glass pipettes, so exercise care when transferring MeCl.
9) For PEG 10K, use glass pipettes to add 10 ml MeCl to volumes of FuCl and TEA calculated above (10K: 0.4866 ml FuCl and 1.2545 ml TEA). Add MeCl to dropping funnels first, then FuCl and TEA. MeCl removes the markings from glass pipettes, so exercise care when transferring MeCl.
10) Flush system with N_2 gas, using the N_2 tank and hose and the N_2 filled balloon. Lift the glass stoppers from the dropping funnels slightly to purge excess air. Make sure the N_2 valve remains open.
11) Stir PEG solution on the stir plate at ~5.
12) Start reaction by dropping the FuCl and TEA at the same rate of 1 drop per ~3-4 seconds. A slower drop rate will result in a more efficient reaction.
13) Reaction will turn dark brown.
14) When necessary, siphon melted water from the ice bin, and replace the ice.

15) When dropping is complete, allow the reaction to continue on ice for the rest of the day.

16) When necessary, siphon melted water from the ice bin, and replace the ice.

17) At the end of the day, remove the ice bin, remove the dropping funnels, and replace the funnels with glass stoppers.

18) Allow the reaction to continue at room temperature with stirring on a cork ring for at least 2 days.

19) Check the N_2 balloon over the next 2 days, and refill the balloon if necessary (close valve when refilling the balloon).

20) Glassware can be dried in the hood, and cleaned with acetone and the base bath.

Rotovaporing of MeCl

Warning: Use nitrile or silver-shield gloves when handling MeCl.

1) Wash and dry:

   1 x 1000 ml round-bottom flask,

   1 x glass funnel.

2) Turn on Rotovapor by switching Vacuum Controller V-800, Rotovapor R-200, and Vacuum V-500 on.

3) Fill the water bath with distilled H2O, and heat to 40°C.

4) Use the circulating pump to flow cold, ice water through the condensing tube.

5) Use the funnel to pour the OPF solution into a 1000 ml round-bottom flask.

6) Clamp and vacuum grease the flask to the Rotovapor.

7) Lower the flask into the water bath, so the OPF solution and water levels are the same.

8) Slowly rotate the flask in the water bath.

9) Turn on the vacuum on at 850 mbar ("Set" → Up or down → "Run").

10) Gradually decrease the vacuum as necessary to maintain a steady drip of condensation into the collecting flask. Vacuum can be decreased as low as 700 mbar.

11) When OPF/MeCl solution is thick and "stew-like" consistency, remove OPF from Rotovapor.

12) Dispose of the MeCl waste in the chlorinated organic solvents waste container.

13) Glassware can be dried in the hood, and cleaned normally.

Wash in Ethyl Acetate

Warning: Use nitrile or silver-shield gloves when handling ethyl acetate.

1) Wash and dry:

   2 x 2 L aspiration flasks, 1-2 x 2 L Erlenmeyer flasks, 1-2 x 2 L beakers,

   2 x Buchner funnels, 1-2 x glass funnels, 1 x stir bar, 2 x spatulas.

2) Add ethyl acetate (EA) to the OPF solution until the flask is ~2/3 full.

3) Stir the solution while heating with the heatgun (low speed, med heat) for 15-20 min, rotating every 5 minutes.

4) Solution will become less viscous and salts become visible at the surface. Ethyl acetate is a solvent for the OPF, but not for the salts produced in the TEA reaction.

5) Connect the vacuum and filter the solution through a Buchner funnel with #1 Whatman filter paper (11 µm pores) into a 2 L aspiration flask.

6) The salts will be filtered out of the solution by the filter paper. Discard these salts.

7) Add EA to the OPF to a total volume of 1500-1700 ml.

8) Stopper the flask with a #9 rubber stopper and parafilm the stopper and aspiration neck, and place the flask into the -20°C explosion-proof freezer for at least 2 hours or overnight if necessary.
9) If necessary, clean glassware for the next step.
10) After cooling, remove the OPF/EA from the freezer. The decreased temperature alters the solubility of the OPF, causing the OPF to precipitate out.
11) Connect the vacuum and filter the solution through a Buchner funnel with #1 Whatman filter paper, capturing the OPF in the filter paper and pulling the EA into an aspiration flask.
12) While filtering, stir the solution, allowing the EA to be pulled through the filter paper. Discard the EA.
13) When nearly dry, transfer the OPF from the filter paper to a beaker.
14) Add 1 L ethyl acetate to the solution.
15) Stir the solution while heating with the heat gun to redissolve the OPF in the EA. Solution goes from light brown to dark brown and becomes less viscous.
16) Use a clean glass funnel to transfer the OPF and EA to a 2 L Erlenmeyer flask and add EA to a total volume of 1500-1700 ml.
17) Stopper the flask with a #10 rubber stopper, and recrystallize the OPF/EA solution in a 2 L aspiration flask at -20°C for 1.5 hours or overnight.
18) Dispose of the EA waste in the nonchlorinated organic solvent waste container.
19) After cooling, filter the solution through a clean Buchner funnel with #4 Whatman filter paper (20-25 µm pores), capturing the OPF in the filter paper and pulling the EA into an aspiration flask.

20) The second filtering step may proceed much more slowly than the first. If EA/OPF is solid after removing from the freezer, add more EA to the solution. Tape 2 spatulas together to scoop product from the bottom of the flask.
21) Dispose of the EA waste in the nonchlorinated organic solvent waste container.
22) Optional: Repeat steps 13-19 for a third filtering step. This may be necessary if OPF appears too dark.
23) Dispose of the EA waste in the nonchlorinated organic solvent waste container.
24) Glassware can be dried in the hood, and cleaned normally.

Wash in Ethyl Ether

Warning: Use nitrile or silver-shield gloves when handling ethyl acetate and/or ethyl ether.

1) Wash and dry:

   1 x 2 L beaker, 1 x stir bar, 1 x Buchner funnel, 2 x PTFE coated jars.
2) When OPF is nearly dry and EA is mostly gone, add 1 L ethyl ether (EE) directly to the funnel to remove the EA.
3) Once mostly dry, transfer the OPF from the funnel and filter paper to a 2 L beaker.
4) Add 1 L ethyl ether (EE) to the OPF for a second wash with stirring.
5) Filter the solution through a Buchner funnel with #4 Whatman filter paper (20-25 µm pores), capturing the OPF in the filter paper and pulling the EE into an aspiration flask.
6) Optional: Add EE to the OPF for a third wash.
7) As the EE filters through and the OPF dries, use a spatula to break up any clumps of OPF.

8) By the end, you should have a fine powder that is mostly dry.

9) Scoop the OPF powder evenly into 2 Teflon-coated jars with the spatula.

10) Leave the OPF in the hood overnight with the lid on loosely.

11) Dispose of the EE waste in the nonchlorinated organic solvent waste container.

12) Glassware can be dried in the hood, and cleaned normally.

Vacuum Dry OPF

1) Clamp a lyophilizer tube to the scaffolding in the back of the fume hood as shown:

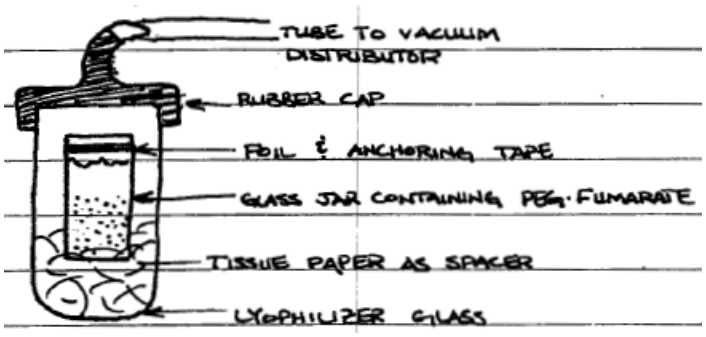

2) Tape aluminum foil to the top of the OPF jars and poke holes in the foil with a small gauge needle.

3) Add liquid nitrogen to the solvent trap.

4) Connect the vacuum to the solvent trap.

5) Close the valves to the samples (3rd and 4th from the top). Open the valve to the manometer (bottom).

6) The top 2 valves are open to the atmosphere and should remain closed.

7) Turn on manometer, and then the vacuum pump.

8) Once a vacuum is established, gradually open the valves to the samples. Open the valve to the first sample until a vacuum is established, then close that valve. Then

open the valve to the second sample until a vacuum is established. Now you can reopen the first sample.

9) Pressure should be less than 10 mbar (preferably 1-2 mbar).
10) Check the pressure and the liquid nitrogen level every 30-45 minutes.
11) Refill the liquid nitrogen if necessary.
12) When OPF is dry and you cannot smell any EE in the powder, open the valve to break the vacuum and turn off the pump.
13) Dispose of solvent from the solvent trap.
14) Parafilm OPF and store it at -20°C.

Verify Product

1) A lighter brown color is preferred.
2) Polymerize a 100% OPF hydrogel with thermal and photo-initiation to test crosslinking.
3) Run GPC on the OPF in chloroform to verify molecular weight.

B.2 PEG-DA Synthesis

Reaction Calculations

1) Begin with **24 g PEG, MW 3400**.
2) React with 100% excess acryloyl chloride (AcCl; 2 AcCl:1 PEG).
3) 24 g PEG / (3400 g/mol PEG) = 7.06 mmol PEG
4) 7.06 mmol PEG * 2 end groups * 2 (100% excess) = 28.24 mmol AcCl
5) 0.02824 mol AcCl * 90.51 g/mol / (1.114 g/mL) = **2.294 mL AcCl**
6) React with 1:1 AcCl:triethylamine (TEA)
7) 0.00706 mmol PEG * 2 end groups = 0.0141 mol TEA

8) 0.0141 mol TEA * 101.9 g/mol / (.726 g/mL) = **1.982 mL TEA**

9) Workup with anhydrous potassium carbonate (K_2CO_3)

10) 0.02824 mol AcCl * 2 mol K_2CO_3/mol AcCl / 2 M K_2CO_3 = **28.2 mL 2M K_2CO_3** (aq)

11) 138.205 g/mol = 276.41 g in 1L = 27.641 g in 100 mL = 8.2923 g K_2CO_3 in 30 mL ddH_2O

Day 1 – Methylene Chloride Distillation

Distill MeCl following the instructions in the OPF synthesis protocol. Keep in mind that you only need approximately 100 mL. Distillation is necessary to remove aqueous contamination (make MeCl anhydrous) that might generate unwanted side reactions in Day 2.

Day 2 – Reaction

What's going on? PEG is being acrylated. TEA acts as a catalyst by sequestering HCl to allow the reaction to proceed to completion. MeCl is the solvent used for this reaction.

Caution: AcCl doesn't smell as bad as FuCl, but it is worse for you (eye, throat irritant)!

Equipment:	
1x 500 mL 3-arm round bottom flask	1x balloon
1x dropping funnel	Glass pipettes
1x PTFE gas valve	1x stir plate
3x glass stoppers	1x clamp
1x glass stopcock	6x green clamps
1x PTFE stopcock	
	Chemicals:
1x stirbar	MeCl (anhydrous)
1x glass funnel	PEG
1x graduated cylinder	TEA
	AcCl

1) Set up 3-arm round bottom flask in the fume hood on a stir plate. Weigh and add PEG to the flask. Add stirbar.
2) Attach one dropping funnel, with a glass stopper, and a PTFE valve for N_2 gas flow. Vacuum grease glass-glass connections for the dropping funnel (excluding glass stopper) and the PTFE valve. Do not grease the PTFE valve itself.
3) Hook up N_2 tubing to the valve. Continually purge the whole system as you add 40 mL MeCl to the round bottom flask through the ungreased arm using a glass funnel. Stir. Gently float a glass stopper in the arm on the air being pushed out.

4) When dissolved, use a glass pipette to add TEA. Vacuum grease a glass stopper and gently float the dropping funnel's glass stopper as before. Let stir for 5 min.
5) Use a glass pipette to add 20 mL MeCl and the appropriate amount of AcCl to the dropping funnel. Be aware that MeCl (and its fumes) will remove markings from glass pipettes. Vacuum grease and stopper the funnel while you are adding and turn off N_2 flow.
6) Remove the N_2 hose and attach an N_2 balloon.
7) Drip the AcCl/MeCl mixture into the round bottom flask (about 1 drop every 3-4 seconds). Drip AcCl in MeCl very slowly (about 1 drop every 4 seconds).
8) After dripping is complete, you can replace the funnels with stopcocks.
9) Let stir overnight.

Day 3 – Workup

What's going on? To remove TEA-HCl, we first react the mixture with potassium carbonate to produce KCl, which will transfer to the aqueous phase. Some TEA will remain in the organic phase for Day 3 filtration.

Equipment:
1x 250 mL separatory funnel
1x glass stopper
1x glass funnel
1x glass stopcock
1x ring clamp

Chemicals:
K_2CO_3, anhydrous

1) Use a glass funnel to transfer the mixture from the round bottom flask to a separatory funnel with a greased stopcock. (Don't forget to close the stopcock prior to transfer. Also, remember to wipe vacuum grease from connections before pouring.)
2) Add appropriate amount of 2M K_2CO_3 to the separatory funnel.
3) Stopper funnel, hold vertically, and give it a quick shake or two. Immediately open the stopper to release CO_2. Repeat a few times.
4) Hold the separatory funnel horizontally, but with the tip tilted higher. One hand should hold the glass stopper, the other holding the stopcock knob up. Rotate vigorously, and open the

stopcock periodically to release CO_2. Repeat until all gas is released. Solution should have the consistency of a milky-white emulsion.

5) Leave overnight. Place a beaker underneath to capture any leaked product.

Day 4 – Filtration and Drying

What's going on? We isolate the mixture from KCl in the aqueous phase, add $MgSO_4$ to remove any additional aqueous solution, and precipitate PEG-DA in ethyl ether. TEA should remain in solution.

1) Drain the two organic phases into a 250 mL beaker on a stir plate with stir bar.
2) While stirring, add $MgSO_4$ until the mixture goes from a lumpy consistency to a well dispersed mixture of powder and organic solvent. It should appear as opaque milk – if it doesn't look like milk, add more $MgSO_4$. Add ~20-40 mL MeCl to keep the PEG-DA in solution (may help to have a smaller bottle or beaker with MeCl). The goal here is to add as little MeCl as possible to keep the solution saturated with PEG-DA. But, if you add too much, no sweat.
3) Prepare a Buchner funnel with aspiration flask and filter paper and pre-wet the filter paper with MeCl.
4) Pour the mixture into the filter and a clear liquid should be collected (containing PEG-DA). If the liquid is cloudy, filtration should be performed again. The vacuum will also begin to evaporate MeCl. Thus, you can elect to evaporate MeCl if necessary.

Equipment:
2x 250 mL beakers
1x 1L aspiration beaker
1x 2-3L beaker
2x stir bars
2x Buchner funnels
Filter paper (fine pores, 42)

Chemicals:
$MgSO_4$, MeCl
Ethyl ether

5) Prepare a 2L beaker with 1.7L ethyl ether and a stir bar. Pour in the PEG-DA solution and wait 10 min to precipitate PEG-DA.
6) Prepare another Buchner funnel with two filter paper sheets, and pre-wet with ethyl ether.

7) Filter to separate PEG-DA. If the filtrate is not clear, re-filter. Pound into bits. See an older grad student to measure your performance.
8) Dry under vacuum until no ether can be smelled (at least 5 hours). At least some of this vacuum drying must be performed immediately after filtration.
9) Store at -20ºC. Expected recovery is approximately 75%.

Note: If necessary, you may need to dialyze the resulting product to remove impurities. Use a 1000 MWCO dialysis membrane at 0.2 g/mL and lyophilize after dialysis.

B.3 Desulfation of Chondroitin Sulfate with Acidic Methanol to Form Chondroitin

Adapted from: *Schubert M. Chondroitin From Chondroitin Sulfate. Methods Carbohyd Chem. 1965;5:109-10.*

Materials:

Chondroitin-6-sulfate – Wako 032-14612, 25 g

Acetyl chloride – Fisher AC21947-2500, 250 ml

Can scale quantities/volumes accordingly.

Desulfation of Chondroitin Sulfate to Form Methyl Ester of Chondroitin

1) Slowly add 5 ml acetyl chloride in 1000 mL methanol (very acidic, pH 0.0)
2) Let the solution stir for a few hours
3) Add 5.0 g chondroitin sulfate in 1000 ml of acidic methanol
4) Stir for 1 day at room temperature
5) Centrifuge (4000 RPM for 5 min) and discard clear solution
6) Repeat on days 3 and 7
7) Dissolve white residue in 100 mL water
8) Precipitate in 600 mL 95% ethanol

9) Separate by centrifugation

10) Wash with ethanol and separate by centrifugation at least twice

11) Wash with ether and separate by centrifugation at least twice

12) Vacuum dry

13) Yields ~2.8 g methyl ester of chondroitin

14) Store product at 4°C

Demethylation to Form Chondroitin

1) 2.5 g methyl ester of chondroitin in 100 mL 0.1M aqueous KOH

2) Keep 1 day at room temperature on shaker plate

3) Add to 1 mL glacial acetic acid, 1 g potassium acetate in 10 ml water

4) Precipitate product with 400 ml ethanol

5) Separate by centrifugation (4000 RPM for 5 min)

6) Wash with ethanol and separate by centrifugation at least twice

7) Wash with ether and separate by centrifugation at least twice

8) Vacuum dry

9) Yields ~2.3 g chondroitin

10) Store product at 4°C

B.4 Chondroitin Sulfate Methacrylamide Synthesis with EDC/NHS

Purpose: To add methacrylamide group to chondroitin sulfate chains.

Materials:

Small glass vial and small stir bar

Chondroitin sulfate A, 1 mg (Sigma)

N-(3-dimethylpropyl)-N-ethylcarbodiimide hydrochloride (EDC)

N-3-aminopropyl methacrylamide

NaCl

Dialysis tubing

Dialysis clips

Methacrylation

1) Add 1.14 mg chondroitin sulfate (~0.0025 mmol by -mer MW, 457.4 Da) per mL of distilled water.
2) Add 0.96 mg (0.005 mmol) of EDC and 0.89 mg (0.005 mmol) of N-3-aminopropyl methacrylamide for every 1 mL of solution.

   Optional: Add 1.09 mg (0.005 mmol) of Sulfo-NHS.
3) Incubate the mixture for 2 hrs at pH 5.0 with stirring at room temperature.
4) Add another 0.96 mg (0.005 mmol) of EDC and 0.89 mg (0.005 mmol) of N-3-aminopropyl methacrylamide for every 1 mL of solution.
5) Incubate the mixture for 2 more hrs at pH 5.0.

Dialysis

1) Dialyze (1,000 MW cutoff) solution against 10 mM NaCl solution for 1 day.
2) Cut the dialysis tubing into strips a little shorter than the beaker that will be used for dialysis.
3) Since the dialysis tubing is stored in sodium azide it needs to be rinsed. To do this put the dialysis tubing in a beaker with about 1L of dH_2O and mix. Refresh the dH_2O every 15 minutes (3x) in order to thoroughly rinse the tubing.
4) After the tubing is thoroughly rinsed remove it from the beaker and close one end of

the dialysis tubing with a weighted closure. After the reaction in step 5 is complete, use a transfer pipette to add the mixture to the tubing until the tubing is about half full. Close the open end of the tubing with a non-weighted closure.

5) Use teflon tape to hold the tubing high in the water as it stirs.
6) Dialyze (1,000 MW cutoff) solution against distilled water for another 2 days.
7) If starting on the morning of the first day change the water the morning and night of the second day.
8) Lyophilize product for 4 days.

B.5 Chondroitin Sulfate Methacrylate Synthesis with Methacrylic Anhydride

Purpose:

To conjugate methacrylate groups onto a chondroitin sulfate polymer that enable photopolymerization into a cohesive CS-MA hydrogel that maintains degradative properties. The goal of this experiment is to create CS-MA with various degrees of methacrylate (MA) substitution by reacting chondroitin sulfate with methacrylic anhydride (MAA) in the presence of sodium hydroxide (NaOH).

References:

Bryant SJ et al. Synthesis and characterization of photopolymerized multifunctional hydrogels: water-soluble poly(vinyl alcohol) and chondroitin sulfate macromers for chondrocyte encapsulation. *Macromolecules.* (2004). 37:6726-6733.

Wang L-F et al. Synthesis and characterization of chondroitin sulfate-methacrylate hydrogels. *Carbohydrate Polymers*. (2003). 52:389-396.

Huang S-J et al. Controlled immobilization of chondroitin sulfate in polyacrylic acid networks. *Journal of Biomaterials Science. Polymer Edition*. (2007). 18(1):17-34.

Tsai M-F et al. Characterization of hydrogels prepared from copolymerization of the different degrees of methacrylate-grafted chondroitin sulfate macromers and acrylic acid. *Journal of Biomedical Materials Research. Part A.* (2008). 84A:727-739.

Reaction Chemistry:

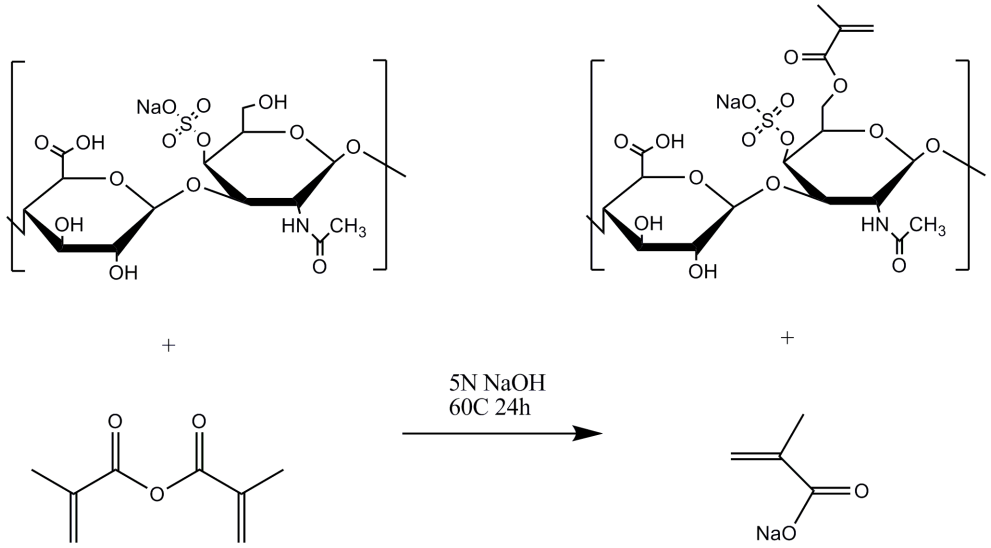

The synthesis of CS-MA is shown above. Any of 3 hydroxyl groups in each disaccharide unit of CS may under nucleophilic acyl substitution via a carbonyl group in methacrylic anhydride to form an ester bond, producing a methacrylic acid by-product. The reaction is driven forward by the addition of excess strong base (NaOH) to neutralize the methacrylic acid (pKa = 4.58) that is formed (Le-Châtelier's principle). Since the solubility of highly charged CS is limited in organic solvents, this methacrylation scheme is carried out in an aqueous environment MAA. To compensate for the tendency of MAA to react with water and form methacrylic acid, an excess of MAA is used in all cases.

Reagents:

- chondroitin sulfate A (Chondroitin 4-sulfate, C 9819, Sigma)

- Storage temperature 2-8°C
- Approximate MW 48,700 Da and PI 1.49 per Bryant et al, MW of disaccharide unit = 458.37 Da

- ddH_2O
- methacrylic anhydride (Product # 276685-500mL, Aldrich)
  - Stored liquid at RT, acids cabinet
  - Use respiratory and contact precautions, wear eye protection
  - Must be added dropwise to aqueous solutions
  - Assay 94%; MW 154.16; density 1.042 g/mL at 25 °C; FP 84°C, BP 87°C
- 5N NaOH
  - Stored solid pellets at RT, bases cabinet
- Methanol
  - Stored 4°C, explosion-proof refrigerator
- D_2O

Equipment:

- 100mL beaker and stir bar for dissolving CS
- 500mL, 3-neck round-bottom flask for reaction, thermometer fitted into glass stopper for flask, 125mL dropping funnels (2), glass valves and clips (2), glass stoppers and clips (3)
- Heating mantle, magnetic stir plate and stir bar
- Pipette pump and glass serological pipettes
- Silicone vacuum grease
- Cork ring

- 2L Erlenmeyer flask
- Large Buchner funnel and 125mm diameter #42 Whatman quantitative cellulose filter membranes, 1L filtration flask
- High vacuum system, lyophilizer tube (1), liquid nitrogen, scintillation vials (1), aluminum foil, syringe needle

Procedure:

Day 1

Preparation

1) Clean stir bars and any glassware. For glassware, begin with soap and water, followed by dH_2O, and then acetone. For plastics, use ethanol in lieu of acetone. Dry in oven or at room temp.
2) Make solution (>150mL) of 5N NaOH (NaOH MW: 40.00).
3) Prepare scintillation vials that will contain solution for pH readings.
4) Bring CS to room temperature (~20min).
5) Place small heating mantle on stir plate inside the fume hood and connect power to nearby transformer. Plug in transformer and stir plate into hood outlet.

   Conjugation

6) Dissolve 15g chondroitin sulfate in 60mL ddH_2O (yields a volume of ~100mL) using a beaker. This will take ~30-45 min at moderate stir velocity. Transfer to 3-neck round bottom flask and place on heating mantle on stir plate inside fume hood, setting at speed 7. Begin stirring. The flask now contains a 25% w/v solution of chondroitin sulfate, which has 19.062×10^{-3} moles of hydroxyl groups that are available for conjugation.

7) Cap the flask with a rubber stopper fitted with a thermometer that is submerged in the reaction solution (left-most neck of the flask). Switch on the transformer at setting 0 and raise the temperature to 60°C (~ transformer setting of 30).
8) Assemble dropping funnels. Place an *extremely thin layer* of silicone vacuum grease on either side of the hole on the glass valve, being careful to avoid getting any in the hole. Place the valve in its corresponding slot on the dropping funnel and fix in place with a metal clip on the other side. Mount a dropping funnel on the middle neck of the flask after coating the male end with a very thin layer of vacuum grease. For now, cap the right-most neck with a glass stopper that has also been coated with a very thin layer of vacuum grease.
9) Using a manual pipette pump and glass serological pipette, slowly add specified volume of methacrylic anhydride via the top end of the dropping funnel, making sure the valve is in the closed position first. Cap the dropping funnel with a glass stopper (coated with vacuum grease) until intended time of addition.
10) Once the temperature of the reaction vessel has stabilized, add methacrylic anhydride in specified amount in the table below to the flask in a dropwise fashion via the dropping funnel, making sure that the rate of dropping is slow and consistent over time until all MAA has been added. To enable a slow addition, partially open the valve.
11) Replace the MAA dropping funnel with one containing 5N NaOH. [Note: This is a highly corrosive base! Wear silver nitrate gloves and face shield!] Add 5N NaOH dropwise (consistent rate) into the flask to reach a pH ~10. Measure and record the pH of the reaction vessel by drawing 10mL of solution after mixing from the

rightmost neck of the flask. Once the appropriate pH is reached, cap the dropping funnel and all open necks with glass stoppers until next measurement/adjustment.

Volume Methacrylic Anhydride (mL)	Moles Methacrylic Anhydride	MAA:CS-Hydroxyl Ratio	Volume 5N Sodium Hydroxide Added (mL)	Moles Sodium Hydroxide Added	NaOH:MAA Ratio
60	*405.6 x 10^{-3}*	*20.6:1*		*x 10^{-3}*	*:1*

12) Stir reaction vigorously at 60°C for 24h under fume hood. Extract 10mL of reaction volume to pH at start of reaction, and again after 2, 4, 8 and 24h. Maintain pH at ~10 as necessary.

Day 2

Preparation

13) Prior to setting up equipment, make sure ***all*** glassware and related equipment is washed and dried. For glassware, begin with soap and water, followed by dH_2O, and then acetone. For plastics, use ethanol in lieu of acetone. Dry in oven or at room temp. Weigh scintillation vials that will be used to later store CSMA (will be used to calculate an approximate percent yield).

14) Set up filtration apparatus: a) Place filter membrane in Buchner funnel and mount in neck of 1L filtration flask; b) Attach plastic tubing to connection in neck of flask and secure to vacuum nozzle in hood; c) secure to mounted clamp in back of hood to stabilize flask.

Precipitation, Filtration, Washing, and Drying

15) Turn off transformer, cap all necks of flask with glass stoppers, and (using thermal gloves) place reaction flask on cork ring to allow reaction to cool to room temperature. Carefully pour reaction through a single neck (wipe vacuum grease off

with a Kimwipe first) into a 2L Erlenmeyer flask. Add ~500mL of methanol to flask to precipitate CS-MA and remaining CS. Following complete precipitation, thoroughly mix the solution and pour into filtration funnel in increments. Wash the resulting filtrate 5x with 50mL methanol (10mL methanol:1g CS reacted). Transfer filtrate to scintillation vial, cover with aluminum foil secured with tape, and poke several small holes in foil with small gage needle.

16) Place vial inside glass lyophilizer tube and connect tube to a vacuum pump via a liquid N_2 condenser trap.

17) Establish vacuum and dry for ~12h or until no methanol is detected by wafting. [Note: Vacuum must be monitored every 30min while running and cannot be left unattended longer than 1h, thus cannot be left on overnight. Doing so presents a significant explosion hazard.]

18) Store vials at 4°C.

Characterization by ^1H NMR

19) Rinse NMR glass tubes with acetone and dry in oven.

20) Prepare 10mg/mL sample of CS-MA in D_2O in microcentrifuge tube and transfer to NMR tubes (~1mL). Cap and number tubes with sample identifier. In addition, prepare a D_2O blank, a CS control, and a MAA control in NMR tubes.

21) Perform ^1H NMR and analyze data for the following peaks:

    a) **Residual MAA or MA acid:** Integrate peak corresponding to methyl groups on MAA is observed at 1.6ppm

b) **Confirmation of MA substitution:** Integrate peaks corresponding to methylene portion of conjugated methacrylate moiety at 5.65 and 6.10ppm. Peak corresponding to methyl portion of conjugated methacrylate moiety at 1.89ppm.

c) **Determination of degree of substitution:** Expand region from 1.6 to 2.1ppm, then deconvolute and integrate peaks at 1.89 (see above) and 1.99ppm (methyl group of native CS). Calculate ratio of peak intensity at 1.89ppm to that at 1.99ppm to calculate degree of MA substitution on CS. [Since there are 3 hydroxyl groups that could be substituted by methacrylate, maximum DS is 3. According to Bryant et al, a heteronuclear shift correlation through multiple bond connectivities (HMBC) experiment (analyzes relationship between protons and carbons in structure) did not reveal a preferred substitution site.]

B.6 Chondroitin Sulfate Methacrylate Synthesis with Glycidyl Methacrylate

1) Dissolve 1 g of chondroitin sulfate (CS) per 50 mL dH_2O

   CS disaccharide: 457.4 Da (Chondroitin disaccharide: 378.35 Da)

   1 g = 2.19 mmol = 1 equivalent

2) Add 50 mL acetone, resulting in a 1% w/v solution of CS in 50:50 mixture of acetone:water

3) Stir overnight at room temperature

4) Add 20 molar equivalents of triethylamine (TEA)

   TEA: 101.19 Da, 0.726 g/mL

   20 equivalents = 43.7 mmol = 4.42 g = 6.09 mL

5) Slowly drip in 20 molar equivalents of glycidyl methacrylate (GMA)

GMA: 142.15 Da, 1.042 g/mL

20 equivalents = 43.7 mmol = 6.22 g = 5.97 mL

6) Stir for 24 hr at room temperature
7) Rotovap to concentrate if necessary
8) Dialyze in 50:50 acetone:water for 1 day using 1,000 Da MWCO regenerated cellulose membrane
9) Dialyze in dH_2O for 2 days
10) Lyophilize product for 4 days
11) Store product at -20°C

B.7 CSMA Microparticle Formation

Remove CSMA from -20°C and allow to sit at room temperature for 30 minutes. Keep ALL ingredients on ice.

1) Place 60 mL of corn oil in the 4°C refrigerator.
2) Make APS solution in 1.5 mL tube: 34.2 mg APS in 500 µL PBS
3) Make TEMED solution in 1.5 mL tube: 22.5 µL in 500 µL PBS
4) Weigh out 55.6 mg Chondroitin Sulfate Methacrylate (CSMA) in a scintillation vial and add 440uL of PBS.
5) Homogenize corn oil at 3900 rpm for 5 minutes.
6) Add 30 uL of APS and 30 uL of TEMED to the CSMA solution, mix, and add solution dropwise to corn oil. Make sure everything is on ice to prevent crosslinking. Homogenize for 5 minutes.

**DO NOT MIX APS AND TEMED TOGETHER BEFORE ADDING TO CSMA SOLUTION-ALWAYS ADD SEPERATELY*

7) Place corn oil mixture on a hot plate (set to 100°C) with the largest stir bar that will fit in the container (to keep particles moving so as not to crosslink with one another) and a thermometer (to monitor temperature-I usually let it go up to 50-60°C). Allow to crosslink for 30 minutes.
8) Separate mixture into two 50 mL conical tubes and centrifuge at 1500 rpm for 5 minutes at 4°C.
9) Remove oil from microparticles and resuspend pellet in ddH2O and transfer to 1.5 mL tube (if possible). Wash 3 times to remove oil. Store at 4°C.

B.8 Passive Adsorption of Aggrecan to TCPS Sufrfaces

Materials:

Aggrecan (Sigma)

Sterile D-PBS (w/o Ca^{2+} or Mg^{2+})

24-well tissue culture-treated polystyrene plates

Protocol:

Aggrecan pre-treatment

1) Sterile filter a 0.05 mg/mL aggrecan solution in PBS.
2) Warm up the aggrecan solution to 37°C.
3) Dispense 100 µL of aggrecan solution into each well of a 24-well tissue culture-treated polystyrene plate. This gives each well 5 µg of aggrecan.

4) Leave plates, with the lids askew, in the sterile hood overnight (with the blower running, UV lights off) to allow the D-PBS to evaporate and aggrecan to adsorb.

B.9 Bovine BMSC Harvest

Purpose: Isolation of bMSCs from a bovine tibia and femur bone.

Materials:

Saw + saw blade

Tweezers, Spatulas

MSC media - Low glucose DMEM, FBS, Antibiotic/Antimicotic, bFGF

PBS+ solution – Sterile PBS, Antibiotic/Antimicotic

PBS+ bottle

Acetic Acid

Trypan blue

Isopropyl alcohol (for Mr. Frostys)

*** Contact Kim x51547 in IBB to make sure there's enough room for our bag in the meat freezer***

Protocol:

1) Make sure to autoclave all appropriate tools (saw blade, tweezers, spatulas, PBS+ bottle).
2) Make up MSC media.

   500 ml Low glucose DMEM

   56.18 ml FBS

   5.62 ml Antibiotic/Antimycotic

562 ul Fungizone

56.2 µl bFGF

3) Make up PBS+

500 ml Sterile PBS

5 ml Antibiotic/Antimicotic

4) Prepare the hood area by laying down sterile drapes and taping them down.
5) Cut away all tissue from the leg. This can be done non-sterilely outside of the hood.
6) Bring the bone into the tissue culture hood. Using a bone saw cut the bone into two roughly equal pieces. Squirt the cut with PBS+.
7) Remove bone marrow using tweezers and spatulas and transfer into a 50 ml tube.
8) Squirt PBS+ solution into the tube.
9) Pippette up and down in a 50 ml pipette until the solution starts to flow smoothy. Tapping the pipette on the bottom of the tube as pipetting will help to break up clumps faster.
10) Repeat using a 10 ml pipette.
11) Run the solution through needles of 16 G, 18 G, 20 G. If the needle becomes clogged try pulling back on the plunger and then adding pressure again. If there is still an obstruction remove the needle and replace.
12) Repeat previous step.
13) Spin down at 1200 rpm for 15 min.
14) Aspirate supernatant, not blood.
15) Pool remainder and spin down if needed.

16) Add PBS+ to bring the solution up to a desired level. Take a 1 ml sample for counting and spin down.

17) Make a 4% acetic acid soln. by mixing 80 uL acetic acid in 2 mL sterile PBS.

18) Add 100 uL 4% acetic acid solution to 100 uL cell suspension to lyse RBCs

19) Add 175 µl media, 100 µl trypan blue, and 25 µl of the cell solution/acetic acid to a tube for counting. This creates a 1:12 dilution. The cells can be spun down in the centrifuge while the counting process in taking place.

20) Inject approximately 10-15 µl of the cell solution into the groove of the hemocytometer.

21) Look at the hemocytometer under the microscope and count the cells in the 4 sections at the corners of the grid.

22) Resuspend in DMEM for a concentration of 40e6 cells/25 ml of media (1.6e6 cells/ml).

Calculations

- (Total number of cells in the 4 grids) x (2500) = Concentration of solution in cells/ml. Multiply this number by 12 to get the concentration of the full solution.
- Multiply the concentration by the volume in the tube to get the total number of cells.

23) Add 40e6 cells in 25 ml of media to a 150x25 mm dish and leave in incubator for 30 min. Neutrophils and fast adhering cells will stick to the plate. MSCs won't.

24) Add 12.5 ml of fluid from the plate and 12.5 ml of media to a T-150 flask. Tilt the flask to make sure the fluid is reaches all corners of the flask and cells get distributed somewhat evenly.

25) Incubate overnight x2 (for two days).

26) Aspirate media from the T-150s.

27) Wash in 10 ml PBS.

28) Aspirate the PBS.

29) Repeat the previous two steps.

30) Add 20-25 ml of media to the flasks.

31) Grow till confluency (~10 days).

32) Freeze down cells (use Mr. Frosty!). Note: You will probably have less than the 20e6 cells/plate that were first plated.

Dispose of leg as appropriate. Double bag the remains in biohazard bags and take it to IBB 0230 (basement) before 4 pm and ring the doorbell for assistance.

B.10 Bovine Tendon/Ligament Fibroblast Harvest

Purpose: Tendon and ligament will be digested to remove matrix (i.e. collagen) and isolate the fibroblasts for use in experiments. Approximately 10g of tendon and ligament tissue can be obtained with each harvest, resulting in around 100e6 cells.

Materials Needed:

Tissue:

Mammal legs (intact joint capsule)

Solutions:

Sterile PBS w/o Ca^{++} and Mg^{++}

Antibiotic/antimycotic (100X)

PSN (100X)

Kanamycin (100X)

Gentamicin (1000X)

Fungizone (1000X)

70% ETOH or IPA solution

DMEM

Collagenase type II, Gibco, 17101-015

Supplies:

#4 blade handles

#22 blades

Sterilized razor blades

Autoclaved Forceps

Autoclaved Nalgene squirt bottle

Hemostats

For cell isolation:

Autoclaved cell strainer (with 74 µm mesh)

60 ml syringes and 0.2 µm filters

T-75 flasks

Shaker plate

*** Contact Kim x51547 in IBB to confirm room for our bag in the meat freezer***

Solution Preparation

Harvest

1. PBS+
    a. Use undiluted 1x bottle of Dulbecco's PBS w/o Ca^{++} and Mg^{++}.

b. Add 10ml/L antibiotic/antimycotic (stock @ 100x).

2. DMEM+ a.k.a. Arnold (overnight antiobiotics for tissue samples)
   a. Use sterile high glucose DMEM. Add 10 ml/L PSN (stock @ 100x), 10 ml/L kanamycin (stock @ 100x), 1 ml/L gentamicin (stock @ 1000x), and 1 ml/L fungizone (stock @ 1000x).

Cell isolation

1. 0.4% collagenase digest solution
   a. In DMEM+ (see above) add 0.4% collagenase. Make enough for 10 ml digest solution per 1 gram tissue + extra volume.
   b. CALCULATION: [total mass of tissue]*10 ml/g tissue * 0.004 = ___ g of collagenase.
   c. Sterile filter collagenase solution using 60 ml syringe and 0.2 µm filter.

Procedure for Tissue Isolation

1) Prepare sterile PBS and place in a sterile 500ml Nalgene squirt bottle.
2) Cut the majority of the meat away from around the joint capsule, but do not penetrate the capsule. Make sure to cut enough meat away from around the capsule in order for someone to hold the bones comfortably.
3) Transfer the leg to the hood.
4) Wash the capsule surface with EtOH and then PBS+.
5) Articulate the joint to identify the femoral heads and patella.
6) Using a #4 scalpel with a #22 blade, take light slices on the outside of the joint capsule along the imaginary line immediately below the femoral condyles. These slices will expose the lateral and medial collateral ligaments.

7) Penetrate the joint capsule on the anterior side exposing the patellar ligament (inferior to the patella) and the fat pads. Squirt the inside of the capsule with PBS+.
8) Use a second scalpel and blade to transect the collateral ligaments and the patellar ligament.
9) Transect the anterior and posterior cruciate ligaments (between the two femoral condyles) without damaging the menisci or the cartilage on the condyles.
10) At this point the femur and the tibia should be easy to separate, if not, go back and see which ligaments have not been fully transected.
11) Cut through the meat on the posterior side of the leg to fully separate the tibia and femur.
12) Detach the tendons and ligaments from bone.
13) Transfer ligaments and tendon to Petri dishes and squirt with PBS+.
14) Dispose of leg as appropriate. Double bag the remains in biohazard bags and take it to IBB 0230 (basement) before 4 pm and ring the doorbell for assistance.

Procedure for Cell Isolation

1) With a new scalpel blade, attempt to remove any excess soft tissue and fibrous tissue.
2) Dice the tissue into roughly 1-3 mm^3 cubes.
3) Record weight of empty Petri dish. Aspirate excess PBS and weigh tissue in Petri dish to get tissue only weight.
4) Place tissue into T-75 flasks so that there is about 2-3 grams of tissue per flask.
5) Add 10 ml of 0.4% collagenase digest solution per 1 gram of tissue to each T-flask. T-flasks should be placed on their sides and secured firmly to the shaker plate. The whole assembly is then placed into the incubator for 12-48 hours. Agitate at 3-5 Hz.

After digestion (~48 hr)

6) When fully digested, filter cell suspension by pipetting suspension into a 60 ml syringe attached to a metal cell strainer with 74μm mesh. Strain cell solution into a 50 ml conical. Dilute the suspension 1:1 with warm PBS to decrease the viscosity of the collagenase solution.
7) Centrifuge all samples at 1300 rpm for 10 minutes. For ligament and tendon the solution above the pellet may appear murky due to cells that did not completely separate out during the centrifugation. If this occurs leave at least 5 ml of solution above the pellet when aspirating. Then, dilute and repeat centrifugation to get the maximum number of cells to pellet down.
8) Aspirate off collagenase solution and resuspend cells in 10 ml sterile PBS w/o IONS or DMEM. Recombine and repeat if necessary.
9) Count cells to determine how much media to later add for the desired cell density.
10) Spin the cells at 1300 rpm for 7 min. Aspirate off the PBS.
11) Add an appropriate amount of media with 10% FBS and 10% DMSO. Use the auto to pipette up and down to mix cells thoroughly throughout the solution.
12) Add 1 ml of cell solution to each tube you will be freezing down.
13) Place the cell vials in the appropriate cooling container and place them in a -80°C freezer.
14) After enough time has passed put the now cold vials into the liquid nitrogen for long-term storage.

B.11 Cell Encapsulation

Purpose: Gels will be created with cells incorporated in them.

Materials:

Media (prepared day before)

Sterile PBS

15 and 50 mL conicals as needed

3 and 10 mL syringes, with one 18G needle for each.

1 mL syringe

Sterile filters

12-well plates

Sterile containers for your gels (Teflon molds, or other molds)

Spatulas, sterilized

The day before your encapsulation

1) Combine the polymers desired in a scintillation vial. You can freeze this vial down until the day of encapsulation. Note: You will lose about 200-300 µL due to sterile filtration, so adjust accordingly by making a gel that requires 300 µL more than the PBS you would have added to your polymers.
2) Sterilize Teflon molds and spatulas as required. Always a good idea to have extra.
3) Make sure you have enough sterile filters and other items for your encapsulation.

Day of encapsulation

Polymer side

4) Warm up your polymer powders, trypsin, and your media.

5) If doing a thermal encapsulation, create 0.3 M stock solutions of APS and TEMED in scintillation vials as you would normally.
    a. APS: 684.6 mg in 10 mL PBS
    b. TEMED: 0.348 g (~350 µL) in 10 mL PBS
6) Add sterile PBS to each vial according to your calculations and vortex.
7) Let the solutions sit at 37 °C for at least 30 min in order to remove bubbles.
8) Filter sterilize APS and TEMED solutions (if you're using them) into 15 mL tubes. Make sure to cover the tubes with aluminum foil to prevent photoinitiation.
    a. Open the packaging of a syringe filter, but leave the filter in its container.
    b. Attach a needle to a 10 mL syringe, and draw up the contents of a scintillation vial.
    c. Invert the syringe and remove the needle.
    d. Grip the sides of the filter container, and screw the syringe onto the filter.
    e. Filter into an open 15 mL tube.
9) Prepare the UV lamp and warm it up if you're doing a photo encapsulation.
10) Place sterile, autoclaved molds into petri dishes (one mold per dish).
11) Filter sterilize your prepolymer mixtures. **Tip:** For a gel less than 1 mL, use a 3 mL syringe, then after pulling up the gel, pull up additional air. The air helps with sterile filtering.
12) Transfer the correct amount of gel to a separate 15 mL tube.
13) Place your sterile spatulas.
14) Prepare and label your 12-well plates.

Important note: At minimum, steps 4-11 **must** be completed before the actual encapsulation itself.

Cell side

15) Rinse your flasks twice with PBS, and trypsinize your flasks as normal.

16) While you count your cells, spin down the cells in the centrifuge. **Caution:** Before you spin down the cells in this step, make sure steps 4-11 are done.

17) Aspirate the media off the cells, then resuspend the pellet in sterile media, typically at a concentration of $50x10^6$ cells/mL.

- Amount of media to resuspend in µL = # of cells/desired concentration x 1000
- e.g., with 10,000,000 cells total, then 10e6 / 50e6 x 1000 = resuspend my cell pellet in 200 µL of media.

Crosslinking/encapsulation

18) Add cell solution according to your calculations and quickly mix with the pipette (do **not** vortex). If the cell solution has a concentration of $50x10^6$ cells/mL and you used the standard gel calculator, this will give a final solution of $10x10^6$ cells/mL.

19) If doing a thermal encapsulation, add APS according to your calculations and mix with pipette. Then, add TEMED according to your calculations and mix with pipette.

20) If doing a photo encapsulation, add sterile D2959 to your solution and mix with pipette.

21) Deposit the appropriate amount of the resulting solution in your molds. The standard is 30 µL of gel in a 1.0-mm Teflon mold well.

22) Cover petri dish and place it in the incubator for 10 min for thermal polymerization; leave under lamp for photo polymerization.

23) Aliquot 2 mL media into each well of a 12-well plate, depending on how many gels you have.

24) Remove from the heat and carefully move the gels into the 12-well plate using a sterile spatula. Put the 12-well plate into the incubator.

25) Repeat steps 18-24 as necessary with other polymer solutions.

26) Recommended: Change media one hour after encapsulation.

B.12 Dimethylmethylene Blue (DMMB) Assay

Materials:

Chondroitin sulfate A or B (B = Dermatan sulphate) Sigma Aldrich C-4384

9-dimethylmethylene blue chloride (DMMB) Sigma Aldrich 341088

Na_2HPO_4 Fisher Sci BP332-500

Di-sodium-EDTA Fisher Sci S311-100

NaCl Fisher Sci S640-500

Glycine Fisher Sci G46-500

Cysteine-HCl Sigma Aldrich C7477

0.1 M stock HCl solution

Regular flat-bottom 96-well plates (clear)

Reagent Preparation:

PBE buffer, pH 6.5: Dissolve 7.1 g Na_2HPO_4 and 1.86 g Na_2EDTA in 495 mL of ddH_2O. Calibrate pH meter, then read and adjust pH to 6.5 +/- 0.1 with concentrated HCl (~3 mL 12 M stock HCl and ~8 mL 1 M HCl), using a glass pipette. Adjust volume to 500 mL and filter sterilize (buffer can be stored for 1-2 months under refrigeration).

GAG standard: Dissolve 17.5 mg of cysteine-HCl in 10 mL of PBE buffer. Make a stock GAG soln of 20 mg/mL in PBE/cysteine, aliquot, and store at -20C. For the GAG standard, a working solution of 200 ug/mL is needed (100 X dilution of stock – 10 uL stock in 990 uL PBE)

DMMB solution: Add 95 mL of 0.1 M HCl solution (792 uL of 12 M HCl in 94.2 mL ddH_2O) to 905 mL ddH_2O and dissolve 3.04 g glycine and 2.37 g NaCl. Verify the pH = 3 (correct if necessary) and, while stirring, add 16 mg DMMB to the buffer. When stored in the dark at RT, the solution is stable for 3 months – may have to filter before use.

NaCl solution, 2.3 M: Dissolve 13.4 g of NaCl in 100 mL ddH2O.

GAG Assay:

1) Pipette standards into wells of a clear bottom 96-well assay plate.

Standard Curve: Should be linear from 0-2 µg/well.

µg GAG/well	µL GAG stock (200 µg/mL)	µL PBE
2	10 µL	15 µL
1.5	7.5	17.5
1.25	6.25	18.75
1	5	20
0.75	3.75	21.25
0.5	2.5	22.5
0.25	1.25	23.75
0	0	25

2) Add 25 µL of sample to empty wells.

Samples: Often need 2-3X dilution to get in linear range.

3) Add 5 µL of 2.3 M NaCl to each well.

4) Add 200 µL of DMMB solution to each well (can use multichannel pipette).

5) Read absorbance at 520 nm.

B.13 PicoGreen Assay

Purpose: The Pico Green assay quantifies the amount of DNA present which is an indirect measure of the number of cells.

Materials:

12 well plates

Sterile PBS

Spatulas, sterilized

Tweezers, sterilized

96 well plates

For Gels

1) Remove media.
2) Add 2ml iPBS.
3) Remove iPBS.
4) Add 3-4ml iPBS
5) Place in incubator for at least 30 min. Leave in incubator until gels are no longer the color of the media and have become clear.
6) Transfer the gels between pieces of weigh paper to remove excess water and weigh the gels. Then put the gels in 1.7 ml eppendorf tubes.
7) Homogenize the gels with a pellet grinder in the tubes. Be careful not to lose any of the gel.
8) When the gel is well ground add ddH_2O to the tube depending on the size of the gel (500 µl for 30 µl gels from 1.0 mm Teflon molds). Some of the ddH_2O can be used to

wash the pellet grinder tip into the tube and to wash the side of the tube. This will maximize the amount of gel that is available for the bioassay.

9) Let sit at room temperature for 30 min.
10) Store at -80 °C if needed.

For Plated Cells in a well plate

1) Aspirate liquid from the wells of the plate
2) Add 2 ml PBS to rinse.
3) Repeat steps 1-2.
4) Add 1 ml distilled, deionized water (ddH_2O).
5) Let sit at room temperature for 30 min.
6) Store at -20 °C if needed.

Lysing the cells

1) Freeze the cells at -80 °C for a minimum of 1 hour.
2) Thaw at room temperature for 30 minutes.
3) Sonicate for 30 min. to lyse the cells.

   Note: The sonicator will heat up after each usage. Ice should be added to the water in order to cool the sonicator down. If this is not done the DNA in the sample could break down.

   Safety note: The sonicator is meant to lyse the cells. Do not put fingers into the water bath while the sonicator is on or cells in your fingers will be lysed.
4) Repeat steps 1-3 two additional times.
5) If the samples are being stored before the assay is done freeze them at -80°C .

Making the plates

Standards

1) Make sure to thaw out samples and PicoGreen reagents for about 20 minutes before doing the assay.
2) Make up buffer solution and PicoGreen according to the PicoGreen calculator. Vortex both solutions to make sure they are mixed thoroughly.

   Note: When creating the buffer solution make sure to take the volume in the DNA standards into account. Also, cover the PicoGreen solution in aluminum foil to protect it from light.
3) Make up DNA standards according to the table below.

Conc. (ug/ml)	DNA (ul)	Buffer Solution
5	25	475
3	15	485
1	5	495
0.5	50 of 5 ug/ml	450
0.3	50 of 3 ug/ml	450
0.1	50 of 1 ug/ml	450
0.05	50 of 0.5 ug/ml	450
0.03	50 of 0.3 ug/ml	450
0.01	50 of 0.1 ug/ml	450
0	0	1000

4) Add 43 µl of your sample solutions into the appropriate wells of a 96 well plate. Make sure to change tips between samples.
5) Add 107 µl of the buffer solution into the wells.
6) Add 150 of the PicoGreen Solution to the wells.
7) Read in a plate reader: ex 485, em 528.

B.14 Confocal Microscopy

Notes

- **You must be trained to use the confocal microscopes.** Email steve.woodard@ibb.gatech.edu for the next training session.
- There are three scopes that you can use:
  - LSM 510 UV, in room 1328.
  - LSM 510 NLO, in room 1326. This is "the multi-photon" confocal microscope.
  - LSM 510 VIS, in room 1326. This is currently the preferred scope.
- Make sure to reserve a spot on the confocal microscope up to one week in advance at http://my.ilabsolutions.com/account/login/. You will need to make an account there if you haven't already.
- These instructions are for the LSM 510 VIS.

Materials Needed

- Bring a box containing gloves and your samples.
- When working with gels, bring additional equipment:
  - Attofluor cell chamber and round glass coverslips
  - PBS squirt bottle (Complete PBS with Ca^{2+}, Mg^{2+})
  - Spatulas and tweezers as necessary, plus Kimwipes for any spills.

Setting Up

1) Turn on the two switches to the left of the microscope – turn these on if needed, plus the computer.
2) At the login screen, login with your Georgia Tech AD username and password.
3) Click on ZEN 2008, in the middle of the screen, and click Start System.

4) Adjust the workspace zoom using the slider on the upper right side of the screen. Use an existing preset or make your own, clicking the "open folder" or "save" icons to save or apply changes.
5) Turn the first two lasers on (488 must go to "standby" first, 543 is simply on/off). No need for 633.
6) Below the laser controls, open the Temenoff Lab setting. This is specially configured for Live/Dead imaging.
7) At the top of the second column, note the current objective being used.
    a) On the LSM 510 VIS, there are 10x, 20x and 40x air objectives. 10x is the most commonly used. 20x and 40x objectives give better magnification, but have less light exposure (and thus produce less bright images as a result).
    b) Two objectives, 40x and 63x objectives are oil-based.
        i) Select the objective using the software and place one drop of oil on the objective.
        ii) Mount your sample and raise the objective until it just touches and oil spreads out.
        iii) When you are done, wipe off the oil with lens paper, **not kimwipes**.
8) Note other settings for averaging images (usually 1, with more for 20x/40x objectives), the resolution of your images (preferred is 1024x1024), and make sure scan speed is set to "Max" (9).
9) Note your physical controls. To the right of the microscope is an X-Y controller. Below your monitor is a touchscreen with a coarse and fine control for controlling Z direction.

Preparing Samples

1) Prepare a sample for viewing.
    a) If you've got a plate, just place the plate on top and you are all set.

b) To prepare for viewing a gel, place a glass cover slip on the bottom piece of the cell chamber. Screw both pieces together and squirt some PBSi into the chamber to keep the gel hydrated. Then load your sample into the circular grooves on the microscope platform.

2) Control your imaging using the Channels area in the 2nd column.
   a) Pinhole size refers to how much light is let through. Higher pinholes let through more light but will increase the amount of light captured in the Z-direction (that is, above and below your image). A preferred pinhole size is 1 AU (Airy unit, showing the lowest Z distance that will be captured). You can increase this if necessary.
   b) Detector Gain amplifies light received by the detector. Higher gain, brighter images, but also more noise. You should settle for a max of around 800 on both channels; sometimes you may even go below 700.
   c) Digital Offset eliminates light below a certain threshold. Use this to eliminate stray bright pixels.
3) Click Fast on the upper left hand of the screen to begin continuously scanning.
4) How to make images clear
   a) Something important is that imaging is **highly subjective** and depends on what you are looking for. Microscopy experts don't like saturating images, but our lab usually tends towards that. Use your experience and be consistent in how you image, and things'll turn out fine.
   b) Set the offset and gain on each channel to near maximum. Lots of noise should fill the screen.

c) To the left of the image, choose Split to separate the red and green signals.

d) Scan to where you can find cells. This can be done by moving up and down (using the focus knob on the side) or by xy translation. Look at where the laser hits the gel to determine where you are. For Z location, check the Z Stack section (lower right, 2nd column) for your height.

e) Below the image, there are colors indicating what is being shown. Click the colors below the "Merged" button to change the display to Range Indicator mode. Red mean oversaturation, blue means undersaturation, and black/gray is somewhere in between.

f) For each channel, you can use the Detector Gain and Offset controls to change how things look. You want just a tiny amount of red, and any spots NOT of interest should be totally blue. Eliminate as much noise as possible without losing areas of interest.

g) Exit Range Indicator mode and see how your images look. You may want to retweak as necessary.

h) Your calibration should be good for the rest of your wells/gels.

Taking Pictures

1) Taking single pictures

a) Use Fast to assist as you scan for areas of interest. When you find one, click Single in the upper left, then save the current image.

b) Images should be saved in D:\[your name] in .lsm format.

2) Taking Z stacks

a) The Z Stack section is below Channels. Check the box to the right of the title to activate it (without it, the Start button in the upper left will be grayed out).
b) Use Fast to select your bottom image (if imaging whole gel, start with a completely black image) and click Set First.
c) Use Fast to select your top image and click Set Last, then click Stop.
d) Make sure Keep Interval is selected. This will keep the z slice size constant, even if you later decide to change the # of slices or the upper and lower limits in your stack. Typically the slice size in our lab is set to 10 µm.
e) Click Start. A scan will automatically begin. To view the images as they are being generated, click Gallery to the left of the image.
f) Don't forget to save your Z stack (also in .lsm format).

Saving Data

Note: Do not expect your data to be backed up. It usually is, but there's no guarantee. We make it easy for you to save your data to the Temenoff lab drive.

1) Click Start > Run: \\zoe.bme.gatech.edu\temenoff-lab
2) When it asks for a username and password, give it your BME credentials.
3) The Temenoff lab server should now be mounted. Copy your images over as appropriate.

Cleaning Up

1) Lasers
   a) Shut down the Argon laser (or put it on Standby if you know someone else will use it).
   b) Shut down the HeNe laser (or leave it on).

2) If you need to shut down the system, give the lasers a few minutes to finish cooling (you should hear a noise stop in 2-3 minutes). Shut down the computer first, then flip both switches (the ones to the left of the scope) off.
3) If working with gels, rinse out the cell chamber and throw away the glass cover slip in biohazard glass trash. Wash the cell chamber with soap and distilled water and leave the individual pieces on the rack in the cell culture room to dry. Do not use ethanol; it dries out the rubber O-ring.

Working with Pictures

1) The free LSM 510 Image Browser (downloadable from Zeiss) can be used to view images. Pretty much the only reason you'd really need to use it, other than viewing pictures and exporting them to various formats, is the Projection feature.
    a) Select your Z stack and open it.
    b) Select Projection. Rotate around the Y axis, and choose the most projection images (64/panorama) to generate to ensure a smooth 3D projection.
    c) The created projection can be slowed and manipulated, as well as stored along with the database.
    d) This can also be exported to a movie file.
2) You can also use the image browser to create your own databases with custom images. Use the Copy and Paste functions in the toolbar.
3) You can also use the Zeiss ZEN LE software (essentially, ZEN without the microscope controls).
4) You can also use ImageJ, especially if you're not on Windows.

Confocal Microscope Settings

You can use the FITC/CY3 as an initial setting.

Below the imaging buttons, check Z-Stack.

Turn on the Argon and HeNe543 lasers. (Argon must go to standby first, and after a while you can set it to On. This is very important - don't forget to turn it off of Standby.)

Imaging Setup

Mode	Switch track every
Channel Mode	Frame

First channel name: Fluorescein 488-517 (FITC)

Second channel name: Rhodamine 543-600

Select the fluorescein channel.

Light path: To the left of laser, select HFT 488/543.

Above HFT 488/543, select NFT 545.

To the right of NFT 545, select BP 505-530, and check Ch2. Select green for Ch2.

Above NFT 545, select Plate.

Next on the path, select LP 560. Check Ch1 and select Red.

Select the rhodamine channel and perform the exact same steps.

Acquisition mode:

Objective	Scan mode	Frame size	Line step	Speed	Averaging
10x	Frame	Click X*Y 1024 x 1024	1	Click Max 9	1

Averaging isn't important unless you want to fiddle around with how it averages images.

Useful for poor visibility.

Channels: Fluorescein

Laser power	Pinhole	Gain	Digital offset	Digital gain
3.0	1 AU	1100-1200 set; 700-750 operating	> -0.10 set; -0.30 operating	1.00 operating

Channels: Rhodamine

Laser power	Pinhole	Gain	Digital offset	Digital gain
35.0	1 AU	1100-1200 set; 800 operating	> -0.10 set; -0.30 operating	1.00 operating

Z Stack: Rhodamine

Interval	Keep
10 microns	Interval

Use "Set First" and "Set Last" to specify the beginning and end of a stack.

Once all of this has been set up, click the Save icon near the Configuration name near the upper left corner, and save it under your own custom preferences.

B.15 Reverse Transcription Polymerase Chain Reaction (RT-PCR)

RNA Extraction

Extract RNA using Qiagen RNeasy Mini Kit

(Consult the RNeasy kit manual for more specific protocols depending on your cell/tissue source)

Materials

Molecular BioProducts RNase Away Spray (VWR 17810-491; 475 ml)

Aerosol Filter Pipette Tips for Rainin LTS, 20 µl (VWR 83009-688; pack of 960)

Aerosol Filter Pipette Tips for Rainin LTS, 200 µl (VWR 82003-196; pack of 960)

Aerosol Filter Pipette Tips for Rainin LTS, 1000 µl (VWR 82003-198; pack of 576)

QIAshredder (Qiagen 79654 or 79656; 50 or 250 runs)

RNeasy Mini Kit (Qiagen 74104 or 74106; 50 or 250 runs)

Optional Alternative: RNeasy Protect Mini Kit (Qiagen 74124 or 74126; 50 or 250 runs)

EMD 2-Mercaptoethanol (VWR EM-6010; 100 ml)

RNAse-free DNase Set (Qiagen 79254; 50 runs)

Protocol

For plated cells

I) Trypsinize cells and centrifuge (10 min, 1000 rpm).

II) Aspirate supernatant, resuspend pellet in media, and centrifuge (10 min, 1000 rpm).

III) Aspirate supernatant, rinse pellet with PBS, and centrifuge again (10 min, 1000 rpm), aspirate PBS.

For gels

I) Soak gels in PBS for ~ 1h to remove media.

II) Transfer the gel to an RNase free, DNase free microcentrifuge tube.

III) Break the gel into small pieces using a pellet grinder.

1) Lyse cell pellet or cells in gel in **350 µl Buffer RLT with β-mercaptoethanol** (add 10 µl BME per 1 ml Buffer RLT).
2) Put solution in **purple QIAshredder column** and centrifuge **(2 min, 14000 rpm)**.
3) Discard filter and add **350 µl 70% ethanol** to eluted substance.

4) Transfer suspension to **pink RNeasy column** and centrifuge **(15 sec, 14000 rpm)**.
5) Discard eluted substance and put filter back on. (Do NOT mix Buffer RLT or RW1 with bleach when discarding. Contact with acids forms highly reactive guanidine salts and liberates very toxic gas)
6) Add **350 µl Buffer RW1** to column and centrifuge **(15 sec, 14000 rpm)**.
7) Discard eluted substance and put filter back on.
8) Add **10 µl DNase I** (lyophilized DNase I is resuspended in 550 µl RNase-free water) to **70 µl Buffer RDD** for each sample.
9) Add **80 µl of DNase/RDD solution** directly onto RNeasy membrane and incubate at **room temperature for 15 min**.
10) Add **350 µl Buffer RW1** to column and centrifuge **(15 sec, 14000 rpm)**.
11) Discard eluted substance and put filter back on.
12) Add **500 µl Buffer RPE** (add 44 ml of 96-100% ethanol to starting 11 ml of Buffer RPE concentrate before first time use) to column and centrifuge **(15 sec, 14000 rpm)**.
13) Discard eluted substance and put filter back on.
14) Add **500 µl Buffer RPE** to column and centrifuge **(2 min, 14000 rpm)**.
15) Discard eluted substance and transfer column to new 2 ml collection tube.
16) Centrifuge **(1 min, 14000 rpm)**.
17) Discard 2 ml collection tube, and transfer column to new 1.5 ml collection tube with cap.
18) Add **30 µl RNase-free water** and centrifuge **(1 min, 14000 rpm)**.
19) The water elutes the RNA into the collection tube – cap the tube and store RNA at -80˚C.

Quantify and check purity of RNA

Materials

MP Biomedicals RNase, DNase-free water (VWR IC821739; 500 ml)

Protocol

1) Take absorbance readings of 2 µl of undiluted RNA at 260 nm and 280 nm light in NanoDrop.
2) Quantity of RNA can be calculated using the following equations:
    - Corrected A_{260} = average sample A_{260} – average blank A_{260}
    - Concentation in µg/ml = (corrected A_{260}) * (44 µg/ml) * (dilution factor)

      (using above protocol, dilution factor = 50)
    - Total mass in µg = (µg/ml concentration value) * (µl volume) / 1000

      (volume of RNA extraction sample; using above extraction protocol, volume = 30-50 µl)
    - Volume in µl needed for 1 µg RNA = (1 µg RNA) * 1000 / (µg/ml concentration value)

      (1 ng to 5 µg RNA can be used for Reverse Transcription)
    - Volume of water in µl needed = 10 µl total volume – RNA volume determined above
3) Purity of RNA can be calculated using the following equation:
    - Purity = A_{260} / A_{280}
    - This value should be between 1.5 and 1.9.

Reverse Transcription

Reverse Transcription with SuperScript III Reverse Transcriptase

Materials

Oligo(dT)$_{15}$ Primer (Promega C1101; 20 µg)

PCR Nucleotide Mix, 10 mM (Promega C1141; 200 µl)

SuperScript III Reverse Transcriptase (Invitrogen 18080-093 or 18080-044; 2000 or 10000 units)

Invitrogen RNaseOUT RNase Inhibitor, 40 units/ml (Invitrogen 10777-019; 5000 units)

Protocol

1) Add the following components to a nuclease-free PCR tube:
   - **1 ng to 5 µg total RNA: 10 µl**
   - **Oligo(dT)$_{15}$ (500 µg/ml): 1 µl**
   - **dNTP Mix (10 mM each): 1 µl**
   - **RNase, DNase-free water: to 12 µl final volume**
2) Heat mixture to 65˚C for 5 min and chill on ice for at least 1 min. Collect the contents of the tube by brief centrifugation and add:
   - **5X First-Strand Buffer (250 mM Tris-HCl, 375 mM KCl, 15 mM $MgCl_2$): 4 µl**
   - **0.1 M DTT**: **1 µl**
   - **RNaseOUT (40 units/µl)**: **1 µl**
3) Mix contents of the tube gently. Incubate at 42˚C for 2 min.

4) Add **1 µl (200 units) of SuperScript III RT** and mix by pipetting gently up and down.

5) Incubate at 50˚C for 30-60 min.

6) Inactivate the reaction by heating at 70˚C for 15 min.

7) Store cDNA at -20˚C.

8) Amplification of PCR targets (>1 kb) may require the removal of RNA complementary to the cDNA. To remove RNA complementary to the cDNA, add 1 µl (2 units) of *E. coli* RNase H and incubate at 37˚C for 20 min.

Primer Preparation

Reconstitute primers (100 µM)

Materials

Custom Primers/Oligonucleotides, desalted (Invitrogen; 25 nmol)

Protocol

1) Find the total nmoles from the information sheet that came with the primer.

2) The volume of DNase-free water needed to create a 100 µM stock can be calculated using the following equation:

   - Volume of DNase-free water in µl = (nmoles of primer) *1000 / (100 µM)

Make 10 µM aliquots

Protocol

1) Briefly spin the primers and add the needed amount of water for a 10-fold dilution.

2) Make a 10-fold dilution (1 part primer: 9 parts DNase-free water) to obtain a 10 µM aliquot.

Polymerase Chain Reaction

Run PCR

Materials

SYBR Green Master Mix (Applied Biosystems 4309155; 5 ml)

Applied Biosystems StepOnePlus Real-Time PCR System and Materials

- MicroAmp Fast 96-Well Reaction Plates, 0.1 ml (Applied Biosystems 4346906; 20 plates)
- MicroAmp Optical Adhesive Films (Applied Biosystems 4360954; 25 films)

OR

- MicroAmp Fast 8-Tube Strips, 0.1 ml (Applied Biosystems 4358293; 125 strips)
- MicroAmp Optical 8-Cap Strips (Applied Biosystems 4323032; 300 strips)
- MicroAmp 96-Well Trays for Veriflex Blocks (Applied Biosystems 4379983; 10 trays)

Protocol

1) Thaw the following components on ice:
    - SYBR Green mix
    - 10 µM forward primer of interest
    - 10 µM reverse primer of interest
    - Sample cDNA
2) To make **Master Mix**, count the number of wells needed for each primer, add 2, and multiply this number by the following to obtain enough Master Mix for all wells of the primer:

- **12.5 µl SYBR Green mix**
- **10.5 µl DNase-free water**
- **0.5 µl 10 µM forward primer**
- **0.5 µl 10 µM reverse primer**

3) Load PCR wells:
   - Load **24 µl of Master Mix** into each well for that primer (target sequence of interest).
   - Add **1 µl of sample cDNA** into the well with Master Mix and mix by pipetting up and down (change pipette tips between each well).
4) After all wells are loaded, cover with optical tape or caps, and put entire plate on ice until ready to run PCR.
5) Load plate into StepOnePlus system:
   - Load plate into machine (A1 in upper-left, H12 in lower-right).
   - Open "StepOne Software v2.0" program.
   - Click "Advanced Setup" button.
   - Under "Experiment Properties," enter an Experiment Name, select "StepOnePlus Instrument (96 Wells)" for the instrument, select "Quantitation – Comparative C_T ($\Delta\Delta C_T$)" for the experiment, select "SYBR Green Reagents" for the reagent (melt curve is optional), and select "Standard" for the ramp speed.
   - Under "Plate Setup," add your targets and samples under "Define Targets and Samples," changing the Reporter to "SYBR" and the Quencher to "None." Under "Assign Targets and Samples," assign the appropriate targets and samples to each

well, selecting your control sample as the reference sample, GAPDH as the endogenous control, and "ROX" as the "dye to use as a passive reference."

- Under "Run Method," change the reaction volume to 25 µl and set the method to the following:
  - Hold at 95˚C for 10 min (100% ramp).
  - Cycle 40 times at 95˚C for 15 sec and 60˚C for 1 min, collecting data at 60˚C.
  - Optional melt curve: 95˚C for 15 sec, 60˚C for 1 min, and +0.3˚C ramp, ending at 95˚C for 15 sec and collecting data during the +0.3˚C ramp.
- Save the file.

  (Templates can be saved to reduce setup time.)
- Select "Start Run."
- After the run, click "Analyze" (settings can be modified under "Analysis Settings") and resave the file.
- Export results to Excel by clicking "Export…" and export "Results" as "One File" with ".xls" file type.

B.16 Quantitative PCR Analysis

Adapted from:

Ruijter JM, Ramakers C, Hoogaars WMH, Karlen Y, Bakker O, van den Hoff MJB, and Moorman AFM. Amplification efficiency: linking baseline and bias in the analysis of quantitative PCR data. Nucleic Acids Res. 2009 Apr;37(6):e45.

Introduction

Let's review the basics of PCR amplification and detection. We start with a few basic equations:

$$N_c = N_0 E^c \qquad E = \frac{N_{c+1}}{N_c} \qquad N_0 = \frac{N_t}{E^{C_t}}$$

where ***N*** = concentration of amplicon, ***E*** is the efficiency of the PCR reaction (where 1 means no amplification, and 2 is 100% amplification), and ***C*** is a cycle threshold of interest. If you want to compare a gene's amplification to its target gene,

$$\frac{N_{0,\text{collagen I}}}{N_{0,\text{GAPDH}}} = \frac{\frac{N_{t,\text{collagen I}}}{E_{\text{collagen I}}^{C_{t,\text{collagen I}}}}}{\frac{N_{t,\text{GAPDH}}}{E_{\text{GAPDH}}^{C_{t,\text{GAPDH}}}}} \approx \frac{E_{\text{GAPDH}}^{C_{t,\text{GAPDH}}}}{E_{\text{collagen I}}^{C_{t,\text{collagen I}}}}$$

assuming the concentrations of the two genes are the same (given, say, a fluorescence threshold). If you then make the next assumption that the efficiencies are the same (say, 100%), then

$$E_{\text{common}}^{C_{t,\text{GAPDH}} - C_{t,\text{collagen I}}} = E_{\text{common}}^{-\left(C_{t,\text{collagen I}} - C_{t,\text{GAPDH}}\right)} \approx 2^{-\Delta C_t}$$

To compare to day 1, we write

$$\frac{N_{0,\text{collagen I, day 7}}}{N_{0,\text{collagen I, day 1}}} = \frac{E_{\text{common}}^{-\left(C_{t,\text{collagen I, day 7}} - C_{t,\text{GAPDH, day 7}}\right)}}{E_{\text{common}}^{-\left(C_{t,\text{collagen I, day 1}} - C_{t,\text{GAPDH, day 1}}\right)}} \approx \frac{2^{-\Delta C_{t,\text{day 7}}}}{2^{-\Delta C_{t,\text{day 1}}}} = 2^{-\left(\Delta C_{t,\text{day 7}} - \Delta C_{t,\text{day 1}}\right)}$$

$$= 2^{-\Delta\Delta C_t}$$

These calculations are contingent on a few assumptions:

- Baseline fluorescence is something that can be eliminated.
- Efficiency is common (and perhaps, also, that it's 100%) among different genes, primer sets, etc.

- Cycle to cycle efficiency does not vary throughout amplification.

Typical PCR analysis errors

If there *is* baseline fluorescence in your sample, you will introduce error into your estimation of *efficiency*:

$$N_c^* = \text{baseline} + N_0 E^c \qquad\qquad E^* = \frac{\text{baseline}+N_{c+1}}{\text{baseline}+N_c}$$

and if you also fail to account for differences in amplification efficiency, you also introduce error:

$$\text{error} = \frac{E_{\text{GAPDH}}^{C_{t,\text{GAPDH}}}}{E_{\text{collagen I}}^{C_{t,\text{collagen I}}}} \div \frac{E_{\text{common}}^{C_{t,\text{GAPDH}}}}{E_{\text{common}}^{C_{t,\text{collagen I}}}} = \left(\frac{E_{\text{GAPDH}}}{E_{\text{common}}}\right)^{C_{t,\text{GAPDH}}} \left(\frac{E_{\text{collagen I}}}{E_{\text{common}}}\right)^{-C_{t,\text{collagen I}}}$$

$$= \left(\frac{E_{\text{gene}}}{E_{\text{common}}}\right)^{C_{t,\text{GAPDH}}+C_{t,\text{collagen I}}}$$

which for even a 5% difference in efficiency can be $1.05^{20+20} = 1.05^{40} = 7.03$ times different.

What LinRegPCR does

- ❖ Estimates individual well baseline by reconstructing the log-linear portion of the amplification curve:
  - ➢ Discards any samples where low amplification is detected.
  - ➢ Calculates the second derivative maximum (SDM) to find the plateau.
  - ➢ Subtracts baseline, then fits both the upper and bottom portions of log-linear region.
  - ➢ When the lower and upper sections' slopes match, the baseline has been found.
- ❖ Calculates individual PCR efficiencies for every well
  - ➢ Calculates mean efficiency and starting amount (N_0) for a given amplicon.
  - ➢ Mean efficiencies are adequate for calculating fold regulation values

- Differences are more a result of statistical error than true differences in efficiency.
- What about running multiple plates for the same gene?
- Individual efficiencies can vary significantly

How to use LinRegPCR

1) Process your data in StepOne first.
   a) Do a quick quality control check on your samples and remove samples that didn't amplify well, that have a high standard deviation, etc.
   b) **Disable** the auto baseline feature in StepOne for each target.
   c) Export the data to Excel – check *Sample Setup* and *Amplification Data*.
2) Open the spreadsheet and then open LinRegPCR.

   Note: LinRegPCR will not work correctly unless Excel is opened beforehand.
3) In LinRegPCR:
   a) Read in your data.
      i) Check the drop-down boxes to make sure Amplification Data is selected.
      ii) Select **Step-One Plus (ABI)** and **DNA binding dye** (SYBR Green).
      iii) Select columns A through D, rows 8 through 3848 (that is, a 40-cycle run. A 50-cycle run would go to row 4808.)
      iv) Make sure ss cDNA is checked, and select No for "Data are baseline-corrected."
   b) Click the red button labeled **determine baselines**.
   c) Check each sample to examine efficiencies and tweak if necessary.
   d) If necessary, use the Amplicon Groups tab to set amplicon groups. The boxes there can help you auto-select amplicon groups quickly for each gene.
   e) Set the log(fluorescence) value on the left.
      i) Note: Make sure to keep this consistent between all plates with the same gene.

ii) Note: In StepOne, the threshold fluorescence is usually less than 1, which is why the log(fluorescence) value in LinRegPCR is negative.

f) Save this data to Excel.

4) Back in Excel:

a) Use the sample setup tab to help re-label your samples and rearrange your data to your liking. You may want to pick up some Excel-fu to summarize and put all of your wells together, do any extra quality control, etc.

i) Note: Remember to use geometric means when averaging data. (Taking the geometric mean is the same as taking the arithmetic mean of the cycle thresholds.)

b) To calculate fold regulation, use the starting concentration of your gene, or N_0. The value of N_0 has already been calculated by LinRegPCR using the mean efficiency for the amplicon group.

i) If many of your wells did not use the mean efficiency to be calculated, it may be a good idea to calculate a new N_0 based on each individual well's PCR efficiency.

ii) You can do this using the equation $N_0^* = \frac{\text{fluorescence threshold value}}{\text{Eff}^{Cq}}$.

c) Calculate a manual ΔΔ method; that is, divide a sample's gene's N_0 by the sample's GAPDH N_0 value, then divide by the geometric mean of your day 1 sample.

d) Perform statistical analysis on the divided-by-GAPDH values.

B.17 Immunostaining

Rules to remember:

- Do not let your sample dry out. This will encourage non-specific binding (and staining) from anything floating around in the air, etc. If you need to stop, make sure samples are wet or otherwise sitting in PBS.
- Store samples at -80°C prior to staining to maintain maximum antigenicity.

- Rinsing with PBS can be done using a slide rack. Place slides into the stain rack, then gently lower into the stain holder with PBS. After two minutes, raise and lower the rack gently, then remove the rack completely. Do this twice, discarding PBS between washes. You'll need ~1000-1200 mL PBS for 12 slides.

Day 1

For Fixed Paraffin Sections

1) Deparaffinize
    a) Deparaffinize slides in xylene and alcohol (Program 4 in autostainer).
2) Antigen retrieval

    For heat-induced:

    a) Citrate Buffer (10 mM, pH 6.0)
        i) Citric acid (anhydrous) – 1.92 g
        ii) Distilled water – 1000 ml
        iii) Mix to dissolve. Adjust pH to 6.0 with 1 N NaOH, and then add 0.5 ml Tween 20 and mix well.
        iv) Store this solution at room temperature for 3 months or at 4°C for longer storage.
    b) Place slides in 10 mM citrate buffer.
    c) Perform heat-induced antigen retrieval in pressure cooker (high setting) in citrate buffer for 15 min.
    d) Allow slides to cool to room temperature before rinsing.
    e) Rinse twice in PBS.

For enzymatic:

a) TE-$CaCl_2$ Buffer (50 mM Tris Base, 1 mM EDTA, 5 mM $CaCl_2$, 0.5% Triton X-100, pH 8.0)
   i) Tris Base – 6.10 g
   ii) EDTA – 0.37 g
   iii) $CaCl_2$ – 0.56 g
   iv) Triton X-100 – 5 ml
   v) Distilled Water – 1000 ml
   vi) Mix to dissolve. Adjust to pH 8.0 using concentrated HCl (10 N).
   vii) Store this buffer at room temperature.
b) Proteinase K Stock Solution (20X, 400 µg/ml)
   i) Proteinase K (30 units/mg) – 8 mg
   ii) TE/$CaCl_2$ Buffer – 10 ml
   iii) Glycerol – 10 ml
   iv) Add proteinase K to TE-$CaCl_2$ buffer until dissolved. Then add glycerol and mix well.
   v) Aliquot and store at -20°C for 2-3 years.
c) Proteinase K Working Solution (1X, 20 µg/ml)
   i) Proteinase K Stock Solution – 1 ml
   ii) TE-$CaCl_2$ Buffer – 19 ml
   iii) Mix well.
   iv) This solution is stable for 6 months at 4°C.
d) Circle samples with PAP pen to create hydrophobic barrier around your samples.

e) Cover sections with Proteinase K working solution, and incubate for 10-20 min at 37°C in humidified chamber.

f) Allow sections to cool at room temperature for 10 min.

g) Rinse twice in PBS.

For Unfixed Frozen Sections

1) Fixation

a) Warm up slides at room temperature for 30-60 minutes.

b) Lightly fix in ice cold acetone for 10 minutes. Place a stain holder containing acetone into an ice bucket, then lower the slide rack inside. Change acetone between slide racks if you're doing more than 12 slides at a time.

c) Let slides air dry for 30 minutes.

2) Wash off OCT

a) Rinse twice in PBS.

b) At this point, samples should be completely free of OCT and other trash. Circle each sample with a PAP pen to isolate future liquids to the sample.

Deglycosylation with Chondroitinase Digestion for Aggrecan Staining

1) Chondroitinase Digestion

a) Activate chondroitinase ABC in buffer of 50mM Tris, 60 mM sodium acetate, 0.02% BSA, pH 8.0. Dilute 1 U/ml chondroitinase 3:4 with 4X activating buffer (eg. 0.75 ml chondroitinase, plus 0.25 ml buffer).

b) Apply 30 µl of 0.75 U/ml of chondroitinase ABC to each sample, and incubate in a humid chamber for 1.5 hr at 37°C, then PBS rinse.

Staining for Immunohistochemistry

1) Preparation (while slides dry)
    a) 1% BSA solution (make 1 g BSA / 100 mL PBS; store at 4°C)
    b) Serum from species of secondary Ab (goat, horse, or rabbit)
    c) Make a humidified chamber using a 150 mm petri dish with a wet paper towel in the bottom, plus 4-5 small petri dishes with water inside. Each chamber can hold 4 or 5 slides.
2) Peroxidase Blocking (For frozen sections only)
    a) Use a slide rack/stain holder to immerse slides in 0.3% peroxide/methanol solution (1 mL 30% H_2O_2 in 100 mL methanol; store in foil < 1 week at 4°C) for 10 minutes at room temperature. You can reuse the peroxide/methanol solution between racks.
3) Serum Blocking
    a) Normal Serum Block Solution (60 µL/sample, mix in 10 mL and store at 4°C):
        i) 1% BSA solution in PBS (stabilizer) – 9.7 mL
        ii) 2% serum (blocking) – 200 µL
        iii) 0.1% Triton X-100 (penetration enhancer) – 100 µL
    b) Incubate sections for 20 min in blocking solution – serum should be same species as secondary antibody. Tap the slide on a kimwipe to remove the solution. Don't do a PBS wash afterwards.

Staining for Immunofluorescence

1) Preparation

a) Make a humidified chamber using a 150 mm petri dish with a wet paper towel in the bottom, plus 4-5 small petri dishes with water inside. Each chamber can hold 4 or 5 slides.

2) Image-iT Signal Enhancer Blocking
   a) Cover section in Image-iT Signal Enhancer (for AlexaFluor488-conjugated IgG)
   b) Incubate sections for 30 min in blocking solution, then PBS wash.

Primary Antibody

1) Primary Antibody
   a) Prepare the working dilution of the primary antibody in 1% BSA. If using an antibody for the first time, you'll need to run a series of dilutions to determine the optimal working concentration). With our antibodies, 1:10, 1:100, 1:500, 1:1000 is a good start.
   b) Use a 10 µL pipette to carefully apply 8 µL primary antibody to each sample.
   c) Incubate sections in a humid chamber at 4°C overnight. Parafilm each chamber to prevent evaporation.

Day 2

For Immunohistochemistry

1) Peroxidase Blocking (For paraffin sections only)
   a) Use a slide rack/stain holder to immerse slides in 0.3% peroxide/methanol solution (1 mL 30% H_2O_2 in 100 mL methanol; store in foil < 1 week at 4°C) for 10 minutes at room temperature. You can reuse the peroxide/methanol solution between racks.

2) Secondary Antibody

a) Remove slides from the humidified chamber and PBS wash.

b) Incubate sections in 1:200 goat biotin conjugated secondary antibody in PBS for 30 minutes at room temperature, then PBS wash.

3) Signal Amplification

a) Solution: Vectastain ABC Elite Standard kit

i) 5 mL PBS + 2 drops of solution A + 2 drops of solution B, added into the provided bottle.

ii) Allow solution to sit for 30 min before use.

b) Drop solution onto slides. Incubate for 30 min, then PBS wash.

4) Chromagen/Substrate Stain

a) Immediately after rinsing, make the peroxidase substrate solution using 1 mL substrate buffer and 20 µL chromogen. There should be no delay between making the solution and adding it to your slides.

b) Allow color to develop for 5-10 minutes (you will need to experiment with this time).

c) Immediately rinse with PBS twice. All DAB waste should be added into a separate waste container and brought to the histology room for disposal.

For Immunofluorescence

1) Secondary Antibody

a) Remove slides from the humidified chamber and PBS wash.

b) Incubate sections in 1:200 goat anti-mouse Alexa Fluor 488-conjugated secondary antibody in PBS for 30 minutes at room temperature, then PBS wash.

2) Nuclear counterstain

a) Incubate sections in 0.1 µg/ml DAPI working solution for 5 min at room temperature, then PBS wash.

Coverslip

1) Cover slip
   a) The slide should be wet from the PBS wash you just did. Place a drop of FluoroGel with Tris buffer on each of your samples within a PAP pen circle. FluoroGel should mix with the water already on the slide.
   b) Place additional FluoroGel (can use two drops; may use more if desired) outside of the PAP pen circles.
   c) Tilt the bottom edge of the cover slip against the bottom edge of the slide. Tilt the slide as necessary so the cover slip catches a consistent edge of liquid along the bottom, then gently lower the top edge so the liquid rides over the PAP pen circles and catches the entire surface of the slide.
   d) Allow slides to dry overnight. You can view them on a microscope sooner than that (a few hours after coverslipping), but sometimes liquid will leak from a slide as it dries. Clean liquid that has leaked onto the outside with wet kimwipes.
   e) Seal the edges of the slides with clear nail polish to prevent bubbles from forming under the coverslip.

REFERENCES

1. Hunziker EB. Articular cartilage repair: are the intrinsic biological constraints undermining this process insuperable? Osteoarthritis Cartilage. 1999;7(1):15-28.

2. Kim S, Bosque J, Meehan JP, Jamali A, Marder R. Increase in outpatient knee arthroscopy in the United States: a comparison of National Surveys of Ambulatory Surgery, 1996 and 2006. J Bone Joint Surg Am. 2011;93(11):994-1000.

3. Lawrence RC, Felson DT, Helmick CG, Arnold LM, Choi H, Deyo RA, et al. Estimates of the prevalence of arthritis and other rheumatic conditions in the United States. Part II. Arthritis Rheum. 2008;58(1):26-35.

4. Leigh JP, Seavey W, Leistikow B. Estimating the costs of job related arthritis. J Rheumatol. 2001;28(7):1647-54.

5. Hollander AP, Dickinson SC, Kafienah W. Stem cells and cartilage development: complexities of a simple tissue. Stem Cells. 2010;28(11):1992-6.

6. Johnstone B, Hering TM, Caplan AI, Goldberg VM, Yoo JU. In vitro chondrogenesis of bone marrow-derived mesenchymal progenitor cells. Exp Cell Res. 1998;238(1):265-72.

7. Hwang NS, Varghese S, Li H, Elisseeff J. Regulation of osteogenic and chondrogenic differentiation of mesenchymal stem cells in PEG-ECM hydrogels. Cell Tissue Res. 2011;344(3):499-509.

8. Varghese S, Hwang NS, Canver AC, Theprungsirikul P, Lin DW, Elisseeff J. Chondroitin sulfate based niches for chondrogenic differentiation of mesenchymal stem cells. Matrix Biol. 2008;27(1):12-21.

9. Nguyen LH, Kudva AK, Guckert NL, Linse KD, Roy K. Unique biomaterial compositions direct bone marrow stem cells into specific chondrocytic phenotypes corresponding to the various zones of articular cartilage. Biomaterials. 2011;32(5):1327-38.

10. French MM, Rose S, Canseco J, Athanasiou KA. Chondrogenic differentiation of adult dermal fibroblasts. Ann Biomed Eng. 2004;32(1):50-6.

11. Chung C, Burdick JA. Influence of three-dimensional hyaluronic acid microenvironments on mesenchymal stem cell chondrogenesis. Tissue Eng Part A. 2009;15(2):243-54.

12. Lohmander S. Proteoglycans of joint cartilage: structure, function, turnover and role as markers of joint disease. Baillieres Clinical Rheumatology. 1988;2(1):37-62.

13. Bhosale AM, Richardson JB. Articular cartilage: structure, injuries and review of management. British Medical Bulletin. 2008;87(1):77-95.

14. Kimata K, Oike Y, Tani K, Shinomura T, Yamagata M, Uritani M, et al. A large chondroitin sulfate proteoglycan (PG-M) synthesized before chondrogenesis in the limb bud of chick embryo. J Biol Chem. 1986;261(29):13517-25.

15. Smith SM, West LA, Govindraj P, Zhang X, Ornitz DM, Hassell JR. Heparan and chondroitin sulfate on growth plate perlecan mediate binding and delivery of FGF-2 to FGF receptors. Matrix Biol. 2007;26(3):175-84.

16. Wilson DG, Phamluong K, Lin WY, Barck K, Carano RA, Diehl L, et al. Chondroitin sulfate synthase 1 (Chsy1) is required for bone development and digit patterning. Developmental Biology. 2012;363(2):413-25.

17. Watanabe Y, Takeuchi K, Higa Onaga S, Sato M, Tsujita M, Abe M, et al. Chondroitin sulfate N-acetylgalactosaminyltransferase-1 is required for normal cartilage development. Biochem J. 2010;432(1):47-55.

18. Kluppel M, Wight TN, Chan C, Hinek A, Wrana JL. Maintenance of chondroitin sulfation balance by chondroitin-4-sulfotransferase 1 is required for chondrocyte development and growth factor signaling during cartilage morphogenesis. Development. 2005;132(17):3989-4003.

19. Fujimoto T, Kawashima H, Tanaka T, Hirose M, Toyama-Sorimachi N, Matsuzawa Y, et al. CD44 binds a chondroitin sulfate proteoglycan, aggrecan. Int Immunol. 2001;13(3):359-66.

20. Bayliss MT, Osborne D, Woodhouse S, Davidson C. Sulfation of chondroitin sulfate in human articular cartilage. The effect of age, topographical position, and zone of cartilage on tissue composition. J Biol Chem. 1999;274(22):15892-900.

21. Villanueva I, Gladem SK, Kessler J, Bryant SJ. Dynamic loading stimulates chondrocyte biosynthesis when encapsulated in charged hydrogels prepared from poly(ethylene glycol) and chondroitin sulfate. Matrix Biol. 2010;29(1):51-62.

22. Sugahara K, Mikami T, Uyama T, Mizuguchi S, Nomura K, Kitagawa H. Recent advances in the structural biology of chondroitin sulfate and dermatan sulfate. Curr Opin Struct Biol. 2003;13(5):612-20.

23. Delise AM, Tuan RS. Analysis of N-cadherin function in limb mesenchymal chondrogenesis in vitro. Dev Dyn. 2002;225(2):195-204.

24. DeLise AM, Fischer L, Tuan RS. Cellular interactions and signaling in cartilage development. Osteoarthritis Cartilage. 2000;8(5):309-34.

25. Hintze V, Miron A, Moeller S, Schnabelrauch M, Wiesmann HP, Worch H, et al. Sulfated hyaluronan and chondroitin sulfate derivatives interact differently with human transforming growth factor-beta1 (TGF-beta1). Acta Biomaterialia. 2012;8(6):2144-52.

26. Nagasawa K, Uchiyama H, Wajima N. Chemical sulfation of preparations of chondroitin 4-sulfate and 6-sulfate, and dermatan sulfate. Preparation of chondroitin sulfate E-like materials from chondroitin 4-sulfate. Carbohydr Res. 1986;158:183-90.

27. Temenoff JS, Mikos AG. Review: tissue engineering for regeneration of articular cartilage. Biomaterials. 2000;21(5):431-40.

28. Dijkgraaf LC, Debont LGM, Boering G, Liem RSB. Normal cartilage structure, biochemistry, and metabolism: a review of the literature. Journal of Oral and Maxillofacial Surgery. 1995;53(8):924-9.

29. Benjamin M, Evans EJ. Fibrocartilage. J Anat. 1990;171:1-15.

30. Cohen NP, Foster RJ, Mow VC. Composition and dynamics of articular cartilage: structure, function, and maintaining healthy state. Journal of Orthopaedic & Sports Physical Therapy. 1998;28(4):203-15.

31. Buckwalter JA, Mankin HJ. Articular cartilage: tissue design and chondrocyte-matrix interactions. Instructional Course Lectures, Vol 47 - 1998. 1998;47:477-86.

32. Buckwalter JA, Mankin HJ. Articular cartilage: degeneration and osteoarthritis, repair, regeneration, and transplantation. Instructional Course Lectures, Vol 47 - 1998. 1998;47:487-504.

33. Watanabe H, Yamada Y, Kimata K. Roles of aggrecan, a large chondroitin sulfate proteoglycan, in cartilage structure and function. J Biochem. 1998;124(4):687-93.

34. Iozzo RV. The biology of the small leucine-rich proteoglycans: functional network of interactive proteins. Journal of Biological Chemistry. 1999;274(27):18843-6.

35. Hildebrand A, Romaris M, Rasmussen LM, Heinegard D, Twardzik DR, Border WA, et al. Interaction of the small interstitial proteoglycans biglycan, decorin and fibromodulin with transforming growth-factor-beta. Biochemical Journal. 1994;302:527-34.

36. Mackie EJ, Thesleff I, Chiquetehrismann R. Tenascin is associated with chondrogenic and osteogenic differentiation in vivo and promotes chondrogenesis in vitro. Journal of Cell Biology. 1987;105(6):2569-79.

37. Durr J, Lammi P, Goodman SL, Aigner T, vonderMark K. Identification and immunolocalization of laminin in cartilage. Experimental Cell Research. 1996;222(1):225-33.

38. Vortkamp A, Lee K, Lanske B, Segre GV, Kronenberg HM, Tabin CJ. Regulation of rate of cartilage differentiation by Indian hedgehog and PTH-related protein. Science. 1996;273(5275):613-22.

39. Karp SJ, Schipani E, St-Jacques B, Hunzelman J, Kronenberg H, McMahon AP. Indian hedgehog coordinates endochondral bone growth and morphogenesis via parathyroid hormone related-protein-dependent and -independent pathways. Development. 2000;127(3):543-8.

40. Mak KK, Kronenberg HM, Chuang PT, Mackem S, Yang Y. Indian hedgehog signals independently of PTHrP to promote chondrocyte hypertrophy. Development. 2008;135(11):1947-56.

41. Buckwalter JA. Articular cartilage: injuries and potential for healing. Journal of Orthopaedic & Sports Physical Therapy. 1998;28(4):192-202.

42. Coutts RD, Sah RL, Amiel D. Effects of growth factors on cartilage repair. Instr Course Lect. 1997;46:487-94.

43. Hunziker EB, Kapfinger E. Removal of proteoglycans from the surface of defects in articular cartilage transiently enhances coverage by repair cells. J Bone Joint Surg Br. 1998;80(1):144-50.

44. Hunziker EB. Articular cartilage repair: basic science and clinical progress. A review of the current status and prospects. Osteoarthritis Cartilage. 2002;10(6):432-63.

45. Temenoff JS, Athanasiou KA, LeBaron RG, Mikos AG. Effect of poly(ethylene glycol) molecular weight on tensile and swelling properties of oligo(poly(ethylene glycol) fumarate) hydrogels for cartilage tissue engineering. J Biomed Mater Res. 2002;59(3):429-37.

46. Kurtz S, Mowat F, Ong K, Chan N, Lau E, Halpern M. Prevalence of primary and revision total hip and knee arthroplasty in the United States from 1990 through 2002. Journal of Bone and Joint Surgery-American Volume. 2005;87A(7):1487-97.

47. Schultz W, Gobel D. Articular cartilage regeneration of the knee joint after proximal tibial valgus osteotomy: a prospective study of different intra- and extra-

articular operative techniques. Knee Surgery Sports Traumatology Arthroscopy. 1999;7(1):29-36.

48. Kanamiya T, Naito M, Hara M, Yoshimura I. The influences of biomechanical factors on cartilage regeneration after high tibial osteotomy for knees with medial compartment osteoarthritis: clinical and arthroscopic observations. Arthroscopy-the Journal of Arthroscopic and Related Surgery. 2002;18(7):725-9.

49. O'Driscoll SW. The healing and regeneration of articular cartilage. Journal of Bone and Joint Surgery-American Volume. 1998;80A(12):1795-812.

50. Wakitani S, Kawaguchi A, Tokuhara Y, Takaoka K. Present status of and future direction for articular cartilage repair. J Bone Miner Metab. 2008;26(2):115-22.

51. Koga H, Engebretsen L, Brinchmann JE, Muneta T, Sekiya I. Mesenchymal stem cell-based therapy for cartilage repair: a review. Knee Surgery Sports Traumatology Arthroscopy. 2009;17(11):1289-97.

52. Lotz M. Cytokines in cartilage injury and repair. Clinical Orthopaedics and Related Research. 2001(391):S108-S15.

53. Pridie KH, Gordon G. A Method of Resurfacing Osteoarthritic Knee Joints. Journal of Bone and Joint Surgery-British Volume. 1959;41(3):618-9.

54. Johnson LL. Arthroscopic abrasion arthroplasty historical and pathologic perspective: present status. Arthroscopy. 1986;2(1):54-69.

55. Minas T, Nehrer S. Current concepts in the treatment of articular cartilage defects. Orthopedics. 1997;20(6):525-38.

56. Steadman JR, Briggs KK, Rodrigo JJ, Kocher MS, Gill TJ, Rodkey WG. Outcomes of microfracture for traumatic chondral defects of the knee: average 11-year follow-up. Arthroscopy. 2003;19(5):477-84.

57. Gudas R, Kalesinskas RJ, Monastyreckiene E, Valanciute A, Trumpickas V. [Osteochondral transplantation (mosaicplasty) in the treatment of knee joint cartilage defects]. Medicina (Kaunas). 2003;39(5):469-75.

58. Hangody L, Fules P. Autologous osteochondral mosaicplasty for the treatment of full-thickness defects of weight-bearing joints: ten years of experimental and clinical experience. J Bone Joint Surg Am. 2003;85-A Suppl 2:25-32.

59. Reddy S, Pedowitz DI, Parekh SG, Sennett BJ, Okereke E. The morbidity associated with osteochondral harvest from asymptomatic knees for the treatment of osteochondral lesions of the talus. Am J Sports Med. 2007;35(1):80-5.

60. Homminga GN, Bulstra SK, Bouwmeester PS, van der Linden AJ. Perichondral grafting for cartilage lesions of the knee. J Bone Joint Surg Br. 1990;72(6):1003-7.

61. Ritsila VA, Santavirta S, Alhopuro S, Poussa M, Jaroma H, Rubak JM, et al. Periosteal and perichondral grafting in reconstructive surgery. Clin Orthop Relat Res. 1994(302):259-65.

62. Alfredson H, Lorentzon R. Autologous periosteum transplantation for the treatment of full thickness patellar cartilage defects. Ortop Traumatol Rehabil. 2001;3(2):216-23.

63. Haddo O, Mahroof S, Higgs D, David L, Pringle J, Bayliss M, et al. The use of chondrogide membrane in autologous chondrocyte implantation. Knee. 2004;11(1):51-5.

64. Kreuz PC, Steinwachs M, Erggelet C, Krause SJ, Ossendorf C, Maier D, et al. Classification of graft hypertrophy after autologous chondrocyte implantation of full-thickness chondral defects in the knee. Osteoarthritis Cartilage. 2007;15(12):1339-47.

65. Benya PD, Shaffer JD. Dedifferentiated chondrocytes reexpress the differentiated collagen phenotype when cultured in agarose gels. Cell. 1982;30(1):215-24.

66. Horas U, Pelinkovic D, Herr G, Aigner T, Schnettler R. Autologous chondrocyte implantation and osteochondral cylinder transplantation in cartilage repair of the knee joint. A prospective, comparative trial. J Bone Joint Surg Am. 2003;85-A(2):185-92.

67. Tins BJ, McCall IW, Takahashi T, Cassar-Pullicino V, Roberts S, Ashton B, et al. Autologous chondrocyte implantation in knee joint: MR imaging and histologic features at 1-year follow-up. Radiology. 2005;234(2):501-8.

68. Jakobsen RB, Engebretsen L, Slauterbeck JR. An analysis of the quality of cartilage repair studies. J Bone Joint Surg Am. 2005;87(10):2232-9.

69. Laurencin CT, Ambrosio AM, Borden MD, Cooper JA, Jr. Tissue engineering: orthopedic applications. Annual review of biomedical engineering. 1999;1:19-46.

70. Freed LE, Guilak F, Guo XE, Gray ML, Tranquillo R, Holmes JW, et al. Advanced tools for tissue engineering: scaffolds, bioreactors, and signaling. Tissue Eng. 2006;12(12):3285-305.

71. Kuo CK, Li WJ, Mauck RL, Tuan RS. Cartilage tissue engineering: its potential and uses. Current Opinion in Rheumatology. 2006;18(1):64-73.

72. Schnabel M, Marlovits S, Eckhoff G, Fichtel I, Gotzen L, Vecsei V, et al. Dedifferentiation-associated changes in morphology and gene expression in

primary human articular chondrocytes in cell culture. Osteoarthritis and Cartilage. 2002;10(1):62-70.

73. Freed LE, Vunjak-Novakovic G. Microgravity tissue engineering. In Vitro Cell Dev Biol Anim. 1997;33(5):381-5.

74. Frondoza C, Sohrabi A, Hungerford D. Human chondrocytes proliferate and produce matrix components in microcarrier suspension culture. Biomaterials. 1996;17(9):879-88.

75. Sittinger M, Bujia J, Minuth WW, Hammer C, Burmester GR. Engineering of cartilage tissue using bioresorbable polymer carriers in perfusion culture. Biomaterials. 1994;15(6):451-6.

76. Duke PJ, Daane EL, Montufar-Solis D. Studies of chondrogenesis in rotating systems. J Cell Biochem. 1993;51(3):274-82.

77. Pittenger MF, Mackay AM, Beck SC, Jaiswal RK, Douglas R, Mosca JD, et al. Multilineage potential of adult human mesenchymal stem cells. Science. 1999;284(5411):143-7.

78. Vunjak-Novakovic G, Altman G, Horan R, Kaplan DL. Tissue engineering of ligaments. Annu Rev Biomed Eng. 2004;6:131-56.

79. Dezawa M, Ishikawa H, Itokazu Y, Yoshihara T, Hoshino M, Takeda S, et al. Bone marrow stromal cells generate muscle cells and repair muscle degeneration. Science. 2005;309(5732):314-7.

80. Kramer J, Hegert C, Guan K, Wobus AM, Muller PK, Rohwedel J. Embryonic stem cell-derived chondrogenic differentiation in vitro: activation by BMP-2 and BMP-4. Mech Dev. 2000;92(2):193-205.

81. Bosnakovski D, Mizuno M, Kim G, Takagi S, Okumura M, Fujinaga T. Chondrogenic differentiation of bovine bone marrow mesenchymal stem cells (MSCs) in different hydrogels: influence of collagen type II extracellular matrix on MSC chondrogenesis. Biotechnol Bioeng. 2006;93(6):1152-63.

82. Lefebvre V, Huang W, Harley VR, Goodfellow PN, de Crombrugghe B. SOX9 is a potent activator of the chondrocyte-specific enhancer of the pro alpha1(II) collagen gene. Mol Cell Biol. 1997;17(4):2336-46.

83. Zuk PA, Zhu M, Ashjian P, De Ugarte DA, Huang JI, Mizuno H, et al. Human adipose tissue is a source of multipotent stem cells. Molecular Biology of the Cell. 2002;13(12):4279-95.

84. Fukumoto T, Sperling JW, Sanyal A, Fitzsimmons JS, Reinholz GG, Conover CA, et al. Combined effects of insulin-like growth factor-1 and transforming

growth factor-beta 1 on periosteal mesenchymal cells during chondrogenesis in vitro. Osteoarthritis and Cartilage. 2003;11(1):55-64.

85. De Bari C, Dell'Accio F, Tylzanowski P, Luyten FP. Multipotent mesenchymal stem cells from adult human synovial membrane. Arthritis and Rheumatism. 2001;44(8):1928-42.

86. Cao BH, Zheng B, Jankowski RJ, Kimura S, Ikezawa M, Deasy B, et al. Muscle stem cells differentiate into haematopoietic lineages but retain myogenic potential. Nature Cell Biology. 2003;5(7):640-6.

87. Bi YM, Ehirchiou D, Kilts TM, Inkson CA, Embree MC, Sonoyama W, et al. Identification of tendon stem/progenitor cells and the role of the extracellular matrix in their niche. Nature Medicine. 2007;13(10):1219-27.

88. Sakaguchi Y, Sekiya I, Yagishita K, Ichinose S, Shinomiya K, Muneta T. Suspended cells from trabecular bone by collagenase digestion become virtually identical to mesenchymal stem cells obtained from marrow aspirates. Blood. 2004;104(9):2728-35.

89. Lee OK, Kuo TK, Chen WM, Lee KD, Hsieh SL, Chen TH. Isolation of multipotent mesenchymal stem cells from umbilical cord blood. Blood. 2004;103(5):1669-75.

90. Barberi T, Willis LM, Socci ND, Studer L. Derivation of multipotent mesenchymal precursors from human embryonic stem cells. PLoS Med. 2005;2(6):e161.

91. Hwang NS, Varghese S, Lee HJ, Zhang Z, Ye Z, Bae J, et al. In vivo commitment and functional tissue regeneration using human embryonic stem cell-derived mesenchymal cells. Proc Natl Acad Sci U S A. 2008;105(52):20641-6.

92. Centrella M, Horowitz MC, Wozney JM, McCarthy TL. Transforming growth factor-beta gene family members and bone. Endocr Rev. 1994;15(1):27-39.

93. Gatherer D, Ten Dijke P, Baird DT, Akhurst RJ. Expression of TGF-beta isoforms during first trimester human embryogenesis. Development. 1990;110(2):445-60.

94. Cals FL, Hellingman CA, Koevoet W, Baatenburg de Jong RJ, van Osch GJ. Effects of transforming growth factor-beta subtypes on in vitro cartilage production and mineralization of human bone marrow stromal-derived mesenchymal stem cells. J Tissue Eng Regen Med. 2012;6(1):68-76.

95. Chimal-Monroy J, Diaz de Leon L. Differential effects of transforming growth factors beta 1, beta 2, beta 3 and beta 5 on chondrogenesis in mouse limb bud mesenchymal cells. Int J Dev Biol. 1997;41(1):91-102.

96. Mueller MB, Fischer M, Zellner J, Berner A, Dienstknecht T, Prantl L, et al. Hypertrophy in mesenchymal stem cell chondrogenesis: effect of TGF-beta isoforms and chondrogenic conditioning. Cells Tissues Organs. 2010;192(3):158-66.

97. Barry F, Boynton RE, Liu BS, Murphy JM. Chondrogenic differentiation of mesenchymal stem cells from bone marrow: differentiation-dependent gene expression of matrix components. Experimental Cell Research. 2001;268(2):189-200.

98. Sekiya I, Vuoristo JT, Larson BL, Prockop DJ. In vitro cartilage formation by human adult stem cells from bone marrow stroma defines the sequence of cellular and molecular events during chondrogenesis. Proc Natl Acad Sci U S A. 2002;99(7):4397-402.

99. Sekiya I, Larson BL, Vuoristo JT, Reger RL, Prockop DJ. Comparison of effect of BMP-2,-4, and-6 on in vitro cartilage formation of human adult stem cells from bone marrow stroma. Cell and Tissue Research. 2005;320(2):269-76.

100. Pei M, He F, Vunjak-Novakovic G. Synovium-derived stem cell-based chondrogenesis. Differentiation. 2008;76(10):1044-56.

101. Longobardi L, O'Rear L, Aakula S, Johnstone B, Shimer K, Chytil A, et al. Effect of IGF-I in the chondrogenesis of bone marrow mesenchymal stem cells in the presence or absence of TGF-beta signaling. J Bone Miner Res. 2006;21(4):626-36.

102. Worster AA, Brower-Toland BD, Fortier LA, Bent SJ, Williams J, Nixon AJ. Chondrocytic differentiation of mesenchymal stem cells sequentially exposed to transforming growth factor-beta1 in monolayer and insulin-like growth factor-I in a three-dimensional matrix. J Orthop Res. 2001;19(4):738-49.

103. Ichinose S, Yamagata K, Sekiya I, Muneta T, Tagami M. Detailed examination of cartilage formation and endochondral ossification using human mesenchymal stem cells. Clinical and Experimental Pharmacology and Physiology. 2005;32(7):561-70.

104. Pelttari K, Winter A, Steck E, Goetzke K, Hennig T, Ochs BG, et al. Premature induction of hypertrophy during in vitro chondrogenesis of human mesenchymal stem cells correlates with calcification and vascular invasion after ectopic transplantation in SCID mice. Arthritis Rheum. 2006;54(10):3254-66.

105. Steck E, Bertram H, Abel R, Chen BH, Winter A, Richter W. Induction of intervertebral disc-like cells from adult mesenchymal stem cells. Stem Cells. 2005;23(3):403-11.

106. Weiss S, Hennig T, Bock R, Steck E, Richter W. Impact of growth factors and PTHrP on early and late chondrogenic differentiation of human mesenchymal stem cells. J Cell Physiol. 2010;223(1):84-93.

107. Kim YJ, Kim HJ, Im GI. PTHrP promotes chondrogenesis and suppresses hypertrophy from both bone marrow-derived and adipose tissue-derived MSCs. Biochem Biophys Res Commun. 2008;373(1):104-8.

108. Fischer J, Dickhut A, Rickert M, Richter W. Human articular chondrocytes secrete parathyroid hormone-related protein and inhibit hypertrophy of mesenchymal stem cells in coculture during chondrogenesis. Arthritis Rheum. 2010;62(9):2696-706.

109. Lee K, Lanske B, Karaplis AC, Deeds JD, Kohno H, Nissenson RA, et al. Parathyroid hormone-related peptide delays terminal differentiation of chondrocytes during endochondral bone development. Endocrinology. 1996;137(11):5109-18.

110. Gawlitta D, Van Rijen MH, Schrijver EJ, Alblas J, Dhert W. Hypoxia impedes hypertrophic chondrogenesis of human multipotent stromal cells. Tissue Eng Part A. 2012.

111. Li WJ, Laurencin CT, Caterson EJ, Tuan RS, Ko FK. Electrospun nanofibrous structure: a novel scaffold for tissue engineering. J Biomed Mater Res. 2002;60(4):613-21.

112. Spadaccio C, Rainer A, Trombetta M, Vadala G, Chello M, Covino E, et al. Poly-L-lactic acid/hydroxyapatite electrospun nanocomposites induce chondrogenic differentiation of human MSC. Annals of Biomedical Engineering. 2009;37(7):1376-89.

113. Richardson SM, Curran JM, Chen R, Vaughan-Thomas A, Hunt JA, Freemont AJ, et al. The differentiation of bone marrow mesenchymal stem cells into chondrocyte-like cells on poly-L-lactic acid (PLLA) scaffolds. Biomaterials. 2006;27(22):4069-78.

114. Chen JW, Wang CY, Lu SH, Wu JZ, Guo XM, Duan CM, et al. In vivo chondrogenesis of adult bone-marrow-derived autologous mesenchymal stem cells. Cell and Tissue Research. 2005;319(3):429-38.

115. Chen GP, Liu DC, Tadokoro M, Hirochika R, Ohgushi H, Tanaka J, et al. Chondrogenic differentiation of human mesenchymal stem cells cultured in a cobweb-like biodegradable scaffold. Biochem Biophys Res Commun. 2004;322(1):50-5.

116. Li WJ, Tuli R, Okafor C, Derfoul A, Danielson KG, Hall DJ, et al. A three-dimensional nanofibrous scaffold for cartilage tissue engineering using human mesenchymal stem cells. Biomaterials. 2005;26(6):599-609.

117. Raghunath J, Rollo J, Sales KM, Butler PE, Seifalian AM. Biomaterials and scaffold design: key to tissue-engineering cartilage. Biotechnology and Applied Biochemistry. 2007;46:73-84.

118. Kim TG, Park TG. Biomimicking extracellular matrix: cell adhesive RGD peptide modified electrospun poly(D,L-lactic-Co-glycolic acid) nanofiber mesh. Tissue Engineering. 2006;12(2):221-33.

119. Ma ZW, Gao CY, Gong YH, Shen JC. Cartilage tissue engineering PLLA scaffold with surface immobilized collagen and basic fibroblast growth factor. Biomaterials. 2005;26(11):1253-9.

120. Park GE, Pattison MA, Park K, Webster TJ. Accelerated chondrocyte functions on NaOH-treated PLGA scaffolds. Biomaterials. 2005;26(16):3075-82.

121. Yoo HS, Lee EA, Yoon JJ, Park TG. Hyaluronic acid modified biodegradable scaffolds for cartilage tissue engineering. Biomaterials. 2005;26(14):1925-33.

122. Drury JL, Mooney DJ. Hydrogels for tissue engineering: scaffold design variables and applications. Biomaterials. 2003;24(24):4337-51.

123. Hoffman AS. Hydrogels for biomedical applications. Advanced Drug Delivery Reviews. 2002;54(1):3-12.

124. Nicodemus GD, Bryant SJ. Cell encapsulation in biodegradable hydrogels for tissue engineering applications. Tissue Engineering Part B-Reviews. 2008;14(2):149-65.

125. Pelaez D, Huang CY, Cheung HS. Cyclic compression maintains viability and induces chondrogenesis of human mesenchymal stem cells in fibrin gel scaffolds. Stem Cells Dev. 2009;18(1):93-102.

126. Baumgartner L, Arnhold S, Brixius K, Addicks K, Bloch W. Human mesenchymal stem cells: influence of oxygen pressure on proliferation and chondrogenic differentiation in fibrin glue in vitro. J Biomed Mater Res A. 2010;93(3):930-40.

127. Im GI. Chondrogenesis from mesenchymal stem cells derived from adipose tissue on the fibrin scaffold. Current Applied Physics. 2005;5(5):438-43.

128. Ponticiello MS, Schinagl RM, Kadiyala S, Barry FP. Gelatin-based resorbable sponge as a carrier matrix for human mesenchymal stem cells in cartilage regeneration therapy. J Biomed Mater Res. 2000;52(2):246-55.

129. Awad HA, Wickham MQ, Leddy HA, Gimble JM, Guilak F. Chondrogenic differentiation of adipose-derived adult stem cells in agarose, alginate, and gelatin scaffolds. Biomaterials. 2004;25(16):3211-22.

130. Kavalkovich KW, Boynton RE, Murphy JM, Barry F. Chondrogenic differentiation of human mesenchymal stem cells within an alginate layer culture system. In Vitro Cell Dev Biol Anim. 2002;38(8):457-66.

131. Xu J, Wang W, Ludeman M, Cheng K, Hayami T, Lotz JC, et al. Chondrogenic differentiation of human mesenchymal stem cells in three-dimensional alginate gels. Tissue Eng Part A. 2008;14(5):667-80.

132. Mauck RL, Yuan X, Tuan RS. Chondrogenic differentiation and functional maturation of bovine mesenchymal stem cells in long-term agarose culture. Osteoarthritis Cartilage. 2006;14(2):179-89.

133. Huang CY, Reuben PM, D'Ippolito G, Schiller PC, Cheung HS. Chondrogenesis of human bone marrow-derived mesenchymal stem cells in agarose culture. Anat Rec A Discov Mol Cell Evol Biol. 2004;278(1):428-36.

134. Tibbitt MW, Anseth KS. Hydrogels as extracellular matrix mimics for 3D cell culture. Biotechnology and Bioengineering. 2009;103(4):655-63.

135. Lee KY, Mooney DJ. Hydrogels for tissue engineering. Chemical Reviews. 2001;101(7):1869-79.

136. Williams CG, Kim TK, Taboas A, Malik A, Manson P, Elisseeff J. In vitro chondrogenesis of bone marrow-derived mesenchymal stem cells in a photopolymerizing hydrogel. Tissue Eng. 2003;9(4):679-88.

137. Salinas CN, Anseth KS. The enhancement of chondrogenic differentiation of human mesenchymal stem cells by enzymatically regulated RGD functionalities. Biomaterials. 2008;29(15):2370-7.

138. Huang CY, Hagar KL, Frost LE, Sun Y, Cheung HS. Effects of cyclic compressive loading on chondrogenesis of rabbit bone-marrow derived mesenchymal stem cells. Stem Cells. 2004;22(3):313-23.

139. Mouw JK, Connelly JT, Wilson CG, Michael KE, Levenston ME. Dynamic compression regulates the expression and synthesis of chondrocyte-specific matrix molecules in bone marrow stromal cells. Stem Cells. 2007;25(3):655-63.

140. Angele P, Schumann D, Angele M, Kinner B, Englert C, Hente R, et al. Cyclic, mechanical compression enhances chondrogenesis of mesenchymal progenitor cells in tissue engineering scaffolds. Biorheology. 2004;41(3-4):335-46.

141. Mauck RL, Byers BA, Yuan X, Tuan RS. Regulation of cartilaginous ECM gene transcription by chondrocytes and MSCs in 3D culture in response to dynamic loading. Biomechanics and Modeling in Mechanobiology. 2007;6(1-2):113-25.

142. Wagner DR, Lindsey DP, Li KW, Tummala P, Chandran SE, Smith RL, et al. Hydrostatic pressure enhances chondrogenic differentiation of human bone

marrow stromal cells in osteochondrogenic medium. Annals of Biomedical Engineering. 2008;36(5):813-20.

143. Angele P, Yoo JU, Smith C, Mansour J, Jepsen KJ, Nerlich M, et al. Cyclic hydrostatic pressure enhances the chondrogenic phenotype of human mesenchymal progenitor cells differentiated in vitro. Journal of Orthopaedic Research. 2003;21(3):451-7.

144. Huang AH, Farrell MJ, Kim M, Mauck RL. Long-term dynamic loading improves the mechanical properties of chondrogenic mesenchymal stem cell-laden hydrogels. European Cells & Materials. 2010;19:72-85.

145. Kisiday JD, Frisbie DD, McIlwraith CW, Grodzinsky AJ. Dynamic compression stimulates proteoglycan synthesis by mesenchymal stem cells in the absence of chondrogenic cytokines. Tissue Engineering Part A. 2009;15(10):2817-24.

146. Guilak F, Cohen DM, Estes BT, Gimble JM, Liedtke W, Chen CS. Control of stem cell fate by physical interactions with the extracellular matrix. Cell Stem Cell. 2009;5(1):17-26.

147. McBeath R, Pirone DM, Nelson CM, Bhadriraju K, Chen CS. Cell shape, cytoskeletal tension, and RhoA regulate stem cell lineage commitment. Dev Cell. 2004;6(4):483-95.

148. Kilian KA, Bugarija B, Lahn BT, Mrksich M. Geometric cues for directing the differentiation of mesenchymal stem cells. Proc Natl Acad Sci U S A. 2010;107(11):4872-7.

149. Kelly DJ, Jacobs CR. The role of mechanical signals in regulating chondrogenesis and osteogenesis of mesenchymal stem cells. Birth Defects Res C Embryo Today. 2010;90(1):75-85.

150. Gao L, McBeath R, Chen CS. Stem cell shape regulates a chondrogenic versus myogenic fate through Rac1 and N-cadherin. Stem Cells. 2010;28(3):564-72.

151. McBride SH, Knothe Tate ML. Modulation of stem cell shape and fate A: the role of density and seeding protocol on nucleus shape and gene expression. Tissue Eng Part A. 2008;14(9):1561-72.

152. McBride SH, Falls T, Knothe Tate ML. Modulation of stem cell shape and fate B: mechanical modulation of cell shape and gene expression. Tissue Eng Part A. 2008;14(9):1573-80.

153. Woods A, Wang G, Beier F. RhoA/ROCK signaling regulates Sox9 expression and actin organization during chondrogenesis. J Biol Chem. 2005;280(12):11626-34.

154. Zanetti NC, Solursh M. Induction of chondrogenesis in limb mesenchymal cultures by disruption of the actin cytoskeleton. J Cell Biol. 1984;99(1 Pt 1):115-23.

155. Lim YB, Kang SS, Park TK, Lee YS, Chun JS, Sonn JK. Disruption of actin cytoskeleton induces chondrogenesis of mesenchymal cells by activating protein kinase C-alpha signaling. Biochem Biophys Res Commun. 2000;273(2):609-13.

156. Lim YB, Kang SS, An WG, Lee YS, Chun JS, Sonn JK. Chondrogenesis induced by actin cytoskeleton disruption is regulated via protein kinase C-dependent p38 mitogen-activated protein kinase signaling. J Cell Biochem. 2003;88(4):713-8.

157. Zhang Z, Messana J, Hwang NS, Elisseeff JH. Reorganization of actin filaments enhances chondrogenic differentiation of cells derived from murine embryonic stem cells. Biochem Biophys Res Commun. 2006;348(2):421-7.

158. Woods A, Beier F. RhoA/ROCK signaling regulates chondrogenesis in a context-dependent manner. J Biol Chem. 2006;281(19):13134-40.

159. Woods A, Wang G, Dupuis H, Shao Z, Beier F. Rac1 signaling stimulates N-cadherin expression, mesenchymal condensation, and chondrogenesis. J Biol Chem. 2007;282(32):23500-8.

160. Engler AJ, Sen S, Sweeney HL, Discher DE. Matrix elasticity directs stem cell lineage specification. Cell. 2006;126(4):677-89.

161. Schuh E, Kramer J, Rohwedel J, Notbohm H, Muller R, Gutsmann T, et al. Effect of matrix elasticity on the maintenance of the chondrogenic phenotype. Tissue Eng Part A. 2010;16(4):1281-90.

162. Park JS, Chu JS, Tsou AD, Diop R, Tang Z, Wang A, et al. The effect of matrix stiffness on the differentiation of mesenchymal stem cells in response to TGF-beta. Biomaterials. 2011;32(16):3921-30.

163. Schuh E, Hofmann S, Stok KS, Notbohm H, Muller R, Rotter N. The influence of matrix elasticity on chondrocyte behavior in 3D. J Tissue Eng Regen Med. 2011.

164. Elbert DL, Hubbell JA. Surface treatments of polymers for biocompatibility. Annu Rev Mater Sci. 1996;26:365-94.

165. Deible CR, Petrosko P, Johnson PC, Beckman EJ, Russell AJ, Wagner WR. Molecular barriers to biomaterial thrombosis by modification of surface proteins with polyethylene glycol. Biomaterials. 1999;20(2):101-9.

166. Gombotz WR, Wang GH, Horbett TA, Hoffman AS. Protein adsorption to poly(ethylene oxide) surfaces. J Biomed Mater Res. 1991;25(12):1547-62.

167. Burdick JA, Anseth KS. Photoencapsulation of osteoblasts in injectable RGD-modified PEG hydrogels for bone tissue engineering. Biomaterials. 2002;23(22):4315-23.

168. Yang F, Williams CG, Wang DA, Lee H, Manson PN, Elisseeff J. The effect of incorporating RGD adhesive peptide in polyethylene glycol diacrylate hydrogel on osteogenesis of bone marrow stromal cells. Biomaterials. 2005;26(30):5991-8.

169. Bryant SJ, Anseth KS. Controlling the spatial distribution of ECM components in degradable PEG hydrogels for tissue engineering cartilage. J Biomed Mater Res A. 2003;64(1):70-9.

170. Moon JJ, Hahn MS, Kim I, Nsiah BA, West JL. Micropatterning of poly(ethylene glycol) diacrylate hydrogels with biomolecules to regulate and guide endothelial morphogenesis. Tissue Eng Part A. 2009;15(3):579-85.

171. Phelps EA, Landazuri N, Thule PM, Taylor WR, Garcia AJ. Regenerative Medicine Special Feature: Bioartificial matrices for therapeutic vascularization. Proc Natl Acad Sci U S A. 2009.

172. Mahoney MJ, Anseth KS. Three-dimensional growth and function of neural tissue in degradable polyethylene glycol hydrogels. Biomaterials. 2006;27(10):2265-74.

173. Gunn JW, Turner SD, Mann BK. Adhesive and mechanical properties of hydrogels influence neurite extension. J Biomed Mater Res A. 2005;72(1):91-7.

174. Brink KS, Yang PJ, Temenoff JS. Degradative properties and cytocompatibility of a mixed-mode hydrogel containing oligo[poly(ethylene glycol)fumarate] and poly(ethylene glycol)dithiol. Acta Biomater. 2009;5(2):570-9.

175. Temenoff JS, Park H, Jabbari E, Conway DE, Sheffield TL, Ambrose CG, et al. Thermally cross-linked oligo(poly(ethylene glycol) fumarate) hydrogels support osteogenic differentiation of encapsulated marrow stromal cells in vitro. Biomacromolecules. 2004;5(1):5-10.

176. Nguyen KT, West JL. Photopolymerizable hydrogels for tissue engineering applications. Biomaterials. 2002;23(22):4307-14.

177. Ifkovits JL, Burdick JA. Review: photopolymerizable and degradable biomaterials for tissue engineering applications. Tissue Engineering. 2007;13(10):2369-85.

178. Hersel U, Dahmen C, Kessler H. RGD modified polymers: biomaterials for stimulated cell adhesion and beyond. Biomaterials. 2003;24(24):4385-415.

179. Salinas CN, Anseth KS. Mixed mode thiol-acrylate photopolymerizations for the synthesis of PEG-peptide hydrogels. Macromolecules. 2008;41(16):6019-26.

180. Elbert DL, Pratt AB, Lutolf MP, Halstenberg S, Hubbell JA. Protein delivery from materials formed by self-selective conjugate addition reactions. J Control Release. 2001;76(1-2):11-25.

181. van de Wetering P, Metters AT, Schoenmakers RG, Hubbell JA. Poly(ethylene glycol) hydrogels formed by conjugate addition with controllable swelling, degradation, and release of pharmaceutically active proteins. J Control Release. 2005;102(3):619-27.

182. Polizzotti BD, Fairbanks BD, Anseth KS. Three-dimensional biochemical patterning of click-based composite hydrogels via thiolene photopolymerization. Biomacromolecules. 2008;9(4):1084-7.

183. Temenoff JS, Mikos AG. Injectable biodegradable materials for orthopedic tissue engineering. Biomaterials. 2000;21(23):2405-12.

184. Lutolf MP, Hubbell JA. Synthetic biomaterials as instructive extracellular microenvironments for morphogenesis in tissue engineering. Nat Biotechnol. 2005;23(1):47-55.

185. Hudalla GA, Eng TS, Murphy WL. An approach to modulate degradation and mesenchymal stem cell behavior in poly(ethylene glycol) networks. Biomacromolecules. 2008;9(3):842-9.

186. Gobin AS, West JL. Cell migration through defined, synthetic ECM analogs. FASEB J. 2002;16(7):751-3.

187. Gobin AS, West JL. Effects of epidermal growth factor on fibroblast migration through biomimetic hydrogels. Biotechnol Prog. 2003;19(6):1781-5.

188. Kloxin AM, Kasko AM, Salinas CN, Anseth KS. Photodegradable hydrogels for dynamic tuning of physical and chemical properties. Science. 2009;324(5923):59-63.

189. Hern DL, Hubbell JA. Incorporation of adhesion peptides into nonadhesive hydrogels useful for tissue resurfacing. J Biomed Mater Res. 1998;39(2):266-76.

190. Mann BK, Schmedlen RH, West JL. Tethered-TGF-beta increases extracellular matrix production of vascular smooth muscle cells. Biomaterials. 2001;22(5):439-44.

191. DeLong SA, Moon JJ, West JL. Covalently immobilized gradients of bFGF on hydrogel scaffolds for directed cell migration. Biomaterials. 2005;26(16):3227-34.

192. Hahn MS, Miller JS, West JL. Laser scanning lithography for surface micropatterning on hydrogels. Adv Mater. 2005;17(24):2939-42.

193. Hahn MS, Miller JS, West JL. Three-dimensional biochemical and biomechanical patterning of hydrogels for guiding cell behavior. Adv Mater. 2006;18(20):2679-84.

194. Hahn MS, Taite LJ, Moon JJ, Rowland MC, Ruffino KA, West JL. Photolithographic patterning of polyethylene glycol hydrogels. Biomaterials. 2006;27(12):2519-24.

195. Liu VA, Bhatia SN. Three-dimensional photopatterning of hydrogels containing living cells. Biomed Microdevices. 2002;4(4):257-66.

196. Liu Tsang V, Chen AA, Cho LM, Jadin KD, Sah RL, DeLong S, et al. Fabrication of 3D hepatic tissues by additive photopatterning of cellular hydrogels. FASEB J. 2007;21(3):790-801.

197. Hammoudi TM, Lu H, Temenoff JS. Long-term spatially defined coculture within three-dimensional photopatterned hydrogels. Tissue Engineering Part C-Methods. 2010;16(6):1621-8.

198. Holland TA, Bodde EW, Baggett LS, Tabata Y, Mikos AG, Jansen JA. Osteochondral repair in the rabbit model utilizing bilayered, degradable oligo(poly(ethylene glycol) fumarate) hydrogel scaffolds. J Biomed Mater Res A. 2005;75(1):156-67.

199. Park H, Temenoff JS, Tabata Y, Caplan AI, Mikos AG. Injectable biodegradable hydrogel composites for rabbit marrow mesenchymal stem cell and growth factor delivery for cartilage tissue engineering. Biomaterials. 2007;28(21):3217-27.

200. Shin H, Quinten Ruhe P, Mikos AG, Jansen JA. In vivo bone and soft tissue response to injectable, biodegradable oligo(poly(ethylene glycol) fumarate) hydrogels. Biomaterials. 2003;24(19):3201-11.

201. Shin H, Jo S, Mikos AG. Modulation of marrow stromal osteoblast adhesion on biomimetic oligo[poly(ethylene glycol) fumarate] hydrogels modified with Arg-Gly-Asp peptides and a poly(ethyleneglycol) spacer. J Biomed Mater Res. 2002;61(2):169-79.

202. Shin H, Temenoff JS, Mikos AG. In vitro cytotoxicity of unsaturated oligo[poly(ethylene glycol) fumarate] macromers and their cross-linked hydrogels. Biomacromolecules. 2003;4(3):552-60.

203. Holland TA, Tessmar JK, Tabata Y, Mikos AG. Transforming growth factor-beta 1 release from oligo(poly(ethylene glycol) fumarate) hydrogels in conditions that model the cartilage wound healing environment. J Control Release. 2004;94(1):101-14.

204. Holland TA, Tabata Y, Mikos AG. Dual growth factor delivery from degradable oligo(poly(ethylene glycol) fumarate) hydrogel scaffolds for cartilage tissue engineering. J Control Release. 2005;101(1-3):111-25.

205. Park H, Temenoff JS, Holland TA, Tabata Y, Mikos AG. Delivery of TGF-beta1 and chondrocytes via injectable, biodegradable hydrogels for cartilage tissue engineering applications. Biomaterials. 2005;26(34):7095-103.

206. Park JS, Yang HJ, Woo DG, Yang HN, Na K, Park KH. Chondrogenic differentiation of mesenchymal stem cells embedded in a scaffold by long-term release of TGF-beta 3 complexed with chondroitin sulfate. J Biomed Mater Res A. 2010;92(2):806-16.

207. Park H, Guo X, Temenoff JS, Tabata Y, Caplan AI, Kasper FK, et al. Effect of swelling ratio of injectable hydrogel composites on chondrogenic differentiation of encapsulated rabbit marrow mesenchymal stem cells in vitro. Biomacromolecules. 2009;10(3):541-6.

208. Park H, Temenoff JS, Tabata Y, Caplan AI, Raphael RM, Jansen JA, et al. Effect of dual growth factor delivery on chondrogenic differentiation of rabbit marrow mesenchymal stem cells encapsulated in injectable hydrogel composites. Journal of Biomedical Materials Research Part A. 2009;88A(4):889-97.

209. Buxton AN, Zhu J, Marchant R, West JL, Yoo JU, Johnstone B. Design and characterization of poly(ethylene glycol) photopolymerizable semi-interpenetrating networks for chondrogenesis of human mesenchymal stem cells. Tissue Eng. 2007;13(10):2549-60.

210. Salinas CN, Cole BB, Kasko AM, Anseth KS. Chondrogenic differentiation potential of human mesenchymal stem cells photoencapsulated within poly(ethylene glycol)-arginine-glycine-aspartic acid-serine thiol-methacrylate mixed-mode networks. Tissue Eng. 2007;13(5):1025-34.

211. Hwang NS, Varghese S, Zhang Z, Elisseeff J. Chondrogenic differentiation of human embryonic stem cell-derived cells in arginine-glycine-aspartate-modified hydrogels. Tissue Eng. 2006;12(9):2695-706.

212. Pankov R, Yamada KM. Fibronectin at a glance. J Cell Sci. 2002;115(Pt 20):3861-3.

213. Connelly JT, Garcia AJ, Levenston ME. Inhibition of in vitro chondrogenesis in RGD-modified three-dimensional alginate gels. Biomaterials. 2007;28(6):1071-83.

214. Liu SQ, Tian Q, Hedrick JL, Po Hui JH, Ee PL, Yang YY. Biomimetic hydrogels for chondrogenic differentiation of human mesenchymal stem cells to neocartilage. Biomaterials. 2010;31(28):7298-307.

215. Lee HJ, Yu C, Chansakul T, Hwang NS, Varghese S, Yu SM, et al. Enhanced chondrogenesis of mesenchymal stem cells in collagen mimetic peptide-mediated microenvironment. Tissue Eng Part A. 2008;14(11):1843-51.

216. Salinas CN, Anseth KS. Decorin moieties tethered into PEG networks induce chondrogenesis of human mesenchymal stem cells. J Biomed Mater Res A. 2009;90(2):456-64.

217. Wight TN. Versican: a versatile extracellular matrix proteoglycan in cell biology. Curr Opin Cell Biol. 2002;14(5):617-23.

218. Shibata S, Fukada K, Imai H, Abe T, Yamashita Y. In situ hybridization and immunohistochemistry of versican, aggrecan and link protein, and histochemistry of hyaluronan in the developing mouse limb bud cartilage. J Anat. 2003;203(4):425-32.

219. Snow HE, Riccio LM, Mjaatvedt CH, Hoffman S, Capehart AA. Versican expression during skeletal/joint morphogenesis and patterning of muscle and nerve in the embryonic mouse limb. Anat Rec A Discov Mol Cell Evol Biol. 2005;282(2):95-105.

220. Knudson CB, Knudson W. Cartilage proteoglycans. Semin Cell Dev Biol. 2001;12(2):69-78.

221. Arikawa-Hirasawa E, Watanabe H, Takami H, Hassell JR, Yamada Y. Perlecan is essential for cartilage and cephalic development. Nat Genet. 1999;23(3):354-8.

222. Costell M, Gustafsson E, Aszodi A, Morgelin M, Bloch W, Hunziker E, et al. Perlecan maintains the integrity of cartilage and some basement membranes. J Cell Biol. 1999;147(5):1109-22.

223. French MM, Smith SE, Akanbi K, Sanford T, Hecht J, Farach-Carson MC, et al. Expression of the heparan sulfate proteoglycan, perlecan, during mouse embryogenesis and perlecan chondrogenic activity in vitro. J Cell Biol. 1999;145(5):1103-15.

224. SundarRaj N, Fite D, Ledbetter S, Chakravarti S, Hassell JR. Perlecan is a component of cartilage matrix and promotes chondrocyte attachment. J Cell Sci. 1995;108 (Pt 7):2663-72.

225. Govindraj P, West L, Smith S, Hassell JR. Modulation of FGF-2 binding to chondrocytes from the developing growth plate by perlecan. Matrix Biol. 2006;25(4):232-9.

226. Handler M, Yurchenco PD, Iozzo RV. Developmental expression of perlecan during murine embryogenesis. Dev Dyn. 1997;210(2):130-45.

227. Domowicz MS, Cortes M, Henry JG, Schwartz NB. Aggrecan modulation of growth plate morphogenesis. Developmental Biology. 2009;329(2):242-57.

228. Thiele H, Sakano M, Kitagawa H, Sugahara K, Rajab A, Hohne W, et al. Loss of chondroitin 6-O-sulfotransferase-1 function results in severe human chondrodysplasia with progressive spinal involvement. Proc Natl Acad Sci U S A. 2004;101(27):10155-60.

229. Caterson B, Mahmoodian F, Sorrell JM, Hardingham TE, Bayliss MT, Carney SL, et al. Modulation of native chondroitin sulphate structure in tissue development and in disease. J Cell Sci. 1990;97 (Pt 3):411-7.

230. Hardingham TE, Fosang AJ. Proteoglycans: many forms and many functions. Faseb J. 1992;6(3):861-70.

231. Plaas AH, Wong-Palms S, Roughley PJ, Midura RJ, Hascall VC. Chemical and immunological assay of the nonreducing terminal residues of chondroitin sulfate from human aggrecan. J Biol Chem. 1997;272(33):20603-10.

232. Chung C, Beecham M, Mauck RL, Burdick JA. The influence of degradation characteristics of hyaluronic acid hydrogels on in vitro neocartilage formation by mesenchymal stem cells. Biomaterials. 2009;30(26):4287-96.

233. Chung C, Erickson IE, Mauck RL, Burdick JA. Differential behavior of auricular and articular chondrocytes in hyaluronic acid hydrogels. Tissue Eng Part A. 2008;14(7):1121-31.

234. Liu Y, Shu XZ, Prestwich GD. Osteochondral defect repair with autologous bone marrow-derived mesenchymal stem cells in an injectable, in situ, cross-linked synthetic extracellular matrix. Tissue Eng. 2006;12(12):3405-16.

235. Bulpitt P, Aeschlimann D. New strategy for chemical modification of hyaluronic acid: preparation of functionalized derivatives and their use in the formation of novel biocompatible hydrogels. J Biomed Mater Res. 1999;47(2):152-69.

236. Liao E, Yaszemski M, Krebsbach P, Hollister S. Tissue-engineered cartilage constructs using composite hyaluronic acid/collagen I hydrogels and designed poly(propylene fumarate) scaffolds. Tissue Eng. 2007;13(3):537-50.

237. Wang DA, Varghese S, Sharma B, Strehin I, Fermanian S, Gorham J, et al. Multifunctional chondroitin sulphate for cartilage tissue-biomaterial integration. Nat Mater. 2007;6(5):385-92.

238. Li Q, Williams CG, Sun DD, Wang J, Leong K, Elisseeff JH. Photocrosslinkable polysaccharides based on chondroitin sulfate. J Biomed Mater Res A. 2004;68(1):28-33.

239. Li Q, Wang DA, Elisseeff JH. Heterogeneous-phase reaction of glycidyl methacrylate and chondroitin sulfate: mechanism of ring-opening-transesterification competition. Macromolecules. 2003;36(7):2556-62.

240. Reyes JMG, Herretes S, Pirouzmanesh A, Wang DA, Elisseeff JH, Jun A, et al. A modified chondroitin sulfate aldehyde adhesive for sealing corneal incisions. Investigative Ophthalmology & Visual Science. 2005;46(4):1247-50.

241. Strehin I, Ambrose WM, Schein O, Salahuddin A, Elisseeff J. Synthesis and characterization of a chondroitin sulfate-polyethylene glycol corneal adhesive. Journal of Cataract and Refractive Surgery. 2009;35(3):567-76.

242. Conovaloff A, Panitch A. Characterization of a chondroitin sulfate hydrogel for nerve root regeneration. J Neural Eng. 2011;8(5):056003.

243. Gilbert RJ, McKeon RJ, Darr A, Calabro A, Hascall VC, Bellamkonda RV. CS-4,6 is differentially upregulated in glial scar and is a potent inhibitor of neurite extension. Mol Cell Neurosci. 2005;29(4):545-58.

244. Yu X, Bellamkonda RV. Dorsal root ganglia neurite extension is inhibited by mechanical and chondroitin sulfate-rich interfaces. J Neurosci Res. 2001;66(2):303-10.

245. Friedlander DR, Milev P, Karthikeyan L, Margolis RK, Margolis RU, Grumet M. The neuronal chondroitin sulfate proteoglycan neurocan binds to the neural cell adhesion molecules Ng-CAM/L1/NILE and N-CAM, and inhibits neuronal adhesion and neurite outgrowth. J Cell Biol. 1994;125(3):669-80.

246. Dou CL, Levine JM. Inhibition of neurite growth by the NG2 chondroitin sulfate proteoglycan. J Neurosci. 1994;14(12):7616-28.

247. Laabs TL, Wang H, Katagiri Y, McCann T, Fawcett JW, Geller HM. Inhibiting glycosaminoglycan chain polymerization decreases the inhibitory activity of astrocyte-derived chondroitin sulfate proteoglycans. J Neurosci. 2007;27(52):14494-501.

248. Bryant SJ, Arthur JA, Anseth KS. Incorporation of tissue-specific molecules alters chondrocyte metabolism and gene expression in photocrosslinked hydrogels. Acta Biomater. 2005;1(2):243-52.

249. Hwang NS, Varghese S, Lee HJ, Theprungsirikul P, Canver A, Sharma B, et al. Response of zonal chondrocytes to extracellular matrix-hydrogels. FEBS Lett. 2007;581(22):4172-8.

250. Kim YJ, Bonassar LJ, Grodzinsky AJ. The role of cartilage streaming potential, fluid flow and pressure in the stimulation of chondrocyte biosynthesis during dynamic compression. J Biomech. 1995;28(9):1055-66.

251. Chen WC, Yao CL, Chu IM, Wei YH. Compare the effects of chondrogenesis by culture of human mesenchymal stem cells with various type of the chondroitin sulfate C. J Biosci Bioeng. 2011;111(2):226-31.

252. Steinmetz NJ, Bryant SJ. Chondroitin sulfate and dynamic loading alter chondrogenesis of human MSCs in PEG hydrogels. Biotechnol Bioeng. 2012.

253. Bishop JR, Schuksz M, Esko JD. Heparan sulphate proteoglycans fine-tune mammalian physiology. Nature. 2007;446(7139):1030-7.

254. Baldwin AD, Kiick KL. Polysaccharide-modified synthetic polymeric biomaterials. Biopolymers. 2010;94(1):128-40.

255. Nie T, Baldwin A, Yamaguchi N, Kiick KL. Production of heparin-functionalized hydrogels for the development of responsive and controlled growth factor delivery systems. J Control Release. 2007;122(3):287-96.

256. Pike DB, Cai S, Pomraning KR, Firpo MA, Fisher RJ, Shu XZ, et al. Heparin-regulated release of growth factors in vitro and angiogenic response in vivo to implanted hyaluronan hydrogels containing VEGF and bFGF. Biomaterials. 2006;27(30):5242-51.

257. Garcia-Olivas R, Hoebeke J, Castel S, Reina M, Fager G, Lustig F, et al. Differential binding of platelet-derived growth factor isoforms to glycosaminoglycans. Histochem Cell Biol. 2003;120(5):371-82.

258. Thomopoulos S, Zaegel M, Das R, Harwood FL, Silva MJ, Amiel D, et al. PDGF-BB released in tendon repair using a novel delivery system promotes cell proliferation and collagen remodeling. J Orthop Res. 2007;25(10):1358-68.

259. Cushing MC, Liao JT, Anseth KS. Activation of valvular interstitial cells is mediated by transforming growth factor-beta1 interactions with matrix molecules. Matrix Biol. 2005;24(6):428-37.

260. Park JS, Woo DG, Yang HN, Na K, Park KH. Transforming growth factor beta-3 bound with sulfate polysaccharide in synthetic extracellular matrix enhanced the biological activities for neocartilage formation in vivo. J Biomed Mater Res A. 2009;91(2):408-15.

261. Deepa SS, Umehara Y, Higashiyama S, Itoh N, Sugahara K. Specific molecular interactions of oversulfated chondroitin sulfate E with various heparin-binding growth factors. Implications as a physiological binding partner in the brain and other tissues. J Biol Chem. 2002;277(46):43707-16.

262. Park YJ, Lee YM, Lee JY, Seol YJ, Chung CP, Lee SJ. Controlled release of platelet-derived growth factor-BB from chondroitin sulfate-chitosan sponge for guided bone regeneration. J Control Release. 2000;67(2-3):385-94.

263. Zafiropoulos A, Fthenou E, Chatzinikolaou G, Tzanakakis GN. Glycosaminoglycans and PDGF signaling in mesenchymal cells. Connect Tissue Res. 2008;49(3):153-6.

264. Mullen LM, Best SM, Brooks RA, Ghose S, Gwynne JH, Wardale J, et al. Binding and Release Characteristics of Insulin-Like Growth Factor-1 from a Collagen-Glycosaminoglycan Scaffold. Tissue Eng Part C Methods. 2010.

265. Aviezer D, Levy E, Safran M, Svahn C, Buddecke E, Schmidt A, et al. Differential structural requirements of heparin and heparan sulfate proteoglycans that promote binding of basic fibroblast growth factor to its receptor. J Biol Chem. 1994;269(1):114-21.

266. Maccarana M, Casu B, Lindahl U. Minimal sequence in heparin/heparan sulfate required for binding of basic fibroblast growth factor. J Biol Chem. 1993;268(32):23898-905.

267. Lundin L, Larsson H, Kreuger J, Kanda S, Lindahl U, Salmivirta M, et al. Selectively desulfated heparin inhibits fibroblast growth factor-induced mitogenicity and angiogenesis. J Biol Chem. 2000;275(32):24653-60.

268. Arai T, Parker A, Busby W, Jr., Clemmons DR. Heparin, heparan sulfate, and dermatan sulfate regulate formation of the insulin-like growth factor-I and insulin-like growth factor-binding protein complexes. J Biol Chem. 1994;269(32):20388-93.

269. Soker S, Goldstaub D, Svahn CM, Vlodavsky I, Levi BZ, Neufeld G. Variations in the size and sulfation of heparin modulate the effect of heparin on the binding of VEGF165 to its receptors. Biochem Biophys Res Commun. 1994;203(2):1339-47.

270. Rickard SM, Mummery RS, Mulloy B, Rider CC. The binding of human glial cell line-derived neurotrophic factor to heparin and heparan sulfate: importance of 2-O-sulfate groups and effect on its interaction with its receptor, GFRalpha1. Glycobiology. 2003;13(6):419-26.

271. Alfano I, Vora P, Mummery RS, Mulloy B, Rider CC. The major determinant of the heparin binding of glial cell-line-derived neurotrophic factor is near the N-terminus and is dispensable for receptor binding. Biochem J. 2007;404(1):131-40.

272. Rider CC. Heparin/heparan sulphate binding in the TGF-beta cytokine superfamily. Biochem Soc Trans. 2006;34(Pt 3):458-60.

273. Hintze V, Moeller S, Schnabelrauch M, Bierbaum S, Viola M, Worch H, et al. Modifications of hyaluronan influence the interaction with human bone morphogenetic protein-4 (hBMP-4). Biomacromolecules. 2009;10(12):3290-7.

274. Lyon M, Rushton G, Gallagher JT. The interaction of the transforming growth factor-betas with heparin/heparan sulfate is isoform-specific. J Biol Chem. 1997;272(29):18000-6.

275. Pellaud J, Schote U, Arvinte T, Seelig J. Conformation and self-association of human recombinant transforming growth factor-beta3 in aqueous solutions. J Biol Chem. 1999;274(12):7699-704.

276. Yamamoto M, Ikada Y, Tabata Y. Controlled release of growth factors based on biodegradation of gelatin hydrogel. J Biomater Sci Polym Ed. 2001;12(1):77-88.

277. Hinck AP, Archer SJ, Qian SW, Roberts AB, Sporn MB, Weatherbee JA, et al. Transforming growth factor beta 1: three-dimensional structure in solution and comparison with the X-ray structure of transforming growth factor beta 2. Biochemistry. 1996;35(26):8517-34.

278. Merceron C, Portron S, Vignes-Colombeix C, Rederstorff E, Masson M, Lesoeur J, et al. Pharmacological modulation of human mesenchymal stem cell chondrogenesis by a chemically oversulfated polysaccharide of marine origin: potential application to cartilage regenerative medicine. Stem Cells. 2012;30(3):471-80.

279. Zanni M, Tamburro A, Rotilio D. IL-1 beta and TGF-beta 1 modulate the sulphation grade of chondro-disaccharides in porcine articular cartilage: a capillary electrophoresis study. J Lipid Mediat Cell Signal. 1995;12(1):29-44.

280. Kim B, Yoon JH, Zhang J, Eric Mueller PO, Halper J. Glycan profiling of a defect in decorin glycosylation in equine systemic proteoglycan accumulation, a potential model of progeroid form of Ehlers-Danlos syndrome. Arch Biochem Biophys. 2010;501(2):221-31.

281. Nicoll SB, Wedrychowska A, Smith NR, Bhatnagar RS. Modulation of proteoglycan and collagen profiles in human dermal fibroblasts by high density micromass culture and treatment with lactic acid suggests change to a chondrogenic phenotype. Connect Tissue Res. 2001;42(1):59-69.

282. Junker JP, Sommar P, Skog M, Johnson H, Kratz G. Adipogenic, chondrogenic and osteogenic differentiation of clonally derived human dermal fibroblasts. Cells Tissues Organs. 2010;191(2):105-18.

283. Mizuno S, Glowacki J. Three-dimensional composite of demineralized bone powder and collagen for in vitro analysis of chondroinduction of human dermal fibroblasts. Biomaterials. 1996;17(18):1819-25.

284. Chen FG, Zhang WJ, Bi D, Liu W, Wei X, Chen FF, et al. Clonal analysis of nestin(-) vimentin(+) multipotent fibroblasts isolated from human dermis. J Cell Sci. 2007;120(Pt 16):2875-83.

285. Woo SL, Abramowitch SD, Kilger R, Liang R. Biomechanics of knee ligaments: injury, healing, and repair. Journal of biomechanics. 2006;39(1):1-20.

286. Martin RB, Burr DB, Sharkey NA. Mechanical properties of ligament and tendon. Skeletal tissue mechanics. New York: Springer; 1998. p. 309-46.

287. Lu HH, Jiang J. Interface tissue engineering and the formulation of multiple-tissue systems. Adv Biochem Eng Biotechnol. 2006;102:91-111.

288. Yang PJ, Temenoff JS. Engineering orthopedic tissue interfaces. Tissue Eng Part B Rev. 2009;15(2):127-41.

289. Doroski DM, Brink KS, Temenoff JS. Techniques for biological characterization of tissue-engineered tendon and ligament. Biomaterials. 2007;28(2):187-202.

290. Marrale J, Morrissey MC, Haddad FS. A literature review of autograft and allograft anterior cruciate ligament reconstruction. Knee Surg Sports Traumatol Arthrosc. 2007;15(6):690-704.

291. Laurencin CT, Freeman JW. Ligament tissue engineering: an evolutionary materials science approach. Biomaterials. 2005;26(36):7530-6.

292. Louboutin H, Debarge R, Richou J, Selmi TA, Donell ST, Neyret P, et al. Osteoarthritis in patients with anterior cruciate ligament rupture: a review of risk factors. Knee. 2009;16(4):239-44.

293. Wang JH. Mechanobiology of tendon. J Biomech. 2006;39(9):1563-82.

294. Louie L, Yannas I, Spector M. Tissue engineered tendon. In: Patrick CW, Mikos AG, McIntire LV, editors. Frontiers in Tissue Engineering. New York: Elsevier Science Ltd.; 1998. p. 412-42.

295. Martin RB, Burr DB, Sharkey NA. Mechanical properties of ligament and tendon. Skeletal Tissue Mechanics. New York: Springer; 1998. p. 309-46.

296. Niyibizi C, Sagarrigo Visconti C, Gibson G, Kavalkovich K. Identification and immunolocalization of type X collagen at the ligament-bone interface. Biochem Biophys Res Commun. 1996;222(2):584-9.

297. Lu HH, El-Amin SF, Scott KD, Laurencin CT. Three-dimensional, bioactive, biodegradable, polymer-bioactive glass composite scaffolds with improved mechanical properties support collagen synthesis and mineralization of human osteoblast-like cells in vitro. J Biomed Mater Res A. 2003;64(3):465-74.

298. Spalazzi JP, Dagher E, Doty SB, Guo XE, Rodeo SA, Lu HH. In vivo evaluation of a multiphased scaffold designed for orthopaedic interface tissue engineering and soft tissue-to-bone integration. J Biomed Mater Res A. 2008;86(1):1-12.

299. Moffat KL, Wang IN, Rodeo SA, Lu HH. Orthopedic interface tissue engineering for the biological fixation of soft tissue grafts. Clin Sports Med. 2009;28(1):157-76.

300. Phillips JE, Burns KL, Le Doux JM, Guldberg RE, Garcia AJ. Engineering graded tissue interfaces. Proc Natl Acad Sci U S A. 2008;105(34):12170-5.

301. Livak KJ, Schmittgen TD. Analysis of relative gene expression data using real-time quantitative PCR and the 2(-Delta Delta C(T)) Method. Methods. 2001;25(4):402-8.

302. Farndale RW, Buttle DJ, Barrett AJ. Improved quantitation and discrimination of sulphated glycosaminoglycans by use of dimethylmethylene blue. Biochim Biophys Acta. 1986;883(2):173-7.

303. Ahn SJ, Costa J, Emanuel JR. PicoGreen quantitation of DNA: effective evaluation of samples pre- or post-PCR. Nucleic Acids Res. 1996;24(13):2623-5.

304. Zhang Z, McCaffery JM, Spencer RG, Francomano CA. Hyaline cartilage engineered by chondrocytes in pellet culture: histological, immunohistochemical and ultrastructural analysis in comparison with cartilage explants. J Anat. 2004;205(3):229-37.

305. Goldberg AJ, Lee DA, Bader DL, Bentley G. Autologous chondrocyte implantation. Culture in a TGF-beta-containing medium enhances the re-expression of a chondrocytic phenotype in passaged human chondrocytes in pellet culture. J Bone Joint Surg Br. 2005;87(1):128-34.

306. Yoo JU, Barthel TS, Nishimura K, Solchaga L, Caplan AI, Goldberg VM, et al. The chondrogenic potential of human bone-marrow-derived mesenchymal progenitor cells. J Bone Joint Surg Am. 1998;80(12):1745-57.

307. Bosnakovski D, Mizuno M, Kim G, Ishiguro T, Okumura M, Iwanaga T, et al. Chondrogenic differentiation of bovine bone marrow mesenchymal stem cells in pellet cultural system. Exp Hematol. 2004;32(5):502-9.

308. DeLise AM, Stringa E, Woodward WA, Mello MA, Tuan RS. Embryonic limb mesenchyme micromass culture as an in vitro model for chondrogenesis and cartilage maturation. Methods Mol Biol. 2000;137:359-75.

309. Schulze-Tanzil G, Mobasheri A, Clegg PD, Sendzik J, John T, Shakibaei M. Cultivation of human tenocytes in high-density culture. Histochem Cell Biol. 2004;122(3):219-28.

310. Gungormus C, Kolankaya D. Characterization of type I, III and V collagens in high-density cultured tenocytes by triple-immunofluorescence technique. Cytotechnology. 2008;58(3):145-52.

311. de Wreede R, Ralphs JR. Deposition of collagenous matrices by tendon fibroblasts in vitro: a comparison of fibroblast behavior in pellet cultures and a novel three-dimensional long-term scaffoldless culture system. Tissue Eng Part A. 2009;15(9):2707-15.

312. Bi Y, Ehirchiou D, Kilts TM, Inkson CA, Embree MC, Sonoyama W, et al. Identification of tendon stem/progenitor cells and the role of the extracellular matrix in their niche. Nat Med. 2007;13(10):1219-27.

313. Seo BM, Miura M, Gronthos S, Bartold PM, Batouli S, Brahim J, et al. Investigation of multipotent postnatal stem cells from human periodontal ligament. Lancet. 2004;364(9429):149-55.

314. Cooper JA, Jr., Bailey LO, Carter JN, Castiglioni CE, Kofron MD, Ko FK, et al. Evaluation of the anterior cruciate ligament, medial collateral ligament, achilles tendon and patellar tendon as cell sources for tissue-engineered ligament. Biomaterials. 2006;27(13):2747-54.

315. Lin VS, Lee MC, O'Neal S, McKean J, Sung KLP. Ligament tissue engineering using synthetic biodegradable fiber scaffolds. Tissue Engineering. 1999;5(5):443-51.

316. Bellincampi LD, Closkey RF, Prasad R, Zawadsky JP, Dunn MG. Viability of fibroblast-seeded ligament analogs after autogenous implantation. J Orthopaed Res. 1998;16(4):414-20.

317. Milev P, Maurel P, Chiba A, Mevissen M, Popp S, Yamaguchi Y, et al. Differential regulation of expression of hyaluronan-binding proteoglycans in developing brain: aggrecan, versican, neurocan, and brevican. Biochem Biophys Res Commun. 1998;247(2):207-12.

318. Lin XH. Functions of heparan sulfate proteoglycans in cell signaling during development. Development. 2004;131(24):6009-21.

319. Taipale J, Keski-Oja J. Growth factors in the extracellular matrix. Faseb J. 1997;11(1):51-9.

320. Panyam J, Dali MM, Sahoo SK, Ma W, Chakravarthi SS, Amidon GL, et al. Polymer degradation and in vitro release of a model protein from poly(D,L-lactide-co-glycolide) nano- and microparticles. J Control Release. 2003;92(1-2):173-87.

321. Kohane DS. Microparticles and nanoparticles for drug delivery. Biotechnol Bioeng. 2007;96(2):203-9.

322. Carpenedo RL, Bratt-Leal AM, Marklein RA, Seaman SA, Bowen NJ, McDonald JF, et al. Homogeneous and organized differentiation within embryoid bodies

induced by microsphere-mediated delivery of small molecules. Biomaterials. 2009;30(13):2507-15.

323. Zauner W, Farrow NA, Haines AMR. In vitro uptake of polystyrene microspheres: effect of particle size, cell line and cell density. Journal of Controlled Release. 2001;71(1):39-51.

324. Lee CT, Huang CP, Lee YD. Preparation of amphiphilic poly(L-lactide)-graft-chondroitin sulfate copolymer self-aggregates and its aggregation behavior. Biomacromolecules. 2006;7(4):1179-86.

325. Lee ES, Park KH, Kang D, Park IS, Min HY, Lee DH, et al. Protein complexed with chondroitin sulfate in poly(lactide-co-glycolide) microspheres. Biomaterials. 2007;28(17):2754-62.

326. Lee CT, Huang CP, Lee YD. Synthesis and characterizations of amphiphilic poly(L-lactide)-grafted chondroitin sulfate copolymer and its application as drug carrier. Biomol Eng. 2007;24(1):131-9.

327. Park YD, Tirelli N, Hubbell JA. Photopolymerized hyaluronic acid-based hydrogels and interpenetrating networks. Biomaterials. 2003;24(6):893-900.

328. Bryant SJ, Davis-Arehart KA, Luo N, Shoemaker RK, Arthur JA, Anseth KS. Synthesis and characterization of photopolymerized multifunctional hydrogels: Water-soluble poly(vinyl alcohol) and chondroitin sulfate macromers for chondrocyte encapsulation. Macromolecules. 2004;37(18):6726-33.

329. Provencher SW. A constrained regularization method for inverting data represented by linear algebraic or integral equations. Comput Phys Commun. 1982;27(3):213-27.

330. Smoluchowski M. Contribution to the theory of electro-osmosis and related phenomena. Bull Int Acad Sci Cracovie. 1903:184-99.

331. Bratt-Leal AM, Carpenedo RL, Ungrin M, Zandstra PW, McDevitt TC. Incorporation of biomaterials in multicellular aggregates modulates pluripotent stem cell differentiation. Biomaterials. In press 2010.

332. Ungrin MD, Joshi C, Nica A, Bauwens C, Zandstra PW. Reproducible, ultra high-throughput formation of multicellular organization from single cell suspension-derived human embryonic stem cell aggregates. PLoS One. 2008;3(2):e1565.

333. Carpenedo RL, Sargent CY, McDevitt TC. Rotary suspension culture enhances the efficiency, yield, and homogeneity of embryoid body differentiation. Stem Cells. 2007;25(9):2224-34.

334. Lindahl U, Hook M. Glycosaminoglycans and their binding to biological macromolecules. Annual Review of Biochemistry. 1978;47:385-417.

335. Freitas S, Merkle HP, Gander B. Microencapsulation by solvent extraction/evaporation: reviewing the state of the art of microsphere preparation process technology. J Control Release. 2005;102(2):313-32.

336. Aggarwal BB, Kohr WJ, Hass PE, Moffat B, Spencer SA, Henzel WJ, et al. Human tumor necrosis factor. Production, purification, and characterization. J Biol Chem. 1985;260(4):2345-54.

337. Jensen M, Birch Hansen P, Murdan S, Frokjaer S, Florence AT. Loading into and electro-stimulated release of peptides and proteins from chondroitin 4-sulphate hydrogels. Eur J Pharm Sci. 2002;15(2):139-48.

338. Schmid P, Cox D, Bilbe G, Maier R, Mcmaster GK. Differential Expression of Tgf Beta-1, Beta-2 and Beta-3 Genes during Mouse Embryogenesis. Development. 1991;111(1):117-30.

339. Boyer AS, Ayerinskas II, Vincent EB, McKinney LA, Weeks DL, Runyan RB. TGF beta 2 and TGF beta 3 have separate and sequential activities during epithelial-mesenchymal cell transformation in the embryonic heart. Developmental Biology. 1999;208(2):530-45.

340. Chimal-Monroy J, deLeon LD. Differential effects of transforming growth factors beta 1, beta 2, beta 3 and beta 5 on chondrogenesis in mouse limb bud mesenchymal cells. International Journal of Developmental Biology. 1997;41(1):91-102.

341. Leonard CM, Fuld HM, Frenz DA, Downie SA, Massague J, Newman SA. Role of transforming growth factor-beta in chondrogenic pattern formation in the embryonic limb: stimulation of mesenchymal condensation and fibronectin gene expression by exogenenous TGF-beta and evidence for endogenous TGF-beta-like activity. Developmental Biology. 1991;145(1):99-109.

342. Wang WG, Lou SQ, Ju XD, Xia K, Xia JH. In vitro chondrogenesis of human bone marrow-derived mesenchymal progenitor cells in monolayer culture: activation by transfection with TGF-beta2. Tissue Cell. 2003;35(1):69-77.

343. Waage A, Brandtzaeg P, Halstensen A, Kierulf P, Espevik T. The complex pattern of cytokines in serum from patients with meningococcal septic shock. Association between interleukin 6, interleukin 1, and fatal outcome. J Exp Med. 1989;169(1):333-8.

344. Klose D, Siepmann F, Elkharraz K, Krenzlin S, Siepmann J. How porosity and size affect the drug release mechanisms from PLGA-based microparticles. International Journal of Pharmaceutics. 2006;314(2):198-206.

345. Holland TA, Tabata Y, Mikos AG. In vitro release of transforming growth factor-beta 1 from gelatin microparticles encapsulated in biodegradable, injectable

oligo(poly(ethylene glycol) fumarate) hydrogels. J Control Release. 2003;91(3):299-313.

346. Huang SJ, Wang JM, Tseng SC, Wang LF, Chen JS. Controlled immobilization of chondroitin sulfate in polyacrylic acid networks. J Biomater Sci Polym Ed. 2007;18(1):17-34.

347. Sui W, Huang LL, Wang J, Bo QB. Preparation and properties of chitosan chondroitin sulfate complex microcapsules. Colloids and Surfaces B-Biointerfaces. 2008;65(1):69-73.

348. Wu YN, Yang Z, Hui JH, Ouyang HW, Lee EH. Cartilaginous ECM component-modification of the micro-bead culture system for chondrogenic differentiation of mesenchymal stem cells. Biomaterials. 2007;28(28):4056-67.

349. Brown KE, Leong K, Huang CH, Dalal R, Green GD, Haimes HB, et al. Gelatin/chondroitin 6-sulfate microspheres for the delivery of therapeutic proteins to the joint. Arthritis Rheum. 1998;41(12):2185-95.

350. Thomson JA. Embryonic stem cell lines derived from human blastocysts (vol 282, pg 1147, 1998). Science. 1998;282(5395):1827-.

351. Kawashima H, Hirose M, Hirose J, Nagakubo D, Plaas AH, Miyasaka M. Binding of a large chondroitin sulfate/dermatan sulfate proteoglycan, versican, to L-selectin, P-selectin, and CD44. J Biol Chem. 2000;275(45):35448-56.

352. ASTM Standard F1903. Standard practice for testing for biological responses to particles in vitro. West Conshohocken, PA: ASTM International; 1998 (2003).

353. ASTM Standard F813. Standard practice for direct contact cell culture evaluation of materials for medical devices. West Conshohocken, PA: ASTM International; 2007.

354. Folkman J, Klagsbrun M, Sasse J, Wadzinski M, Ingber D, Vlodavsky I. A heparin-binding angiogenic protein--basic fibroblast growth factor--is stored within basement membrane. Am J Pathol. 1988;130(2):393-400.

355. Bashkin P, Doctrow S, Klagsbrun M, Svahn CM, Folkman J, Vlodavsky I. Basic fibroblast growth factor binds to subendothelial extracellular matrix and is released by heparitinase and heparin-like molecules. Biochemistry. 1989;28(4):1737-43.

356. Thornton SC, Mueller SN, Levine EM. Human endothelial cells: use of heparin in cloning and long-term serial cultivation. Science. 1983;222(4624):623-5.

357. Moscatelli D. High and low affinity binding sites for basic fibroblast growth factor on cultured cells: absence of a role for low affinity binding in the

stimulation of plasminogen activator production by bovine capillary endothelial cells. J Cell Physiol. 1987;131(1):123-30.

358. Feyzi E, Lustig F, Fager G, Spillmann D, Lindahl U, Salmivirta M. Characterization of heparin and heparan sulfate domains binding to the long splice variant of platelet-derived growth factor A chain. J Biol Chem. 1997;272(9):5518-24.

359. Feyzi E, Trybala E, Bergstrom T, Lindahl U, Spillmann D. Structural requirement of heparan sulfate for interaction with herpes simplex virus type 1 virions and isolated glycoprotein C. J Biol Chem. 1997;272(40):24850-7.

360. Knudson CB, Knudson W. Hyaluronan-binding proteins in development, tissue homeostasis, and disease. Faseb J. 1993;7(13):1233-41.

361. Toole BP. Hyaluronan: from extracellular glue to pericellular cue. Nat Rev Cancer. 2004;4(7):528-39.

362. Bourguignon LY, Singleton PA, Zhu H, Zhou B. Hyaluronan promotes signaling interaction between CD44 and the transforming growth factor beta receptor I in metastatic breast tumor cells. J Biol Chem. 2002;277(42):39703-12.

363. Yang B, Yang BL, Savani RC, Turley EA. Identification of a common hyaluronan binding motif in the hyaluronan binding proteins RHAMM, CD44 and link protein. EMBO J. 1994;13(2):286-96.

364. Underhill C. CD44: the hyaluronan receptor. J Cell Sci. 1992;103 (Pt 2):293-8.

365. Schubert M. Chondroitin from chondroitin sulfate. In: Whistler RL, editor. Methods in Carbohydrate Chemistry. New York: Academic Press; 1965. p. 109-10.

366. Kantor TG, Schubert M. A Method for the Desulfation of Chondroitin Sulfate. J Am Chem Soc. 1957;79(1):152-3.

367. Jo S, Shin H, Shung AK, Fisher JP, Mikos AG. Synthesis and characterization of oligo(poly(ethylene glycol) fumarate) macromer. Macromolecules. 2001;34(9):2839-44.

368. Baier Leach J, Bivens KA, Patrick CW, Jr., Schmidt CE. Photocrosslinked hyaluronic acid hydrogels: natural, biodegradable tissue engineering scaffolds. Biotechnol Bioeng. 2003;82(5):578-89.

369. Saito H, Yamagata T, Suzuki S. Enzymatic methods for the determination of small quantities of isomeric chondroitin sulfates. J Biol Chem. 1968;243(7):1536-42.

370. Yamagata T, Saito H, Habuchi O, Suzuki S. Purification and properties of bacterial chondroitinases and chondrosulfatases. J Biol Chem. 1968;243(7):1523-35.

371. Sigma-Aldrich. Enzymatic assay of chondroitinase ABC, EC 4.2.2.4. 1997.

372. Donnan FG. The theory of membrane equilibria. Chemical Reviews. 1924;1(1):73-90.

373. Lai WM, Hou JS, Mow VC. A triphasic theory for the swelling and deformation behaviors of articular cartilage. Journal of Biomechanical Engineering-Transactions of the Asme. 1991;113(3):245-58.

374. Edmond E, Ogston AG. An approach to study of phase separation in ternary aqueous systems. Biochemical Journal. 1968;109(4):569-&.

375. Chen CC, Boskey AL. Mechanisms of Proteoglycan Inhibition of Hydroxyapatite Growth. Calcif Tissue Int. 1985;37(4):395-400.

376. de Sousa Junior JF, Nader HB, Dietrich CP. Sequential degradation of chondroitin sulfate in molluscs. Desulfation of chondroitin sulfate without prior depolymerization by a novel sulfatase from Anomalocardia brasiliana. J Biol Chem. 1990;265(33):20150-5.

377. Nagasawa K, Inoue Y, Tokuyasu T. Improved method for the preparation of chondroitin by solvolytic desulfation of chondroitin sulfates. J Biochem. 1979;86(5):1323-9.

378. Navarro DA, Flores ML, Stortz CA. Microwave-assisted desulfation of sulfated polysaccharides. Carbohydrate Polymers. 2007;69(4):742-7.

379. Mow VC, Gu WY, Chen FH. Structure and function of articular cartilage and meniscus. In: Mow VC, Huiskes R, editors. Basic Orthopaedic Biomechanics & Mechano-Biology. 3rd ed. Philadelphia: Lippincott Williams & Wilkins; 2005. p. 181-258.

380. Canal T, Peppas NA. Correlation between Mesh Size and Equilibrium Degree of Swelling of Polymeric Networks. J Biomed Mater Res A. 1989;23(10):1183-93.

381. Shing Y, Folkman J, Sullivan R, Butterfield C, Murray J, Klagsbrun M. Heparin affinity: purification of a tumor-derived capillary endothelial cell growth factor. Science. 1984;223(4642):1296-9.

382. Del Rosso M, Cappelletti R, Viti M, Vannucchi S, Chiarugi V. Binding of the basement-membrane glycoprotein laminin to glycosaminoglycans. An affinity-chromatography study. Biochem J. 1981;199(3):699-704.

383. Zou P, Zou K, Muramatsu H, Ichihara-Tanaka K, Habuchi O, Ohtake S, et al. Glycosaminoglycan structures required for strong binding to midkine, a heparin-binding growth factor. Glycobiology. 2003;13(1):35-42.

384. Vlodavsky I, Folkman J, Sullivan R, Fridman R, Ishai-Michaeli R, Sasse J, et al. Endothelial cell-derived basic fibroblast growth factor: synthesis and deposition into subendothelial extracellular matrix. Proc Natl Acad Sci U S A. 1987;84(8):2292-6.

385. Witt DP, Lander AD. Differential binding of chemokines to glycosaminoglycan subpopulations. Curr Biol. 1994;4(5):394-400.

386. Saksela O, Moscatelli D, Sommer A, Rifkin DB. Endothelial cell-derived heparan sulfate binds basic fibroblast growth factor and protects it from proteolytic degradation. J Cell Biol. 1988;107(2):743-51.

387. Turnbull JE, Fernig DG, Ke Y, Wilkinson MC, Gallagher JT. Identification of the basic fibroblast growth factor binding sequence in fibroblast heparan sulfate. J Biol Chem. 1992;267(15):10337-41.

388. Klagsbrun M, Shing Y. Heparin affinity of anionic and cationic capillary endothelial cell growth factors: analysis of hypothalamus-derived growth factors and fibroblast growth factors. Proc Natl Acad Sci U S A. 1985;82(3):805-9.

389. Ruijter JM, Ramakers C, Hoogaars WM, Karlen Y, Bakker O, van den Hoff MJ, et al. Amplification efficiency: linking baseline and bias in the analysis of quantitative PCR data. Nucleic Acids Res. 2009;37(6):e45.

390. Box GEP, Cox DR. An analysis of transformations. Journal of the Royal Statistical Society Series B-Statistical Methodology. 1964;26(2):211-52.

391. Takahashi Y, Tabata Y. Effect of the fiber diameter and porosity of non-woven PET fabrics on the osteogenic differentiation of mesenchymal stem cells. J Biomater Sci Polym Ed. 2004;15(1):41-57.

392. Kasten P, Beyen I, Niemeyer P, Luginbuhl R, Bohner M, Richter W. Porosity and pore size of beta-tricalcium phosphate scaffold can influence protein production and osteogenic differentiation of human mesenchymal stem cells: an in vitro and in vivo study. Acta Biomaterialia. 2008;4(6):1904-15.

393. Seto SP, Casas ME, Temenoff JS. Differentiation of mesenchymal stem cells in heparin-containing hydrogels via coculture with osteoblasts. Cell Tissue Res. 2012;347(3):589-601.

394. Akiyama H, Chaboissier MC, Martin JF, Schedl A, de Crombrugghe B. The transcription factor Sox9 has essential roles in successive steps of the chondrocyte differentiation pathway and is required for expression of Sox5 and Sox6. Genes Dev. 2002;16(21):2813-28.

395. Day TF, Guo X, Garrett-Beal L, Yang Y. Wnt/beta-catenin signaling in mesenchymal progenitors controls osteoblast and chondrocyte differentiation during vertebrate skeletogenesis. Dev Cell. 2005;8(5):739-50.

396. Qiu Y, Lim JJ, Scott L, Jr., Adams RC, Bui HT, Temenoff JS. PEG-based hydrogels with tunable degradation characteristics to control delivery of marrow stromal cells for tendon overuse injuries. Acta Biomater. 2011;7(3):959-66.

397. Ruoslahti E, Engvall E. Complexing of fibronectin glycosaminoglycans and collagen. Biochim Biophys Acta. 1980;631(2):350-8.

398. Scott JE. Proteoglycan-fibrillar collagen interactions. Biochem J. 1988;252(2):313-23.

399. Bos KJ, Rucklidge GJ, Dunbar B, Robins SP. Primary structure of the helical domain of porcine collagen X. Matrix Biol. 1999;18(2):149-53.

400. Nuttelman CR, Tripodi MC, Anseth KS. Synthetic hydrogel niches that promote hMSC viability. Matrix Biol. 2005;24(3):208-18.

401. Tavella S, Bellese G, Castagnola P, Martin I, Piccini D, Doliana R, et al. Regulated expression of fibronectin, laminin and related integrin receptors during the early chondrocyte differentiation. J Cell Sci. 1997;110 (Pt 18):2261-70.

402. Fibbi G, Vannucchi S, Cavallini P, Del Rosso M, Pasquali F, Cappelletti R, et al. Involvement of chondroitin sulphate in preventing adhesive cellular interactions. Biochim Biophys Acta. 1983;762(4):512-8.

403. Chiquet-Ehrismann R. Inhibition of cell adhesion by anti-adhesive molecules. Curr Opin Cell Biol. 1995;7(5):715-9.

404. Attia J, Legendre F, Nguyen QT, Bauge C, Boumediene K, Pujol JP. Evaluation of adhesion, proliferation, and functional differentiation of dermal fibroblasts on glycosaminoglycan-coated polysulfone membranes. Tissue Eng Part A. 2008;14(10):1687-97.

405. Mathews MB. Structural factors in cation binding to anionic polysaccharides of connective tissue. Arch Biochem Biophys. 1964;104:394-404.

406. Heldin CH, Miyazono K, ten Dijke P. TGF-beta signalling from cell membrane to nucleus through SMAD proteins. Nature. 1997;390(6659):465-71.

407. Tuli R, Tuli S, Nandi S, Huang X, Manner PA, Hozack WJ, et al. Transforming growth factor-beta-mediated chondrogenesis of human mesenchymal progenitor cells involves N-cadherin and mitogen-activated protein kinase and Wnt signaling cross-talk. J Biol Chem. 2003;278(42):41227-36.

408. Watanabe H, de Caestecker MP, Yamada Y. Transcriptional cross-talk between Smad, ERK1/2, and p38 mitogen-activated protein kinase pathways regulates transforming growth factor-beta-induced aggrecan gene expression in chondrogenic ATDC5 cells. J Biol Chem. 2001;276(17):14466-73.

409. Ravindran S, Roam JL, Nguyen PK, Hering TM, Elbert DL, McAlinden A. Changes of chondrocyte expression profiles in human MSC aggregates in the presence of PEG microspheres and TGF-beta3. Biomaterials. 2011;32(33):8436-45.

410. Fan H, Zhang C, Li J, Bi L, Qin L, Wu H, et al. Gelatin microspheres containing TGF-beta3 enhance the chondrogenesis of mesenchymal stem cells in modified pellet culture. Biomacromolecules. 2008;9(3):927-34.